Scuola Superiore Meridionale
University of Naples Federico II

Scuola Superiore Meridionale

Doctoral Thesis
in Cosmology, Space Science & Space Technology

The Effective Metric Description:
a parametrization for black hole spacetimes beyond General Relativity

Author:
Manuel Del Piano

Supervisors:
Prof. Francesco Sannino
Prof. Stefan Hohenegger

Submitted in fulfillment of the requirements for the degree of Doctor of Philosophy in Cosmology, Space Science & Space Technology.
Coordinator: Prof. Salvatore Capozziello.

PhD SPACE
Cosmology, Space Science & Space Technology

Abstract

This thesis develops a comprehensive and model-independent framework for studying static and spherically symmetric black holes (BHs) subjected to deformations of the classical solutions. Central to this construction is the *Effective Metric Description* (EMD), which parametrizes deviations from classical geometries, such as Schwarzschild and Reissner–Nordström, through one or two functions of a physical quantity, typically the proper distance from the event horizon. By defining the deformation functions in terms of this physical quantity, the EMD ensures coordinate invariance of the deformations and consistency with the classical symmetries of the spacetime.

We provide a systematic method to solve the self-consistency equations near the horizon via series expansions, imposing regularity conditions that guarantee finite curvature scalars and a well-defined Hawking temperature. To extend the applicability of the framework beyond the near-horizon region, we introduce Padé approximants, allowing accurate computation of astrophysical observables, including the photon-sphere radius and the black hole shadow. Our results show that effective expressions capture the leading corrections to these observables and can be directly compared with experimental measurements, enabling model-independent constraints on the deformation functions.

The EMD framework is further generalized to incorporate charged black holes, yielding consistent expressions for the Hawking temperature and clarifying the role of extremal configurations. Additionally, we establish explicit mappings between EMDs based on other spacetime invariants and other widely used parametrization schemes, such as Johannsen–Psaltis and Rezzolla–Zhidenko, demonstrating the fundamental equivalence of these approaches and facilitating the translation of quantum-gravity–inspired deformations across different frameworks. Applications to quasi normal modes in the eikonal limit and various regular black hole models illustrate the versatility and predictive power of the framework.

Overall, this thesis provides a unified and flexible basis to study black hole spacetimes in classical and quantum regimes. The formalism developed here not only advances theoretical understanding but also bridges the gap to phenomenology, offering practical tools to confront upcoming high-precision observations with predictions of quantum gravity and general relativity.

Acknowledgements

I would like to express my deepest gratitude to my supervisors Prof. Francesco Sannino and Stefan Hohenegger for their constant guidance, insightful discussions, and invaluable support throughout these years. Their scientific rigor and encouragement have been essential in shaping both this work and my growth as a researcher.

I am sincerely grateful to Professor Salvatore Capozziello, PhD coordinator, for his constant support, constructive feedback, and for fostering an inspiring research environment that made this project possible.

I also wish to thank all the members of our research group for their collaboration, stimulating conversations, and for creating a friendly and motivating atmosphere in which ideas could freely evolve. Their passion for science and enthusiasm made this journey truly enjoyable.

Finally, I extend my thanks to all colleagues and friends who, in different ways, have accompanied me along this path, sharing not only scientific challenges but also the everyday moments that made this experience memorable.

Publication List

This thesis is based on the following publications:

[45] E. Binetti, M. Del Piano, S. Hohenegger, F. Pezzella, and F. Sannino, *Effective theory of quantum black holes*, Phys. Rev. D **106**, 046006 (2022), arXiv:2203.13515 [gr-qc] .

[46] M. Del Piano, S. Hohenegger, and F. Sannino, *Quantum black hole physics from the event horizon*, Phys. Rev. D **109**, 024045 (2024), arXiv:2307.13489 [gr-qc] .

[47] M. Del Piano, S. Hohenegger, and F. Sannino, *Effective metric descriptions of quantum black holes*, Eur. Phys. J. C **84**, 1273 (2024), arXiv:2403.12679 [gr-qc] .

[49] M. Del Piano, S. Hohenegger, and F. Sannino, *Black hole shadow and other observables away from the horizon: Extending the effective metric descriptions*, Phys. Rev. D **111**, 064070 (2025), arXiv:2412.13673 [gr-qc] .

[48] M. Damia Paciarini, M. Del Piano, S. Hohenegger, and F. Sannino, *Effective metric description of charged black holes*, Eur. Phys. J. C **85**, 848 (2025), arXiv:2504.20810 [gr-qc] .

[69] M. Del Piano, C. De Simone, M. Damia Paciarini, V. De Falco, M. Myszkowski, F. Sannino, and V. Vellucci, *Toward a unified view of agnostic parametrizations for deformed black holes*, Submitted to Phys. Rev. D (2025), arXiv:2510.14707 [gr-qc]

Additional publications which are not included in this thesis are listed below:

[7] B. Bajc, M. Del Piano, and F. Sannino, *UV finite GUT with SUSY breaking*, Phys. Rev. D **109**, 055043 (2024), arXiv:2308.13311 [hep-ph] .

[119] A. Alonso-Serrano, M. de Cesare, and M. Del Piano, *Black hole solutions in quantum phenomenological gravitational dynamics*, Phys. Rev. D **112**, 084031 (2025), arXiv:2504.01539 [gr-qc]

Contents

Abstract **iii**

Acknowledgements **iv**

Publication List **v**

1 Introduction **1**

2 Black hole spacetimes within General Relativity **5**
2.1 Black hole solutions in General Relativity . . . 5
2.1.1 Vacuum solutions . . . 6
2.1.2 Non-vacuum solutions . . . 9
2.1.3 Uniqueness and the No-Hair Theorems . . . 10
2.2 Black hole thermodynamics . . . 10
2.3 Spherically symmetric black hole shadow . . . 12
2.4 Quasi-Normal Modes . . . 14
2.4.1 Eikonal limit . . . 15

3 The Effective Metric Description **17**
3.1 Definitions and Review . . . 17
3.2 The proper distance EMD . . . 20
3.2.1 Solving the distance function . . . 20
3.2.2 Metric functions and curvature scalars . . . 22
3.2.3 Regular higher order derivatives . . . 25
3.2.4 Conditions for regularity at inner horizons . . . 27
3.3 EMD redefinitions . . . 28
3.4 Ricci Scalar EMD . . . 29
3.4.1 Definition of the EMD . . . 30
3.4.2 Relation to the Distance EMD . . . 32
3.5 Kretschmann Scalar EMD . . . 35
3.5.1 Definition of the EMD . . . 35
3.5.2 Relation to other EMDs . . . 37
3.5.3 Overview of the relations . . . 38
3.6 EMD for charged black holes . . . 40
3.6.1 Near horizon expansion and EMD coefficients . . . 41

3.6.2 Hawking temperature and Ricci scalar . . . 43
3.6.3 Small charge expansion . . . 44
3.6.4 Solution of the Maxwell field . . . 45
3.6.5 Effective description of an extremal BH . . . 46

4 Applications **53**
4.1 Minimal metric deformation . . . 53
4.2 Bonanno-Reuter asymptotically safe black hole . . . 57
4.3 Hayward black hole . . . 61
4.4 Dymnikova black hole . . . 63
4.5 Extremal Frolov space-time . . . 65
4.6 Weak gravity conjecture . . . 68
4.7 Computing the proper distance . . . 69

5 Extending the EMD **73**
5.1 Effective Metric Approach and Approximations . . . 73
5.2 Padé Approximation . . . 75
5.2.1 Padè Approximant of a Series Expansion . . . 75
5.2.2 Padé Approximant of the Metric and Horizon Distance . . . 76
5.2.3 Padé Approximation for the Photon Radius . . . 79
5.3 Simple Examples of Corrected Schwarzschild Geometries . . . 83
5.3.1 Metrics and Deformation Parameters . . . 83
5.3.2 Dilaton black hole . . . 89
5.4 Convergence . . . 92

6 Comparison of Parametrized Black Hole Metrics **93**
6.1 Agnostic parametrizations . . . 93
6.1.1 Johannsen-Psaltis parametrization . . . 94
6.1.2 Rezzolla-Zhidenko parametrization . . . 95
6.1.3 Effective Metric Description parametrization . . . 95
6.2 Transformation maps relating the different parametrizations . . . 98
6.2.1 Eikonal limit in different parametrizations . . . 103
6.2.2 Application to BH models . . . 108

7 Concluding remarks and outlooks **113**

Appendix **117**
A.1 Series relations . . . 117
A.1.1 Series expansion of inverse radial coordinate . . . 118
A.1.2 Power of a power series . . . 119
A.2 Series expansions for $\xi_1 \neq 0$ . . . 120
A.3 Transition from Ricci to Distance EMD . . . 121
A.4 Signs in the Kretschmann Scalar EMD . . . 122
A.5 Conditions in the extremal case with $Q^2 \neq M\, r_H$ . . . 124

Bibliography **127**

1 Introduction

Black holes (BHs) are among the most intriguing and fundamental objects predicted by Einstein's theory of General Relativity (GR) [1–3]. Defined by regions of spacetime from which no signal can escape, black holes provide a unique stage to probe gravitational physics in extreme regimes. Classical solutions in GR, such as the Schwarzschild, Reissner–Nordström (RN), and Kerr black holes, are characterized by only a few parameters: mass, charge, and angular momentum. This simplicity, often encapsulated in the *no-hair conjecture* [4–12], belies the profound richness of their physical and mathematical properties. For instance, RN and Kerr black holes exhibit inner and outer horizons, whose coalescence defines an extremal configuration with vanishing surface gravity [13–16]. Similarly, the Kerr solution introduces rotation, leading to frame-dragging effects and a more intricate causal structure.

Astrophysical observations have now reached a level of accuracy that allows for the direct probing of black hole properties. The Event Horizon Telescope (EHT) has provided unprecedented imaging of the supermassive black holes M87* and Sgr A*, revealing their shadows and constraining their mass and spin parameters [17–20]. Simultaneously, gravitational wave observatories, including LIGO, Virgo, and KAGRA, have detected numerous BH binary mergers, providing detailed information about their mass, spin distributions, and merger dynamics [21–23]. These observations not only confirm the existence of black holes as predicted by GR but also open the door to probing potential deviations from classical solutions, thereby providing a unique window into physics beyond GR and hints of quantum gravity effects.

Despite these advances, a fully consistent and predictive theory of quantum gravity remains elusive. Consequently, understanding the modifications of black hole spacetimes due to quantum or otherwise beyond-GR effects poses a significant challenge. Many approaches have been proposed, ranging from concrete quantum gravity models to phenomenological modifications inspired by symmetry or regularity principles. The resulting plethora of individual models [24–43] often employ distinct metric deformations, making direct comparison with observational data and cross-model generalization difficult [44].

To address this challenge, an *Effective Metric Description* (EMD) framework has been developed [45–48]. The core idea is to construct a model-independent and systematic representation of black hole deformations in terms of physical quantities, typically invariants of the spacetime geometry. In the case of non-extremal, static, and spherically symmetric black holes, a natural choice for such a quantity is the proper radial distance from the event horizon. For extremal black holes, where this invariant is not well-defined, one can instead use the proper time for a free-falling observer to reach the horizon.

In the EMD framework, the metric is expanded in a series around the horizon in terms of these physical quantities. Regularity conditions, such as finiteness of the Hawking temperature and curvature scalars, impose constraints on the coefficients of these expansions. These constraints are coordinate-independent and provide universal conditions for physically admissible black hole spacetimes [49, 50]. By formulating deformations in this manner, the EMD allows a coherent description of a wide class of black holes, whether classical, regular, or quantum-deformed, in a way that is both physically meaningful and well-defined.

Parameterizing observationally relevant quantities is central to the EMD's applicability. The black hole shadow, corresponding to the apparent shape of the photon capture region as seen by a distant observer, probes the geometry near the photon sphere and provides relevant insights on the spacetime structure. To this aim, the EMD went through deep improvements in order to connect the near horizon parametrization with observables that lie at a finite distance from it. This was eventually achieved by the employment of Padé approximants [51], which enjoy large applications in very different fields [52–56]. The successful extension of the EMD to observables away from the event horizon [49], sparkled the idea of applying such approach to other interesting physical quantities, such as the orbital frequency and Lyapunov exponent of photon orbits which determine the real and imaginary parts of quasi-normal mode (QNM) frequencies [57–61] in the eikonal limit [62–64]. As a result, the shadow radius and eikonal QNMs are tightly linked to the underlying spacetime geometry and can be computed within the EMD framework to assess deviations from classical predictions.

Many other parametrizations exist in the literature. Johannsen–Psaltis [65, 66] introduced a quadrupole moment independent of mass and spin, facilitating tests of the no-hair theorem through ISCO and lensing observations. Cardoso, Pani and Rico [67] extended this approach to include additional parameters affecting both weak- and strong-field regimes. Rezzolla–Zhidenko [61, 68] introduced a continued-fraction expansion for static, spherically symmetric spacetimes, providing superior convergence properties compared to Taylor series. Our EMD framework complements these approaches by focusing on invariants, series expansions near the horizon, and the connection to directly observable quantities. Establishing a map between these frameworks allows a coherent comparison of different parametrizations, revealing their respective strengths and limitations [69].

Several works have applied the EMD framework to explore different aspects of black hole physics. Li *et al.* [70] analyzed timelike and lightlike geodesics in a quantum black hole described within the EMD, studying the periapsis precession of bounded orbits and angular shadow size. They found that quantum corrections enhance both the precession and the shadow relative to the classical case, particularly for smaller black holes. Belfiglio *et al.* [71] investigated entanglement entropy for a massive non-minimally coupled scalar field in several quantum black hole models, showing a significant deviation from the classical area law near the origin, with convergence to classical results at larger distances. D'Alise *et al.* [50] explored positivity conditions and asymptotic stress-energy tensors, demonstrating how physicality requirements constrain metric deformations, with results applicable to both classical and quantum black holes.

Further extensions of the EMD framework have been applied to lower-dimensional models and regular spacetimes. Damia Paciarini *et al.* [72] developed an EMD for 2+1-dimensional BTZ black holes, computing effective metrics near the horizon, origin, and spatial infinity, while deriving corrected Hawking temperatures. In [73], they systematically investigated regularity conditions in spherically symmetric spacetimes, classifying cores based on asymptotic behavior and ensuring geodesic completeness. Hohenegger [74] linked EMD expansion coefficients to observable quantities via a gedankenexperiment, establishing a connection between metric deformations and effective stress-energy tensors, and illustrated their approach using the Hayward spacetime.

These works collectively demonstrate the versatility of the EMD, highlighting its ability to:

- Capture universal features of black hole physics across models,
- Provide a systematic parametrization of quantum or regularized deformations,
- Enable computation of physically observable quantities such as Hawking temperature, shadows, and geodesic precession in a model-independent fashion,
- Connect theoretical parameters to observable quantities measurable by external probes.

Moreover, modifications of near-horizon metrics can significantly affect gravitational wave emission, particularly during the ringdown phase after perturbations. The EMD provides a practical approach to compute these corrections systematically, enabling predictions for potential deviations in future gravitational wave detections. By connecting these observables to series expansion coefficients of the EMD, one can, in principle, constrain or measure quantum corrections using astrophysical data.

This thesis aims to provide a unified view of model-independent black hole parametrizations, with a particular focus on the EMD framework. We explore its construction, theoretical consistency, and practical applications, while reviewing and extending its previous uses in the literature. Special attention is given to physical observables, including shadows and eikonal QNMs, and their sensitivity to quantum or regularized deformations. The EMD framework is not merely a theoretical tool, but a bridge connecting fundamental black hole physics, quantum gravity-inspired modifications, and observable astrophysical signatures. It provides a systematic, physically meaningful, and model-independent approach to study the rich phenomenology of black holes, paving the way for rigorous confrontation with current and future observations.

The thesis is organized as follows. Chapter 2 provides a review of classical black hole solutions, introducing the key physical quantities of interest, such as the Hawking temperature, the black hole shadow, and quasi-normal modes (QNMs). Chapter 3 introduces the Effective Metric Description (EMD) framework. Building on [45, 46], we present the general idea of the approach, including the self-consistency and regularity conditions of the solutions. The chapter then explores, following [47], how EMDs formulated in terms of different physical quantities are connected, establishing the robustness of the framework. Finally, based on [48], the generalization to charged black holes is discussed, with particular attention to extremal configurations. In chapter 4, the approach is tested on various black hole models. Chapter 5 extends the near-horizon parametrization using Padé approximants and demonstrates their application to the computation of the black hole shadow. Chapter 6, based on [69], compares EMDs near the horizon and at large distances with other parametrizations in the literature, namely Johannsen–Psaltis and Rezzolla–Zhidenko, and tests all frameworks by computing QNMs in the eikonal limit for different black hole models. In the concluding chapter 7, we summarize the main results obtained throughout the thesis. We emphasize how the EMD framework provides a consistent, model-independent approach to describing quantum and classical deformations of black holes, including charged and extremal configurations.

The conclusions highlight the versatility and robustness of EMDs, their connections to other parametrizations, and the applicability of the framework to key observables such as the black hole shadow and QNMs. Finally, we outline potential directions for future research, including the extension of the EMD framework to rotating black holes, the study of interior black hole structures, and the exploration of additional physical observables. These perspectives open the way to both deeper theoretical insights into quantum gravity effects and potential applications to astrophysical observations.

Throughout the thesis we adopt the geometric unit convention $c = G_\mathrm{N} = 1$.

2 Black hole spacetimes within General Relativity

This chapter introduces the essential theoretical background of black hole physics forming the basis of the effective metric description. We review the main BH solutions of general relativity (GR), *i.e.* Schwarzschild, Reissner–Nordström, and briefly Kerr, highlighting their geometric structure, causal properties, and the implications of the no-hair theorems. We then discuss key thermodynamic aspects such as surface gravity, Hawking radiation, and the area law, which link gravity, quantum theory, and thermodynamics. The chapter also examines light propagation and the formation of the BH shadow, followed by an introduction to BH perturbations and their quasi-normal modes (QNMs), which characterize the ringdown phase of gravitational-wave emission. Altogether, these topics provide the conceptual and mathematical foundation for the effective metric framework developed in the following chapters.

2.1 Black hole solutions in General Relativity

General Relativity is a dynamical theory of the spacetime, whose action in 4 dimensions is the Einstein-Hilbert action. The total system action composed of matter and spacetime reads

$$S_{\mathrm{tot}} = S_{\mathrm{EH}} + S_m \quad \text{with} \quad S_{\mathrm{EH}} = \frac{1}{16\pi}\int \mathrm{d}^4x\sqrt{-g}\,R \quad \text{and} \quad S_m = \int \mathrm{d}^4x\sqrt{-g}\,\mathcal{L}_m\,, \tag{2.1}$$

where g is the determinant of the metric tensor $g_{\mu\nu}$, R is the Ricci scalar and $\mathcal{L}_m$ is the matter Lagrangian density. A possible additional term in S_{EH} is the cosmological constant Λ which models the spacetime dynamics driven by the presence of dark energy in the system, which is appreciable at cosmological scales and hence, we can neglect it in the action. Variation of the total action (2.1) with respect to the metric tensor yields the second-order non-linear field equations

$$R_{\mu\nu} - \frac{1}{2}R\,g_{\mu\nu} = 8\pi\,T_{\mu\nu}\,, \tag{2.2}$$

notably known as the Einstein equations, where $R_{\mu\nu}$ is the Ricci tensor obtained from the contraction of the diagonal components of the Riemann curvature tensor $R_{\mu\nu} := R^{\rho}{}_{\mu\rho\nu}$, computed from $g_{\mu\nu}$, and $T_{\mu\nu}$ is the energy-momentum tensor defined by the matter Lagrangian density as

$$T_{\mu\nu} := -\frac{2}{\sqrt{-g}}\frac{\delta\left(\sqrt{-g}\,\mathcal{L}_m\right)}{\delta g^{\mu\nu}}\,. \tag{2.3}$$

This tensor acts as the source term in the Einstein equations (2.2), allowing us to distinguish between vacuum and non-vacuum solutions.

2.1.1 Vacuum solutions

Firstly, let us examine the case of vacuum solution, namely we impose in Eq. (2.2) that

$$T_{\mu\nu} = 0\,, \tag{2.4}$$

in some region of the spacetime. Typically, the choices that can be made depend on the type of matter distribution and the most used is a spatially limited distribution and a vacuum exterior space. Thus, in order to proceed with the solution of the field equations, which they now read

$$R_{\mu\nu} = 0\,, \tag{2.5}$$

we have to impose the symmetries of the spacetime.

The Schwarzschild solution

The simplest case is the static and spherically symmetric spacetime, which is described in spherical coordinates (t, r, θ, φ) by the following line element

$$\mathrm{d}s^2 = -h(r)\mathrm{d}t^2 + f(r)^{-1}\mathrm{d}r^2 + r^2\mathrm{d}\theta^2 + r^2\sin^2\theta\mathrm{d}\varphi^2\,. \tag{2.6}$$

The Ricci scalar in terms of f and h is[1]

$$R = \frac{f(h^{(1)})^2}{2h^2} - \frac{\left(rf^{(1)} + 4f\right)h^{(1)}}{2rh} - \frac{f\,h^{(2)}}{h} - \frac{2\left(rf^{(1)} + f - 1\right)}{r^2}\,. \tag{2.8}$$

and the Kretschmann scalar is given by

$$K \coloneqq R_{\rho\sigma\mu\nu}R^{\rho\sigma\mu\nu}\,, \tag{2.9}$$

where $R_{\rho\sigma\mu\nu} = g_{\rho\lambda}R^{\lambda}{}_{\sigma\mu\nu}$ is the fully covariant Riemann tensor.
Inserting such metric into the field equations (2.2) with the condition (2.4), and imposing the asymptotic flatness as well as the weak field limit as boundary conditions, one obtains the noteworthy Schwarzschild solution

$$h(r) \equiv f(r) = f_S(r) = 1 - \frac{2M}{r}\,, \tag{2.10}$$

where M is the mass of the object at $r = 0$ sourcing the exterior gravitational field. The time-independence and spherical symmetry of not a particular choice for symmetries of the exterior gravitational field but are actually related to the uniqueness of the solution in light of the Birkhoff's

[1] From here on out the notation $F^{(n)}$ is used to indicate the n-th derivative of a function F with respect to its argument. For example, we define

$$f^{(n)}(r) := \frac{\mathrm{d}^n f(r)}{\mathrm{d}r^n} \quad \text{and} \quad \Phi^{(n)}\left(\frac{1}{x}\right) := \left.\frac{\mathrm{d}^n\Phi(y)}{\mathrm{d}y^n}\right|_{y=\frac{1}{x}}\,. \tag{2.7}$$

The subscript $_H$ denotes the evaluation of a quantity at the horizon, which corresponds to taking $r = r_H$, *e.g.* $f_H^{(n)} := f^{(n)}(r = r_H)$.

theorem. The theorem states the Schwarzschild spacetime is the only spherically symmetric and asymptotically flat solution to the Einstein equations in vacuum. Hence, even in the case of a time-evolving matter distribution, for instance in a radially pulsating or collapsing spherical star, the exterior region is described by the Schwarzschild metric.
Let us remark that the metric elements $-g_{tt}(r) = g_{rr}^{-1} = 1 - 2M/r$ have two singular points: the first one is $r = 0$ where $g_{tt} \to +\infty$ and $g_{rr} \to 0^-$. The second point is $r = 2M$ where $g_{tt} \to 0^-$ and $g_{rr} \to +(-)\infty$ (respectively when it is approach from $(2M)^+$ and $(2M)^-$), however each singular point has different nature. In order to investigate which point is properly a curvature singularity, one has to construct the invariants of the Riemann curvature tensor. A naive example of such an invariant would be the Ricci scalar in Eq. (2.8) but given the vacuum condition (2.4), and so Eq. (2.5), it is identically vanishing. Alternatively, we can consider the Kretschmann scalar in Eq. (2.9)

$$K = \frac{48M^2}{r^6} \,, \tag{2.11}$$

which exhibits a pole only at $r = 0$. Hence, the singularity at $r = 2M$ is called *coordinate singularity*, because it can be removed with some appropriate coordinate transformations, for example the Eddington-Finkelstein in-falling or out-going null coordinate sets. Nonetheless, the surface at $r = 2M$ has remarkable features. Considering the hypersurface Σ

$$\Sigma = r - 2M = 0 \,, \tag{2.12}$$

the dual normal vector is given by the gradient

$$n_\alpha = \partial_\alpha \Sigma \,, \tag{2.13}$$

and whose norm is

$$n_\alpha n^\alpha = g^{\alpha\beta} n_\alpha n_\beta = g^{rr}(\partial_r \Sigma)^2 = 1 - \frac{2M}{r} \,. \tag{2.14}$$

Hence, we can examine three cases:

- Any sphere with radius $r > 2M$ is a collection of timelike points where signals can be sent towards the origin $r \to 0$ and the spatial infinity $r \to \infty$, hence they are all causally connected.
- The spheres with radii $r < 2M$ are spacelike, and any light signal is forced to converge towards the origin, therefore any observer located in this region is unable to communicate with observers at $r > 2M$.
- The 2-sphere $r = 2M$ is a lightlike surface that separates the two causally disconnected regions described above, therefore it is called the **event horizon**.

The same conclusions can be drawn from the investigation of the timelike Killing vector

$$(\chi^t)^\mu = (1, 0, 0, 0) \,, \tag{2.15}$$

which is such that the Lie derivative vanishes, *e.g.* $\mathcal{L}_{\chi^t} g_{\mu\nu} = \partial_t g_{\mu\nu} = 0$, reflecting the time-translational invariance of the metric (namely the assumption of staticity). A timelike *Killing horizon* is defined as the collection of points where the norm $(\chi^t)_\mu (\chi^t)^\mu = -f_S(r)$ vanishes. Hence, for the Schwarzschild spacetime the event horizon coincides with the timelike Killing horizon. From these observations, the Schwarzschild solution is said to describe the geometry of a black hole.

The Kerr solution

For the completeness of the review on the GR vacuum solutions, let us now examine the case in which we relax the spherical symmetry of the spacetime and briefly introduce the metric of a rotating black hole with mass M and angular momentum J, known as Kerr BH [75]. As an isolated rotating object, we can find a coordinate frame in which we can align one axis along the conserved angular momentum. The most commonly used coordinates are the Boyer-Lindquist coordinates (t, r, θ, φ) and the line element reads

$$\begin{aligned} \mathrm{d}s^2 = -\left(1 - \frac{2M\,r}{\Sigma}\right)\mathrm{d}t^2 + \frac{\Sigma}{\Delta}\mathrm{d}r^2 + \Sigma\,\mathrm{d}\theta^2 + \\ + \left(r^2 + a^2 + \frac{2Ma^2\,r}{\Sigma}\sin^2\theta\right)\sin^2\theta\,\mathrm{d}\varphi^2 - \frac{4Ma\,r}{\Sigma}\sin^2\theta\,\mathrm{d}t\,\mathrm{d}\varphi\,. \end{aligned} \tag{2.16}$$

where $a \coloneqq J/M$ and we have introduced the auxiliary functions

$$\Sigma \coloneqq r^2 + a^2\cos^2\theta \quad \text{and} \quad \Delta \coloneqq r^2 - 2M\,r + a^2\,. \tag{2.17}$$

We note the appearance of the cross term $g_{t\phi} \propto a$ in the line element, which vanishes when the angular momentum is switched off and the entire metric (2.16) reduces to the Schwarzschild one. Rotation leads to two distinct surfaces of interest. The roots of Δ determine the inner and outer horizons

$$r_\pm = M \pm \sqrt{M^2 - a^2}\,. \tag{2.18}$$

The stationary limit surface is defined by $g_{tt} = 0$, *i.e.*

$$r_{\rm ergo}(\theta) = M + \sqrt{M^2 - a^2\cos^2\theta}\,, \tag{2.19}$$

which encloses the ergoregion, where no static observer can exist and the angular velocity of the BH horizon is

$$\Omega_H \coloneqq \left.\frac{g_{t\varphi}}{g_{\varphi\varphi}}\right|_{r=r_+} = \frac{a}{2Mr_+}\,. \tag{2.20}$$

The distinction between the ergoregion boundary and the horizon, $r_{\rm ergo}(\theta) > r_+$ for $0 < \theta < \pi$, enables extraction of rotational energy, which is an important feature for the Penrose process [76, 77] and for the effect of superradiance of fields around the BH [78–80].[2]

From Eq. (2.18), the existence of two real and distinct roots requires $a < M$ ensuring that the metric describes a rotating black hole. The limiting case $a = M$ corresponds to an *extremal* Kerr black hole, for which the inner and outer horizons coincide. If instead $a > M$, the function Δ has no real roots and the curvature singularity at $r = 0$ becomes exposed to distant observers, resulting in a *naked singularity* [81]. Such configurations would violate the *cosmic censorship conjecture* [82], which posits the existence of an event horizon that shields singularities from the exterior universe. Consequently, the bound

$$a \leq M\,, \tag{2.21}$$

is enforced as a necessary condition for physically acceptable Kerr spacetimes.

[2] Kerr supports the superradiant scattering of classical scalar fields if the field frequency ω is such that $\omega < m\Omega_H$ leading to amplification of waves with azimuthal number m. If the wave is trapped, a superradiant instability can arise, constraining ultralight fields.

2.1.2 Non-vacuum solutions

Before studying the presence of matter content in the system, we remark that the cosmological constant Λ behaves like and effective geometrical source in vacuum Einstein equations, *e.g.* $R_{\mu\nu} = \Lambda\, g_{\mu\nu}$, realizing the condition for Einstein spaces. The solution to such equations are known as de Sitter ($\Lambda > 0$) or Anti-de Sitter ($\Lambda < 0$) which are maximally symmetric spaces.
While vacuum black holes already capture essential aspects of strong-gravity physics, realistic astrophysical environments and fundamental interactions demand the inclusion of matter fields. In this Section, we investigate the class of solutions in GR that are supported by electromagnetic charges.

Reissner-Nordström black holes

The classical Reissner-Nordström (RN) geometry [13–15, 83] represents a static and spherical solution to the Einstein field equations (2.2) in presence of an electromagnetic field. In the region outside of the event horizon, the source term in the field equation reads

$$T_{\mu\nu} = \frac{1}{4\pi}\left(F_{\mu}{}^{\rho}F_{\nu\rho} - \frac{1}{4}g_{\mu\nu}F^{\rho\sigma}F_{\rho\sigma}\right) , \tag{2.22}$$

which is the energy-momentum tensor related to $U(1)$ gauge vector field A^{μ}, with $F_{\mu\nu} = -F_{\nu\mu} = \nabla_{\mu}A_{\nu} - \nabla_{\nu}A_{\mu}$ being the field strength tensor, which is subject to the Maxwell equations in the curved background as well as the Bianchi identity:

$$g^{\rho\mu}\nabla_{\rho}F_{\mu\nu} = 0 \quad \text{and} \quad \nabla_{[\mu}F_{\nu\rho]} = 0 \, . \tag{2.23}$$

Here ∇_{μ} is the covariant derivative obtained through the metric $g_{\mu\nu}$. Assuming spherical symmetry and time invariance, as in the metric (2.6), we notably obtain the Reissner-Nordström solution, that takes the following form [84]:

$$h(r) = f(r) = 1 - \frac{2M}{r} + \frac{Q^2}{r^2} , \tag{2.24}$$

in which M is the mass of the black hole and $Q^2 = q^2 + m^2$, where q and m are its electric and magnetic charges respectively. We also remark that the limit $Q \to 0$, leads to the Schwarzschild space-time. On this metric, the solution to the electromagnetic field equations (2.23) are given by the point-like charge Coulomb electric field and the magnetic monopole field

$$E_r = F_{rt} = \frac{q}{r^2} \quad \text{and} \quad B_r = \frac{F_{\theta\varphi}}{r^2\sin^2\theta} = \frac{m}{r^2} . \tag{2.25}$$

Similarly as in the Kerr BH, we have two roots for the metric function

$$r_{\pm} = M \pm \sqrt{M^2 - Q^2} , \tag{2.26}$$

representing the inner and outer horizons. They are real and distinct if $Q < M$, they coincide in the case of $Q = M$ giving an extremal RN BH and if $Q > M$ we will have a naked singularity. However, many studies has proven that the inner horizon (also known as a Cauchy horizon) is unstable under perturbations [85–88].

2.1.3 Uniqueness and the No-Hair Theorems

Within classical general relativity, the family of stationary, asymptotically flat black hole solutions in four dimensions is remarkably restricted to the ones discussed above. According to the *black hole uniqueness theorems* [5–7], any such solution of the Einstein–Maxwell equations is completely characterized by only three global conserved quantities: mass M, angular momentum J, and electric charge Q. This implies that, under reasonable physical assumptions (such as the presence of an event horizon and the absence of naked singularities), the only admissible stationary black holes are the Schwarzschild, Reissner–Nordström, and Kerr (or Kerr–Newman in the charged and rotating case) solutions. This simplicity is encapsulated in the *no-hair theorem* [4, 8–12], which states that all higher multipole moments of the gravitational and electromagnetic fields are determined by these three parameters alone. Consequently, any additional structure or deviation from these metrics must arise from new physics beyond classical general relativity, such as modifications of the gravitational action, coupling to non-linear matter fields, or quantum-gravity effects.

2.2 Black hole thermodynamics

We consider a static, spherically symmetric metric of the form in Eq. (2.6) and assume an non-extremal event horizon at $r = r_H$ where $h(r_H) = f(r_H) = 0$. The *surface gravity* κ associated with the horizon generator $(\chi^t)^\mu = \delta^{\mu 0}$ can be defined geometrically by

$$(\chi^t)^\nu \, \nabla_\nu (\chi^t)^\mu = \kappa \, (\chi^t)^\mu \quad \text{on} \quad r = r_H \, . \tag{2.27}$$

Equivalently, for the metric (2.6) one obtains the convenient expression

$$\kappa \;=\; \frac{1}{2}\sqrt{h_H^{(1)} \, f_H^{(1)}} \, . \tag{2.28}$$

In most cases one has $h(r) = f(r)$ which yields $\kappa = \frac{1}{2} f_H^{(1)}$.

The Hawking temperature follows from the requirement of regularity of the Euclidean section of the black-hole geometry. Introduce the Euclidean time with a Wick rotation $\tau = it$ and expand the metric (2.6) near the horizon. Let $r = r_H + \delta r$ with $\delta r \ll r_H$. To leading order

$$h(r) \simeq h_H^{(1)} \, \delta r \quad \text{and} \quad f(r) \simeq f_H^{(1)} \, \delta r \, . \tag{2.29}$$

Define a radial coordinate ρ by

$$\rho \coloneqq 2\sqrt{\frac{\delta r}{f_H^{(1)}}} \quad \Longrightarrow \quad \delta r = \tfrac{1}{4} f_H^{(1)} \, \rho^2 \, . \tag{2.30}$$

Substituting into the Euclidean metric gives, to leading order,

$$\mathrm{d}s_E^2 \simeq \rho^2 \left(\frac{h_H^{(1)} f_H^{(1)}}{4} \right) \mathrm{d}\tau^2 + \mathrm{d}\rho^2 + r_H^2 \mathrm{d}\Omega^2 \, . \tag{2.31}$$

Using (2.28) this becomes the flat polar form

$$\mathrm{d}s_E^2 \simeq \rho^2 \kappa^2 \mathrm{d}\tau^2 + \mathrm{d}\rho^2 + r_H^2 \mathrm{d}\Omega^2 \, . \tag{2.32}$$

Absence of a conical singularity at $\rho = 0$ (the horizon) requires the Euclidean time τ to be periodic with period

$$\beta = \frac{2\pi}{\kappa} \,. \tag{2.33}$$

Interpreting β as the inverse temperature of the quantum field state regular on the horizon yields the Hawking temperature [2, 89–92]

$$T_H = \frac{1}{\beta} = \frac{\kappa}{2\pi} \,. \tag{2.34}$$

For the Schwarzschild, Reissner-Nordström and Kerr metrics we have that the respective temperatures read

$$T_{\rm H}^{\rm Schw} = \frac{1}{8\pi M} \,, \quad T_{\rm H}^{\rm RN} = \frac{\sqrt{M^2 - Q^2}}{2\pi (M + \sqrt{M^2 - Q^2})^2} \quad \text{and} \quad T_{\rm H}^{\rm Kerr} = \frac{\sqrt{M^2 - a^2}}{2\pi \left[(M + \sqrt{M^2 - a^2})^2 + a^2 \right]} \tag{2.35}$$

showing that the temperatures decrease with increasing mass, implying that large astrophysical BHs are extremely cold.

Bekenstein first proposed that BHs possess an entropy proportional to the area of their event horizon [91, 93, 94], leading to the *Bekenstein–Hawking entropy*

$$S_{\rm BH} = \frac{A_H}{4} \,, \tag{2.36}$$

where A_H is the event horizon area measured in units of the Planck length $\ell_{\rm P}$. This entropy–area relation establishes BHs as the most entropic objects for a given mass.

These results complete the analogy between BH mechanics and standard thermodynamics:

- The surface gravity plays the role of temperature.
- The horizon area plays the role of entropy.
- The ADM mass serves as internal energy.

and culminate in the *first law of BH thermodynamics*

$$\mathrm{d}M = T_{\rm H}\, \mathrm{d}S + \Omega_H\, \mathrm{d}J + \Phi_H\, \mathrm{d}Q \,, \tag{2.37}$$

holding for the most general stationary BH with angular momentum J and electric charge Q, whose conjugate variables are respectively the angular velocity at the horizon Ω_H and the scalar potential at the horizon Φ_H. Notably, for static neutral and non-rotating BHs, one can read the entropy as

$$S = \int \frac{\mathrm{d}M}{T_{\rm H}} \,, \tag{2.38}$$

which, for the Schwarzschild case in Eq. (2.35), yields the Bekenstein-Hawking entropy (2.36) $S = 4\pi M^2$.

In the context of the AdS/CFT correspondence [43, 95–100], the Bekenstein–Hawking area law finds a natural realization in the Ryu–Takayanagi prescription [101, 102]. There, the von Neumann entropy (also called entanglement entropy) of a quantum subsystem in the boundary conformal field theory (CFT) is given by the area of an extremal codimension-two surface in the bulk spacetime,

$$S_{\rm EE} = \frac{\text{Area}(\gamma_A)}{4}\,, \tag{2.39}$$

where γ_A is the minimal surface homologous to the boundary region A. This result establishes a direct link between quantum entanglement and spacetime geometry, providing a microscopic interpretation of the gravitational entropy and reproducing the area law as a manifestation of boundary entanglement.

Several approaches to quantum gravity, however, predict logarithmic corrections to the entropy–area law [103–113]. In a complementary direction, the seminal work by Jacobson [114–116] interpreted the Einstein field equations as an equation of state: by requiring that the Clausius relation $\delta Q = T\,\delta S$ hold for all local Rindler horizons, one can recover the Einstein equations as a thermodynamic consistency condition. This thermodynamics-of-spacetime viewpoint suggests that gravity may emerge from microscopic degrees of freedom whose coarse-grained behaviour is encoded by horizon thermodynamics. The program of quantum phenomenological gravitational dynamics [117–119] extends this insight by investigating how modifications of the entropy–area relation affect the gravitational field equations and the dynamics of spacetime.

Quantum emission implies BHs are not eternally stable: they lose mass via Hawking radiation and eventually evaporate. This process raises deep questions regarding information conservation and the microscopic origin of BH entropy. For extremal configurations ($Q = M$ for RN and $a = M$ for Kerr) the temperatures in Eq. (2.35) vanish implying that the BH does not emit thermal radiation, reaching a state that is known as *remnant*, which is speculated to be the possible endpoint of the evolution of a BH that would preserve information [120–122]. Altogether, Hawking radiation and the entropy–area law establish BHs as legitimate thermodynamic systems, bridging general relativity, quantum theory, and statistical mechanics.

2.3 Spherically symmetric black hole shadow

Let us now examine the dynamics of point-like particles around spherical and static background (2.6). The Lagrangian of a free uncharged particle reads

$$\mathcal{L} = \frac{1}{2} g_{\mu\nu} \frac{\mathrm{d}x^\mu}{\mathrm{d}\lambda}\frac{\mathrm{d}x^\nu}{\mathrm{d}\lambda} \equiv \frac{u}{2}\,, \tag{2.40}$$

where x^μ is the coordinate of the particle, λ is an affine parameter and $u = +1, 0, -1$ respectively for space-like (tachyons), light-like (or null) and time-like (massive) particles and comes from the normalization of the four-velocity $u^\mu = \mathrm{d}x^\mu/\mathrm{d}\lambda$. It is remarkable that the symmetries of the spacetime become also symmetries of the particle's motion. We can see it by writing out the Lagrangian (2.40) and, for convenience, set on the equatorial plane $\theta = \pi/2$

$$\mathcal{L} = -\frac{h(r)}{2}\left(\frac{\mathrm{d}t}{\mathrm{d}\lambda}\right)^2 + \frac{1}{2f(r)}\left(\frac{\mathrm{d}r}{\mathrm{d}\lambda}\right)^2 + \frac{r^2}{2}\left(\frac{\mathrm{d}\varphi}{\mathrm{d}\lambda}\right)^2\,. \tag{2.41}$$

We see that the Lagrangian does not depend on the time coordinate t and azimuthal angle φ, hence their conjugate momenta p_t and p_φ are constants of motion

$$p_t \coloneqq \frac{\partial\mathcal{L}}{\partial(\mathrm{d}t/\mathrm{d}\lambda)} = -h(r)\frac{\mathrm{d}t}{\mathrm{d}\lambda} \equiv E \longrightarrow \frac{\mathrm{d}t}{\mathrm{d}\lambda} = -\frac{E}{h(r)}\,, \tag{2.42a}$$

$$p_\varphi := \frac{\partial \mathcal{L}}{\partial(\mathrm{d}\varphi/\mathrm{d}\lambda)} = r^2\frac{\mathrm{d}\varphi}{\mathrm{d}\lambda} \equiv L \longrightarrow \frac{\mathrm{d}\varphi}{\mathrm{d}\lambda} = \frac{L}{r^2} \,, \tag{2.42b}$$

where we have defined the total energy of the particle E and the angular momentum L as conserved quantities. Using the relations (2.42a) and (2.42b) into the Lagrangian in Eq. (2.40), we obtain

$$-\frac{E^2}{h(r)} + \frac{1}{f(r)}\left(\frac{\mathrm{d}r}{\mathrm{d}\lambda}\right)^2 + \frac{L^2}{r^2} = u \,, \tag{2.43}$$

which can be re-arranged in the form

$$\left(\frac{\mathrm{d}r}{\mathrm{d}\lambda}\right)^2 = \frac{f(r)}{h(r)}\left[E^2 - h(r)\left(\frac{L^2}{r^2} - u\right)\right] \,. \tag{2.44}$$

Dividing both members by (2.42b) for $u = 0$, we have the radial equation of massless particles in the geometry (2.6)

$$\left(\frac{\mathrm{d}r}{\mathrm{d}\varphi}\right)^2 = r^2 f(r)\left(\frac{r^2}{b^2h(r)} - 1\right) \quad \text{with} \quad b := L/E \,, \tag{2.45}$$

where b is the impact parameter. Equation (2.45) can be read as a one-dimensional energy conservation law [123, 124] in the sense $(\mathrm{d}r/\mathrm{d}\varphi)^2 + V_{\rm eff} = 0$, with the effective potential $V_{\rm eff}$ given by the right hand side in (2.45). The particle follows a circular orbit (*i.e.* with $r = r_{\rm ps}$ =const.) for $(r_{\rm ps}, b)$ that satisfy

$$V_{\rm eff} = 0 \quad \text{and} \quad \frac{\mathrm{d}V_{\rm eff}}{\mathrm{d}r} = 0 \qquad \text{such that} \qquad \left.\frac{\mathrm{d}r}{\mathrm{d}\varphi}\right|_{r=r_{\rm ps}} = \left.\frac{\mathrm{d}^2r}{\mathrm{d}\varphi^2}\right|_{r=r_{\rm ps}} = 0 \,, \tag{2.46}$$

It is convenient to re-formulate the problem in terms of the minimal radius distance $r_{\rm min}$ of a massless particle on a general open trajectory [123–125] (see Figure 2.1), such that (2.45) becomes [126]

$$\left(\frac{\mathrm{d}r}{\mathrm{d}\varphi}\right)^2 = r^2 f(r)\left(\frac{U(r_{\rm min})^2}{U(r)^2} - 1\right) \,, \qquad \text{with} \qquad U(r)^2 = \frac{h(r)}{r^2} \,, \tag{2.47}$$

where the new effective potential satisfies $U(r_{\rm min}) = b^{-1}$. Furthermore, the inclination angle α measured by a static observer located at a (large) radial distance $r_{\rm obs}$ is [123, 127–129]

$$\cot\alpha = \frac{1}{\sqrt{r^2 f(r)}}\left.\frac{\mathrm{d}r}{\mathrm{d}\varphi}\right|_{r=r_{\rm obs}} \qquad \text{such that} \qquad \sin^2\alpha = \frac{U(r_{\rm obs})^2}{U(r_{\rm min})^2} \,, \tag{2.48}$$

from which we can obtain the angular aperture of the black hole shadow as an observer-dependent quantity

$$\sin^2\alpha_{\rm sh} = U(r_{\rm obs})^2 b_{\rm sh}^2 \quad \text{with} \quad b_{\rm sh} := U(r_{\rm ps})^{-1} \,. \tag{2.49}$$

Here $b_{\rm sh}$ is usually called the *radius of the black hole shadow* [123] and, as before, $r_{\rm ps}$ is the radius of the photon sphere, which is computed from (2.46). Using the potential in (2.47), the latter condition becomes

$$\left.\frac{\mathrm{d}U^2(r)}{\mathrm{d}r}\right|_{r=r_{\rm ps}} = 0 \implies r_{\rm ps}h'(r_{\rm ps}) = 2h(r_{\rm ps}) \quad . \tag{2.50}$$

In principle, there may be more than one solution to this equation, allowing for the presence of several photon rings, some of which are stable (around which photons oscillate) and some unstable (towards which photons spiral) [130]. However, following [131] and [132], we expect at least one local maximum for the effective potential U outside of the event horizon.

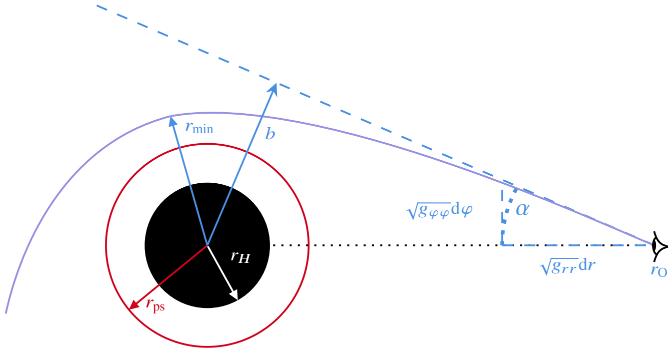

Figure 2.1: Observer-dependent inclination angle α and the minimal radial distance $r_{\min}$ for a photon on an open trajectory around the black hole. The impact parameter b is measured by an observer at the (large) distance $r_{\rm obs}$. The red circle $r_{\rm ps}$ represents the photon ring (*i.e.* a circular orbit for massless particles around the black hole).

2.4 Quasi-Normal Modes

Perturbations of BH spacetimes play a central role in probing their stability and dynamical properties. When a BH is perturbed, the spacetime geometry responds by emitting gravitational radiation that carries information about its intrinsic properties such as mass, charge, and angular momentum and eventually settles back to equilibrium. The intermediate stage of this relaxation process is characterized by a discrete set of damped oscillations known as *quasi-normal modes* (QNMs) [133–138]. These modes are intrinsic to the black hole itself and depend solely on its parameters (mass, charge, angular momentum), being independent of the details of the perturbation.

The analysis of perturbations around a static, spherically symmetric metric can be traced back to the seminal work of Regge and Wheeler [139], who studied the stability of the Schwarzschild geometry under odd-parity (axial) perturbations. Later, Zerilli [140] extended this analysis to even-parity (polar) perturbations, deriving the corresponding effective potential and wave equation.

Consider a generic field perturbation $\Psi(t, r, \theta, \varphi)$ of spin s ($s = 0, 1, 2$ respectively for scalar, electromagnetic and gravitational perturbations) on a static, spherically symmetric background of the form as in Eq. (2.6). After decomposing the perturbation into spherical harmonics and separating variables

$$\Psi(t, r, \theta, \varphi) = \sum_{\ell \geq 0} e^{-i\omega t} \frac{\psi_\ell(r)}{r} {}_sY_\ell^m(\theta, \varphi) \,, \tag{2.51}$$

the linearized response of the BH to such perturbations is governed by a one-dimensional Schrödinger-like equation for the radial component $\psi_\ell(r)$ [136, 138–141]

$$\frac{\mathrm{d}^2\psi_\ell}{\mathrm{d}r_*^2} + \left[\omega^2 - V_{\ell,s}(r)\right] \psi_\ell = 0 \,, \tag{2.52}$$

where r_* is the *tortoise coordinate* defined by $\mathrm{d}r_*/\mathrm{d}r \coloneqq \sqrt{-g_{rr}/g_{tt}} = \sqrt{f(r)/h(r)}$, and $V_{\ell,s}(r)$ is an effective potential determined by the background metric, the multipole moment ℓ and the spin s of the perturbation.

The quasi-normal modes correspond to the solutions of Eq. (2.52) satisfying the boundary conditions of *purely ingoing waves* at the event horizon and *purely outgoing waves* at spatial infinity (or at the cosmological horizon in de Sitter backgrounds):

$$\psi(r_*) \sim \begin{cases} e^{-i\omega r_*} , & r_* \to -\infty \; (r \to r_H) , \\ e^{+i\omega r_*} , & r_* \to +\infty \; (r \to \infty) . \end{cases} \tag{2.53}$$

These boundary conditions quantize the complex frequency spectrum $\omega = \omega_R + i\omega_I$, where ω_R governs the oscillation frequency and $\omega_I < 0$ describes the damping rate due to energy loss through gravitational radiation.

The QNM spectrum encodes the linear response of the spacetime and provides a characteristic *ringdown* signal in gravitational-wave observations [142, 143]. In particular, the detection of ringdown frequencies allows one to test the no-hair theorem by verifying that the observed modes are consistent with those predicted for a Kerr black hole [144]. Moreover, deviations from the general-relativistic spectrum may signal the presence of new physics, such as quantum-gravity corrections, extra dimensions, or modified theories of gravity [145–147].

Analytically, QNMs can be computed using various approximation methods such as the Pöschl-Teller potential [148], the WKB expansion [149–152], continued fractions [137, 153], or numerical integration of the wavelike equations [135, 154].

2.4.1 Eikonal limit

In the semiclassical eikonal limit (namely the limit of large angular momentum $\ell \gg 1$) or high overtones, the spectrum exhibits universal scaling properties closely linked to the structure of the effective potential barrier and, in the eikonal limit, to the properties of unstable null geodesics near the photon sphere [155, 156]. In this limit, the QNM frequency reads

$$\omega_{n\ell} = \Omega\,\ell - i\left(n + \frac{1}{2}\right)|\lambda| , \tag{2.54}$$

where $n \in \mathbb{N}$ is the overtone number, Ω is the orbital frequency of light rays at the photon-sphere radius $r_{\rm ps}$, and λ is the Lyapunov exponent [63].

The eikonal limit establishes a correspondence between the QNMs and the properties of the photon sphere, under the following two criteria [60]: (*i*) the perturbation potential is positive definite (to avoid instabilities), single peaked, and decays to zero at the boundaries; and (*ii*) the perturbation is a test scalar field or other field minimally coupled to gravity. This implies that the eikonal QNMs associated with gravitational perturbations may not, in general, be directly related to the properties of the unstable photon orbit. For this reason, we will restrict our analysis to perturbations of test scalar and electromagnetic fields.

Given a static and spherically symmetric spacetime in Eq. (2.6), the photon dynamics can be described using the effective potential U defined in Eq. (2.47). The radius, orbital frequency [77], and Lyapunov exponent of the photon sphere are then given by [63][3]

$$r_{\rm ps}\, g_{tt}'(r_{\rm ps}) = 2\, g_{tt}(r_{\rm ps}) , \tag{2.55a}$$

$$\Omega^2 = U^2(r_{\rm ps}) = -\frac{g_{tt}(r)}{r^2}\bigg|_{r=r_{\rm ps}} , \tag{2.55b}$$

[3] Note the change of the metric signature with respect to eqs. (35), (37), and (40) reported in Ref. [63].

$$\lambda^2 = -\frac{r_{\rm ps}^2}{2\, g_{rr}(r_{\rm ps})} \frac{\mathrm{d}^2 U^2(r)}{\mathrm{d}r^2}\bigg|_{r=r_{\rm ps}} , \tag{2.55c}$$

respectively. We note that Ω is closely related to the radius of the BH shadow through $b_{\rm sh} := U(r_{\rm ps})^{-1} \equiv \Omega^{-1}$ [123].[4]

Altogether, quasi-normal modes represent the "spectroscopic fingerprint" of black holes, encoding information about their geometry and offering a unique observational window into the strong-field regime of gravity.

[4]In Ref. [63], the authors use a different potential $V_r(r)$ instead of $U^2(r)$.

3 The Effective Metric Description

This chapter is based on and extends the results presented in [45–48], where the Effective Metric Deformation (EMD) framework was first introduced and applied to static, spherically symmetric spacetimes. Building on those foundations, we further develop the formalism by constructing the proper-distance EMD and exploring its mapping to curvature-based schemes such as the Ricci and Kretschmann EMDs. The final sections are devoted to the EMD for charged BHs, including the analysis of the extremal limit and the introduction of a proper-time EMD suited for dynamical observers.

3.1 Definitions and Review

This Section serves the purpose of illustrating what is the Effective Metric Description (EMD) and how it is used to describe (quantum) deformed Schwarzschild black holes.

The staring point is the metric of a spherically symmetric and static black hole of mass M written in terms of the Schwarzschild coordinates (t, r, θ, φ)

$$\mathrm{d}s^2 = -h(r)\mathrm{d}t^2 + \frac{\mathrm{d}r^2}{f(r)} + r^2\mathrm{d}\theta^2 + r^2 \sin^2\theta\, \mathrm{d}\varphi^2 \,, \tag{3.1}$$

where

$$h(r) = 1 - \frac{\Psi}{r} \quad \text{with} \quad f(r) = 1 - \frac{\Phi}{r} \,. \tag{3.2}$$

where Ψ and Φ parametrize deformations of the Schwarzschild encoding corrections due to physical effects beyond GR, either classical or quantum in nature.

In order to describe a black hole, it is assumed that the metric functions $h(r)$ and $f(r)$ possess a simple zero at some finite radius $r_H > 0$, corresponding to the position of the (outer) event horizon. In the following, Eq. (3.1) will be considered only for $r \geq r_H$, where both $h(r)$ and $f(r)$ are taken to be positive definite.

To ensure the regularity of the geometry and its derivatives in the vicinity of the horizon, the metric functions can be expanded in Taylor series around $r = r_H$ as

$$f(r) = \sum_{n\geq 1} \frac{f_H^{(n)}}{n!} (r - r_H)^n, \qquad h(r) = \sum_{n\geq 1} \frac{h_H^{(n)}}{n!} (r - r_H)^n \,. \tag{3.3}$$

These expansions make explicit that the first derivatives $f_H^{(1)}$ and $h_H^{(1)}$ are finite and non-vanishing, thereby guaranteeing a regular and non-degenerate horizon.

Then we require that the geometry is asymptotically flat. Concretely, one assumes that the geometry approaches the Schwarzschild metric (with mass parameter M) for very large distances from the origin

$$\lim_{r\to\infty} \Psi(r) = 2M = \lim_{r\to\infty} \Phi(r) \,. \tag{3.4}$$

Furthermore, in order for coordinate transformations of the undeformed space-time to be also realized in the deformed case, we demand that Ψ and Φ are invariant quantities. This can be achieved by writing them as functions of a physical quantity, for which in [45, 157] the proper distance from the origin was proposed.[1]

An Effective Metric Description is largely determined by identifying the latter with a physical quantity $\mathcal{X}$, which is invariant under reparameterization and which is a monotonic function of the Schwarzschild coordinate r. Hence, we can denote the deformation functions as $\Psi^{(\mathcal{X})}$ and $\Phi^{(\mathcal{X})}$ when they are parametrized in terms of a physical quantity $\mathcal{X}$. [2]

To formalize the discussion, an EMD for describing a (quantum) deformed spherically symmetric and static black hole is characterized by the following set of quantities:

(i) a defining **physical quantity** $\mathcal{X}$. The symbol $\mathcal{X}$ is mostly used to loosely label the EMD, *e.g.* the EMD outlined below is simply called the *distance*-EMD. Furthermore, additional **(normalisation) condition(s)** may be required that supplement (and sharpen) the definition of the physical quantity: these can act as boundary conditions for the self-consistency condition (point *(iii)* below), or are related to the classical limit (in which the metric deformation is switched off). In the example of the distance EMD, this condition is the convention to measure the distance from the horizon of the black hole *i.e.* $\rho(r_H) = 0$ as well as the choice of the sign $\nu = +1$ in (3.14) (which allows for the recovery of the Schwarzschild geometry in the limit $\xi_{2n} \to 0\ \forall n \geq 1$).

(ii) a **set of free parameters** which are used to deform the functions h and f in the metric (3.1). More concretely, one typically refers to the expansion coefficients of $\Psi^{(\mathcal{X})}$ and $\Phi^{(\mathcal{X})}$ close to the horizon (as *e.g.* in (3.7)).

(iii) a **self-consistency equation** which encodes how $\mathcal{X}$ is computed from the metric. This equation usually takes the form of a (non-linear) differential equation (see (3.6) in the case of the distance EMD).

Once the EMD has been defined, physical quantities related to the black hole geometry, can be computed in terms of the free parameters. For example, as we will show in Sec. 3.2.2, the Hawking temperature (cf. Sec. 2.2) can be parametrized as[3]

$$T_H = \frac{1}{4\pi} \left.\frac{\mathrm{d}f}{\mathrm{d}r}\right|_{r=r_H} = \frac{1+\varpi}{8\pi r_H} \,, \tag{3.5}$$

that is indeed only a function of r_H and ϖ (or equivalently $\xi_{0,2}$), which will be defined in the following Section.

[1] One can choose a more general geodesic distance to prove a Taylor theorem for general tensor calculus shown in [158–160]. However, as mentioned in these works, explicit computations become rapidly involved.

[2] The (slightly abusive) notation $\Psi^{(\mathcal{X})}(r)$ and $\Phi^{(\mathcal{X})}(r)$ will be used to signify $\Psi^{(\mathcal{X})}(\mathcal{X}(r))$ and $\Phi^{(\mathcal{X})}(\mathcal{X}(r))$. Furthermore, since the goal is to compare EMDs defined by different physical quantities, various different deformation functions will be introduced and the superscript $(\mathcal{X})$ simply serves as a naming convention.

[3] This expression takes into account that here we only consider a single metric deformation function $h = f$.

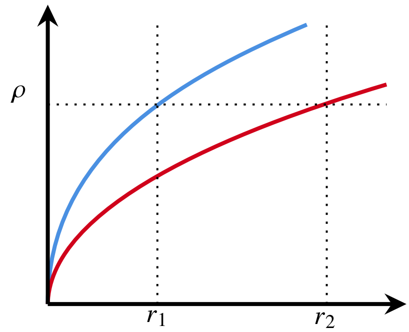

Figure 3.1: Since the proper distance from the horizon ρ can be the only physically and unambiguous quantity that an observer measures, one should relate such observable to the shape of the spacetime. Given two models of deforming the spacetime (Φ_1 and Φ_2), we have that in the Schwarzschild coordinates, in order to obtain the same physical distance ρ, one has to evaluate each model in each own corresponding value of r (namely r_1 and r_2). The advantage of parameterizing the deformations in the proper distance (such as in this case), is that the ambiguity about the position with respect to the black hole, at which one performs experiments and measurements, is lifted and the coefficients that appear in the expansions can be readily read off from the observational point of view.

The motivation for introducing the Effective Metric Deformation lies in the need for a coordinate-independent and physically transparent way to parametrize deviations from classical spacetimes. In conventional approaches, metric deformations are expressed as functions of coordinate variables such as the Schwarzschild radius r, which, although geometrically convenient, lack diffeomorphism-invariant meaning. The functional form $\Phi(r)$ is not preserved under coordinate transformations, while only $\Phi(\mathcal{X})$, with $\mathcal{X}$ an invariant scalar constructed from the spacetime, is truly physical. This issue becomes critical when defining the notion of *smallness* of a deformation, as what appears small in one coordinate system may not be so in another. The EMD framework addresses this by parametrizing metric deformations directly in terms of observable and invariant quantities, ensuring that both the expansion coefficients and the definition of proximity to the classical theory are physically meaningful and coordinate-independent.

In spherical symmetry, the areal radius r already provides an invariant definition, related to the quadratic Casimir of the rotation group and to the Misner-Sharp mass, making it a useful testing ground for the formalism. However, from an operational point of view, observables such as the proper distance from the horizon offer a more direct and measurable way to quantify deviations, free from coordinate ambiguities. The EMD thus provides a general and flexible framework in which quantum or phenomenological corrections to black hole geometries can be encoded in terms of physically interpretable, observer-independent quantities, offering a robust bridge between theoretical parametrizations and measurable effects, which is a property sought after by other QG approaches [161].

3.2 The proper distance EMD

To explain the framework in more detail, as in the references [45, 46], the physical quantity is chosen to be the proper distance ρ measured from the horizon of the black hole, *i.e.* $\Phi^{(\rho)}(r)$. In writing $f(r)$ in (3.1), we implicitly understand ρ to be a (monotonic) function of the Schwarzschild coordinate r, which is fixed through the first order differential equation

$$\frac{\mathrm{d}\rho}{\mathrm{d}r} = \frac{1}{\sqrt{f}} = \left(1 - \frac{\Phi^{(\rho)}(\rho)}{r}\right)^{-1/2} \quad \text{with} \quad \rho(r_H) = 0\,. \tag{3.6}$$

This differential equation is non-linear, since the right hand side through $\Phi^{(\rho)}$ is also a function of the distance ρ. The surface gravity and the Ricci scalar are fundamental quantities that must be well-defined at and near the horizon (cf. Sec. 2.2), while here we give the definition of the Ricci scalar as a geometric quantity, which directly follows from Eq. (3.1): it is a scalar quantity which appears in the equation of motion of the gravitational field (*i.e.* the Einstein equations). Therefore, its regularity (notably at the horizon) in the deformed metric ensures that in the deformed case no additional singularities arise beyond the classical ones. We mainly focus on the finiteness of the Ricci scalar defined in eq (2.8) at the horizon but, in some examples, we shall also examine the behavior of the Kretschmann scalar in eq. (2.9).

In [46] two equivalent approaches were proposed to find regularity conditions of the curvature scalars at the horizon and solve Eq. (3.6) in a self-consistent way. The first method uses an exponential definition of the deformation function and used the Taylor expansions in Eqs.(3.3) to find regularity of the first and second derivatives at the horizon. In this thesis, the second approach, which is based on self-consist methods, will be discussed, in light of the further applications of such parametrization. To solve Eq. (3.6) in a self-consistent fashion as a series expansion close to the horizon, the following series expansions are defined

$$\Psi^{(\rho)}(\rho) = r_H + 2M\sum_{n=0}^{\infty}\theta_n\left(\frac{\rho}{2M}\right)^n \quad \text{and} \quad \Phi^{(\rho)}(\rho) = r_H + 2M\sum_{n=0}^{\infty}\xi_n\left(\frac{\rho}{2M}\right)^n\,, \tag{3.7}$$

such that the deformation of the classical Schwarzschild geometry is fully encoded in r_H and the real dimensionless parameters $\{\theta_n, \xi_n\}_{n\in\mathbb{N}_0}$. The series in (3.7) is assumed to have a non-vanishing radius of convergence (see [158–160] where a Taylor theorem for more general tensor calculus, based on (various) geodesic distances, was developed).

3.2.1 Solving the distance function

Series expansion of the radial coordinate

Using the expansion (3.7) allows to express the distance ρ as a function of the Schwarzschild coordinate r and vice-versa

$$r(\rho) = r_H + 2M\sum_{n=1}^{\infty}a_n\left(\frac{\rho}{2M}\right)^n \quad \text{and} \quad \rho(r) = 2M\sum_{n=1}^{\infty}b_n\left(\frac{r-r_H}{2M}\right)^{n/2}\,. \tag{3.8}$$

We can solve for the coefficients a_n in terms of the ξ_n by inserting the series on the left of Eq. (3.8) into the differential equation (3.6), that we write in the form

$$r(\rho)\left[1-\left(\frac{\mathrm{d}r}{\mathrm{d}\rho}\right)^2\right]=\Phi^{(\rho)}(\rho)\ . \tag{3.9}$$

We can expand the square of the series using the Cauchy product of two series as shown in the Appendix A.1.2, then use again the Cauchy product to expand the left-hand side in series of ρ while the right-hand side is expanded as in Eq. (3.7). Thus, we have

$$\begin{aligned} r_H\,(1-a_1)^2+\sum_{p=1}^{\infty}\Bigg[&2M(1-a_1^2)a_p-r_H\sum_{m=1}^{p+1}m(p-m+2)a_m a_{p-m+2}+\\ &-2M\sum_{n=1}^{p-1}\sum_{m=1}^{n+1}m(n-m+2)a_{p-n}a_m a_{n-m+2}\Bigg]\left(\frac{\rho}{2M}\right)^p=r_H+2M\sum_{p=1}^{\infty}\xi_p\left(\frac{\rho}{2M}\right)^p\ . \end{aligned} \tag{3.10}$$

Identifying the coefficients order by order for $p\in\{0,1,2\}$ leads to

$$r_H=r_H(1-a_1^2)\ , \tag{3.11a}$$

$$\xi_1=(1-a_1^2)a_1-\frac{2r_H}{M}a_1a_2\ , \tag{3.11b}$$

$$\xi_2=(1-a_1^2)a_2-\frac{r_H}{M}(3a_1a_3+2a_2^2)-4a_1^2a_2\ . \tag{3.11c}$$

The first of these equations requires $a_1=0$, which implies that $\xi_1=0$. The last equation becomes

$$\xi_2=\left(1-\frac{2r_H}{M}a_2\right)a_2\ , \tag{3.12}$$

which is solved for

$$a_2=\frac{M(1+\nu\,\varpi)}{4r_H}\quad\text{with}\quad\varpi:=\sqrt{1-\frac{8r_H}{M}\xi_2}\quad\text{and}\quad\nu:=\pm1\ . \tag{3.13}$$

The choice of the sign parameter $\nu=+1$ picks the solution that is smoothly connected to the Schwarzschild case when turning off the deformation parameter, *i.e.* when $\xi_2\to0$. Moreover, the requirement for ϖ to be real imposes an upper bound on $\xi_2\le M/8r_H$. Equating the remaining powers of $(\rho/2M)^p$, for $p\ge3$, Eq. (3.10) becomes a recursive equation, which allows to express a_p in terms of ξ_p and the a_q with $q<p$:

$$a_p=\frac{\xi_p+r_H/2M\ \sum_{n=3}^{p-1}(p-n+2)\,n\,a_n\,a_{p-n+2}+\sum_{n=2}^{p-2}\sum_{m=2}^{n}(n-m+2)\,m\,a_{p-n}\,a_m\,a_{n-m+2}}{1-2p\,r_H\,a_2/M}\ . \tag{3.14}$$

The coefficients b_n in Eq. (3.8) follow from inversion of the series (3.8) [4]

$$b_1=\frac{1}{a_2^{1/2}}\ ,\qquad b_2=-\frac{a_3}{2a_2^2}\ ,\qquad b_n=\frac{(-1)^{n-1}}{2^{n-1}\,n!\,a_2^{n/2}}\det(\mathcal{M}_n)\qquad\forall n\ge3\ . \tag{3.15}$$

[4]Notice that for $\xi_2\le\frac{M}{8r_H}$, the coefficient $a_2\ne0$.

where $\mathcal{M}_n$ is a $(n-1)\times(n-1)$ matrix explicitly written as

$$\mathcal{M}_n = \begin{pmatrix}
n\frac{a_3}{a_2} & 1 & 0 & 0 & 0 & 0 & 0 & 0 & \cdots & 0 \\
4n\frac{a_4}{a_2} & (n+2)\frac{a_3}{a_2} & 2 & 0 & 0 & 0 & 0 & 0 & \cdots & 0 \\
12n\frac{a_5}{a_2} & (4n+4)\frac{a_4}{a_2} & (n+4)\frac{a_3}{a_2} & 3 & 0 & 0 & 0 & 0 & \cdots & 0 \\
32n\frac{a_6}{a_2} & (12n+8)\frac{a_5}{a_2} & (4n+8)\frac{a_4}{a_2} & (n+6)\frac{a_3}{a_2} & 4 & 0 & 0 & 0 & \cdots & 0 \\
80n\frac{a_7}{a_2} & (32n+16)\frac{a_6}{a_2} & (12n+16)\frac{a_5}{a_2} & (4n+12)\frac{a_4}{a_2} & (n+8)\frac{a_3}{a_2} & 5 & 0 & 0 & \cdots & 0 \\
\vdots & \vdots & \vdots & \vdots & \vdots & \ddots & \ddots & \cdots & \cdots & \vdots \\
2^{k-1}kn\frac{a_{k+2}}{a_2} & 2^{k-2}((k-1)n+2)\frac{a_{k+1}}{a_2} & 2^{k-3}((k-2)n+4)\frac{a_k}{a_2} & \cdots & \cdots & \cdots & (n+2^{k-1})\frac{a_3}{a_2} & k & \cdots & 0 \\
\vdots & \vdots & \vdots & \vdots & \vdots & \vdots & \vdots & \ddots & \ddots & \vdots \\
2^{n-3}n(n-2)\frac{a_n}{a_2} & \vdots & \vdots & \vdots & \vdots & \vdots & \vdots & \ddots & \ddots & n-2 \\
2^{n-2}n(n-1)\frac{a_{n+1}}{a_2} & 2^{n-3}\big(n(n-2)+2\big)\frac{a_n}{a_2} & \cdots & \cdots & \cdots & \cdots & \cdots & \cdots & \cdots & (n+2^{n-2})\frac{a_3}{a_2}
\end{pmatrix} . \tag{3.16}$$

Concretely, we find for the first few coefficients with $n \geq 3$

$$b_3 = \frac{5a_3^2 - 4a_2a_4}{8a_2^{7/2}} , \qquad b_4 = \frac{3a_2a_3a_4 - 2a_3^3 - a_2^2a_5}{2a_2^5} ,$$
$$b_5 = \frac{231a_3^4 - 504a_2a_3^2a_4 + 224a_2^2a_3a_5 + 112a_2^2a_4^2 - 64a_2^3a_6}{129a_2^{13/2}} . \tag{3.17}$$

Remarkably, expanding the above expressions, one finds that

$$b_{2n-1} = \frac{2^{2n-1}r_H^{n+1}\sqrt{\frac{4M(1+\varpi)}{r_H}}\,\xi_{2n}}{M^{n+1}(1+\varpi)^{n+1}((n-1)+n\varpi)} + \widetilde{b}_{2n-1}(\xi_2,\ldots,\xi_{2n-2}) \qquad \forall n \geq 2 , \tag{3.18}$$

where notably $\widetilde{b}_{2n-1}$ is independent of ξ_{2k} for $k > n$. For completeness, in Appendix A.2 we analyze the impact of $\xi_1 \neq 0$.

3.2.2 Metric functions and curvature scalars

In the previous Subsection, the differential equation (3.9) was solved assuming an integer series expansion of the radial coordinate r as a function of the distance (from the event horizon) ρ. In this Subsection, this result is used to compute the Ricci scalar.

Using (3.7) and (3.8), as well as the following expansion (see App. A.1.1)

$$\frac{1}{r(\rho)} = \sum_{n=0}^{\infty} \mathfrak{p}_n \left(\frac{\rho}{2M}\right)^n , \quad \text{with} \quad \begin{array}{l} \mathfrak{p}_0 = \frac{1}{r_H}, \quad \mathfrak{p}_1 = -\frac{2Ma_1}{r_H^2}, \quad \mathfrak{p}_2 = \frac{2M\left(2Ma_1^2 - a_2r_H\right)}{r_H^3} , \\ \mathfrak{p}_p = -\frac{2M\,a_p}{r_H^2} - \frac{2M}{r_H}\sum_{n=1}^{p-1}\mathfrak{p}_n a_{p-n} , \quad \forall p \geq 3 , \end{array} \tag{3.19}$$

(with $a_0 \equiv r_H$) we can express the metric functions as power series in ρ

$$f = 1 - \sum_{k=0}^{\infty}\left(\frac{\rho}{2M}\right)^k \sum_{n=0}^{k} \mathfrak{p}_n\,\xi_{k-n} , \quad \text{and} \quad h = 1 - \sum_{k=0}^{\infty}\left(\frac{\rho}{2M}\right)^k \sum_{n=0}^{k} \mathfrak{p}_n\,\theta_{k-n} , \quad \forall \rho \geq 0 , \tag{3.20}$$

which reads explicitly to leading orders

$$f = \frac{a_2 - \xi_2}{2Mr_H}\rho^2 + \frac{a_3 - \xi_3}{4M^2r_H}\rho^3 + O(\rho^4) , \tag{3.21a}$$

$$h = -\frac{\theta_1}{r_H}\,\rho + \frac{a_2-\theta_2}{2Mr_H}\,\rho^2 + \frac{(a_3-\theta_3)r_H + a_2\theta_1}{4M^2r_H^2}\,\rho^3 + \mathcal{O}(\rho^4)\,. \tag{3.21b}$$

We can equivalently write these as expansions in $(r-r_H)$

$$f = \frac{a_2-\xi_2}{a_2\,r_H}\,(r-r_H) + \frac{a_3\xi_2 - a_2\xi_3}{(2M)^{1/2}(a_2)^{5/2}r_H}\,(r-r_H)^{3/2} + \mathcal{O}((r-r_H)^2)\,, \tag{3.22a}$$

$$h = -\frac{\theta_1}{r_H}\sqrt{\frac{2M}{a_2}}\,(r-r_H)^{1/2} + \frac{2a_2^2 + a_3\theta_1 - 2a_2\theta_2}{2a_2^2\,r_H}\,(r-r_H) + \mathcal{O}((r-r_H)^{3/2})\,, \tag{3.22b}$$

which shows certain similarities with the Taylor series expansions in Eq. (3.3), but also some differences: on the one hand, comparing the expansion for the function f in Eq. (3.22a) with the first in Eq. (3.3), we can read off the first derivative at the horizon in terms of the parameters

$$\frac{a_2-\xi_2}{a_2\,r_H} = 4\,a_2 = \frac{M(1+\varpi)}{r_H} = 2M\,f_H^{(1)}\,. \tag{3.23}$$

On the other hand, (3.22a) contains a term of order $(r-r_H)^{3/2}$ (and (3.21a) a term of order ρ^3), which is absent in (3.3). Indeed (3.22a) is not an integer series expansion and therefore more general than (3.3). Similarly, (since the condition $\theta_1 = 0$ is not imposed), the function h even starts from a term $(r-r_H)^{1/2}$ in (3.22b) (order ρ in (3.21b)), which is absent in the second equation in Eq. (3.3). The series from Eqs. (3.7) and (3.20) are therefore more general than the Taylor expansion in $r-r_H$ in Eq. (3.3). However, it is notable that for generic values of ξ_3 and θ_1 one has

$$\lim_{r\to r_H} f^{(2)}(r) \to \infty\,, \qquad \text{and} \qquad \lim_{r\to r_H} h^{(1)}(r) \to \infty\,. \tag{3.24}$$

Indeed, the finiteness of the derivatives of the metric functions at the horizon was not the initial assumption and in the next Subsubsection the absence of a physical curvature singularity instead as a more general condition shall be imposed. Before doing so, however, it is stressed that the conditions for the absence of the singularities (3.24) from (3.22a) and (3.22b) can be deduced in a straightforward manner:

$$\theta_1 = 0\,, \qquad \text{and} \qquad a_3\xi_2 = a_2\xi_3\,, \qquad \text{and} \qquad a_3\theta_2 = a_2\theta_3\,. \tag{3.25}$$

Using Eq. (3.14), the second of these relations implies

$$\left(\frac{M(1+\varpi)}{4r_H} + \frac{2\xi_2}{1+3\varpi}\right)\xi_3 = 0\,, \tag{3.26}$$

which has as only solution $\xi_3 = 0$, which further implies $a_3 = 0$ and so, from the third relation in (3.25), yields $\theta_3 = 0$. Notice that the conditions

$$\xi_1 = \xi_3 = \theta_1 = \theta_3 = 0\,, \tag{3.27}$$

which guarantee existence of the first and second derivative of f and h for $r = r_H$ (which are necessary for the expansions in Eq. (3.3)). The upper bound $\xi_2 \leq M/8r_H$ was already obtained previously to guarantee reality of ϖ in Eq. (3.13).

Ricci scalar and Hawking temperature

Next, the Ricci scalar is considered, however, for simplicity, we shall work out its series expansions only to leading order. Moreover, we shall start out by only assuming $\xi_1 = 0$ (which is required for the consistent expansion (3.22)), but the remaining conditions in (3.27) shall not be assumed. Let us notably first consider the case of $\theta_1 \neq 0$. Inserting (3.22a) and (3.22b) into the Ricci scalar in Eq. (2.8), we obtain the following series expansion (for $r \geq r_H$)

$$R = \frac{a_2 - \xi_2}{8a_2 r_H}(r - r_H)^{-1} + \frac{(2a_2^2 + a_3\theta_1 - 2a_2\theta_2)(a_2 - \xi_2)}{8\sqrt{2M}a_2^{5/2}\theta_1 r_H}(r - r_H)^{-1/2} + O((r - r_H)^0)\,. \tag{3.28}$$

Using (3.14) the coefficient of the leading term becomes

$$\frac{a_2 - \xi_2}{8a_2 r_H} = \frac{\sqrt{1 - 8r_H\xi_2/M}}{8r_H}\,, \tag{3.29}$$

which is non-vanishing for all values of $\xi_2 \leq M/8r_H$ and therefore signals a curvature singularity at the event horizon. To avoid the latter, we now impose $\theta_1 = 0$, which also leads to a well defined derivative $h_H^{(1)}$:

$$h_H^{(1)} = \frac{a_2 - \theta_2}{a_2 r_H}\,, \tag{3.30}$$

Moreover, the condition $\theta_1 = 0$ also changes the series expansion in (3.28), which now becomes

$$R = \frac{\sqrt{2}\sqrt{r_H(1+\varpi)}\,((1+3\varpi)\theta_3 + 2\xi_3)}{M^4(1+3\varpi)(1+\varpi - 4r_H\theta_2/M)}(r - r_H)^{-1/2} + O((r - r_H)^0)\,. \tag{3.31}$$

We have furthermore verified that the singularity of R at $r = r_H$ cannot be removed if $1 + \varpi - 4r_H\theta_2/M = 0$ and we, therefore, require $\theta_2 \neq a_2$.[5] In this case, the necessary condition for regularity of R at the horizon is $(1 + 3\varpi)\theta_3 + 2\xi_3 = 0$. We have verified that under the same condition also the Kretschmann scalar is finite at the horizon. To summarize, the consistency conditions for the approach outlined in Section 3.2.1, the conditions for the absence of a singularity of the Ricci scalar, and the bounds for positive metric functions f and h for $r > r_H$ are therefore

$$\xi_1 = 0\,, \qquad \theta_1 = 0\,, \qquad \xi_3 = -\frac{1}{2}(1+3\varpi)\,\theta_3\,, \qquad \xi_2 \leq \frac{M}{8r_H}\,, \qquad \theta_2 < \frac{M(1+\varpi)}{4r_H}\,. \tag{3.32}$$

We further remark that the series coefficients (3.14) and (3.15) along with the expansions (3.20) allow to compute the (finite) value of R at the horizon. While the general form is rather complicated, here we only give the expression in the particular case $f = h$ (*i.e.* $\xi_n = \theta_n\ \forall n \geq 1$) with $\xi_1 = \xi_3 = 0$

$$\begin{aligned} R\Big|_{r=r_H} &= \frac{(1-\varpi^2)(2Ma_2^2 - r_H\,a_4)}{8r_H^3 a_2^3} + \frac{\xi_4}{Mr_H a_2^2} = \\ &= \frac{(1-\varpi)(33\varpi^4 + 14\varpi^3 + 2\varpi - 1)}{16r_H^2\varpi^3(1+2\varpi)} + \frac{24r_H\,\xi_4}{M^3(1+\varpi)(1+2\varpi)}\,. \end{aligned} \tag{3.33}$$

[5] This condition is compatible with $\theta_2 < \frac{M(1+\varpi)}{4r_H}$ which guarantees that $h_H^{(1)} > 0$ in (3.30). The latter is necessary such that $h(r) > 0$ for $r > r_H$ (with a simple zero at $r = r_H$).

which we shall use in the examples in Chapter 4.

Before closing this Section, we also provide the expression for the Hawking temperature

$$T_{\rm H} = \frac{\sqrt{f_H^{(1)} h_H^{(1)}}}{4\pi} = \frac{\sqrt{1+\varpi - 8r_H\theta_2/M}}{4\sqrt{2}\,\pi\, r_H}\,. \tag{3.34}$$

The upper bound on θ_2 in (3.32) guarantees that $T_{\rm H} > 0$. Indeed, $T_{\rm H} = 0$ would require $f_H^{(1)} = 0$ and/or $h_H^{(1)} = 0$, which translate into $a_2 = \xi_2$ and $a_2 = \theta_2$ respectively. The former has no real solution, while the latter leads to a singularity of the Ricci scalar at the horizon. We remark, however, that black hole solutions with $T_{\rm H} = 0$ are possible upon choosing the solution with $\nu = -1$ giving $a_2 = \frac{M(1-\varpi)}{4r_H}$ in Eq. (3.13).

3.2.3 Regular higher order derivatives

In the previous subsections we have derived the conditions (3.32) by assuming that the first and second derivatives of the metric functions f and h are finite at the horizon r_H. In this subsection, we explore further conditions that stem from assuming that also higher derivatives (*i.e.* beyond the second) are finite. For simplicity, we shall focus on the function f, while the same considerations also apply to h. Concretely, let $N \in \mathbb{N}$ and let us assume that all derivatives $f_H^{(k)}$ for $k \in \{1, \dots, N\}$ at $r = r_H$ are finite. This allows us to go beyond the second order in Eq. (3.3) and write

$$f(z) = \sum_{k=1}^{N} \frac{f_H^{(k)}}{k!}(r-r_H)^k + O((r-r_H)^{n+1})\,, \qquad \text{with} \qquad f_H^{(k)} := \left.\frac{\mathrm{d}^k f}{\mathrm{d}r^k}\right|_{z=r_H}\,. \tag{3.35}$$

Distance function

We can truncate the series for the proper distance ρ in series of $r - r_H$ in Eq. (3.8) at order N

$$\rho = \sum_{k=1}^{2N-1} b_k\,(r-r_H)^{k/2} + O\left((r-r_H)^N\right)\,, \tag{3.36}$$

Note that the coefficients b_k of this series are re-scaled by absorbing some powers of $2M$ and they can be found as the solutions of the differential equation (3.6) up to order N, which we re-write in the form

$$\left(\frac{\mathrm{d}r}{\mathrm{d}\rho}\right)^2 = \frac{1}{f(r)}\,. \tag{3.37}$$

The right-hand side of this equation has a simple pole at $r = r_H$ and we can write the Laurent series expansion

$$\frac{1}{f(r)} = \sum_{m=-1}^{N-2} \ell_m\,(r-r_H)^m + O((r-r_H)^{N-1}) \quad \text{with} \quad \ell_m \in \mathbb{R}\,. \tag{3.38}$$

Multiplying both sides of this equation by $(r - r_H)$ and taking the limit $r \to r_H$, we find for the leading coefficient $\ell_{-1} = 1/f_H^{(1)}$. To extract the remaining coefficients, we consider the relation

$$f(r)\,\frac{\mathrm{d}}{\mathrm{d}r}\frac{1}{f(r)} = -\frac{1}{f(r)}\,\frac{\mathrm{d}f}{\mathrm{d}r}\,, \tag{3.39}$$

and expand both sides in powers of $(r - r_H)$. Comparing order by order (see Appendix A.1) we then find

$$\ell_0 = -\frac{\ell_{-1} f_H^{(2)}}{2 f_H^{(1)}} = -\frac{f_H^{(2)}}{2(f_H^{(1)})^2} \,,$$
$$\ell_p = \frac{-1}{(p+1) f_H^{(1)}} \left[\frac{(p+1)\ell_{-1}\, f_H^{(p+2)}}{(p+2)!} + \sum_{k=1}^{p-1} \frac{k \ell_k f_H^{(p-k+1)}}{(p-k+1)!} + \sum_{k=2}^{p+1} \frac{\ell_{p-k+1} f_H^{(k)}}{(k-1)!} \right] , \quad 1 \le p \le N-2 \,, \tag{3.40}$$

which fixes the coefficients ℓ_p iteratively (in terms of the $f_H^{(n)}$). Inserting (3.38) into (3.37), we find the following recursive structure for the coefficients b_p

$$b_1 = 2\sqrt{\ell_{-1}} = \frac{2}{\sqrt{f_H^{(1)}}} \,, \qquad\qquad b_2 = 0 \,,$$
$$b_p = \begin{cases} \frac{2}{(2s+3)b_1} \left[\ell_p - \sum_{n=2}^{2s+2} \frac{n(2s-n+4)}{4}\, b_n\, b_{2s-n+4} \right] & \text{if} \quad p = 2s+3 \in \mathbb{N}_{\text{odd}} \,, \\ -\frac{1}{(s+1)b_1} \sum_{n=2}^{2s+1} \frac{n(2s-n+3)}{4} b_n b_{2s-n+3} & \text{if} \quad p = 2s+2 \in \mathbb{N}_{\text{odd}} \,, \end{cases} \quad 3 \le p \le 2N-1 \,, \tag{3.41}$$

which allows to fix them iteratively in terms of the $f_H^{(n)}$. Since $b_2 = 0$, the recursive structure in (3.41) implies that $b_{2s} = 0$ for $s \in \{1, \ldots, N-2\}$. For the odd coefficients, we find for the first few instances (for sufficiently large N)

$$b_1 = \frac{2}{(f_H^{(1)})^{1/2}} \,, \qquad b_3 = -\frac{f_H^{(2)}}{6(f_H^{(1)})^{3/2}} \,, \qquad b_5 = \frac{9(f_H^{(2)})^2 - 8 f_H^{(1)} f_H^{(3)}}{240 (f_H^{(1)})^{5/2}} \,. \tag{3.42}$$

These results are indeed compatible with the expressions in Eqs. (3.17).

Conditions for the regularity of higher derivatives $f^{(n)}$

The results of the previous subsection can be used to derive necessary conditions for the function $\Phi^{(\rho)}$ such that the first N derivatives of the function f (with respect to r) are finite, which is required for (3.35). Assuming an expansion of the latter of the form (3.7) (rescaling the coefficients $\xi_n \mapsto (2M)^{n-1}\xi_n$ and $\xi_0 \equiv r_H$), we have with (3.36)

$$f(r) = 1 - \frac{1}{r} \sum_{n=0}^{2N} \xi_n \left(\sum_{k=1}^{2N-1} b_k \,(r - r_H)^{k/2} \right)^n + \mathcal{O}\left((r - r_H)^N \right) \,, \tag{3.43}$$

which is only a function of r. Due to the fact that this expression contains half-integer powers of $(r - r_H)$, derivatives of f can contain negative powers unless certain conditions for the coefficients ξ_n are satisfied. To understand these conditions, we first re-write the summation in eq. (3.43), taking into account that $b_{2s} = 0$ for $s \in \{1, \ldots, N-2\}$

$$f(r) = 1 - \frac{1}{r} \sum_{m=0}^{N} \xi_{2m} (r - r_H)^m \left(\sum_{k=0}^{N-1} b_{2k+1} \,(r - r_H)^k \right)^{2m}$$

$$-\frac{1}{r}\sum_{m=1}^{N}\xi_{2m-1}\left(\sum_{k=0}^{N-1}b_{2k-1}\left(r-r_H\right)^{k+1/2}\right)^{2m-1}+\mathcal{O}\left(\left(r-r_H\right)^N\right)\,. \tag{3.44}$$

Re-writing the above result by expressing the Cauchy product with the expansion of $1/r$ in power series in $r-r_H$

$$\frac{1}{r}=\frac{1}{r_H}\sum_{n=0}^{N}\frac{(-1)^n}{r_H^n}\left(r-r_H\right)^n+\mathcal{O}\left(\left(r-r_H\right)^{N+1}\right)\,, \tag{3.45}$$

it is clear that the terms in the first line of (3.44) contain no half-integer powers of $r-r_H$ and thus cannot contribute to singularities of derivatives of f at $r=r_H$. The terms in the second line of (3.44), however, contain terms that lead to negative powers of $r-r_H$ for derivatives of f. The conditions to eliminate these singular terms for all $f_H^{(k)}$ for $k\in\{1,\ldots,N\}$ are therefore

$$\xi_{2n-1}=0 \qquad \forall n\in\{1,\ldots,N\}\,. \tag{3.46}$$

To see this, let $s\in\{1,\ldots,N\}$ and assume that $\xi_{2s-1}\neq 0$, while $\xi_{2m-1}=0\;\forall m\in\{1,\ldots,s-1\}$. In this case, $f_H^{(s)}$ has a singularity of the form $(r-r_H)^{-1/2}$

$$\begin{aligned}\frac{\mathrm{d}^s}{\mathrm{d}r^s}f(r)&=-\frac{\xi_{2s-1}}{r_H}\,b_1^{2s-1}\,\frac{\mathrm{d}^s}{\mathrm{d}r^s}(r-r_H)^{s-1/2}+\mathcal{O}((r-r_H)^0)\\&=-\frac{(2s-1)!!}{2^s r_H}\,\xi_{2s-1}\,b_1^{2s-1}\,(r-r_H)^{-1/2}+\mathcal{O}((r-r_H)^0)\,.\end{aligned} \tag{3.47}$$

Absence of this singular contribution therefore requires $\xi_{2s-1}=0$. Generalizing the procedure for $N\to\infty$, similar conclusions can be drawn for the function $\Psi^{(\rho)}$ in h, which read

$$\theta_{2n+1}=0 \quad \text{with} \quad \forall n\in\mathbb{N}_0\,. \tag{3.48}$$

Using these conditions into the recursive relation in Eq. (3.14) and repeat the procedure for Eq. (3.15), we have that

$$a_{2n+1}=0=b_{2n} \quad \text{with} \quad n\in\mathbb{N}_0\,. \tag{3.49}$$

3.2.4 Conditions for regularity at inner horizons

The sufficient conditions summarized in Eq. (3.32) at the end of Section 3.2.2 for regularity of the Ricci tensor at r_H, have been derived assuming that the latter is the position of the outer horizon: notably, we have assumed in various instances that $f(r)>0$ for $r>r_H$. Generalized Schwarzschild BHs, however, may have further horizons, (for example, the BHs with regularized cores [24, 26, 32, 157, 162]) which are characterized by a vanishing of the function $f(r)$ in (3.1), such that the derivative of the distance (3.6) diverges. The latter can (in the same way as discussed in Section 3.2.2) lead to curvature singularities that are physically not acceptable. Assuming that the metric functions h and f are of the form

$$h=1-\frac{\Psi^{(d)}}{r} \quad \text{and} \quad f=1-\frac{\Phi^{(d)}}{r}\,, \tag{3.50}$$

where the full proper distance d is defined as

$$\frac{\mathrm{d}d}{\mathrm{d}r}:=\frac{1}{\sqrt{|f(r)|}}\,, \tag{3.51}$$

and the presence of an inner horizon, therefore, puts further conditions on the functions Φ and Ψ. We can obtain these conditions by straightforwardly generalizing the discussion of Section 3.2.2. Here we shall briefly sketch them, assuming a black hole with $f = h$ and two (simple) horizons at $r_{H,\pm}$ (with $r_{H,+} > r_{H,-}$).[6] At $r = r_{H,-}$, one can introduce the series expansion analogous to Eq. (3.7) as

$$\Phi^{(\zeta)} = r_{H,-} + 2M \sum_{n=0} \overline{\xi}_n \left(\frac{\zeta}{2M}\right)^n , \tag{3.52}$$

where ζ is the the proper distance from the inner event horizon $r_{H,-}$. The solution of the series expansion of $\zeta(r)$ (or equivalently of $r(\zeta)$) in power series of $r - r_{H,-}$ from Eq. (3.51), leads to the condition $\overline{\xi}_1 = 0$ which makes the first derivative of f regular at $r_{H,-}$. Investigating the regularity of the second derivative through the Ricci scalar, one finds that $\overline{\xi}_3 = 0$, in complete analogy with the conditions summarized in Eqs. (3.32) for the external horizon.

3.3 EMD redefinitions

Before discussing EMDs based on different physical quantities (that is curvature scalars rather than the physical distance), we shall first consider EMD redefinitions, in which the physical quantity $\mathcal{X}$ is replaced by simple functions of it: indeed, consider the starting point

$$\Phi^{(\mathcal{X})}(\mathcal{X}) = \sum_{n=0}^{\infty} x_n\, \mathcal{X}^n \qquad \text{with} \qquad x_n \in \mathbb{R} \;\; \forall n \geq 0 , \tag{3.53}$$

which we assume to have finite radius of convergence $\mathcal{X}_c$, and replace $\mathcal{X}$ by a continuous, monotonic function of $\mathcal{X}$, which we denote $\sigma : [0, \mathcal{X}_c] \longrightarrow \mathbb{R}$. Then we define $\widetilde{\mathcal{X}} = \sigma(\mathcal{X})$, along with the deformation function

$$\Phi^{(\widetilde{\mathcal{X}})}(\widetilde{\mathcal{X}}) = \sum_{n=0}^{\infty} \widetilde{x}_n\, \widetilde{\mathcal{X}}^n \qquad \text{with} \qquad \widetilde{x}_n \in \mathbb{R} \;\; \forall n \geq 0 . \tag{3.54}$$

A very simple example of this idea was already used in [50], where a physical distance shifted by a constant was considered, *i.e.* $\widetilde{\mathcal{X}} = \sigma(\mathcal{X}) = \mathcal{X} + c$ for $c \in \mathbb{R}$. In this case, the two sets of coefficients $\{x_n\}_{n\in\mathbb{N}_0}$ and $\{\widetilde{x}_n\}_{n\in\mathbb{N}_0}$ are related

$$x_n = \sum_{\ell=n}^{\infty} \frac{\widetilde{x}_\ell\, c^{\ell-n}}{(\ell-n)!} , \qquad \widetilde{x}_n = \sum_{\ell=n}^{\infty} \frac{x_\ell\, (-c)^{\ell-n}}{(\ell-n)!} , \qquad \forall n \in \mathbb{N} . \tag{3.55}$$

Notice that in this case, any single x_n depends on infinitely many of the $\{\widetilde{x}_{n'}\}_{n'\geq n}$ and vice-versa.

In order to describe the relation between (3.53) and (3.54) for a more general function σ, we assume that the latter can be expanded

$$\sigma(\mathcal{X}) = \sum_{k=1}^{\infty} \sigma_k\, \mathcal{X}^k , \qquad \text{with} \qquad \sigma_k \in \mathbb{R} , \tag{3.56}$$

[6] Here $r_{H,+}$ is understood to be the position of the outer horizon, which we denote by r_H throughout the remainder of this thesis.

which has a radius of convergence $\mathcal{X}_c' \geq \mathcal{X}_c$.[7] By demanding $\Phi^{(\mathcal{X})}(\mathcal{X}) = \Phi^{(\widetilde{\mathcal{X}})}(\widetilde{\mathcal{X}})$

$$\Phi^{(\widetilde{\mathcal{X}})}(\widetilde{\mathcal{X}}) = \sum_{n=0}^{\infty} \widetilde{x}_n \left(\sum_{k=1}^{\infty} \sigma_k \, \mathcal{X}^k \right)^n = \Phi^{(\mathcal{X})}(\mathcal{X}) \,, \tag{3.57}$$

and using (A.7) in Appendix A.1, we obtain the following relation

$$\begin{aligned} &x_0 = \widetilde{x}_0 \,, \qquad x_1 = \sigma_1 \, \widetilde{x}_1 \,, \\ &x_m = \sigma_m \, \widetilde{x}_1 + \sum_{p=2}^{m} \widetilde{x}_p \sum_{\substack{0 \leq \ell_{p-1} \leq \ell_{p-2} \leq \ldots \leq \ell_1 \leq n \\ \ell_1 + \ldots + \ell_{p-1} = p-n}} \frac{n! \, \sigma_1^{n-\ell_1} \ldots \sigma_{p-1}^{\ell_{p-2}-\ell_{p-1}} \sigma_p^{\ell_{p-1}}}{(n-\ell_1)! \ldots (\ell_{p-2}-\ell_{p-1})! \ell_{p-1}!} \,. \end{aligned} \tag{3.58}$$

This identification is a linear relation, which expresses x_m as a linear combination of *finitely* many $\widetilde{x}_n$ with $n \leq m$. Formally, this relation can be written as a linear transformation with an infinite dimensional lower triangular matrix

$$\begin{pmatrix} x_0 \\ x_1 \\ x_2 \\ x_3 \\ x_4 \\ x_5 \\ \vdots \end{pmatrix} = \begin{pmatrix} 1 & 0 & 0 & 0 & 0 & 0 & \cdots \\ 0 & \sigma_1 & 0 & 0 & 0 & 0 & \cdots \\ 0 & \sigma_2 & \sigma_1^2 & 0 & 0 & 0 & \cdots \\ 0 & \sigma_3 & 2\sigma_1\sigma_2 & \sigma_1^3 & 0 & 0 & \cdots \\ 0 & \sigma_4 & \sigma_2^2 + 2\sigma_1\sigma_3 & 3\sigma_1^2\sigma_2 & \sigma_1^4 & 0 & \cdots \\ 0 & \sigma_5 & 2(\sigma_1\sigma_4 + \sigma_2\sigma_3) & 3(\sigma_1\sigma_2^2 + \sigma_1^2\sigma_3) & 4\sigma_1^3\sigma_2 & \sigma_1^5 & \cdots \\ \vdots & \vdots & \vdots & \vdots & \vdots & \vdots & \ddots \end{pmatrix} \cdot \begin{pmatrix} \widetilde{x}_0 \\ \widetilde{x}_1 \\ \widetilde{x}_2 \\ \widetilde{x}_3 \\ \widetilde{x}_4 \\ \widetilde{x}_5 \\ \vdots \end{pmatrix} . \tag{3.59}$$

Combining (3.55) with (3.59) allows to describe more general EMD redefinitions.

3.4 Ricci Scalar EMD

Let us note that the most general static space-time metric compatible with spherical symmetry is not considered here yet, but to streamline the discussion, a family of metrics, parametrized by a single function $\Phi^{(\mathcal{X})}$ of a single argument, are examined. In this Section we shall discuss a new EMD that is not based on the physical distance to the black hole (horizon), but instead to the Ricci scalar. Indeed, outside of the horizon of the black hole, the latter is expected to be a monotonic function of the Schwarzschild coordinate r. Here we shall first discuss how to define such deformations in a self-consistent fashion and then explain how such descriptions can be linked to the distance EMD that we have reviewed in the previous Section.

[7] Since (3.55) already describes the relation for a shift by a constant, we have assumed $\sigma_0 = 0$. Furthermore, in the following we shall implicitly assume $\sigma_1 \neq 0$.

3.4.1 Definition of the EMD

To define the Ricci scalar EMD, we shall use for the deformation of the metric (3.1)) a function $\Phi^{(R)}$ of the Ricci scalar:

$$f(r) = 1 - \frac{\Phi^{(R)}(R(r))}{r} \,. \tag{3.60}$$

As before, we consider the outer horizon of the black hole to be located at $r = r_H$, such that $f(r_H) = 0$. The Ricci scalar R is fixed in terms of the metric function in the following manner[8]

$$R(r) = \frac{1}{r^2}\left(2 - 2f - 4rf' - r^2 f''\right) = \frac{2}{r^2}\frac{\mathrm{d}\Phi^{(R)}}{\mathrm{d}r} + \frac{1}{r}\frac{\mathrm{d}^2\Phi^{(R)}}{\mathrm{d}r^2} \,, \tag{3.61}$$

which is a second order, non-linear differential equation for R as a function of the Schwarzschild coordinate r. Solving (3.61) in general in the regime $r \geq r_H$ is a difficult task and we limit ourselves to studying a series expansion in the vicinity of the horizon. Concretely, we define the following series expansions

$$\Phi^{(R)}(R) = 2M \sum_{n=0}^{\infty} \frac{q_n}{n!} R^n \,, \qquad \text{and} \qquad R(r) = \sum_{n=0}^{\infty} \frac{R_n}{n!}(r - r_H)^n \,, \tag{3.62}$$

which we assume to have a non-zero radius of convergence for $r \geq r_H$. Notice that the sets of expansion coefficients $\{q_n\}_{n\in\mathbb{N}_0}$ and $\{R_n\}_{n\in\mathbb{N}_0}$ play very different roles: the $\{q_n\}$ implicitly define the function $\Phi^{(R)}$ and are therefore external input parameters that *define* the metric deformation. They are therefore part of the free parameters that define the Ricci scalar EMD. The coefficients $\{R_n\}$ are a priori not free, but instead fixed by (3.61) in terms of the $\{q_n\}$. However, since (3.61) is a second order differential equation, its general solution depends on two further (unfixed) parameters. Thus, in order to fully describe the Ricci scalar EMD, we first need to understand how to parametrise this freedom.

First of all, the condition of the horizon being located at r_H (*i.e.* $f(r_H) = 0$) imposes

$$\sum_{n=0}^{\infty} \frac{q_n}{n!}(R_0)^n = \frac{r_H}{2M} \,. \tag{3.63}$$

Furthermore, the expansion of R in (3.62) allows to expand $\Phi^{(R)}$ in terms of the Schwarzschild coordinate

$$\Phi^{(R)}(r) = 2M \sum_{n=0}^{\infty} \frac{q_n}{n!}\left(\sum_{k=0}^{\infty} \frac{R_k}{k!}(r - r_H)^k\right)^n =: 2M \sum_{p=0}^{\infty} \tau_p \,(r - r_H)^p \,. \tag{3.64}$$

This series can be developed in the following form (see Appendix A.1 for a discussion on the technical details of expanding powers of series)

$$\Phi^{(R)} = 2M \sum_{n=0}^{\infty} \frac{q_n}{n!} \sum_{\ell_1=0}^{n} \sum_{\ell_2=0}^{\ell_1} \cdots \sum_{\ell_p=0}^{\ell_{p-1}} \binom{n}{\ell_1}\binom{\ell_1}{\ell_2}\cdots\binom{\ell_{p-1}}{\ell_p} (R_0)^{n-\ell_1}\left(\tfrac{R_1}{1!}\right)^{\ell_1-\ell_2} \cdots \left(\tfrac{R_{p-1}}{(p-1)!}\right)^{\ell_{p-1}-\ell_p} \times$$

[8] In this work, primes denote derivatives with respect to the Schwarzschild coordinate r. Furthermore we have used the shorthand notation $\frac{\mathrm{d}\Phi^{(R)}}{\mathrm{d}r} = \frac{\mathrm{d}\Phi^{(R)}}{\mathrm{d}R}\frac{\mathrm{d}R}{\mathrm{d}r}$, and similarly for the second derivative.

$$\times \left(\frac{R_p}{p!}\right)^{\ell_p} (r-r_H)^{\ell_1+\ell_2+\ldots\ell_{p-1}+\ell_p} + \mathcal{O}((r-r_H)^{p+1}) \,, \tag{3.65}$$

such that we can read off the coefficients

$$\tau_0 = \sum_{n=0}^{\infty} \frac{q_n}{n!} (R_0)^n \equiv \frac{r_H}{2M} \,,$$

$$\tau_p = \sum_{n=0}^{\infty} q_n \sum_{\substack{0\le\ell_p\le\ell_{p-1}\le\ldots\le\ell_1\le n\\ \ell_1+\ell_2+\ldots+\ell_p=p}} \frac{(R_0)^{n-\ell_1}\left(\frac{R_1}{1!}\right)^{\ell_1-\ell_2}\cdots\left(\frac{R_{p-1}}{(p-1)!}\right)^{\ell_{p-1}-\ell_p}\left(\frac{R_p}{p!}\right)^{\ell_p}}{(n-\ell_1)!\,(\ell_1-\ell_2)!\ldots(\ell_{p-1}-\ell_p)!\ell_p!} \,, \quad \forall p\ge 1 \,. \tag{3.66}$$

Furthermore, using the expansions

$$\frac{1}{r} = \sum_{n=0}^{\infty} \frac{(-1)^n}{r_H^{n+1}} (r-r_H)^n \,, \qquad \text{and} \qquad \frac{1}{r^2} = \sum_{n=0}^{\infty} \frac{(-1)^n (n+1)}{r_H^{n+2}} (r-r_H)^n \,, \tag{3.67}$$

we can further expand the two terms on the right hand-side of eq. (3.61) by using the Cauchy product of two series

$$\frac{1}{r^2}\frac{\mathrm{d}\Phi^{(R)}}{\mathrm{d}r} = 2M\sum_{p=0}^{\infty}(r-r_H)^p\sum_{n=0}^{p}\frac{(-1)^n(n+1)(p+1-n)}{r_H^{n+2}}\,\tau_{p+1-n} \,, \tag{3.68}$$

$$\frac{1}{r}\frac{\mathrm{d}^2\Phi^{(R)}}{\mathrm{d}r^2} = 2M\sum_{p=0}^{\infty}(r-r_H)^p\sum_{n=0}^{p}\frac{(-1)^n(p+2-n)(p+1-n)}{r_H^{n+1}}\,\tau_{p+2-n} \,. \tag{3.69}$$

Combining these results, (3.61) can be expanded in powers of $(r-r_H)$

$$\sum_{p=0}^{\infty}\frac{R_p}{p!}(r-r_H)^p = 2M\sum_{p=0}^{\infty}(r-r_H)^p\sum_{n=0}^{p}\frac{(-1)^n}{r_H^{n+2}}\Big[2r_H(n+1)(p+1-n)\,\tau_{p+1-n}+$$
$$+(p+2-n)(p+1-n)\,\tau_{p+2-n}\Big] \,, \tag{3.70}$$

such that, by comparing order by order, we find

$$\frac{R_p}{p!} = 2M\sum_{n=0}^{p}\frac{(-1)^n}{r_H^{n+2}}\left[2(n+1)(p+1-n)\,\tau_{p+1-n}+r_H(p+2-n)(p+1-n)\,\tau_{p+2-n}\right] \,. \tag{3.71}$$

To understand this relation, we recall that the τ_p in (3.66) are functions of the coefficients $\{q_n\}$ and $\{R_n\}$. Therefore, a priori (3.71) allows to express the latter in terms of the former. Concretely, however, (3.71) can be seen as a recursive equation that allows to express iteratively the $\{R_n\}_{n\ge2}$ in terms of $\{R_0, R_1, q_{n\ge0}\}$. To see this, we re-write the second equation of (3.66) in the form

$$\tau_{p+2} = \frac{R_{p+2}}{(p+2)!}\sum_{n=1}^{\infty}\frac{q_n\,R_0^{n-1}}{(n-1)!} + \tau_{p+2}^{\text{sub-}R}(R_0,\ldots,R_{p+1},\{q_n\}) \,, \tag{3.72}$$

where $\tau_{p+2}^{\text{sub-}R}$ is notably independent of $R_{k\ge p+2}$

$$\tau_{p+2}^{\text{sub-}R} := \sum_{n=0}^{\infty} q_n \sum_{\substack{0\le\ell_{p+1}\le\ldots\le\ell_1\le n\\ \ell_1+\ell_2+\ldots\ell_{p+1}=p+2}} \frac{R_0^{n-\ell_1}\left(\frac{R_1}{1!}\right)^{\ell_1-\ell_2}\cdots\left(\frac{R_{p+1}}{(p+1)!}\right)^{\ell_{p+1}}}{(n-\ell_1)!\,(\ell_1-\ell_2)!\ldots(\ell_p-\ell_{p+1})!\ell_{p+1}!} \,. \tag{3.73}$$

Therefore (3.71) is a linear equation in R_{p+2} that allows to express it in terms of $R_{p'}$, with $p' < p+2$ and $\{q_n\}$

$$R_{p+2} = \frac{r_H\, p!}{2M \sum_{k=1}^{\infty} \frac{q_k R_0^{k-1}}{(k-1)!}} \left[\frac{R_p}{p!} - \frac{2M(p+2)(p+1)}{r_H} \tau_{p+2}^{\text{sub}\,R} + \right. \\ \left. - 4M \sum_{n=0}^{p} \frac{(-1)^n (n+1)(p+1-n)}{r_H^{n+2}} \tau_{p+1-n} - 2M \sum_{n=1}^{p} \frac{(-1)^n (p+2-n)(p+1-n)}{r_H^{n+1}} \tau_{p+2-n} \right] . \tag{3.74}$$

Thus, we can choose as the free parameters to describe this EMD the parameters R_0, R_1 and $\{q_n\}_{n\in\mathbb{N}_0}$. The discussion so far is summarised in Figure 3.2, which formalises the definition of the Ricci scalar EMD to describe (quantum) deformations of a spherically symmetric and static black hole. Notice that this EMD a priori gives a different description of the black hole deformation as the distance EMD discussed in the previous Section. Moreover, given the different sets of input parameters (*i.e.* $\{\xi_n\}_{n\in\mathbb{N}_0}$ for the distance EMD and $(R_0, R_1, \{q_n\})$ for the Ricci scalar EMD) it is not clear whether these two descriptions are equivalent. In the following Subsection we shall therefore discuss how to connect the two EMDs, that is, we shall try to formulate relations among the two sets of parameters that lead to identical deformations and therefore the same geometry.[9]

3.4.2 Relation to the Distance EMD

Our strategy in relating the distance EMD to the Ricci scalar EMD is to identify the deformation functions, *i.e.* $\Phi^{(R)} = \Phi^{(\rho)}$. This can for example be achieved by expanding both functions in the Schwarzschild coordinate and identify the coefficients τ_p (as defined in (3.64)) order by order. However, a major technical complication on the Ricci scalar side is the fact that τ_p for fixed p generally depends on all $\{q_n\}_{n\in\mathbb{N}_0}$. We therefore first slightly re-define the Ricci scalar EMD before relating it to the distance EMD.

Redefinition of the Ricci Scalar EMD

We may slightly re-define the Ricci scalar EMD by choosing as physical quantity $\widetilde{R}(r) := R(r) - R_0$. Since R_0 is a constant (namely the value of the Ricci scalar at the horizon), $\widetilde{R}$ is a physical quantity and (outside of the horizon) a monotonic function of r. We thus consider the expansion of the modified deformation function

$$\Phi^{(\widetilde{R})} = 2M \sum_{n=0}^{\infty} \frac{\widetilde{q}_n}{n!} \widetilde{R}^n , \qquad \text{and} \qquad \widetilde{R}(r) = \sum_{n=1}^{\infty} \frac{R_n}{n!} (r - r_H)^n . \tag{3.75}$$

Following the same logic as explained in Section 3.3 (see (3.55)), the coefficients q_p in (3.62) and the $\widetilde{q}_p$ in (3.75) can be related through

$$q_p = \sum_{n=p}^{\infty} \frac{\widetilde{q}_n\, (-R_0)^{n-p}}{(n-p)!} , \qquad \text{and} \qquad \widetilde{q}_p = \sum_{n=p}^{\infty} \frac{q_n\, R_0^{n-p}}{(n-p)!} . \tag{3.76}$$

[9] Notice that we shall impose that the two deformations are indeed *identical*. We shall not discuss the much more general possibility of the two space-times described by these deformations being equivalent and related to one another through coordinate transformations.

Furthermore, the identification (3.76) allows to write

$$\Phi^{(\widetilde{R})}(\widetilde{R}) = 2M \sum_{p=0}^{\infty} \tau_p \,(r - r_H)^p \,, \tag{3.77}$$

with the same coefficients τ_p as in (3.64). Concretely, we find the following form for τ_p as a function of $\{\widetilde{q}_n\}_{n\in\mathbb{N}_0}$ and $\{R_n\}_{n\in\mathbb{N}}$

$$\begin{aligned}
&\tau_0 = \widetilde{q}_0\,,\\
&\tau_p = \sum_{\substack{0\leq \ell_{p-1}\leq\ldots\leq\ell_1\leq n\leq p\\ \ell_1+\ell_2+\ldots+\ell_{p-1}+n=p}} \frac{\widetilde{q}_n \left(\frac{R_1}{1!}\right)^{n-\ell_1}\left(\frac{R_2}{2!}\right)^{\ell_1-\ell_2}\ldots\left(\frac{R_{p-1}}{(p-1)!}\right)^{\ell_{p-2}-\ell_{p-1}}\left(\frac{R_p}{p!}\right)^{\ell_{p-1}}}{(n-\ell_1)!\,(\ell_1-\ell_2)!\ldots(\ell_{p-2}-\ell_{p-1})!\ell_{p-1}!} \qquad \forall p\geq 1\,.
\end{aligned} \tag{3.78}$$

Inserting this relation in the self-consistency relation (3.71) leads to a recursive relation that fixes R_n for $n\geq 2$ in terms of R_0, R_1 and $\{\widetilde{q}_n\}_{n\in\mathbb{N}_0}$:

$$\begin{aligned}
R_{p+2} = \frac{r_H\, p!}{2M\widetilde{q}_1}\Bigg[&\frac{R_p}{p!} - \frac{2M(p+2)(p+1)}{r_H} \sum_{\substack{0\leq\ell_p\leq\ldots\leq\ell_1\leq n\leq p+2\\ \ell_1+\ell_2+\ldots\ell_p+n=p+2}} \frac{\widetilde{q}_n\left(\frac{R_1}{1!}\right)^{n-\ell_1}\ldots\left(\frac{R_p}{p!}\right)^{\ell_{p-1}-\ell_p}\left(\frac{R_{p+1}}{(p+1)!}\right)^{\ell_p}}{(n-\ell_1)!\ldots(\ell_{p-1}-\ell_p)!\ell_p!}\\
&-4M\sum_{n=0}^{p}\frac{(-1)^n(n+1)(p+1-n)}{r_H^{n+2}}\tau_{p+1-n} - 2M\sum_{n=1}^{p}\frac{(-1)^n(p+2-n)(p+1-n)}{r_H^{n+1}}\,\tau_{p+2-n}\Bigg]\,.
\end{aligned} \tag{3.79}$$

Together with (3.78) this solution allows to express the coefficients τ_n in the expansion of the deformation function (3.77) in terms of R_0, R_1 and $\{\widetilde{q}_n\}_{n\in\mathbb{N}_0}$. For the $\tau_{0,\ldots,4}$ we obtain

$$\begin{aligned}
&\tau_0 = \widetilde{q}_0\,,\quad \tau_1 = R_1\,\widetilde{q}_1\,,\quad \tau_2 = \frac{R_0 r_H}{4M} - \frac{R_1}{r_H}\,\widetilde{q}_1\,,\quad \tau_3 = \frac{R_1}{r_H^2}\,\widetilde{q}_1 - \frac{R_0 - r_H R_1}{12M}\,,\\
&\tau_4 = \frac{R_0}{192 r_H M^3\widetilde{q}_1}\,(r_H^3 + 12M\widetilde{q}_1) - R_1\left(\frac{1}{24M} + \frac{\widetilde{q}_1}{r_H^3}\right) - \frac{R_1^2 r_H\widetilde{q}_2}{48M\widetilde{q}_1}\,.
\end{aligned} \tag{3.80}$$

The form of τ_4 suggests that the coefficients τ_n for $n>4$ are more complicated, however, we remark that (3.78) implies that they depend linearly on $\widetilde{q}_{n-2}$ in the following fashion

$$\tau_n = -\frac{R_1^{n-2} r_H}{2Mn!}\,\frac{\widetilde{q}_{n-2}}{\widetilde{q}_1} + \tau_n^{\text{sub-}\widetilde{R}}(R_0, R_1, \widetilde{q}_0, \ldots, \widetilde{q}_{n-3})\,, \qquad \forall n\geq 4\,, \tag{3.81}$$

where $\tau_n^{\text{sub-}\widetilde{R}}$ is independent of $\widetilde{q}_{k\geq n-2}$.

EMD identification

To relate the (redefined) Ricci scalar- and distance- EMD, we next identify the deformation functions $\Phi^{(\rho)}$ in (3.7) with $\Phi^{(\widetilde{R})}$ in (3.75)

$$\Phi^{(\rho)} = \sum_{p=0}^{\infty} \tau_p \, (r - r_H)^p = \Phi^{(\widetilde{R})} \,, \tag{3.82}$$

To this end we express the coefficients τ_p in terms of $\{\xi_{2n}\}_{n\in\mathbb{N}_0}$ using the result of the previous Section and taking into account the full regular function at the horizon with the conditions (3.46), (3.48) and (3.49)

$$\begin{aligned} &\tau_0 = \xi_0 \,, \qquad \tau_1 = \xi_2 b_1^2 \,, \\ &\tau_p = \sum_{\substack{0\leq \ell_{p-1}\leq \ldots \leq \ell_1 \leq 2n \leq 2p \\ n+\ell_1+\ell_2+\ldots+\ell_{p-1}=p}} \frac{(2n)!\, \xi_{2n} b_1^{2n-\ell_1} b_3^{\ell_1-\ell_2} \ldots b_{2p-3}^{\ell_{p-2}-\ell_{p-1}} b_{2p-1}^{\ell_{p-1}}}{(2n-\ell_1)!(\ell_1-\ell_2)!\ldots(\ell_{p-2}-\ell_{p-1})!\ell_{p-1}!} \qquad \forall p \geq 2 \,. \end{aligned} \tag{3.83}$$

Using (3.15) to express the coefficients $\{b_{2n-1}\}_{n\in\mathbb{N}}$ in terms of the $\{a_{2n-2}\}_{n\in\mathbb{N}}$ and (3.14) to express the latter in terms of $\{\xi_{2n-2}\}_{n\in\mathbb{N}}$, we find for the coefficients $\tau_{0,\ldots,3}$ of (3.83)

$$\begin{aligned} &\tau_0 = \xi_0 \,, \qquad \tau_1 = \frac{8 r_H \xi_2}{1+\varpi} \,, \qquad \tau_2 = \frac{4\xi_2}{1+2\varpi} + \frac{64 r_H^2 (1+\varpi(3+2\varpi)+8r_H\xi_2)\xi_4}{(1+\varpi)^3(1+2\varpi)} \,, \\ &\tau_3 = \frac{1280 r_H^3 \xi_6}{(1+\varpi)^2(2+3\varpi)} + \frac{4096 r_H^4 (7+8\varpi)\xi_4^2}{(1+\varpi)^3(1+2\varpi)(2+3\varpi)} + \frac{48 r_H (5+9\varpi+6\varpi^2)\xi_4}{(1+\varpi)(1+2\varpi)^2(2+3\varpi)} \\ &\qquad + \frac{(1+\varpi)^2(1-3\varpi+2\varpi^2)}{8 r_H^2 (1+2\varpi)^2(2+3\varpi)} \,. \end{aligned} \tag{3.84}$$

The general form (3.18) of the coefficients b_{2n-1} implies

$$\tau_p = \frac{2^{3p} r_H^p}{(1+\varpi)^p} \left(\frac{8\xi_2 r_H}{(1+\varpi)((p-1)+p\varpi)} + 1 \right) \xi_{2p} + \tau_p^{\text{sub-}\rho} \left(\xi_0, \ldots, \xi_{2p-2}\right) \,, \tag{3.85}$$

where $\tau_p^{\text{sub-}\rho}$ is independent of ξ_{2k} for $k \geq p+1$. Identifying (3.81) with (3.85) allows to relate the coefficients $\{\xi_{2n}\}_{n\in\mathbb{N}_0}$ to $(R_0, R_1, \{\widetilde{q}_n\}_{n\in\mathbb{N}_0})$. Concretely, identifying $\tau_{0,\ldots,3}$ gives relations between $(\xi_0, \xi_2, \xi_4, \xi_6)$ and $(R_0, R_1, \widetilde{q}_0, \widetilde{q}_1)$, which are explicitly given in Appendix A.3. Once these parameters are fixed, the identification of $\tau_{p\geq 4}$ (*i.e.* (3.81) and (3.85)) is a linear relation relating ξ_{2p} and $\widetilde{q}_{p-2}$, which therefore allows to completely express the distance EMD in terms of the Ricci-scalar EMD and vice versa. Notice that this identification also allows to write physical quantities unambiguously in either EMD. For example, the Hawking temperature in the distance scheme (3.5) can be given more generally in terms of $\tau_{0,1}$ as follows

$$T_H = \frac{1 - 2M\,\tau_1}{8\pi M\,\tau_0} \,. \tag{3.86}$$

Using (3.66) and (3.80) we can therefore write the Hawking temperature in terms of the free parameters of the Ricci-scalar EMD

$$T_H = \frac{1 - 2MR_1 \sum_{n=1}^{\infty} \frac{q_n R_0^{n-1}}{(n-1)!}}{8\pi M \sum_{m=0}^{\infty} \frac{q_m R_0^m}{m!}} = \frac{1 - 2MR_1\widetilde{q}_1}{8\pi M \widetilde{q}_0} \,. \tag{3.87}$$

Before closing this Section, we briefly remark that the condition $\xi_2 \leq \frac{M}{8r_H}$ for the coefficient ξ_2 in the distance EMD is automatically satisfied in the Ricci scalar EMD. Indeed, for any value of $\widetilde{q}_1\, R_1 \in \mathbb{R}$, $\xi_2 \leq \frac{M}{8r_H}$ is automatically satisfied in (A.27).

3.5 Kretschmann Scalar EMD

3.5.1 Definition of the EMD

Following the example of the Ricci scalar, we can define further EMDs based on other curvature scalars. As an example of a second-order curvature invariant, we shall consider the Kretschmann scalar [163], which in terms of the Riemann tensor $R^{\mu}{}_{\nu\rho\lambda}$ is defined as $K = R_{\mu\nu\rho\lambda}R^{\mu\nu\rho\lambda}$, and define the deformed metric function

$$f(r) = 1 - \frac{\Phi^{(K)}(K(r))}{r} \,. \tag{3.88}$$

The Kretschmann scalar is related to the deformation function through the following differential equation

$$\begin{aligned} K(z) &= \frac{1}{r^4}\left(4 - 8f + 4f^2 + 4r^2(f')^2 + r^4(f'')^2\right) \\ &= \frac{2}{r^2}\left[\frac{\mathrm{d}^2}{\mathrm{d}r^2}\left(\frac{(\Phi^{(K)})^2}{r^2}\right) + \frac{r^4}{2}\left(\frac{\mathrm{d}}{\mathrm{d}r}\left(\frac{1}{r^2}\frac{\mathrm{d}\Phi^{(K)}}{\mathrm{d}r}\right)\right)^2\right] \,. \end{aligned} \tag{3.89}$$

Following the example of (3.62), in order to solve this self-consistency relation, we expand the function $v^{(K)}$ as

$$\Phi^{(K)}(K) = 2M\sum_{n=0}^{\infty}\frac{s_n}{n!}K^n \,, \qquad \text{and} \qquad K(z) = \sum_{n=0}^{\infty}\frac{K_n}{n!}(r - r_H)^n \,, \tag{3.90}$$

where the coefficients $\{s_n\}_{n\in\mathbb{N}_0}$ are external input parameters that define the EMD. We choose them in such a way to satisfy the normalisation condition $\sum_{n=0}^{\infty}\frac{s_n}{n!}K_0^n = \frac{r_H}{2M}$. As we shall explain, the coefficients $\{K_n\}_{n\in\mathbb{N}_0}$ are a priori not all independent, but related to the $\{s_n\}_{n\in\mathbb{N}_0}$ via (3.89). To study these dependencies, we expand $\Phi^{(K)}$ in the Schwarzschild coordinate[10]

$$\Phi^{(K)}(K(r)) = 2M\sum_{p=0}^{\infty}\tau_p(r - r_H)^p \,, \tag{3.91}$$

where the coefficients τ_n can be expressed in terms of the $\{K_n\}_{n\in\mathbb{N}_0}$ as follows

$$\begin{aligned} \tau_0 &= \sum_{n=0}^{\infty}\frac{s_n}{n!}(K_0)^n \,, \\ \tau_p &= \sum_{n=0}^{\infty}s_n \sum_{\substack{0\leq \ell_p\leq \ell_{p-1}\leq\ldots\leq\ell_1\leq n \\ \ell_1+\ell_2+\ldots+\ell_p=p}} \frac{(K_0)^{n-\ell_1}\,(K_1)^{\ell_1-\ell_2}\ldots\left(\frac{K_p}{p!}\right)^{\ell_p}}{(n-\ell_1)!\,(\ell_1-\ell_2)!\ldots(\ell_{p-1}-\ell_p)!\ell_p!} \,. \end{aligned} \tag{3.92}$$

[10] In view of later identifying this EMD with the ones discussed previously, we use the same coefficients $\{\tau_n\}_{n\in\mathbb{N}_0}$ as in (3.64) and (3.82).

Furthermore, from (3.89) we obtain

$$\begin{aligned}
\frac{K_p}{p!} &= 8M^2 \sum_{m=0}^{p} \sum_{n=0}^{m+2} \sum_{\ell=0}^{m+2-n} \frac{(-1)^{p+\ell-m}(p-m+1)(\ell+1)(m+2)(m+1)}{r_H^{p-m+\ell+4}} \tau_n \, \tau_{m+2-n-\ell} \\
&+ 4M^2 \sum_{n=1}^{p-1} \sum_{\ell=0}^{p-n} \sum_{k=0}^{n} \frac{(-1)^{\ell+k}(\ell+1)(k+1)(p-n)n(p-n+1-\ell)(n+1-k)}{r_H^{k+\ell+4}} \tau_{p-n-\ell+1} \, \tau_{n-k+1} \\
&+ 8M^2 \sum_{n=1}^{p} \sum_{\ell=0}^{p-n+1} \sum_{k=0}^{n} \frac{(-1)^{\ell+k}(\ell+1)(k+1)(p-n+1)n(p-n+2-\ell)(n+1-k)}{r_H^{k+\ell+3}} \tau_{p-n-\ell+2} \, \tau_{n-k+1} \\
&+ 4M^2 \sum_{n=1}^{p+1} \sum_{\ell=0}^{p-n+2} \sum_{k=0}^{n} \frac{(-1)^{\ell+k}(\ell+1)(k+1)(p-n+2)n(p-n+3-\ell)(n+1-k)}{r_H^{k+\ell+2}} \tau_{p-n-\ell+3} \, \tau_{n-k+1} \, .
\end{aligned} \tag{3.93}$$

Notice that for $p > 0$

$$\begin{aligned}
\frac{K_p}{p!} &= \frac{16M^2(p+1)(p+2)}{r_H^4} \left(\tau_0 - r_H \, \tau_1 + r_H^2 \, \tau_2\right) \tau_{p+2} + \widehat{\tau}_{p+2}^{\text{sub-}K}(\tau_0, \dots, \tau_{p+1}) \\
&= \frac{16M^2 K_{p+2}}{r_H^4 p!} \left(\sum_{m=0}^{\infty} s_m K_0^{m-2} \left(\frac{K_0^2}{m!} - \frac{r_H K_0 K_1}{(m-1)!} + \frac{r_H^2 K_0 K_2}{2(m-1)!} + \frac{r_H^2 K_1^2}{2(m-2)!}\right)\right) \left(\sum_{n=1}^{\infty} \frac{s_n (K_0)^{n-1}}{(n-1)!}\right) \\
&\qquad + \tau_{p+2}^{\text{sub-}K}(K_0, \dots, K_{p+1}, \{s_n\}) \, ,
\end{aligned} \tag{3.94}$$

where $\widehat{\tau}_{p+2}^{\text{sub-}K}$ and $\tau_{p+2}^{\text{sub-}K}$ denote terms independent of $\tau_{n>p+2}$ and $K_{n>p+2}$ respectively. Furthermore, in the second line we have used an expansion of the coefficients τ_{p+2} similar to (3.72) or (3.81). We therefore find that (3.94) is a linear equation for K_{p+2}, which, similar to the case of the Ricci scalar EMD, allows to express the K_{p+2} uniquely in terms of $K_{p'<p+2}$ for all $p \geq 3$. For $p = 0$, (3.93) is a quadratic equation for K_2 with the following solutions

$$K_2 = \frac{2\zeta_1(K_1(2\zeta_1 - K_1 r_H \zeta_2)M - 1) + u|\zeta_1|\sqrt{16K_1\zeta_1 M(1 - K_1\zeta_1 M) - 8 + K_0 r_H^4}}{2M r_H \zeta_1^2} \, , \tag{3.95}$$

where we have introduced a phase factor $u = \pm 1$ and defined the following shorthand notation

$$\zeta_1 = \sum_{n=1}^{\infty} s_n \frac{K_0^{n-1}}{(n-1)!} \quad \text{and} \quad \zeta_2 = \sum_{n=2}^{\infty} s_n \frac{K_0^{n-2}}{(n-2)!} \, . \tag{3.96}$$

Furthermore, we have used $\tau_0 = \frac{r_H}{2M}$ to simplify the expression. Based on this solution, the Kretschmann scalar EMD is summarized in Figure 3.2. Here we consider as free parameters $(K_0, K_1, \{s_n\}_{n\in\mathbb{N}_0})$ (which are real parameters), while the phase factor $u = \pm 1$ is an additional condition. This is similar to our choice for dealing with a sign ambiguity when resolving the self-consistency condition in the distance EMD. Finally, we remark that with (3.92) the Hawking temperature (3.86) in the Kretschmann-scalar EMD takes the following form

$$T_H = \frac{1 - 2MK_1 \sum_{n=1}^{\infty} \frac{s_n K_0^{n-1}}{(n-1)!}}{8\pi M \sum_{m=0}^{\infty} \frac{s_m K_0^m}{m!}} = \frac{1 - 2MK_1 \, \zeta_1}{4\pi r_H} \, . \tag{3.97}$$

3.5.2 Relation to other EMDs

After having introduced the Kretschmann scalar EMD, we now relate it to other EMDs. To this end, following the example of the Ricci scalar EMD, we shall first propose a slight redefinition, before making contact to the distance- and Ricci scalar EMD.

Instead of working with the Kretschmann scalar directly, we instead subtract from it its value at the horizon, *i.e.* we introduce $\widetilde{K}(r) := K(r) - K_0$ and define

$$\Phi^{(\widetilde{K})}(\widetilde{K}) = 2M \sum_{n=0}^{\infty} \frac{\widetilde{s}_n}{n!}\,\widetilde{K}^n\,, \qquad \text{and} \qquad \widetilde{K}(z) = \sum_{n=1}^{\infty} \frac{K_n}{n!}\,(r-r_H)^n\,, \tag{3.98}$$

The relation between the coefficients $\{s_n\}_{n\in\mathbb{N}_0}$ and $\{\widetilde{s}_n\}_{n\in\mathbb{N}_0}$ follows in the same manner as in (3.76), namely

$$s_p = \sum_{n=p}^{\infty} \frac{\widetilde{s}_n\,(-K_0)^{n-p}}{(n-p)!}\,, \qquad \text{and} \qquad \widetilde{s}_p = \sum_{n=p}^{\infty} \frac{s_n\,K_0^{n-p}}{(n-p)!}\,. \tag{3.99}$$

To make contact with other EMDs, we expand $v^{(\widetilde{K})}$ in terms of the Schwarzschild coordinate

$$\Phi^{(\widetilde{K})} = 2M \sum_{p=0}^{\infty} \tau_p\,(r-r_H)^p\,. \tag{3.100}$$

and interpret the coefficients τ_p to be the same as in (3.64), (3.82) and (3.91), while being expanded as a function of the $\{\widetilde{s}_n\}_{n\in\mathbb{N}_0}$ and $\{K_n\}_{n\in\mathbb{N}}$

$$\begin{aligned}
&\tau_0 = \widetilde{s}_0\,,\\
&\tau_p = \sum_{\substack{0\le \ell_{p-1}\le\ldots\le\ell_1\le n\le p\\ \ell_1+\ell_2+\ldots+\ell_{p-1}+n=p}} \frac{\widetilde{s}_n\left(\frac{K_1}{1!}\right)^{n-\ell_1}\left(\frac{K_2}{2!}\right)^{\ell_1-\ell_2}\cdots\left(\frac{K_{p-1}}{(p-1)!}\right)^{\ell_{p-2}-\ell_{p-1}}\left(\frac{K_p}{p!}\right)^{\ell_{p-1}}}{(n-\ell_1)!\,(\ell_1-\ell_2)!\ldots(\ell_{p-2}-\ell_{p-1})!\ell_{p-1}!} \qquad \forall p\ge 1\,.
\end{aligned} \tag{3.101}$$

Using (3.93) we can explicitly express the τ_p in terms of $\{\widetilde{s}_n\}_{n\in\mathbb{N}_0}$ and (K_0, K_1, u), *e.g.* we find for the first few instances

$$\begin{aligned}
&\tau_0 = \widetilde{s}_0\,, \qquad \tau_1 = K_1\,\widetilde{s}_1\,, \qquad \tau_2 = \frac{4M\widetilde{s}_1(K_1 r_H\widetilde{s}_1 - \widetilde{s}_0) + \mathfrak{p}}{4M\widetilde{s}_1 r_H}\,,\\
&\tau_3 = \frac{6K_0\widetilde{s}_1 r_H^6 - 64K_1^2\widetilde{s}_1^3 M^2 r_H^2 + K_1\widetilde{s}_1 r_H\left(-16\mathfrak{p}M + 96\widetilde{s}_0\widetilde{s}_1 M^2 + r_H^6\right) + 16\widetilde{s}_0 M(\mathfrak{p} - 4\widetilde{s}_0\widetilde{s}_1 M)}{24\mathfrak{p}M r_H^3}\,,
\end{aligned} \tag{3.102}$$

with the abbreviation $\mathfrak{p} = u|\widetilde{s}_1|\sqrt{K_0 r_H^6 - 16(2\widetilde{s}_0^2 - 2K_1 r_H\widetilde{s}_0\widetilde{s}_1 + K_1^2 r_H^2\widetilde{s}_1^2)M^2}$. Higher orders in τ_n are more complicated, however, we remark that they depend linearly on $\widetilde{s}_{n-2}$

$$\tau_n = -\frac{K_1^{n-2} r_H^4}{4M\,\mathfrak{p}\,n!}\,\widetilde{s}_{n-2} + \tau_n^{\text{sub-}\widetilde{K}}(K_0, K_1, u, \widetilde{s}_0, \ldots, \widetilde{s}_{n-3})\,, \qquad \forall n\ge 4\,, \tag{3.103}$$

where $\tau_n^{\text{sub-}\widetilde{K}}$ is independent of $\{\widetilde{s}_{k\ge n-1}\}$. Identifying the τ_p in (3.102) and (3.103) with (3.64), (3.82) and (3.91) yields equations that allow to relate the Kretschmann scalar EMD to the distance-and Ricci scalar EMD. Indeed, identifying $\tau_{0,1,2,3}$ fixes $(K_0, K_1, \widetilde{s}_0, \widetilde{s}_1)$ in terms of $(R_0, R_1, \widetilde{q}_0, \widetilde{q}_1)$ or $(\xi_0, \xi_2, \xi_4, \xi_6)$ (and vice-versa). Notice, that the space of solutions for these equations is fairly restricted: for example, for given $(\tau_0, \tau_1, \tau_2, \tau_3)$ (either given in terms of $(\xi_0, \xi_2, \xi_4, \xi_6)$ or $(R_0, R_1, \widetilde{q}_0, \widetilde{q}_1)$), consistent solutions of $(K_0, K_1, \widetilde{s}_0, \widetilde{s}_1)$ not only require a specific choice of u, but they are in fact uniquely fixed. To see this, we realise that the third equation in (3.102) can be rewritten in the form

$$\frac{u\,\mathrm{sign}(\widetilde{s}_1)}{4Mr_H}\sqrt{K_0 r_H^6 - 16(2\tau_0^2 - 2\tau_1\tau_0 r_H + \tau_1^2 r_H^2)M^2} = \tau_2 - \tau_1 + \frac{\tau_0}{r_H}\,, \tag{3.104}$$

which only has a solution if $u\,\mathrm{sign}(\widetilde{s}_1) = \mathrm{sign}\,(\tau_2 - \tau_1 + 1)$, in which case K_0 is uniquely fixed. This, however, renders the last equation in (3.102) linear in $\widetilde{s}_1$, with the solution

$$\widetilde{s}_1 = \frac{r_H^6 \tau_1}{32 r_H(\tau_1 - 2\tau_2 + 2\tau_1\tau_2 + 3r_H^2\tau_3(1 - \tau_1 + \tau_2) - 6K_0}\,. \tag{3.105}$$

Since this fixes (the sign of) $\widetilde{s}_1$, (3.104) is consistent only for a specific value of u. Finally, as in the previous cases, once (3.102) is solved, (3.103) are linear equations for $\widetilde{s}_{n-2}$ in terms of τ_n. Due to the length of the ensuing expressions, we refrain from reproducing the explicit form of the solution,[11], however, we provide a concrete mapping from the distance to the Kretschmann scalar EMD for a particular small deformation of the Schwarzschild solution in Appendix A.4. Higher orders $\tau_{n\geq 4}$ are linear in $\widetilde{s}_{n-2}$ and thus uniquely allow to fix them in terms of $\widetilde{q}_{n-2}$ or ξ_{2n} (or vice-versa).

3.5.3 Overview of the relations

In the previous three Sections, we have defined EMDs as coherent frameworks to describe (quantum) deformedm relative to the classical Schwarzschild geometry [1], spherically symmetric and static black holes in 4 dimensions. Such black hole geometries are captured by one[12] deformation function of a physical quantity $\mathcal{X}$ to ensure compatibility of the quantum geometry with the same symmetries as its classical counterpart.

In 3.2 the physical distance, measured from the (horizon of the) black hole, was chosen. However, other physical quantities (*e.g.* curvature scalars of different orders) are equally viable. In each case, in order to remain self-consistent, $\mathcal{X}$ is computed from the deformed metric, thus leading to an involved equation to tackle (see eqs. (3.6), (3.61) and (3.89) respectively for the distance, Ricci scalar and Kretschmann scalar). To solve this equation, we follow the general framework developed in 3.2 and consider series expansions in the vicinity of the event horizon of the black hole. In this way, we not only provide self-consistent solutions for metric deformations based on the physical distance, Ricci- and Kretschmann scalar, but also propose clear definitions of each of the EMDs, as shown in the overview in Figure 3.2. Moreover, as also indicated in the schematic drawing, by expressing the deformation functions as expansions in the Schwarzschild coordinate,

[11] For the same reason, we also do not provide the (unique) inverse transformations that express $(\xi_0, \xi_2, \xi_4, \xi_6)$ or $(R_0, R_1, \widetilde{q}_0, \widetilde{q}_1)$ in terms of $(K_0, K_1, \widetilde{s}_0, \widetilde{s}_1)$)): they follow from replacing τ_n in (3.84), (3.85) and (3.80), (3.81) respectively with (3.102) and (3.103). We furthermore remark in passing that, similar to the case of the Ricci scalar EMD, the condition $\xi_2 \leq \frac{M}{8r_H}$ also poses no further conditions on $(K_0, K_1, \{\widetilde{s}_n\}_{n\in\mathbb{N}_0})$.

[12] In Sections 3.4 and 3.5 we only focused on the case of a single deformation function. The more general case of two such functions, which is compatible with spherical symmetry and static behaviour of the black hole, can be tackled using the same methods described here.

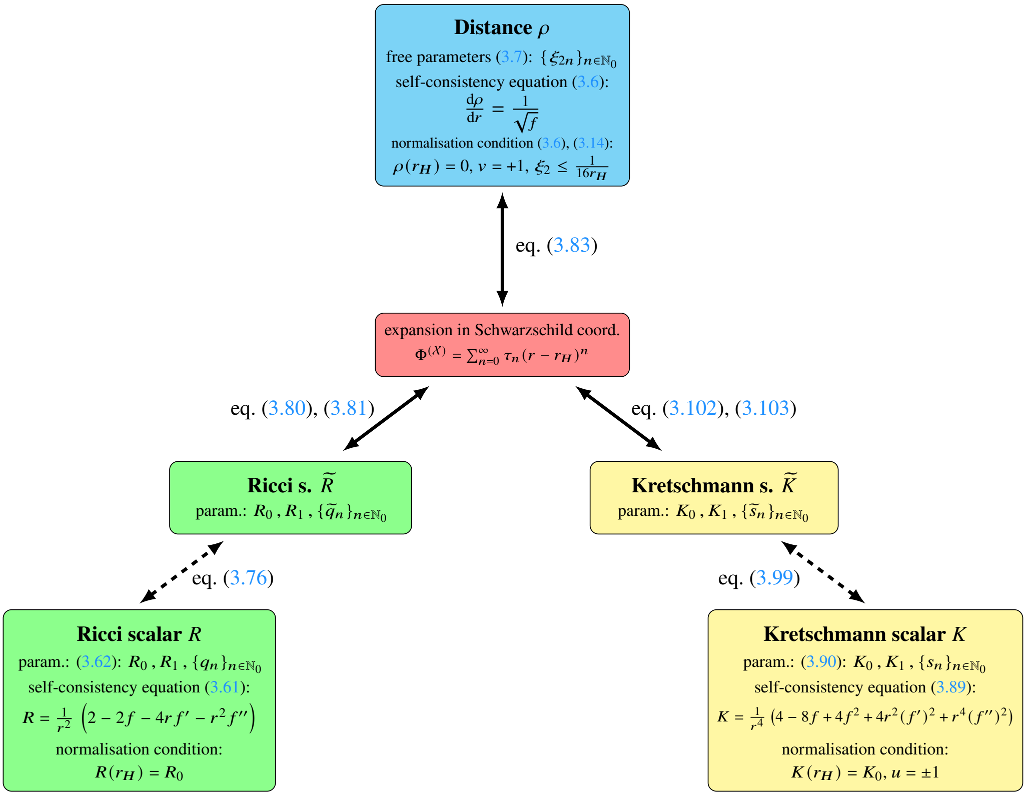

Figure 3.2: Relation between the three EMDs for a deformed Schwarzschild metric discussed in this Chapter.

we find equations which allow to relate the different EMDs to one another. In the case of the EMDs based on curvature invariants, we first perform a slight re-definition of the EMD ((3.76)) and (3.99) respectively), by subtracting the value at the horizon: in this way, the equations relating the (modified) EMD to the distance EMD, can be solved in an iterative fashion.

From a conceptual perspective, the relation between the distance EMD and EMDs based on curvature scalars is non-trivial: indeed, the former is a non-local physical quantity (since it is defined as an integral between two points in space-time), while the latter are local invariants. Nevertheless, at least sufficiently close to the horizon, they are both expected to be monotonic functions of the Schwarzschild coordinate, which thus allows the mapping between the EMDs.

We furthermore also remark that a basic assumption of our work is a sufficient level of regularity of the geometry close to the horizon, such that series expansions remain well-defined. While here we have defined EMDs based on full (*i.e.* infinite) series expansions with suitable radius of convergence, in practice the relations among different EMDs remain (approximately) valid if these series are truncated after certain orders. This property is useful for practical computations, when geometries are approximated by their leading coefficients (see *e.g.* [50, 74] for an example).

3.6 EMD for charged black holes

In order to go beyond the classical geometry of a charged black hole discussed in Sec. 2.1.2, we now introduce deformations in the form of an EMD, keeping the general form (2.24) of the metric and introducing deformations in the functions $f(r)$ and $h(r)$. In order for these deformations to not only be compatible with the symmetries of the classical RN spacetime, but also to be formulated in a universal way, we write them as functions of a physical quantity: indeed, since such a formulation is based on a measurable observable (which needs to be calculable in any given model), this approach allows to directly compare solutions stemming from different theories beyond GR, regardless of model-specific features.

Following the reasoning of the previous Sections, we start by describing the metric within the proper distance-EMD, introduced in Sec. 3.2. Keeping in mind that already the classical RN geometry features generally more than one horizon (*i.e.* a radial position r_0 such that $f(r_0) = 0 = h(r_0)$), in the following we consider r_H the position of the outermost horizon and we shall restrict ourselves to describing the space-time for $r \geq r_H$ (*i.e.* $\rho \geq 0$) which is physically accessible. To this end, we modify the metric functions $f(r)$ and $h(r)$ in (2.24):

$$h(r) = 1 - \frac{2M}{r}\Psi^{(\rho)}(\rho) + \frac{Q^2}{r^2}X^{(\rho)}(\rho)\,, \quad \text{and} \quad f(z) = 1 - \frac{2M}{r}\Phi^{(\rho)}(\rho) + \frac{Q^2}{r^2}\Upsilon^{(\rho)}(\rho)\,, \tag{3.106}$$

with $\Psi^{(\rho)}$, $X^{(\rho)}$, $\Phi^{(\rho)}$ and $\Upsilon^{(\rho)}$ functions that define the ρ EMD (along with the position r_H) and[13]

$$\rho(r) := \int_{r_H}^{r} \frac{\mathrm{d}r'}{\sqrt{|f(r')|}} \quad \text{for} \quad r \geq r_H\,. \tag{3.107}$$

A priori $\Psi^{(\rho)}$, $X^{(\rho)}$, $\Phi^{(\rho)}$ and $\Upsilon^{(\rho)}$ are independent of each other, however, in order to describe an asymptotically flat space-time (similar to the classical RN geometry), we require

$$\lim_{\rho\to\infty}\Phi(\rho) = \lim_{\rho\to\infty}X(\rho) = \lim_{\rho\to\infty}\Psi(\rho) = \lim_{\rho\to\infty}\Upsilon(\rho) = 1, \quad \forall Q \in \mathbb{R}\,. \tag{3.108}$$

Furthermore, in order to have an horizon at $\rho = 0$, we require

$$\Phi_H - \frac{Q^2}{2Mr_H}X_H = \Psi_H - \frac{Q^2}{2Mr_H}\Upsilon_H\,, \qquad \forall Q \in \mathbb{R}\,. \tag{3.109}$$

Therefore, the horizon at $\rho = 0$ constitutes a Killing horizon with a time-like Killing vector $(\chi^t)^\mu = \delta^{0\mu}$:

$$(\chi^t)^\mu(\chi^t)_\mu\big|_{r=r_H} = g_{00}|_{r=r_H} = -h(r_H) = 0\,. \tag{3.110}$$

[13] We remark that (3.106) as well as (3.107) are in principle well defined also for $\rho < 0$, provided that the space-time geometry in the interior of the black hole is still described by a metric. In the following, however, we shall focus exclusively on $\rho \geq 0$, *i.e.* the space-time region outside of the black hole.

3.6.1 Near horizon expansion and EMD coefficients

In the remainder of this section we shall mostly be interested in developing the EMD in a region close to (but outside of) the event horizon located at $\rho = 0$. In order to render the geometry fully manifest, we shall solve (3.107) in the form of a series expansion, using similar techniques developed in Sec. 3.2.

Before entering into the details of the series expansion, we shall first simplify the metric deformations in eq. (3.106). Indeed, locally, the deformation functions $\Psi^{(\rho)}$, $X^{(\rho)}$, $\Phi^{(\rho)}$ and $\Upsilon^{(\rho)}$ can be reabsorbed into only two, which will make computations more compact in the following. Indeed, we shall consider the metric functions

$$f(r) = 1 - \left(\frac{2M}{r} - \frac{Q^2}{r^2}\right)\Gamma^{(\rho)}(\rho)\,, \quad h(r) = 1 - \left(\frac{2M}{r} - \frac{Q^2}{r^2}\right)\Omega^{(\rho)}(\rho)\,, \tag{3.111}$$

where

$$\Gamma^{(\rho)}(\rho) = \frac{2M\,r(\rho)\,\Phi^{(\rho)}(\rho) - Q^2\Upsilon^{(\rho)}(\rho)}{2M\,r(\rho) - Q^2}\,, \quad \Omega^{(\rho)}(\rho) = \frac{2M\,r(\rho)\,\Psi^{(\rho)}(\rho) - Q^2X^{(\rho)}(\rho)}{2M\,r(\rho) - Q^2}\,. \tag{3.112}$$

Here we have used that locally (*i.e.* close to the horizon), r can be written as an invertible function of ρ. Furthermore, for sufficiently small values of ρ, we assume that $\Gamma^{(\rho)}$ and $\Omega^{(\rho)}$ can be expanded in (convergent) power series

$$\Gamma(\rho) = \sum_{n=0}\xi_n\rho^n\,, \qquad \text{and} \qquad \Omega(\rho) = \sum_{n=0}\theta_n\rho^n\,. \tag{3.113}$$

The condition $f(r_H) = 0 = h(r_H)$ implies

$$\xi_0 = \Gamma_H = \frac{r_H^2}{2M\,r_H - Q^2} = \Omega_H = \theta_0\,, \tag{3.114}$$

such that locally, the EMD is *defined* by the expansion coefficients $\{\xi_n, \theta_n\}_{n\in\mathbb{N}}$ (along with r_H), which we consider as physical input parameters that explicitly determine the near horizon geometry. In order to demonstrate this, we shall solve (3.107) in a self-consistent fashion. However, to this end, we shall require the BH to be non-extremal, *i.e.* we shall assume that the metric functions f and h have a simple zero at $r = r_H$ and thus admit series expansions of the form

$$f(r) = f_H^{(1)}(r - r_H) + O\Big((r - r_H)^{3/2}\Big)\,, \quad \text{and} \quad h(r) = h_H^{(1)}(r - r_H) + O\Big((r - r_H)^{3/2}\Big)\,, \tag{3.115}$$

with $f_H^{(1)} \neq 0 \neq h_H^{(1)}$ non-vanishing series coefficients.[14] We also remark that eq. (3.115) guarantees that eq. (3.107) is integrable at r_H and therefore ρ is well-defined:

$$\rho(r) = \frac{2\sqrt{r - r_H}}{\sqrt{f_H^{(1)}}} + O((r - r_H))\,. \tag{3.116}$$

[14] We shall discuss in Section 3.6.5 how to generalise this approach to the extremal case.

As mentioned before, locally this result can be inverted $r(\rho) = r_H + \frac{f_H^{(1)}}{4}\rho^2 + \mathcal{O}(\rho^3)$ and we shall re-write the series (3.8) in the following fashion

$$r = r_H + \sum_{n=1}^{\infty} a_n \rho^n \,. \tag{3.117}$$

In order to find the coefficients $\{a_n\}_{n\in\mathbb{N}}$, we need to solve (3.107) order by order in ρ. To this end, we re-write this equation as the following differential equation

$$r\left(1-\left(\frac{\mathrm{d}r}{\mathrm{d}\rho}\right)^2\right) = \left(2M - \frac{Q^2}{r}\right)\Gamma(\rho)\,. \tag{3.118}$$

Substituting the series (3.113) and (3.117) into (3.118), we find:

$$\begin{aligned}\sum_{p=0}^{\infty}\left(2M\,\xi_p - Q^2\sum_{n=0}^{p}\xi_n\mathfrak{p}_{p-n}\right)\rho^p = r_H(1-a_1^2) + \sum_{p=1}^{\infty}\Bigg[(1-a_1^2)a_p - r_H\sum_{m=1}^{p+1}(p-m+2)m a_m a_{p-m+2}\\ - \sum_{n=1}^{p-1}\sum_{m=1}^{n+1}(n-m+2)m a_{p-n}a_m a_{n-m+2}\Bigg]\rho^p\,,\end{aligned} \tag{3.119}$$

where we have used (3.19) to introduce the coefficients $\mathfrak{p}_n$.

From equation (3.119), we can extract recursive conditions for the coefficients $\{a_n\}_{n\in\mathbb{N}}$: for $p = 1, 2$ and 3, we find

$$\begin{aligned}&r_H^2(1-a_1^2) = r_H 2M\,\xi_0 - Q^2\xi_0\,,\\ &-2a_1 r_H\left(2a_2 r_H + a_1^2 - 1\right) = 2M\,r_H\,\xi_1 + 2M\,a_1\,\xi_0 - Q^2\xi_1\,,\\ &a_1^2\,(1-10a_2 r_H) - 6a_3 a_1 z_H^2 + 2a_2 r_H\,(1-2a_2 r_H) - a_1^4 - a_2 a_1^3 = 2M\,r_H\,\xi_2 + a_1 2M\,\xi_1 + 2M\,a_2\xi_0 - Q^2\xi_2\,.\end{aligned} \tag{3.120}$$

Using (3.114), the first relation indeed implies $a_1 = 0$, in which case the last two equations in (3.120) reduce to

$$\left(2M\,r_H - Q^2\right)\xi_1 = 0\,, \quad \text{and} \quad 2a_2 r_H\,(1-2a_2 r_H) = \left(2M\,r_H - Q^2\right)\xi_2 + 2M\,a_2\,\xi_0\,. \tag{3.121}$$

In this paper, we shall exclusively be interested in the case $Q^2 \neq 2M\,r_H$,[15] in which case the first equation requires $\xi_1 = 0$, which is therefore a constraint on the EMD coefficients. The second equation in (3.121) is a quadratic equation fixes the coefficient a_2:

$$a_2 = \frac{r_H - M\,\xi_0 + \sqrt{(r_H - M\,\xi_0)^2 + 4r_H^2\,\xi_2\,(Q^2 - 2M\,r_H)}}{4r_H^2}\,, \tag{3.122}$$

where the + in front of the square root is chosen to be consistent with the classical RN result when the deformation coefficients ξ_0, ξ_2 are switched off. Moreover eq. (3.122) represents a generalization

[15]Indeed, as we shall discuss in more detail in Section 3.6.5 (see in particular footnote [18]), the black holes with $Q^2 = 2M\,, r_H$ have no classical limit and therefore cannot be understood as small deformations of a geometry that appears as solution in GR. We shall not consider such scenarios in this work.

of the result obtained in eq. (3.13) in Sec. (3.2). The further coefficients of the series (3.117) can uniquely be determined to arbitrary order using the following recursive relation

$$a_p = \frac{1}{1-4p\,r_H a_2}\Bigg[2M\xi_p - Q^2\sum_{n=0}^{p}\xi_n \mathfrak{p}_{p-n} + r_H\sum_{n=3}^{p-1}(p-n+2)na_n a_{p-n+2}+ \\ +\sum_{n=2}^{p-2}\sum_{m=2}^{n}(n-m+2)m a_{p-n}a_m a_{n-m+2}\Bigg] \quad \text{for} \quad p\geq 3\,. \tag{3.123}$$

Notably, switching off the charge $Q \to 0$, one recovers the same iterative relation as in Eq. (3.14) for the uncharged BH (with the proper rescaling with respect to the BH mass).

3.6.2 Hawking temperature and Ricci scalar

Besides $\xi_1 = 0$, we need to impose further constraints on the EMD coefficients $\{\xi_n, \theta_n\}_{n\in\mathbb{N}}$, in order to ensure regularity of the geometry: more concretely, we require finiteness of the Hawking temperature (2.34) and the regularity of the Ricci scalar (2.8).

As discussed in Sec 2.2, the Hawking temperature is given in Eq. (2.34) in terms of $f_H^{(1)}$ and $h_H^{(1)}$ that are given in (3.115). In order to obtain derivatives at the horizon, we first use eq. (3.19) to expand the metric functions in power series in ρ, supposing that the series converge in a neighborhood of the horizon

$$f(\rho) = 1-\left(\frac{2M}{r(\rho)}-\frac{Q^2}{r(\rho)^2}\right)\Gamma^{(\rho)}(\rho) = 1+\sum_{n=0}^{\infty}\left(\sum_{k=0}^{n}\xi_k\left(\sum_{l=0}^{n-k}Q^2\mathfrak{p}_l\mathfrak{p}_{n-k-l}-2M\,\mathfrak{p}_{n-k}\right)\right)\rho^n\,, \tag{3.124}$$

$$h(\rho) = 1-\left(\frac{2M}{r(\rho)}-\frac{Q^2}{r(\rho)^2}\right)\Omega^{(\rho)}(\rho) = 1+\sum_{n=0}^{\infty}\left(\sum_{k=0}^{n}\theta_k\left(\sum_{l=0}^{n-k}Q^2\mathfrak{p}_l\mathfrak{p}_{n-k-l}-2M\,\mathfrak{p}_{n-k}\right)\right)\rho^n\,. \tag{3.125}$$

Using (3.117), we can then locally also write the metric functions as series expansions in $r - r_H$, for which we find to leading order

$$\begin{aligned} f(r) &= \frac{r_H\xi_2\left(Q^2-2M\,r_H\right)+a_2\left(r_H^2-Q^2\xi_0\right)}{a_2 r_H^3}(r-r_H)+\mathcal{O}\Big((r-r_H)^{3/2}\Big)\,,\\ h(r) &= \frac{\theta_1\left(Q^2-2M\,r_H\right)}{\sqrt{a_2}r_H^2}\sqrt{r-r_H}+\left(\frac{\theta_2 r_H\left(Q^2-2M\,r_H\right)-2a_2\theta_0\left(Q^2-M\,r_H\right)}{a_2 r_H^3}+\right.\\ &\left.-\frac{a_3\theta_1\left(Q^2-2M\,z_H\right)}{2a_2^2 r_H^2}\right)(r-r_H)+\mathcal{O}\Big((r-r_H)^{3/2}\Big)\,. \end{aligned} \tag{3.126}$$

Here the a_p are understood to be $a_p = a_p\left(\{\xi_n\}_{2\leq n\leq p}\right)$ through (3.123), which, however, we shall not spell out in the interest of compactness of the notation. For $T_{\rm H}$ in Eq. (2.34) to be well-defined, we first require the term of order $\mathcal{O}\big((r-r_H)^{1/2}\big)$ in the expansion of h to vanish. Recalling that we assumed $Q^2 \neq 2M\,r_H$, this imposes the constraint $\theta_1 = 0$. The Hawking temperature (squared) is then well-defined and can be written as

$$T_{\rm H}^2 = \frac{(r_H^2 - Q^2\xi_0)\left(r_H - M\,\xi_0 + \sqrt{4r_H^2\,\xi_2\,(Q^2 - 2M\,r_H) + (r_H - M\,\xi_0)^2}\right) + 4r_H^3\,\theta_2\,(Q^2 - 2M\,r_H)}{16\pi^2\,r_H^5}\,. \tag{3.127}$$

Since ξ_0 is given in (3.114), from the coefficients defining the EMD, the Hawking temperature depends only on three deformation parameters which are r_H, ξ_2 and θ_2. Among these, we furthermore require

$$\xi_2 \leq \frac{(r_H - M\,\xi_0)^2}{4r_H^2\,(2M\,r_H - Q^2)}\,,\ \theta_2 < \frac{\left(r_H - M\,\xi_0 + \sqrt{4r_H^2\,\xi_2\,(Q^2 - 2M\,r_H) + (r_H - M\,\xi_0)^2}\right)(r_H^2 - Q^2\xi_0)}{4r_H^3\,(2M\,r_H - Q^2)}\,, \tag{3.128}$$

to ensure that $T_H \in \mathbb{R}_+$. Finally, we also require the that the Ricci scalar R is regular at the horizon. The constraints imposed above are not sufficient to make the Ricci finite. Indeed, a residual divergence is still present at the horizon, *i.e.* $R \propto \rho^{-1}$. The exact expression for the divergent term of R is not relevant, however, it vanishes provided

$$\xi_3 = \frac{1}{2}\theta_3\left(\frac{3\varpi\,(Q^2 - 2M\,r_H)}{2(M\,r_H - Q^2)} - 1\right)\,,\quad \text{with}\quad \varpi = 2\sqrt{\frac{4\xi_2\,(Q^2 - 2M\,r_H)^3 + (Q^2 - M\,r_H)^2}{(Q^2 - 2M\,r_H)^2}}\,. \tag{3.129}$$

This constraint smoothly reduces to the condition found in Eq. (3.32) in the limit $Q \to 0$ and $(\xi_n, \theta_n) \mapsto (2M)^{-n}(\xi_n, \theta_n)$.

3.6.3 Small charge expansion

The aim of this subsection is to provide a description of the Hawking temperature $T_{\rm H}$ for a (quantum) deformed black hole in presence of a small charge Q. In this approximation, the deformations receive sub-leading corrections in Q: the presence of a charge enters the equations at the same order as in the classical small charge limit. We shall use a subscript $_*$ to indicate that a quantity is evaluated for $Q = 0$. In order to give a concrete example, we assume that the radial coordinate evaluated at the horizon can be written in the form

$$r_H = r_* - \frac{Q^2}{2M} + O(Q^3)\,, \tag{3.130}$$

Implementing these approximations into the temperature (3.127), one gets:

$$T_{\rm H} = T_* - \frac{(8M\,r_*\,(\xi_{2*}\,(32M\,\theta_{2*}\,r_* - 10\varpi_* - 6) - \theta_{2*}) + 3\varpi_*)}{512\pi^2 M^2\,r_*^4\varpi_* T_*}Q^4 + O(Q^5)\,, \tag{3.131}$$

in which T_* represents the Hawking temperature for the uncharged black hole defined as in 3.2, that we now rewrite with the re-scaled coefficeints as follows:

$$T_* = \frac{\sqrt{1 + \varpi_* - 8M\,\theta_{2*} r_*}}{4\pi\,r_*}\,,\qquad \varpi_* = \sqrt{1 - 32M\,\xi_{2*}\,r_*}\,. \tag{3.132}$$

Thus, the assumption (3.130) leads to corrections of the temperature of order Q^4, which matches predictions by semi-classical approximations [164]. However, the correction differs from the classical prediction by the presence of the derivatives of the deformation functions, which enter in a non trivial way.

Other computations have been carried out to improve the semi-classical result, such as implementing EFT techniques [165]. In this reference, the author derives corrections to the horizon position stemming from higher curvature terms in the action, which affect the behavior of the Hawking temperature in the small charge regime, and which are in fact not of the form we have assumed in (3.130). Consequently, the expression for the temperature found in [165] exhibits corrections at order $O(Q^2)$, differing from (3.131), which shows modifications proportional to $O(Q^4)$.

3.6.4 Solution of the Maxwell field

Once the divergences of the Ricci scalar have been removed, and the Hawking temperature T_{H} is well-defined, one can study the behaviour of the modified electromagnetic tensor $F_{\mu\nu}$.
We suppose that deformations due to (quantum) gravitational effects generated by a spherical source preserve the spherical symmetry. Because of this, one may add deformations to the classical field strength tensor $F^{\mathrm{cl}}_{\mu\nu}$ which only depends on the radial coordinate r:

$$F_{\mu\nu} = -F_{\nu\mu} = F^{\mathrm{cl}}_{\mu\nu} + F^{\mathrm{def}}_{\mu\nu} , \tag{3.133}$$

where $F^{\mathrm{cl}}_{rt} = E_r$ and $F^{\mathrm{cl}}_{\theta\varphi} = B_r$ are given in Eq. (2.25), with $Q^2 = q^2 + m^2$ as defined in Sec. 2.1.2, and we define

$$E^{\mathrm{def}}_r = F^{\mathrm{def}}_{rt} := w(r) , \qquad \text{and} \qquad B^{\mathrm{def}}_r = \frac{F^{\mathrm{def}}_{\theta\phi}}{r^2 \sin\theta} := k(r) , \tag{3.134}$$

in which $w(r)$ and $k(r)$ are unknown functions of the radial coordinate. The first Maxwell equations in Eq. (2.23) can be written as:

$$\partial_\mu \left(\sqrt{-g} F^{\mu\nu}\right) = 0 , \qquad \text{with} \qquad g := \det g_{\mu\nu} = -\frac{h(r)}{f(r)} r^4 \sin^2\theta , \tag{3.135}$$

which imply:

$$\left(\partial_r \sqrt{-g}\right) F^{rt} + \sqrt{-g}\left(\partial_r F^{rt}\right) = 0 , \tag{3.136}$$

$$\left(\partial_\theta \sqrt{-g}\right) F^{\theta\phi} + \sqrt{-g}\left(\partial_\theta F^{\theta\phi}\right) = 0 , \tag{3.137}$$

The first equation in (3.136) gives the following condition for $w(z)$:

$$w(r) = -\frac{q}{r^2} + \frac{c_1}{r^2}\sqrt{\frac{h(r)}{f(r)}} , \tag{3.138}$$

where c_1 is a constant, which can be fixed requiring $w(r) = 0$ when the deformations are switched off. This condition yields $c_1 = q$. On the other hand, equation (3.137) is always satisfied, independently of the choice of $k(r)$.

Regarding the Bianchi identity

$$\partial_\mu F_{\nu\rho} + \partial_\nu F_{\rho\mu} + \partial_\rho F_{\mu\nu} = 0 , \tag{3.139}$$

the only non-trivial condition is $\partial_r F_{\theta\phi} = 0$, which implies $\partial_r [r^2 k(r)] = 0$ and which gives the following solution for $k(r)$

$$k(r) = \frac{c_2}{r^2} \,, \tag{3.140}$$

where c_2 is an integration constant which must be determined. One can fix the latter by requiring that when $k(r) \to 0$, the classical result is reproduced. Indeed, this is satisfied if $c_2 = 0$. Then, the overall expression for the non-trivial components of $F_{\mu\nu}$ take the following form:

$$-F_{tr} = F_{rt} = \frac{q}{r^2}\sqrt{\frac{h(r)}{f(r)}} = \frac{q}{r^2}\frac{\sqrt{Q^2\Omega^{(\rho)}(\rho) - 2M\,r\,\Omega^{(\rho)}(\rho) + r^2}}{\sqrt{Q^2\Gamma^{(\rho)}(\rho) - 2M\,r\,\Gamma^{(\rho)}(\rho) + r^2}} \,, \qquad -F_{\phi\theta} = F_{\theta\phi} = m\sin\theta \,. \tag{3.141}$$

In summary, the electric field gets modified by the factor $\sqrt{\frac{h(r)}{f(r)}}$, while the magnetic field remains unchanged with respect to the classical one. This is not surprising, since the metric deformations (3.111) were introduced in a way to keep the geometry static.

3.6.5 Effective description of an extremal BH

In this Section we develop an EMD for extremal (charged), spherically symmetric and static black holes. Extremality in this context amounts to assuming that the metric functions f and h have higher order zeros at the horizon (when seen as functions of $r - r_H$): concretely, this amounts to assuming that $f_H^{(1)}$ in (3.115) (and its counterpart $h_H^{(1)}$) vanish. In more physical terms, this condition also implies that the surface gravity given in Eq. (2.28) of the black hole vanishes.

From a technical perspective, $f_H^{(1)} = 0$ renders the expansion in Eq. (3.116) (and all subsequent steps depending on it) ill-defined. This problem can also be understood from the definition of the distance in eq. (3.107): indeed, f having a second order zero at $r = r_H$ introduces a non-integrable singularity at the horizon and therefore makes the distance ρ of a space-time point to the horizon logarithmically divergent. Thus, in the case of extremal spherically symmetric and static black holes, the (spatial) distance is not a suitable physical quantity to define an EMD, at least in the immediate vicinity of the horizon. In the following, we shall therefore introduce an EMD based on the proper time of a free-falling observer (see [74] for the full EMD developed in the case of uncharged black holes), which can be generalized also to the extremal case.

EMD based on Proper Time

We introduce the proper time τ as the time that a free-falling, time-like observer measures along a radial geodesic. Let us recall a generic static spherically symmetric metric

$$ds^2 = -h(r)dt^2 + \frac{dr^2}{f(r)} + r^2 d\theta^2 + r^2\sin^2\theta d\phi^2 \,, \tag{3.142}$$

the infinitesimal distance for a geodesic radial motion in the equatorial plane, *i.e.* for $\theta = \pi/2$, is

$$-d\tau^2 = \frac{u\,h(r)}{f(r)}\frac{dr^2}{(1 + u\,h(r))} \,, \tag{3.143}$$

where the choice $u = +1$ or -1 correspond, respectively, to either a space-like or a time-like radial geodesic. Thus, the finite proper time $\tau(r)$ that a time-like observer measures to fall from a point in space-time labeled by r to the event horizon at r_H is

$$\tau(r) = \int_{r_H}^{r} \sqrt{\frac{h(r')}{f(r')}} \frac{\mathrm{d}r'}{\sqrt{1 - h(r')}} . \tag{3.144}$$

Here the overall sign has been fixed to represent an in-falling motion along the geodesic. As an example, we consider the classical Reissner-Nordström black hole geometry, which is characterised by $f(r) = h(r) = 1 - \frac{2M}{r} + \frac{Q^2}{r^2}$. In this case, the proper time for a a radially in-falling time-like observer can be written in the form

$$\tau(r) = \frac{M}{3}\left(\mathfrak{q}^2\left(\sqrt{2\mathfrak{r} - \mathfrak{q}^2} - \sqrt{2\mathfrak{r}_H - \mathfrak{q}^2}\right) + \mathfrak{r}\sqrt{2\mathfrak{r} - \mathfrak{q}^2} - \mathfrak{r}_H\sqrt{2\mathfrak{r}_H - \mathfrak{q}^2}\right) , \tag{3.145}$$

with the short-hand notation

$$\mathfrak{q} = \frac{|Q|}{M} , \qquad \mathfrak{r} = \frac{r}{M} , \qquad \mathfrak{r}_H = \frac{r_H}{M} = 1 + \sqrt{1 - \mathfrak{q}^2} . \tag{3.146}$$

The proper time (3.145) is schematically shown in Figure 3.3 for different values of the charge-to-mass ratio $\mathfrak{q} \in [0, 1]$. The case $\mathfrak{q} = 0$ corresponds to the un-charged (Schwarzschild) black hole,

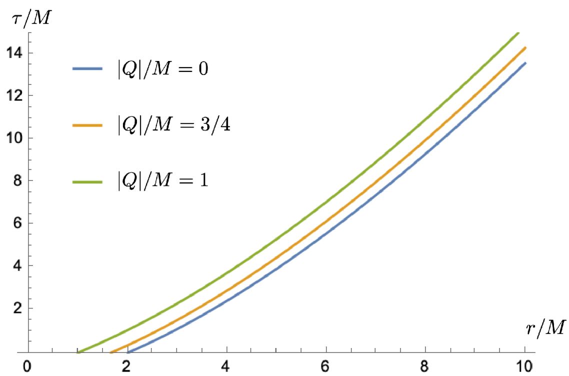

Figure 3.3: Proper time measured by a time-like observer falling along a radial geodesic from a space-time point labeled by r to the horizon of a Reissner-Nordström black hole, as given in (3.145). The case $|Q|/M = 1$ represents the extremal case, which is still a finite function.

while the extremal case is $\mathfrak{q} = 1$.[16] As can be seen from Figure 3.3, $\tau(r)$ remains a finite function (even for $\mathfrak{q} = 1$) at the horizon located at $r_H = M\,\mathfrak{r}_H = M(1 + \sqrt{1 - \mathfrak{q}^2})$, where $\tau(r_H) = 0$. We next write the metric-deformation functions f and h in eq. (3.142) in terms of τ as follows

$$f(r) = 1 - \left(\frac{2M}{r} - \frac{Q^2}{r^2}\right)\Gamma^{(\tau)}(\tau) \quad \text{and} \quad h(r) = 1 - \left(\frac{2M}{r} - \frac{Q^2}{r^2}\right)\Omega^{(\tau)}(\tau) . \tag{3.147}$$

[16] $\mathfrak{q} > 1$ does not represent a black hole geometry, but rather a naked singularity, which is generally considered unphysical (cf. Sec. 2.1.2).

Here, the functions $\Gamma^{(\tau)}(\tau)$ and $\Omega^{(\tau)}(\tau)$ (along with r_H) define the EMD based on the proper time τ. In order to avoid confusion with the EMD based on the spatial distance to the horizon,[17] as discussed in Section 3.6.1, and now we expand the functions in power series of the proper time from the horizon in the following manner

$$\Gamma^{(\tau)}(\tau) = \sum_{n=0}^{\infty} \widetilde{\xi}_n \tau^n \,, \qquad \Omega^{(\tau)}(\tau) = \sum_{n=0}^{\infty} \widetilde{\theta}_n \tau^n \,, \qquad \text{with} \qquad \widetilde{\xi}_n\,,\widetilde{\theta}_n \in \mathbb{R}\,. \tag{3.148}$$

In order to solve (3.144) iteratively, we also introduce the expansions

$$r = r_H + \sum_{n=1}^{\infty} \widetilde{a}_n \tau^n \,, \qquad \tau(r) = \sum_{n=1}^{\infty} \widetilde{b}_n\,(r-r_H)^n \,, \qquad \text{with} \qquad \widetilde{a}_n\,,\widetilde{b}_n \in \mathbb{R}\,, \tag{3.149}$$

where the coefficients $\{\widetilde{a}_n\}_{n\in\mathbb{N}}$ are implicitly determined by (3.144), while $(\widetilde{b}_n)_{n\in\mathbb{N}}$ are fixed through series inversion [46, 47, 166]. Notably, for the first few instances we find (see also [74])

$$\widetilde{b}_1 = \frac{1}{\widetilde{a}_1}\,, \qquad \widetilde{b}_2 = -\frac{\widetilde{a}_2}{\widetilde{a}_1^3}\,, \qquad \widetilde{b}_3 = \frac{2\widetilde{a}_2^2 - \widetilde{a}_1\widetilde{a}_3}{\widetilde{a}_1^5}\,, \qquad \widetilde{b}_4 = \frac{5\widetilde{a}_1\widetilde{a}_2\widetilde{a}_3 - 5\widetilde{a}_2^3 - \widetilde{a}_1^2\widetilde{a}_4}{\widetilde{a}_1^7}\,. \tag{3.150}$$

In order to represent a black hole horizon, the metric functions f and h in (3.147) need to vanish for $r \longrightarrow r_H$, which is equivalent to $\tau \longrightarrow 0$. Since (3.148) and (3.149) lead to

$$f(r) = \left(1 - \frac{\widetilde{\xi}_0(2M\,r_H - Q^2)}{r_H^2}\right) + O(r-r_H)\,, \quad h(r) = \left(1 - \frac{\widetilde{\theta}_0(2M\,r_H - Q^2)}{r_H^2}\right) + O(r-r_H)\,, \tag{3.151}$$

$\widetilde{\xi}_0$ and $\widetilde{\theta}_0$ cannot be arbitrary, but need to satisfy

$$\widetilde{\xi}_0 = \frac{r_H^2}{2M\,r_H - Q^2} = \widetilde{\theta}_0\,. \tag{3.152}$$

Here, for simplicity, we restrict to the case $2M\,r_H \neq Q^2$.[18] Among the remaining parameters, we consider $\{\widetilde{\xi}_n\}_{n\in\mathbb{N}}$ and $\{\widetilde{\theta}_n\}_{n\in\mathbb{N}}$ along with r_H, Q and M as (physical) input parameters to the black hole geometry (outside of the horizon) and thus the EMD coefficients. Indeed, the coefficients $\{\widetilde{a}_n\}_{n\in\mathbb{N}}$ (and thus through (3.150) also $\{\widetilde{b}_n\}_{n\in\mathbb{N}}$) are fixed by expanding (3.144) order by order in $(r-r_H)$. Notably, using (3.152), we find to leading order $O(r-r_H)$

$$\widetilde{a}_1 = \sqrt{\frac{\widetilde{\xi}_1(Q^2-2M\,r_H)^2 + 2\widetilde{a}_1\,r_H(Q^2-M\,r_H)}{\widetilde{\theta}_1(Q^2-2M\,r_H)^2 + 2\widetilde{a}_1\,r_H(Q^2-M\,r_H)}}\,, \tag{3.153}$$

where we have implicitly assumed that the right hand side is well-defined, which, as we shall see in the following Subsection, is related to the behaviour of the subleading terms in (3.151): concretely,

[17] Since both ρ and τ are monotonic functions of r in the vicinity of the horizon and finite in the non-extremal case, we remark that the EMDs based on the two quantities are therefore equivalent and one can be expressed in terms of the other. As mentioned before, this is no longer possible in the extremal case.

[18] In the classical case, this condition is equivalent to $\mathfrak{q}^2 \neq 2(1+\sqrt{1-\mathfrak{q}^2})$, which is always satisfied over the reals, notably for $\mathfrak{q} \in [0,1]$. Thus, deformed black holes with $2M\,r_H = Q^2$ have no classical limit, which is why we do not discuss them in the following.

it is related to the non-vanishing of the terms of order $\mathcal{O}(r - r_H)$ and thus assumes that $r = r_H$ constitutes a *simple* horizon. In this case, $\widetilde{a}_1$ is fixed in terms of $(\widetilde{\xi}_1, \widetilde{\theta}_1, Q, r_H, M)$.[19] Higher orders $\mathcal{O}((r - r_H)^p)$ (for $p > 1$) in (3.144) only depend on $\widetilde{a}_{p'}$ with $p' \leq p$ and are linear in $\widetilde{a}_p$. These equations therefore uniquely fix the expansion (3.149), and therefore the black hole geometry (see also [74] for a more detailed discussion in a related case). The proper time allows therefore for an EMD that is capable of describing the charged black hole geometry. We also remark in passing that the condition for $\widetilde{a}_1 \in \mathbb{R}$ in (3.153) as well $f(r) > 0$ and $h(r) > 0$ for $r > r_H$ requires

$$(Q^2 - 2M\,r_H)\,\widetilde{\xi}_1 > -2\widetilde{a}_1\,r_H\,\frac{Q^2 - M\,r_H}{Q^2 - 2M\,r_H}\,, \quad \text{and} \quad (Q^2 - 2M\,r_H)\,\widetilde{\theta}_1 > -2\widetilde{a}_1\,r_H\,\frac{Q^2 - M\,r_H}{Q^2 - 2M\,r_H}\,, \tag{3.154}$$

with $\widetilde{a}_1$ fixed from (3.153). Finally, unlike the EMD based on the spatial proper distance, finiteness of curvature invariants such as the Ricci- and Kretschmann scalar pose no further constraints on the parameter space, since the second derivatives of f and h are finite at the horizon.

Extremal Black Holes

General Charged Extremal Black Holes In the previous Subsection, we have argued for an EMD of charged, spherically symmetric black holes in terms of the proper time (3.144): indeed, by inserting (3.148) and (3.149), Eq. (3.144) can be expanded in powers of $(r - r_H)$, which provides conditions on the coefficients $\{\widetilde{a}_n\}_{n\in\mathbb{N}}$ and in fact fixes them iteratively in terms of $\Big(\{\widetilde{\xi}_n\}_{n\in\mathbb{N}}, \{\widetilde{\theta}_n\}_{n\in\mathbb{N}}, Q, r_H, M\Big)$. Here we are interested in the question, which regions of this parameter space allow for *extremal* (charged) black holes. Since these are characterised by the fact that $r = r_H$ is a double zero of f and h in (3.147), we have to impose in addition to (3.152) also the vanishing of the term of order $\mathcal{O}(r - r_H)$ in (3.151):

$$\frac{\widetilde{\xi}_1(Q^2 - 2M\,r_H)^2 + 2\widetilde{a}_1\,r_H(Q^2 - M\,r_H)}{\widetilde{a}_1\,r_H^2(Q^2 - 2M\,r_H)} = 0\,, \quad \text{and} \quad \frac{\widetilde{\theta}_1(Q^2 - 2M\,r_H)^2 + 2\widetilde{a}_1\,r_H(Q^2 - M\,r_H)}{\widetilde{a}_1\,r_H^2(Q^2 - 2M\,r_H)} = 0\,. \tag{3.155}$$

Imposing these conditions renders the right hand side of (3.153) ill-defined and indeed, the leading order term $\mathcal{O}(r - r_H)$ of (3.144) instead becomes

$$\widetilde{a}_1 = \sqrt{\frac{\widetilde{a}_1^2\,Q^4 + (Q^2 - 2M\,r_H)\left(\widetilde{\xi}_2(Q^2 - 2M\,r_H)^2 + 2\widetilde{a}_2 r_H(Q^2 - M\,r_H)\right)}{\widetilde{a}_1^2\,Q^4 + (Q^2 - 2M\,r_H)\left(\widetilde{\theta}_2(Q^2 - 2M\,r_H)^2 + 2\widetilde{a}_2 r_H(Q^2 - M\,r_H)\right)}}\,. \tag{3.156}$$

This equation is qualitatively quite different from (3.153) and (in conjunction with (3.155)) the type of possible solutions depend more heavily on the remaining parameters. Recalling that we still consider $Q^2 \neq 2M\,r_H$, we may distinguish the following subspaces of the parameter space:

(i) $Q^2 \neq M\,r_H$: In this case, the parameter subspace can further be subdivided by considering (see Appendix A.5 for more details)

[19] Although (3.153) has multiple solutions, generally only one of them leads to $\widetilde{a}_1 \in \mathbb{R}$.

- $\widetilde{\xi}_2 = \widetilde{\theta}_2$: In this case, the only solution of (3.156) is $\widetilde{a}_1 = 1$ such that (3.155) can be used to fix

$$\widetilde{\xi}_1 = \widetilde{\theta}_1 = -\frac{2r_H(Q^2 - M\,r_H)}{(Q^2 - 2M\,r_H)^2}\,. \tag{3.157}$$

  Higher order terms $O((r - r_H)^p)$ (for $p > 1$) in the expansion of (3.144) are linear in $\widetilde{a}_p$ (and only contain $\widetilde{a}_{p'}$ with $p' \leq p$), thus uniquely fixing the expansion (3.149) and therefore allowing to define an EMD for an extremal charged black hole, which is parametrised by $\left(\{\widetilde{\xi}_n\}_{n\geq 2}\,, \{\widetilde{\theta}_n\}_{n\geq 2}\,, Q\,, r_H\,, M\right)$.

- $\widetilde{\xi}_2 \neq \widetilde{\theta}_2$: In this case, $\widetilde{a}_2$ does not disappear from the equation (3.156). Moreover, all higher order terms $O((r - r_H)^p)$ (for $p > 1$) in the expansion of (3.144) also acquire a linear dependence on $\widetilde{a}_{p+1}$ (but remain independent of all $\widetilde{a}_{p'}$ with $p' > p + 1$).[20] We therefore use the condition (3.155) to fix

$$\widetilde{\theta}_1 = \widetilde{\xi}_1\,, \qquad \text{and} \qquad \widetilde{a}_1 = \widetilde{\xi}_1\left(2M - \frac{Q^4}{2r_H(Q^2 - M\,r_H)}\right), \tag{3.158}$$

  leaving $\widetilde{\xi}_1$ as an undetermined free parameter. Eq. (3.156) then determines $\widetilde{a}_2$ and the higher order terms $O((r - r_H)^p)$ in (3.144) uniquely fix $\widetilde{a}_{p+1}$ uniquely, without further constraints on any of the $\widetilde{\xi}_n$ and $\widetilde{\theta}_n$, thus leading to an EMD of an extremal charged black hole parametrised by $\left(\{\widetilde{\xi}_n\}_{n\geq 1}\,, \{\widetilde{\theta}_n\}_{n\geq 2}\,, Q\,, r_H\,, M\right)$.

(ii) $Q^2 = M\,r_H$: In this case, (3.155) is solved by $\widetilde{\xi}_1 = 0 = \widetilde{\theta}_1$, while (3.156) fixes $\widetilde{a}_1$ (irrespective of $\widetilde{\xi}_2 = \widetilde{\theta}_2$ or not). Assuming the latter to be non-negative, there are two possible solutions

$$\widetilde{a}_1 = \frac{1}{\sqrt{2}}\sqrt{1 + M\,r_H\,\widetilde{\theta}_2 \pm \sqrt{(1 + M\,r_H\,\widetilde{\theta}_2)^2 - 4M\,r_H\widetilde{\xi}_2}}\,. \tag{3.159}$$

For $\widetilde{\xi}_2, \widetilde{\theta}_2 \longrightarrow 0$ (*i.e.* in the classical case), these become $\widetilde{a}_1 = 1$ and $\widetilde{a}_1 = 0$ respectively. We furthermore assume $\widetilde{a}_1$ to be real, which in particular requires

$$\widetilde{\xi}_2 \leq \frac{(1 + M\,r_H\widetilde{\theta}_2)^2}{4M\,r_H}\,, \qquad \text{and} \qquad \widetilde{\theta}_2 \geq -\frac{1}{M\,r_H} \quad \text{if } \widetilde{\xi}_2 > 0\,, \tag{3.160}$$

The higher order terms $O((r - r_H)^p)$ in (3.144) provide linear relations to uniquely fix $\widetilde{a}_p$, without further constraints on any of the $\widetilde{\xi}_n$ and $\widetilde{\theta}_n$. The region in parameter space $Q^2 = M\,r_H$ therefore leads to an EMD of an extremal charged black hole parametrised by $\left(\{\widetilde{\xi}_n\}_{n\geq 2}\,, \{\widetilde{\theta}_n\}_{n\geq 2}\,, r_H\,, M\right)$.

Furthermore, in all cases, the remaining free parameters still need to be chosen such that

$$f(r) > 0\,, \qquad \text{and} \qquad h(r) > 0\,, \qquad \forall r \geq r_H\,, \tag{3.161}$$

which gives rise to further non-trivial inequalities. However, finiteness of curvature invariants such as the Ricci scalar pose no further constraints also in the extremal case, since the second derivatives of f and h remain finite at the horizon.

[20] We have checked up to $p = 5$, that the term $O((r - r_H)^p)$ in (3.144) depends linearly on $\widetilde{a}_{p+1}$, provided that $\widetilde{\xi}_2 \neq \widetilde{\theta}_2$ and $Q^2 \neq M\,r_H$ (as well as $Q^2 \neq 2M\,r_H$).

Deformed Extremal Reissner-Nordström Geometry Since the above conditions are complicated to represent in full generality (see Appendix A.5), we shall here analyse them in the case of a BH that represents a small deformation of the extremal Reissner-Nordström geometry. In order to parametrise this case within the remaining parameter space, we introduce

$$\epsilon := \frac{M - r_H}{r_H}\,, \qquad \widetilde{\xi}_n := \frac{x_n}{M^n}\,, \qquad \widetilde{\theta}_n := \frac{t_n}{M^n}\,, \tag{3.162}$$

where $\epsilon > -1$ is defined in analogy as in Rezzolla-Zhidenko paramterization [68], which we will discuss in Chapter 6, and is understood as a small deformation parameter. Notice in particular that $r_H = \frac{M}{1+\epsilon}$. In the following, we shall discuss the case *(i)* to leading order in ϵ, while *(ii)* can be compactly discussed to all orders for $\epsilon > -1$:

(i) In order for a black hole in the parameter space with $Q^2 \neq M\, r_H$ to represent a small deformation of the extremal RN geometry, we need to consider ϵ to be a small parameter and shall discuss effects to leading order. In particular, we shall assume

$$x_n = \epsilon\, x_n^{(1)} + \mathcal{O}(\epsilon^2)\,, \quad \text{and} \quad t_n = \epsilon\, t_n^{(1)} + \mathcal{O}(\epsilon^2)\,, \quad \forall n \geq 1\,, \quad |Q| = M(1 + q\,\epsilon) + \mathcal{O}(\epsilon^2)\,, \tag{3.163}$$

where

$$x_n^{(p)} := \left.\frac{\mathrm{d}^p x_n}{\mathrm{d}\epsilon^p}\right|_{\epsilon=0}\,, \quad t_n^{(p)} := \left.\frac{\mathrm{d}^p t_n}{\mathrm{d}\epsilon^p}\right|_{\epsilon=0} \quad \text{and} \quad q := \left.\frac{\mathrm{d}(|Q|/M)}{\mathrm{d}\epsilon}\right|_{\epsilon=0}\,, \tag{3.164}$$

which allows to write for the coefficients in (3.149)

$$\widetilde{a}_n = \widetilde{a}_n^{(0)} + \epsilon\, \widetilde{a}_n^{(1)} + \mathcal{O}(\epsilon^2)\,, \qquad \text{with} \qquad \begin{cases} \widetilde{a}_1^{(0)} = 1\,, \\ \widetilde{a}_2^{(0)} = 0\,, \\ \widetilde{a}_3^{(0)} = -\frac{1}{6M^2}\,. \end{cases} \tag{3.165}$$

Furthermore, to leading order in ϵ, eq. (3.152) and (3.155) impose respectively

$$\widetilde{\xi}_0 = \widetilde{\theta}_0 = 1 + 2q\,\epsilon + \mathcal{O}(\epsilon^2)\,, \qquad \text{and} \qquad t_1^{(1)} = -2(1+2q) = x_1^{(1)}\,, \tag{3.166}$$

while (3.156) (and higher orders in the expansion of (3.144)) uniquely fix the leading deformations $\widetilde{a}_n^{(1)}$, *i.e.* for all values of $x_2^{(1)}$ and $t_2^{(1)}$ we find at leading order in ϵ

$$\begin{aligned} \widetilde{a}_1^{(1)} &= \frac{t_2^{(1)} - x_2^{(1)}}{2}\,, \qquad \widetilde{a}_2^{(1)} = \frac{2(t_2^{(1)} - x_2^{(1)}) + t_3^{(1)} - x_3^{(1)}}{4M}\,, \\ \widetilde{a}_3^{(1)} &= -\frac{36 + 48q + t_2^{(1)} - 7x_2^{(1)} - 12(t_3^{(1)} - x_3^{(1)}) - 6(t_4^{(1)} - x_4^{(1)})}{36M^2}\,. \end{aligned} \tag{3.167}$$

Finally, the conditions (3.161) become to leading order

$$1 + (6 + 8q - x_2^{(1)})\epsilon > 0\,, \qquad \text{and} \qquad 1 + (6 + 8q - t_2^{(1)})\epsilon > 0\,. \tag{3.168}$$

(ii) For the RN geometry, the extremality condition corresponds to $Q^2 = M^2$, which leads to $r_H = M$ ($\epsilon = 0$) and thus $Q^2 = M\, r_H$. The latter relation can therefore be understood as

a deformation of the classical case for any value of $\epsilon > -1$. Furthermore, since $\widetilde{a}_1 = 1$ classically, we shall focus on the positive sign in (3.159):

$$\widetilde{a}_1 = \frac{\sqrt{1+\epsilon+t_2+\sqrt{(1+\epsilon+t_2)^2-4(1+\epsilon)x_2}}}{\sqrt{2(1+\epsilon)}} \tag{3.169}$$

Finally, the conditions (3.161) can be formulated as follows

$$\begin{cases} x_2 < 0 & \text{if} \quad t_2 \leq -(1+\epsilon)\,, \\ x_2 \leq \frac{(1+\epsilon+t_2)^2}{4(1+\epsilon)} & \text{if} \quad -(1+\epsilon) < t_2 < 1+\epsilon\,, \\ x_2 < t_2 & \text{if} \quad t_2 \geq 1+\epsilon\,. \end{cases} \tag{3.170}$$

These conditions are represented by the green region in Figure 3.4: the interior satisfies the inequalities (3.161), while only the solid black line of its boundary is compatible.

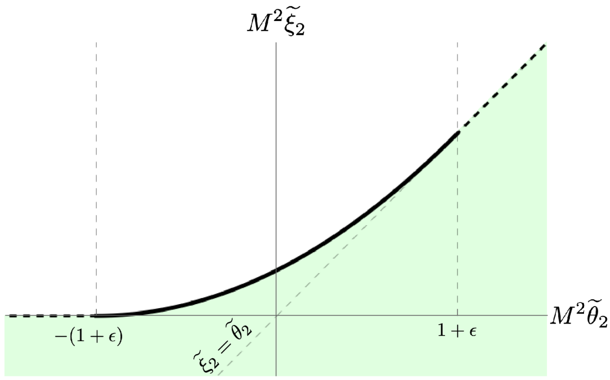

Figure 3.4: Allowed parameter region of $\widetilde{\xi}_2$ and $\widetilde{\theta}_2$ in the case $Q^2 = M\, r_H$. The interior of the green coloured region leads to extremal geometries satisfying all relevant conditions. On its boundary, only the solid black line is allowed, while the dashed black line is excluded.

4 Applications

In this Chapter, we illustrate applications of the approach presented in the previous Sections, in particular, the conditions (3.32) which are sufficient for a finite Ricci scalar at the horizon, we shall consider five concrete examples: the first one is the specifically constructed metric to satisfy (3.32) in a minimal fashion. The second one is Bonanno-Reuter [157] black hole arising from the Asymptotically safe quantum gravity program. The third and fourth examples are the the Hayward black hole [24] and the Dymnikova space-time [167], and although we are aware that these examples do not exhibit any divergent physical quantities, it is still interesting to demonstrate how our approach can be applied to deformation functions that explicitly depend on coordinates other than the proper distance. The last application is the electrically charged Frolov spacetime [32] in the case of extremal BH. Finally, we discuss a connection of our framework to the Weak Gravity Conjecture within the Swampland program [168–170] and discuss the efficiency of the approach to describe the proper distance within some models.

4.1 Minimal metric deformation

As a first example, we introduce a novel model which is an *ad hoc* construction based on the constraints (3.32). The physical motivations behind such toy model are irrelevant as we aim at showing the utility of the framework a model-building tool. We consider the following form of the metric function

$$h_{\mathrm{MM}}(r) = f_{\mathrm{MM}}(r) = 1 - \frac{2M}{r} e^{\Phi\left(\frac{1}{d_H+\rho(r)}\right)} \,, \tag{4.1}$$

We can model the deformation Φ in such a way to abide by a minimal set of conditions. Namely, the requirements that the Ricci scalar is finite at the horizon, summarized in eq. (3.32), and that all the derivatives of Φ on the horizon of order higher than the third vanish translate into the following conditions:

$$\Phi_H = \phi_0 \,, \quad \Phi_H^{(1)} = 0 \,, \quad \Phi_H^{(2)} = \phi_2 \,, \quad \Phi_H^{(3)} = -6 d_H \phi_2 \quad \text{and} \quad \Phi_H^{(n)} = 0 \quad \forall n \geq 4 \,. \tag{4.2}$$

The solution to (4.2) can be written compactly in the form

$$\Phi\left(\frac{1}{d_H+\rho}\right) = \phi_0 + \frac{\rho^2(d_H+3\rho)\phi_2}{2d_H^2(d_H+\rho)^3} \,. \tag{4.3}$$

Here we consider d_H as a parameter of the model, which encodes information about the interior of the black hole. Moreover, $\phi_0, \phi_2 \in \mathbb{R}$ are arbitrary parameters, which, however, are not independent:

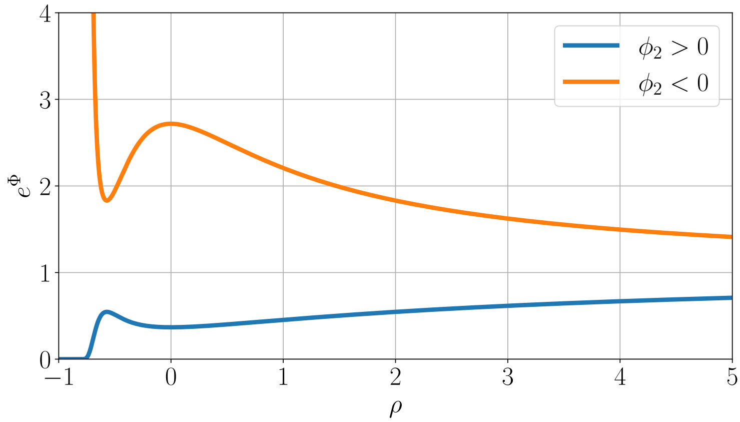

Figure 4.1: *Function e^Φ in eq. (4.3) with $\phi_0 = -3\phi_2/2d_H^2$ and $d_H = 1$.*

indeed, in order for the metric to asymptotically approach the Schwarzschild one (with mass parameter M), we require the asymptotic limit

$$\lim_{\rho\to\infty} e^{\Phi\left(\frac{1}{d_H+\rho}\right)} = e^{\phi_0+\frac{3\phi_2}{2d_H^2}} \overset{!}{=} 1 \qquad \Longrightarrow \qquad \phi_0 = -\frac{3\phi_2}{2d_H^2} \,. \tag{4.4}$$

Choosing $\Phi_H^{(n)} \neq 0$ for some $n \geq 4$ in (4.2) would yield higher modifications of e^Φ of order $O(\rho^4)$, which are negligible close to the horizon. The position of the latter is located at

$$r_H = 2M\, e^{\phi_0} = 2M \exp\left(-\frac{3\phi_2}{2d_H^2}\right) \,. \tag{4.5}$$

A schematic plot of e^Φ as a function of ρ is shown in Figure 4.1. Here we have plotted e^Φ in the entire space-time (*i.e.* also inside of the event horizon for $\rho < 0$): following our general philosophy, we shall discuss the metric function (and all associated quantities) only outside of the horizon (*i.e.* for $\rho \geq 0$) and only make a few brief remarks on the physics inside of the black hole in Section 4.1. The leading coefficients ξ_n (stemming from the series expansion of $2M\, e^\Phi$ in Eq. (3.7)) are exhibited in (4.66). In particular, due to the choice (4.2), we find $\xi_1 = 0 = \xi_3$, which therefore satisfies (3.32).

Curvature and temperature

As a first step to calculating physical quantities for the spacetime metric characterized by (4.2), we compute the first derivative of the function f at the horizon $r_H = 2Me^{\phi_0}$

$$f_H^{(1)} = h_H^{(1)} = \frac{e^{-\phi_0}}{4M}\left(1 + \sqrt{1 - \frac{32e^{2\phi_0}M^2\phi_2}{d_H^4}}\right) \quad \text{with} \quad \phi_0 = -\frac{3\phi_2}{2d_H^2} \,, \tag{4.6}$$

which imposes the condition $\phi_2 \leq \frac{d_H^4}{32\,e^{2\phi_0}\,M^2}$, which with (4.4) therefore becomes the non-linear relation for ϕ_2

$$\phi_2\, e^{3\phi_2/d_H^2} \leq \frac{d_H^4}{32M^2}\,. \tag{4.7}$$

The Ricci scalar at the horizon is finite in this model and takes the value

$$R\big|_{r_H} = \frac{3+(2-5\varpi)\varpi}{2r_H^2(1+2\varpi)} + \frac{24r_H^2\,\phi_2(\phi_2-12d_H^2)}{d_H^8(1+\varpi)(1+2\varpi)}\,, \qquad \text{with} \qquad \varpi = \sqrt{1-\frac{8r_H^2\phi_2}{d_H^4}}\,, \tag{4.8}$$

which vanishes when $\phi_2 \to 0$ ($\varpi \to 1$), recovering the classical case. Finiteness of the derivatives (4.6) (at the event horizon) is a necessary requirement for well-behaved thermodynamical properties of the black hole. Indeed, the Hawking temperature is given by

$$T_{\mathrm{H}} = \frac{f_H^{(1)}}{4\pi} = \frac{1}{8\pi r_H}\left(1+\sqrt{1-\frac{8r_H^2\phi_2}{d_H^4}}\right)\,. \tag{4.9}$$

Determining the entropy using the law of thermodynamics (2.38), requires specifying the M-dependence of d_H and ϕ_2 and thus requires further refinement of the model. To give a concrete example, we shall consider $M \gg 1$ along with

$$\phi_2 = \mathcal{O}(M^0) \quad \text{and} \quad d_H = \pi M + \mathcal{O}(M^0)\,, \tag{4.10}$$

that is, we are assuming only sub-leading corrections to the classical Schwarzschild metric. We, therefore, find the horizon position

$$r_H = 2M - \frac{3\phi_2}{\pi^2 M} + \mathcal{O}(M^{-2})\,, \tag{4.11}$$

and thus for the Hawking temperature

$$T_{\mathrm{H}} = \frac{1}{8\pi M}\left[1+\frac{(3\pi^2-16)\phi_2}{2\pi^4 M^2} + \mathcal{O}(M^{-3})\right]\,, \tag{4.12}$$

and the entropy

$$S = 4\pi M^2\left[1-\frac{(3\pi^2-16)\,\phi_2}{3\pi^2 M^2}\log\left(M^2\right) + \mathcal{O}\left(M^{-4}\right)\right] + \text{const}\,. \tag{4.13}$$

This approximation exhibits a logarithmic correction, compatible with previous results in the literature [103–113]. We remind the reader, however, that (4.13) is based on the assumptions (4.10), which are related to the interior of the black hole solution.

Extending the metric inside the horizon

Following our general philosophy, so far we have considered the metric function only outside of the black hole horizon and have used the horizon distance d_H (and r_H) as the only additional input that is required for the interior of the black hole. Indeed, due to its definition

$$d(r) = \int_0^r \frac{\mathrm{d}r'}{\sqrt{|f(r')|}}\,, \tag{4.14}$$

the calculation of d_H requires knowing the metric in the interior of the black hole, which we have not specified up to this point. In the current example, since the function (4.3) can in fact be extended to the entire space-time (*i.e.* also for $\rho < 0$), as is showcased in Figure 4.1, one can contemplate the possibility to use (4.3) as a model for the entire space-time. Although this discussion is generally outside of the scope of this thesis, here we shall nevertheless make a few remarks regarding this possibility. For concreteness, we shall focus on $\phi_2 > 0$ in the entire Subsubsection.

As a first question, we may ask the behavior of the metric at the origin. In order to get a better understanding of the space-time described by (4.3) for $r \ll 1$, we may use a right rectangular approximation for the integral of the proper distance (4.14)

$$d(r) \simeq \frac{r}{\sqrt{|f(r)|}} \qquad \forall r \ll M\,, \tag{4.15}$$

which is an algebraic equation. Numerical analysis suggests that there are no real positive values for $(r, d(r))$ that satisfy this relation for small r when $f(r) < 0$. We have, however, obtained the following solution of (4.15) for $r(d)$ in the case $f(r) > 0$

$$\begin{aligned}\frac{r}{d} &= \frac{\sqrt{d}\left(3^{1/3}d^{2/3} + \left(-9e^{\Phi}M + \sqrt{-3d^2 + 81e^{2\Phi}M^2}\right)\right)^{2/3}}{3^{2/3}\left(-9e^{\Phi}M + \sqrt{-3d^2 + 81e^{2\Phi}M^2}\right)^{1/3}} \\ &= \cos\left[\frac{1}{3}\ \arcsin\left(\frac{3\sqrt{3}e^{\Phi}M}{d}\right)\right] - \frac{1}{\sqrt{3}}\sin\left[\frac{1}{3}\ \arcsin\left(\frac{3\sqrt{3}e^{\Phi}M}{d}\right)\right]\,. \end{aligned}\tag{4.16}$$

where e^{Φ} is understood to be a function of $d = d_H + \rho$. The function f, therefore, approaches $+1$ for $d \longrightarrow 0$, which hints towards the absence of a singularity at the origin. To verify this, we realize that the function r in (4.16) cannot be expanded in a Taylor series for d. However, noting that (for Φ given in (4.3)) for $\phi_2 > 0$ we have the limit $\lim\limits_{\rho\to -d_H} e^{\Phi}$ in an exponential fashion, we can (formally) write r/d as a series expansion in powers of e^{Φ}

$$\frac{r}{d} = 1 - \sum_{n=1}^{\infty} \frac{2^{n-1}\,\Gamma\left(\frac{3n-1}{2}\right)}{n!\,\Gamma\left(\frac{n+1}{2}\right)}\left(\frac{M\,e^{\Phi}}{d}\right)^n \qquad \text{for} \qquad \frac{M\,e^{\Phi}}{d} \in \left[0, \tfrac{1}{3\sqrt{3}}\right)\,. \tag{4.17}$$

We then find the Ricci scalar close to the origin

$$R = \frac{2M\,e^{\Phi}\,\phi_2}{d_H^2 d^9}\left[d_H^2 d^3(7d - 6d_H) + (3d_H - 4d)^2(d - d_H)^2\phi_2\right] + O(e^{2\Phi})\,, \tag{4.18}$$

which is indeed finite in the limit $d \longrightarrow 0$, due to the exponential suppression of e^{Φ}.[1]

While the above result of the absence of a curvature singularity at the origin is very encouraging conceptually, it also highlights another problem: indeed, if $f(r) > 0$ close to the origin and $f(r) > 0$ for $r > r_H$, with a simple zero at r_H, f necessarily has (at least) one further zero in the interval $r \in (0, r_H)$, more concretely for $\rho \leq -d_H/3$. In other words, the space-time described by (4.3) has at least one more inner horizon. At the latter, we have to verify again if all necessary conditions

[1] We have also verified that the Kretschmann scalar is finite at the origin in this model.

are met for the absence of a curvature singularity. However, since (4.2) is only a minimal solution of the conditions (3.32) (which are tailored to remove unphysical singularities at the outer event horizon), we cannot guarantee the absence of a curvature singularity at this inner horizon. This problem can be circumvented by allowing some of the $\Phi_H^{(n)}$ (for $n \geq 4$) to be non-zero, as we have shown in Section 3.2.4 how to derive local conditions for the absence of curvature singularities at an inner horizon.

4.2 Bonanno-Reuter asymptotically safe black hole

The perturbative quantisation of gravity based on Steven Weinberg's seminal proposal leads to insurmountable divergences due to the negative mass-dimension of Newton's constant. In his 1979 work [171], Weinberg argued that a quantum theory of gravity might still be consistent and predictive if the renormalisation group (RG) flow of all dimensionless couplings approaches a non-Gaussian fixed point in the ultraviolet (UV). In other words, one requires a finite number of relevant directions so the theory remains "safe" from unphysical divergences as the momentum scale $k \to \infty$.

More formally, let $\{g_i(k)\}$ denote the set of dimensionless couplings in the theory; asymptotic safety demands

$$\beta_{g_i}(g_j) \;=\; k\,\frac{\mathrm{d}g_i}{\mathrm{d}k} \;\to\; 0 \quad \text{for } k \to \infty,$$

with $g_i(k) \to g_i^*$ finite and the number of UV-relevant directions finite.

In the gravitational context this idea materialises most concretely within the Functional Renormalisation Group (FRG) formalism for the effective average action Γ_k. The authors of [172] obtained the Newton's constant beta function using some approximate truncations of the gravitational action, thus supporting the idea of a non-perturbatively renormalisable quantum field theory of the metric.

Key reviews of the scenario (see [173–177]) underline its conceptual import and technical challenges. Several phenomenological consequences follow: in the UV the theory becomes scale-invariant and predictive from a finite number of input parameters; in the infrared it must reproduce classical General Relativity; and deviations might appear at Planckian or near-Planckian scales, potentially influencing black-hole physics, cosmology and the structure of singularities.

While not yet providing a complete theory of quantum gravity, the asymptotic-safety programme remains one of the viable frameworks consistent with the basic field-theoretic paradigm, offering a minimal and field-theory–based route to a UV completion of gravity.

Let us consider as an example the black hole metric introduced by Bonanno-Reuter [157] as a renormalization group improved generalization of the Schwarzschild space-time. Indeed, in [157], it has been proposed to replace the (dimensionful) Newton constant G_{Newton} by a running Newton constant

$$G_{\text{Newton}} \longrightarrow G(k) = \frac{G_0}{1 + \omega\, G_0\, k^2}\,, \tag{4.19}$$

where $\omega \in \mathbb{R}$ is a constant and k a (position dependent) scale (with reference scale $k = 0$, at which we measure the Newton's constant $G_0 \equiv G(k = 0)$, whose length dimension is $[G_0] = [L]^2$). The choice of the latter is ambiguous, but it has been proposed in [157] to use an inverse physical distance from the center of the black hole[2] and here we present the re-scaled version with respect

[2] Other options discussed in [157] include distances of the form $\int_C \sqrt{|\mathrm{d}s^2|}$, for different choices of contours C (for example the world-line of a free-falling observer).

to G_0

$$k(r) = (G_0)^{-1/2}\, \xi \,/\, \mathcal{D}(r) \tag{4.20}$$

with ξ a suitable dimensionless constant and $\mathcal{D}(r)$ the dimensionless proper distance function. Such a distance has physical meaning, independent of a specific choice of coordinates. The metric proposed in [157] can be written in the form

$$h(r) = f(r) = f_{\mathrm{BR}}(r) := 1 - \frac{2G_0 M}{r}\frac{1}{1+\widetilde{\omega}/\mathcal{D}(r)^2}\,, \tag{4.21}$$

where $\widetilde{\omega} = \omega\,\xi^2$ is a dimensionless constant. In [157] the concrete value $\widetilde{\omega} = \frac{118}{15\pi}$ was given, however, subsequent works in the literature [178–182] potentially point towards different values (and a different sign). In the following, we shall consider $\widetilde{\omega}$ a generic parameter and discover marked differences between positive and negative values. Furthermore, we shall consider (4.21) to be valid only outside of the event horizon, which is located at $d_{\mathrm{BR},H}$ (which we take as an input of the model.[3]) In order for f_{BR} to remain well defined at the horizon, we shall assume $\widetilde{\omega} + d^2_{\mathrm{BR},H} = \frac{2G_0 M\, d^2_{\mathrm{BR},H}}{r_H} \neq 0$.

For concrete computations, a choice for the physical distance needs to be made. Here we shall discuss three different possibilities that lead to a geometry with an (outer) event horizon, for which we can verify whether the conditions (3.32) are satisfied and whether therefore the Ricci scalar is finite, namely: *(i)* the proper distance computed from the metric (4.21); *(ii)* the proper distance computed from the Schwarzschild metric; *(iii)* an interpolating function. We shall discuss all three possibilities in the following:

(i) choosing $\mathcal{D}(r)$ as the *proper distance* $d_{\mathrm{BR}}(r)$:

$$d_{\mathrm{BR}}(r) = (G_0)^{-1/2}\int_0^r \frac{\mathrm{d}r'}{\sqrt{|f_{\mathrm{BR}}(r')|}}\,, \qquad \forall r \geq 0\,. \tag{4.22}$$

This is a self-consistent choice in the sense that the proper distance is compatible with the metric (4.21). As discussed in [45], this guarantees that the modified metric exhibits the same diffeomorphism invariance as the (classical) Schwarzschild black hole. However, explicitly computing the distance becomes more involved (since (4.22) is an implicit definition). For negative values of $\widetilde{\omega}$, a series expansion close to the horizon is developed in Appendix 4.7. However, for our purposes, this is not in fact required, since we can simply verify the regularity conditions developed in the previous Sections, *i.e.* eq. (3.32). For the concrete function (4.21) with $d(r) = d_{\mathrm{BR}}(r) = d_{\mathrm{BR},H} + G_0^{-1/2}\rho(r)$, we obtain

$$\xi_1 = \theta_1 = \frac{4G_0 M\,\widetilde{\omega}\, d_{\mathrm{BR},H}}{(\widetilde{\omega} + d^2_{\mathrm{BR},H})^2} \neq 0\,, \tag{4.23}$$

such that Eq. (3.32) is not satisfied. In fact, (4.23) implies that already the first derivative of f_{BR}

$$f^{(1)}_{\mathrm{BR}}(r) = (1 - f_{\mathrm{BR}}(r))\left(\frac{1}{r} - \frac{2\widetilde{\omega}}{d_{\mathrm{BR}}(r)(d_{\mathrm{BR}}(r)^2 + \widetilde{\omega})}\frac{1}{\sqrt{f_{\mathrm{BR}}(r)}}\right)\,, \qquad \forall r \geq r_{\mathrm{BR},H}\,,$$

[3] Here we are allowing for the possibility that the metric inside of the black hole is different from (4.21) in which case $d_{\mathrm{BR},H}$ would need to be computed as a separate input to the model. As we shall see, our conclusions will be entirely independent of this choice and thus the concrete value of $d_{\mathrm{BR},H}$.

diverges at the horizon

$$\lim_{\epsilon\to 0^+} f_{\rm BR}^{(1)}(r_{{\rm BR},H}+\epsilon)\to\infty\,. \tag{4.24}$$

This is due to the fact that $f_{\rm BR}(r_{{\rm BR},H})=0$. Following the discussion of Section 2.2, this poses problems with the interpretation of the black hole's thermodynamical properties, notably the Hawking temperature's definition. Furthermore, it also leads to a curvature singularity at the horizon, since for example, the Ricci scalar becomes

$$R=\frac{\widetilde{\omega}(f_{\rm BR}-1)\left(d_{\rm BR}(d_{\rm BR}^2+\widetilde{\omega})(1-5f_{\rm BR})f_{\rm BR}^{1/2}+r\,(6d_{\rm BR}^2f_{\rm BR}-2\widetilde{\omega})\right)}{r\,d_{\rm BR}^2\,(d_{\rm BR}^2+\widetilde{\omega})^2\,f_{\rm BR}^2}\,,\qquad\forall r\geq r_H\,.$$

This expression diverges at the event horizon due to the factor $f_{\rm BR}^2$ in the denominator (while the numerator at the horizon assumes the finite value $2\widetilde{\omega}^2 r_H$).

Finally, we remark since $\xi_1\neq 0$, the results of the series expansion approach developed in Section 3.2 are not directly applicable. In appendix A.2, we show how it can be generalised in this case, and the consequences for the Bonanno-Reuter space-time for $\widetilde{\omega}<0$, are discussed in appendix 4.7 (confirming further our above conclusions in this case).

(ii) choosing $\mathcal{D}(r)$ as the *proper distance* of the (classical) *Schwarzschild geometry* $d_{\rm S}(r)$, *i.e.*

$$d_{\rm S}(r)=(G_0)^{-1/2}\int_0^r\frac{{\rm d}r'}{\sqrt{\left|1-\frac{2G_0M}{r'}\right|}}= \tag{4.25}$$

$$=(G_0)^{-1/2}\times\begin{cases}\pi G_0M-\sqrt{r(2G_0M-r)}-2G_0M\,\arctan\sqrt{\frac{2G_0M}{r}-1} & \text{if}\quad 0<r\leq 2G_0M\,,\\ \pi G_0M+\sqrt{r(r-2G_0M)}+2G_0M\,{\rm arctanh}\sqrt{1-\frac{2G_0M}{r}} & \text{if}\quad r\geq 2G_0M\,.\end{cases} \tag{4.26}$$

This option was initially advocated in [157] and has the advantage that it can be computed as a closed expression in terms of r. This geometry possesses a horizon, whose position is corrected by $\widetilde{\omega}$, *e.g.* for large mass M of the black hole

$$r_{{\rm BR},H}=2G_0M-\frac{2}{\pi^2}\frac{\widetilde{\omega}}{M}+\mathcal{O}\left(|\widetilde{\omega}|^{3/2}/M^2\right)\,. \tag{4.27}$$

For $f_{\rm BR}$ to be well defined at the horizon, we assume that $\widetilde{\omega}+d_{\rm S}^2(r=r_{{\rm BR},H})\neq 0$. The derivative of f in this case becomes

$$f_{\rm BR}^{(1)}(r)=\frac{2G_0M}{r^2\left(1+\frac{\widetilde{\omega}}{d_{\rm S}(r)^2}\right)}-\frac{4G_0M\,\widetilde{\omega}}{r\,d_{\rm S}(r)^3\left|1-\frac{2G_0M}{r}\right|\left(1+\frac{\widetilde{\omega}}{d_{\rm S}(r)^2}\right)^2}\,, \tag{4.28}$$

which is finite at the horizon $r_{{\rm BR},H}$, but diverges for $r=2G_0M$ (which for $\widetilde{\omega}>0$ lies outside the horizon of the black hole). Because of this, while the Ricci scalar is finite at $r=r_{{\rm BR},H}$, the geometry has a curvature singularity at $r=2G_0M$.

(iii) Although a closed function of r, the Schwarzschild proper distance (4.26) is still difficult to work with for concrete computations. Therefore in [157] the following approximation for (4.26) was proposed

$$d_S(r) \simeq \mathfrak{d}_S(r) = \left(\frac{r^3}{G_0(r+\gamma\, G_0 M)}\right)^{1/2}, \quad \text{such that} \quad \begin{aligned} &\lim_{r\to 0} \mathfrak{d}_S(r) \sim (\gamma G_0 M)^{-1/2} r^{3/2}\,, \\ &\lim_{r\to\infty} \mathfrak{d}_S(r) \sim (G_0)^{-1/2}\, r\,. \end{aligned} \tag{4.29}$$

Here $\gamma \in \mathbb{R}$ is a constant, which in order to mimic the same behaviour as (4.26) at the origin ($r \to 0$) needs to be chosen as $\gamma = 9/2$. The function $\mathfrak{d}_S$ has no inflection points, and thus does not feature the same behaviour as a proper distance at a horizon for any value of r.

Identifying $\mathcal{D}$ in (4.21) with $\mathfrak{d}_S$ leads to a zero of f_{BR} at

$$r_{\text{BR},H} = 2G_0 M - \frac{2+\gamma}{4}\,\frac{\widetilde{\omega}}{M} + \mathcal{O}(\widetilde{\omega}^2/M^2)\,. \tag{4.30}$$

At this horizon, both the first and second derivatives of f_{BR} are finite implying that the Ricci scalar takes a finite value.

To summarise, treating (4.21) in a *self-consistent fashion* by identifying $\mathcal{D}$ by the proper distance d_{BR} calculated from f_{BR} itself leads to a divergent first derivative of the metric function at the horizon, which in turn leads to significant problems for physical quantities. Notably, it poses problems for defining a finite Hawking temperature and leads to a curvature singularity at the (outer) event horizon. This is in line with the results of Section 3.2, due to the fact that the function $\Phi^{(\rho)}(\rho) = \frac{2G_0 M}{1+\widetilde{\omega}/(d_{\text{BR},H}+G_0^{-1/2}\rho)^2}$ does not satisfy the conditions (3.32), independent of the geometry of the black hole inside the event horizon (*i.e.* independent of the value of $d_{\text{BR},H}$). The choices *(ii)* and *(iii)* constitute a departure from the original idea presented in [157] (proposed as an approximation in this work) by replacing $\mathcal{D}$ by a function of the radial coordinate r, which does *not* represent a physical distance that has been consistently calculated from the metric characterised by (4.21).

While *(ii)*, depending on the sign of $\widetilde{\omega}$, may have a curvature singularity outside of the event horizon, choice *(iii)* is at least well-behaved from this perspective. However, from the point of view of the original motivation to deform the Schwarzschild metric by a function of a (consistently calculated) distance function, the choice *(iii)* corresponds to a different deformation function than (4.21). Using the approach outlined in Section 3.2.1, we can determine this modified deformation function by reverse engineering the coefficients ξ_n: indeed, by integrating eq. (3.6) we find the coefficients b_n in eq. (3.7)

$$\begin{aligned} b_1 &= \frac{\sqrt{2}\left|r_{\text{BR},H}^3 + \widetilde{\omega} G_0(r_{\text{BR},H} + \gamma\, G_0 M)\right|}{\sqrt{r_{\text{BR},H} G_0 M (r_{\text{BR},H}^3 - \widetilde{\omega} G_0(r_{\text{BR},H} + 2\gamma G_0 M))}}\,, && b_2 = 0\,, \\ b_3 &= \frac{b_1^3 G_0 M \left(r_{\text{BR},H}^6 - 3r_{\text{BR},H}^4 G_0 \widetilde{\omega} - 7\gamma r_{\text{BR},H}^3\, G_0^2 M\, \widetilde{\omega} + (\gamma G_0^2 M\, \widetilde{\omega})^2\right)}{24\sqrt{2}\left(r_{\text{BR},H}^3 + \widetilde{\omega} G_0(\gamma G_0 M + r_{\text{BR},H})\right)^3}\,, && b_4 = 0\,. \end{aligned} \tag{4.31}$$

Therefore with

$$a_1 = 0\,, \qquad a_2 = \frac{1}{b_1^2}\,, \qquad a_3 = 0\,, \qquad a_4 = -\frac{2b_3}{b_1^5}\,, \tag{4.32}$$

we obtain for the leading coefficients of ξ_n (which are equal to θ_n)

$$\xi_1 = 0\,, \qquad \xi_2 = \frac{2r_{\mathrm{BR},H}^2 \widetilde{\omega}\, G_0 M (2r_{\mathrm{BR},H} + 3\gamma\, G_0 M)}{b_1^2 (r_{\mathrm{BR},H}^3 + \widetilde{\omega}\, G_0 (r_{\mathrm{BR},H} + \gamma\, G_0 M))^2}\,, \qquad \xi_3 = 0\,. \tag{4.33}$$

These indeed satisfy the conditions (3.32). Therefore, the "approximation" to use (4.29) for $\mathcal{D}$ in (4.21) instead of the self-consistently calculated proper distance, corresponds to changing the metric function (4.21), in a way characterised by the above expansion coefficients.

4.3 Hayward black hole

The Hayward black hole [24] is a well-known example of a static and spherically symmetric regular black hole solution, designed to eliminate the central singularity while preserving the essential causal structure of the Schwarzschild geometry. The metric was introduced as a simple, phenomenological modification of the Schwarzschild solution that replaces the singularity with a regular de Sitter core, characterized by a finite curvature and energy density at the origin, without committing to any specific modification of General Relativity. The Hayward spacetime smoothly interpolates between a de Sitter region near $r = 0$ and an asymptotically flat Schwarzschild-like behavior at large radii, with the transition governed by a length scale parameter associated with quantum-gravitational effects. Owing to its minimal and physically transparent form, the Hayward model has become a standard prototype in the study of regular black holes, black hole evaporation, and possible quantum modifications of classical horizons. The metric function for the Hayward space-time can be written as

$$f(r) = h(r) = f_{\mathrm{Hay}}(r) := 1 - \frac{2Mr^2}{r^3 + 2M\gamma}\,, \tag{4.34}$$

where γ is a free parameter that determines the scale at which the departure from the classical Schwarzschild solution becomes significant [32]. Here we assume f_{Hay} to hold in the entire space-time. From the metric element, we can directly deduce the form of the deformation function, which explicitly depends on the coordinate r rather than the proper distance d

$$\Phi\,(d(r)) := \frac{2Mr^3}{r^3 + 2M\gamma}\,. \tag{4.35}$$

The Hayward space-time exhibits two event horizons, indicated by the existence of two zeroes of the function f_{Hay}. The position of the outer horizon is:

$$r_{H,+} = \frac{2M}{3}\left(1 + 2\cos\left[\frac{1}{3}\arccos\left(1 - \frac{27\gamma}{8M^2}\right)\right]\right)\,. \tag{4.36}$$

Furthermore, the proper distance can be computed using the integral expression (4.14):

$$d_{\mathrm{Hay}}(r) = \int_0^r \sqrt{\left|\frac{\tilde{r}^3 + 2M\gamma}{\tilde{r}^3 - 2M(\tilde{r}^2 + \gamma)}\right|}\mathrm{d}\tilde{r}\,. \tag{4.37}$$

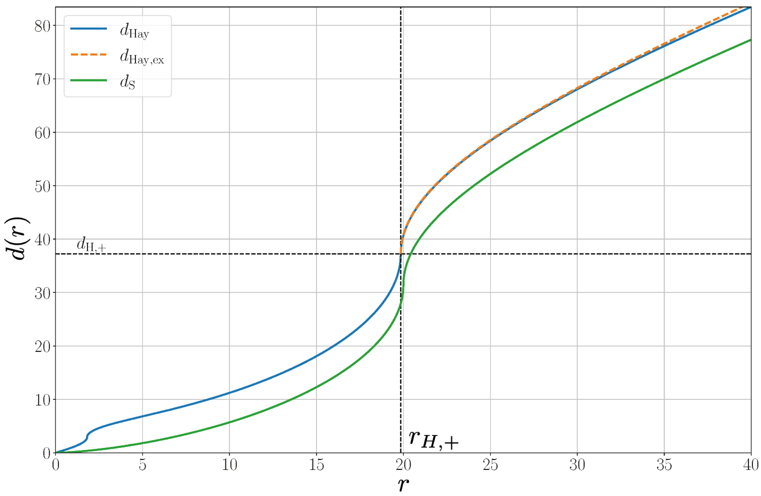

Figure 4.2: *Comparison between the proper distance in the Hayward space-time (blue, calculated using equation (4.37)) and the proper distance in the Schwarzschild space-time $d_{\rm S}$ (green) for specific parameter values: $M = 10$ and $\gamma = 3$. The dashed orange line corresponds to the Taylor series expansion of the proper distance from the event horizon, obtained from equation (4.39).*

Numerical evaluation of this integral suggests the following form of the distance of the horizon for large values of M

$$d_{H,+} = \pi M + c_1\,\gamma^{c_2}\,\ln M + O(M^0)\,, \qquad \text{with} \qquad \begin{aligned} c_1 &= 0.3334 \pm 0.0002\,,\\ c_2 &= 0.4999 \pm 0.0002\,. \end{aligned} \tag{4.38}$$

More importantly, the distance (for a generic point outside of the horizon) can be expanded in powers of $(r - r_{H,+})$, which takes the explicit form

$$\begin{aligned} d_{\rm Hay,ex} = d_{H,+} &+ \frac{\sqrt{2}(r_{H,+}^3 + 2\gamma M)\sqrt{r - r_{H,+}}}{\sqrt{r_{H,+}M(r_{H,+}^3 - 4\gamma M)}} + \frac{M(r_{H,+}^6 - 14r_{H,+}^3\gamma M + 4\gamma^2 M^2)}{3\sqrt{2}(r_{H,+}M(r_{H,+}^3 - 4\gamma M))^{3/2}}\,(r - r_{H,+})^{3/2} \\ &+ O((r - r_{H,+})^{5/2})\,. \end{aligned} \tag{4.39}$$

A comparison between the numerical solution for the distance function (4.37) and (4.39) is shown in Figure 4.2. Using expansion (3.8) we can read off the coefficients b_n from eq. (4.39) and express them in terms of the a_n's using the recursive relation listed in (3.15)

$$a_2^{-1/2} = \frac{\sqrt{2}(r_{H,+}^3 + 2\gamma M)}{\sqrt{r_{H,+}M(r_{H,+}^3 - 4\gamma M)}}\,, \quad -\frac{a_3}{2a_2^2} = 0\,, \quad \frac{5a_3^2 - 4a_2 a_4}{8a_2^{7/2}} = \frac{M(r_{H,+}^6 - 14r_{H,+}^3\gamma M + 4\gamma^2 M^2)}{3\sqrt{2}(r_{H,+}M(r_{H,+}^3 - 4\gamma M))^{3/2}}\,. \tag{4.40}$$

Solving this system yields the solutions for a_2, a_3 and a_4

$$a_2 = \frac{r_{H,+}M(r_{H,+}^3 - 4\gamma M)}{2(r_{H,+}^3 + 2\gamma M)^2}\,, \qquad a_3 = 0\,, \tag{4.41}$$

$$a_4 = \frac{-M^2 r_{H,+}^{10} + 18\gamma M^3 r_{H,+}^7 - 60\gamma^2 M^4 r_{H,+}^4 + 16\gamma^3 M^5 r_{H,+}}{384\gamma^5 M^5 + 12 r_{H,+}^{15} + 120\gamma M r_{H,+}^{12} + 480\gamma^2 M^2 r_{H,+}^9 + 960\gamma^3 M^3 r_{H,+}^6 + 960\gamma^4 M^4 r_{H,+}^3} \,. \tag{4.42}$$

Plugging these coefficients into the series (3.8) allows us to write r as a power series in ρ and then expand around $\rho = 0$

$$\frac{2Mr(\rho)^3}{r(\rho)^3 + 2M\gamma} = r_{H,+} + \frac{6\gamma M^3 r_{H,+}^3 \left(r_{H,+}^3 - 4\gamma M\right)}{\left(2\gamma M + r_{H,+}^3\right)^4}\rho^2 + \\ + \frac{\gamma M^4 \left(-7 r_{H,+}^{12} + 72\gamma M r_{H,+}^9 - 204\gamma^2 M^2 r_{H,+}^6 + 112\gamma^3 M^3 r_{H,+}^3\right)}{\left(2\gamma M + r_{H,+}^3\right)^7}\rho^4 + O(\rho^5) \,, \tag{4.43}$$

from which we can read the coefficients ξ_n. In particular, we obtain

$$\xi_1 = 0 \,, \quad \xi_2 = \frac{6\gamma M^3 r_{H,+}^3 \left(r_{H,+}^3 - 4\gamma M\right)}{\left(2\gamma M + r_{H,+}^3\right)^4} \quad \text{and} \quad \xi_3 = 0 \,. \tag{4.44}$$

Alternatively, we can use the last relation in equation (3.11) and the recursive relation in equation (3.14) for $p = 3$ to determine the values of the coefficients ξ_2 and ξ_3. By doing so, we can establish that the Hayward space-time satisfies the condition (3.27). Consequently, it is not surprising that the Ricci scalar and the Hawking temperature in this space-time are well-defined and free from singularities at the event horizon $r_{H,+}$.

4.4 Dymnikova black hole

The Dymnikova black hole [27, 167] represents one of the earliest and most studied examples of a regular black hole, that is, a spherically symmetric and asymptotically flat solution of Einstein's equations free from curvature singularities at the center. The solution arises from coupling general relativity to a specific form of anisotropic vacuum-like matter with a de Sitter core, which replaces the classical singularity with a smooth region of finite energy density. The metric interpolates between a de Sitter geometry near the origin and a Schwarzschild-like behavior at large radii, yielding a horizon structure similar to that of the Reissner–Nordström spacetime. The Dymnikova model thus provides a self-consistent and physically motivated realization of a nonsingular black hole, serving as a valuable prototype for studying quantum-gravity inspired regular geometries and their thermodynamic or quasi-normal mode properties.

The metric function in the Dymnikova space-time is given by

$$f(r) = h(r) = f_{\text{Dymn}}(r) := 1 - \frac{2M}{r}\left(1 - e^{-r^3/\ell_*^3}\right) \quad \text{with} \quad \ell_*^3 = 2M\ell_0^2 \,, \tag{4.45}$$

which (as for the Hayward black hole) we take to hold for the entire space-time. Also, similar to the Hayward black hole, the parameter ℓ_0 ensures the regularity of the solution near the origin.

Additionally, the density profile of the effective energy-momentum tensor is chosen such that the metric possesses a de Sitter core. Furthermore, the Dymnikova space-time possesses two horizons, which for large masses are located at

$$r_{H,+} = 2M\left(1 - \mathcal{O}\left(e^{-4M^2/\ell_0^2}\right)\right) \quad \text{and} \quad r_{H,-} = 2M\left(1 - \mathcal{O}\left(\frac{\ell_0}{8M}\right)\right) . \tag{4.46}$$

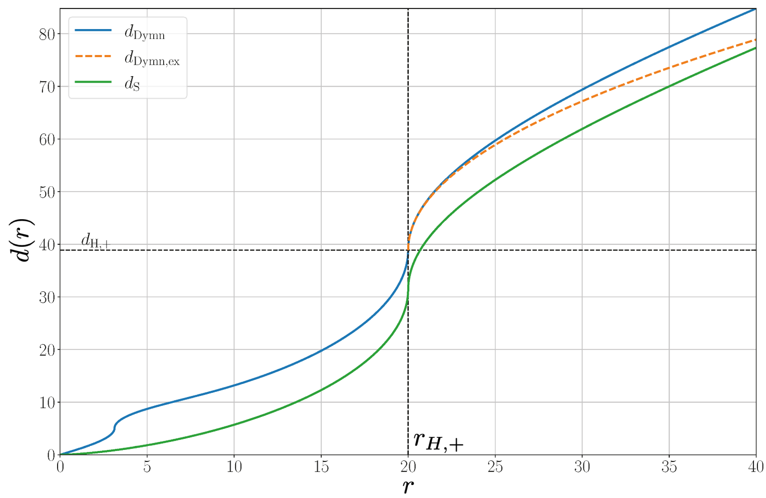

Figure 4.3: *Comparison of the proper distance in the Dymnikova space-time, computed using the definition* (4.14) *(blue), with the proper distance in the Schwarzschild space-time* $d_{\rm S}$ *(green) for* $M = 10$ *and* $\ell_0 = 3$. *The dashed orange line represents the Taylor series expansion of the proper distance from the event horizon, as given by equation* (4.47).

We find from (3.8) that the power series expansion of the proper distance has the following form

$$\begin{aligned} d_{\rm Dymn,ex} = d_{H,+} &+ \frac{2r_{H,+}\sqrt{r - r_{H,+}}}{\sqrt{2M - e^{-r_{H,+}^3/2M\ell_0^2}\left(2M + 3r_{H,+}^3/\ell_0^2\right)}} + \\ &+ \frac{e^{-r_{H,+}^3/2M\ell_0^2}\left(8M^2\ell_0^4\left(e^{r_{H,+}^3/2M\ell_0^2} - 1\right) - 9r_{H,+}^6\right)}{24M\ell_0^4\left(2M + e^{-r_{H,+}^3/2M\ell_0^2}\left(-2M - 3r_{H,+}^3/\ell_0^2\right)\right)^{3/2}}(r - r_{H,+})^{3/2} + \mathcal{O}((r - r_{H,+})^2) . \end{aligned} \tag{4.47}$$

In Figure 4.3 we provide a numerical approximation of the proper distance using the definition (4.14) and compare this expansion for $r > r_{H,+}$. Furthermore, we can recover the coefficients a_2, a_3 and a_4

$$a_2 = \frac{e^{-r_{H,+}^3/2M\ell_0^2}\left(2M\ell_0^2\left(e^{r_{H,+}^3/2M\ell_0^2} - 1\right) - 3r_{H,+}^3\right)}{4\ell_0^2 r_{H,+}^2} , \qquad a_3 = 0 , \tag{4.48}$$

$$a_4 = \frac{e^{-r_{H,+}^3/2M\ell_0^2}\left(2M\ell_0^2\left(e^{r_{H,+}^3/2M\ell_0^2}-1\right)-3r_{H,+}^3\right)\left(9r_{H,+}^6-8M^2\ell_0^4\left(e^{r_{H,+}^3/2M\ell_0^2}-1\right)\right)}{384M\ell_0^6 r_{H,+}^5}\,. \quad (4.49)$$

As for the Hayward space-time, we can expand the function $2M(1-e^{-r(\rho)^3/\ell_*^3})$ around $\rho = 0$

$$2M(1-e^{-r(\rho)^3/\ell_*^3}) = r_{H,+} + \frac{3e^{-r_{H,+}^3/M\ell_0^2}\left(2M\ell_0^2\left(e^{r_{H,+}^3/2M\ell_0^2}-1\right)-3r_{H,+}^3\right)}{4\ell_0^4}\rho^2 + O(\rho^4) \quad (4.50)$$

from which we read off the coefficients ξ_1, ξ_2 and ξ_3

$$\xi_1 = 0\,, \quad \xi_2 = \frac{3e^{-r_{H,+}^3/M\ell_0^2}\left(2M\ell_0^2\left(e^{r_{H,+}^3/2M\ell_0^2}-1\right)-3r_{H,+}^3\right)}{4\ell_0^4} \quad \text{and} \quad \xi_3 = 0\,. \quad (4.51)$$

We observe that the conditions stated in equation (3.27) are satisfied in the Dymnikova space-time as well, leading to the same conclusions as those drawn for the Hayward black hole. These conditions ensure that the Ricci scalar and the Hawking temperature remain well-defined and free from singularities at the event horizons, which is indeed the case for this space-time.

4.5 Extremal Frolov space-time

The Frolov spacetime [32] represents a class of regular black hole solutions designed to capture the essential features of quantum-gravity–induced modifications to the classical black hole interior. In this model, the singularity is replaced by a smooth transition region connecting the trapped and anti-trapped domains through a de Sitter-like core, ensuring that all curvature invariants remain finite. The geometry can be interpreted as an effective semiclassical description of a spherical black hole undergoing evaporation, and it incorporates a bounce that prevents the formation of a curvature singularity. The Frolov metric thus provides a physically motivated and analytically tractable framework to explore non-singular black hole evolution, causal structure, and information recovery scenarios in quantum gravity.

In this Subsection we shall discuss the Frolov spacetime as the extremal configuration of the deformed Reissner-Nordström geometry, or equivalently as an extremal charged Hayward BH (cf. Sec. 4.3). As a concrete example of the EMD based on the proper time (notably in the extremal case), we shall consider here the following metric (using the same notation as in (3.142)), first introduced by Frolov in [32]

$$h(r) = f(r) = 1 - \left(\frac{2M}{r} - \frac{Q^2}{r^2}\right)\widetilde{\Gamma}\,, \quad \text{where} \quad \widetilde{\Gamma} := \frac{r^4}{r^4 + (2Mr + Q^2)\eta^2}\,. \quad (4.52)$$

If $Q = 0$, we recover the Hayward metric [24]. Inspecting the two limits

$$f(r) \overset{r\to\infty}{=} 1 - \frac{2M}{r} + \frac{Q^2}{r^2} + \eta^2 O(r^{-4}) \quad \text{and} \quad f(r) \overset{r\to 0}{=} 1 + \frac{r^2}{\eta^2} + O(r^6)\,, \quad (4.53)$$

the metric (4.52) features asymptotic flatness, while reproducing the Reissner-Nordström metric for $\eta \to 0$. This latter parameter can be interpreted as the radius of an Anti de-Sitter core at the origin. Finally, the position of the event horizon satisfies $f(r_H) = 0$, which has 4 solutions: we shall understand r_H to be the largest (real) value among these.

In the following, we shall be interested in the extremal Frolov space-time. Indeed, extremality (*i.e.* $\frac{\mathrm{d}f}{\mathrm{d}r}(r_H) = 0$) imposes a condition among the three parameters (Q, M, η). In order to characterise this condition, we shall consider η to be parametrically small, by introducing the parameter ϵ as in (3.162) to capture small deformations of the Reissner-Nordström geometry

$$\epsilon := \frac{M - r_H}{r_H} \qquad \text{such that} \qquad r_H = \frac{M}{1+\epsilon}\,, \tag{4.54}$$

where $r_H = M$ corresponds to the classical event horizon of the (extremal) Reissner-Nordström geometry. The conditions for a (deformed) extremal black hole are then solved by

$$\frac{|Q|}{M} = \frac{\sqrt{\epsilon + \sqrt{1+5\epsilon+5\epsilon^2}}}{1+\epsilon}\,, \qquad \frac{\eta^2}{M^2} = \frac{1+2\epsilon-\sqrt{1+5\epsilon+5\epsilon^2}}{(1+\epsilon)^3}\,. \tag{4.55}$$

Reality of Q furthermore requires $\epsilon \geq -\frac{1}{4}$, while $f > 0$ for $r > r_H$ requires $\epsilon \leq \frac{5+\sqrt{105}}{40}$. These results are schematically shown in Figure 4.4, where the green shaded region $\epsilon \in [-1/4, \frac{5+\sqrt{105}}{40}]$ denotes the parameter space that gives rise to an extremal black hole with the correct space-time signature outside of the event horizon. We remark that $\eta^2 > 0$ for $\epsilon \in [-1/4, 0]$, which correspond

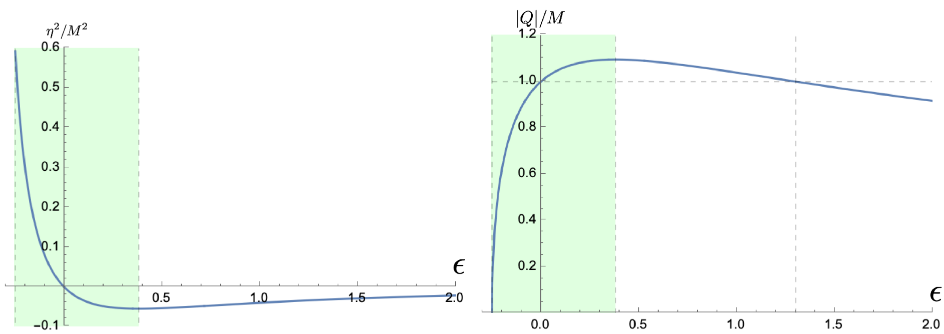

Figure 4.4: Parametrisation of the radius of the Anti de-Sitter core (left) and mass-to-charge ratio (right) of the extremal Frolov-space-time as a function of the deformation parameter ϵ (see eq. (4.55)). The green shaded region leads to a geometry with the correct signature outside of the event horizon. Notice, however, that $\epsilon > 0$ leads to $|Q| > M$ and $\eta^2 < 0$, such that the latter is no longer the radius of a Anti de-Sitter core.

to a horizon radius that is larger than its classical counterpart. Allowing $\eta^2 < 0$, we find $|Q| \geq M$ for $\epsilon \in \left[0, \frac{\sqrt{13}-1}{2}\right]$, thus circumventing the classical bound for the charge of the black hole, known as *super-extremal*. We remark, however, that $\eta^2 < 0$, no longer represents the radius of an Anti de-Sitter core at the origin, which, however, is a priori not visible only from outside of the event horizon. Notice, also that $\epsilon = \frac{5+\sqrt{105}}{40}$ corresponds to the largest possible value of $|Q|/M$ and the smallest possible value of η^2/M^2 (*i.e.* the extrema of the expressions in (4.55)). Furthermore we remark that $Q^2 = 2M r_H$ for $\epsilon = 3/4 > \frac{5+\sqrt{105}}{40}$, which is outside of the green shaded region in Figure 4.4, thus justifying the assumption made in Section 3.6.5.

Figure 4.5 depicts the function f for different values of ϵ outside of the event horizon. The right panel of this Figure indicates that indeed for $\epsilon > \frac{5+\sqrt{105}}{40}$, the function f is negative outside of the double horizon located at $\frac{M}{1+\epsilon}$: moreover, it develops a further single horizon at a position $r > M$.

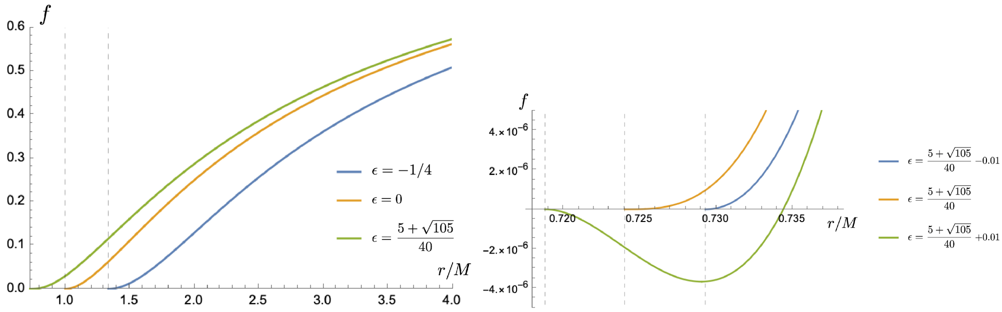

Figure 4.5: Left: plot of the function f outside of the horizon for different values of $\epsilon \in \left[-\frac{1}{4}, \frac{5+\sqrt{105}}{40}\right]$ (*i.e.* the green shaded region in Figure 4.4). Notice that indeed each plot starts with a horizontal tangent, indicating the second order zero at the horizon. Right: for $\epsilon > \frac{5+\sqrt{105}}{40}$, $r_H = \frac{M}{1+\epsilon}$ no longer represents the outermost horizon of the geometry.

Finally, we also provide the expressions for the first few coefficients $(\widetilde{\xi}_n = \widetilde{\theta}_n)_{n\in\mathbb{N}}$ as functions of ϵ

$$\begin{aligned}
\widetilde{\xi}_0 &= \frac{1}{2+\epsilon-\sqrt{1+5\epsilon(1+\epsilon)}} = 1 + \frac{3\epsilon}{2} + \mathcal{O}(\epsilon^2)\,, \\
\widetilde{\xi}_1 &= \frac{2(1+\epsilon)(1-\sqrt{1+5\epsilon(1+\epsilon)})}{(2+\epsilon-\sqrt{1+5\epsilon(1+\epsilon)})^2\, M} = -\frac{5\epsilon}{M} + \mathcal{O}(\epsilon^2)\,, \\
\widetilde{\xi}_2 &= \frac{2(1+\epsilon)^2(1+10\epsilon+8\epsilon^2-(1+2\epsilon)\sqrt{1+5\epsilon(1+\epsilon)})}{(2+\epsilon-\sqrt{1+5\epsilon(1+\epsilon)})^3\, M^2} = \frac{11\epsilon}{M^2} + \mathcal{O}(\epsilon^2)\,.
\end{aligned} \tag{4.56}$$

which are plotted (for $\epsilon \in [-1/4, 0]$) in Figure 4.6.

In order to compare to the leading order computations in Section 3.6.5 (*i.e.* for the case *(i)* of the parameter space), we need to expand (4.55) to obtain $\frac{|Q|}{M} = 1 + \frac{3\epsilon}{4} + \mathcal{O}(\epsilon^2)$, such that $q = \frac{3}{4}$ in (3.163). For small enough values of ϵ (such that the higher orders in ϵ can indeed be neglected), this is compatible with (3.168).

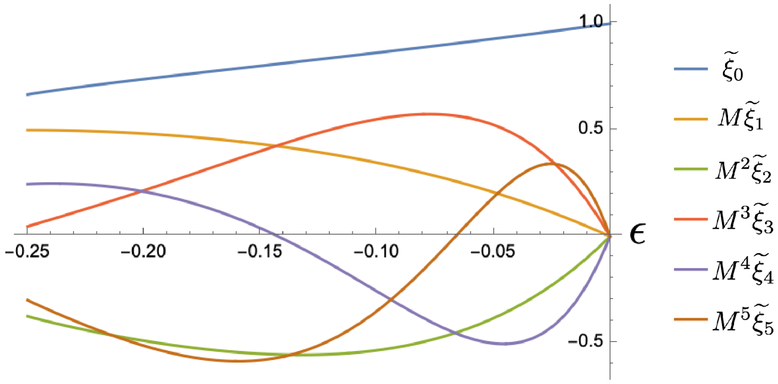

Figure 4.6: Leading Coefficients $\widetilde{\xi}_n(\epsilon)$ for $\epsilon \in \left[-\frac{1}{4}, 0\right]$.

4.6 Weak gravity conjecture

The *Swampland program* [168, 169, 183, 184] aims to delineate the subset of effective field theories (EFTs) that can arise from a consistent theory of quantum gravity, such as string theory. While effective theories are ubiquitous in particle physics and cosmology, only a small fraction of them can be consistently embedded in a UV-complete gravitational framework, the so-called *string landscape*, whereas the remaining inconsistent ones belong to the *Swampland*. The program formulates a series of *Swampland conjectures*, such as the Distance conjecture and the de Sitter conjecture, providing quantitative criteria that low-energy EFTs must satisfy to admit a quantum-gravitational completion. These conjectures have profound implications for cosmology, black hole physics, and the nature of spacetime itself, offering a bridge between phenomenological models and the fundamental constraints imposed by quantum gravity.

The weak gravity conjecture [168, 185, 186] states that the emission spectrum requires a particle with charge-to-mass ratio larger than the black hole's charge-to-mass ratio. In particular, in Planck units, the following relation holds:

$$\frac{M}{q} \geq \left.\left(\frac{\mathfrak{m}}{\mathfrak{q}}\right)\right|_{\min}, \tag{4.57}$$

where $\mathfrak{m}$ and $\mathfrak{q}$ are the mass and charge of the particle with the largest charge-to-mass ratio of the emission spectrum. Subsequent works in the literature have focused on refinements (or corrections) to (4.57), by studying different effects in (effective) quantum theories. As a recent example, we mention [187], which has analysed the impact of selected higher order operators in the effective action. To gain insights on $\widetilde{\xi}_0$ in our framework, we consider the decay of an electrically charged black hole. From the definition of horizon, the ratio between the black hole mass M and its charge q is

$$\frac{M}{q} = \frac{r_H^2 + q^2\widetilde{\xi}_0}{2\,q\,r_H\widetilde{\xi}_0}. \tag{4.58}$$

Close to the classical extremality condition, r_H and the deformation function $\widetilde{\xi}_0$ take the following form:

$$r_H = q(1+\gamma)\,, \quad \tilde{\xi}_0 = 1+\lambda\,, \tag{4.59}$$

where λ and γ play the role of the quantum corrections, and $\gamma \sim O(\lambda)$. Using equation (4.59), we can obtain the following upper limit:

$$\lambda \leq 2 - 2\left.\left(\frac{\mathfrak{m}}{\mathfrak{q}}\right)\right|_{\min}\,, \tag{4.60}$$

which relates the inside of the black hole with its emission spectrum, and may allow to grasp some information of the interior structure of the black hole.

4.7 Computing the proper distance

To showcase the approach developed in Section 3.2.1 to compute the proper distance as a function of the deformation parameters, we consider three simple examples, corresponding to different choices of the coefficients ξ_n.

Schwarzschild distance

The simplest choice is to set $r_H = 2M$ and so $\xi_0 = 1$ and $\xi_n = 0\ \forall n > 0$, which corresponds to the Schwarzschild black hole (*i.e.* $\Phi = 2M$). In this case, we also have $d_H = \pi M$. Using (3.13) and (3.14), the first few coefficients a_{2n} (and their reversions b_n) can be tabulated as follows

	$n=1$	$n=2$	$n=3$	$n=4$	$n=5$	$n=6$
a_{2n}	$\frac{1}{8}$	$-\frac{1}{48}$	$\frac{11}{2880}$	$-\frac{73}{80640}$	$\frac{887}{3628800M^9}$	$-\frac{136883}{1916006400}$
b_{2n-1}	2	$\frac{1}{3}$	$-\frac{1}{20}$	$\frac{1}{56}$	$-\frac{5}{576}$	$\frac{7}{1408}$

which allows to compute a series expansion of the distance function, as in eq. (3.8). These coefficients have previously been obtained in [188, 189] (see also [190]) in a different context, namely solutions for free-falling bodies in Newtonian gravity. We have verified up to $(r-2M)^{500-1/2}$ that these coefficients follow the pattern

$$b_{2n-1} = \frac{(-1)^n(2n-5)!!}{2^{n-2}(2n-1)(n-1)!}\,, \tag{4.61}$$

such that the series expansion of ρ in terms of $(r-r_H)^{1/2}$ has an interval of convergence of $r \in [0, 4M]$. A graphical example (for $M = 5$) is shown in Figure 4.7, with an expansion up to order $(r-r_H)^{500-1/2}$. We have furthermore verified that the coefficients b_n agree with a series expansion of $\rho(r)$: indeed, in the case of the Schwarzschild geometry, the distance ρ can in fact be computed in closed form as a function of r (see eq. (4.26))

$$\rho(r) = \sqrt{r(r-2M)} + 2M\,\mathrm{arctanh}\sqrt{1-\frac{2M}{r}} \quad \text{for} \quad r > 2M\,, \tag{4.62}$$

allowing us to verify whether (3.8) is indeed a good representation of the distance function (see Figure 4.7).

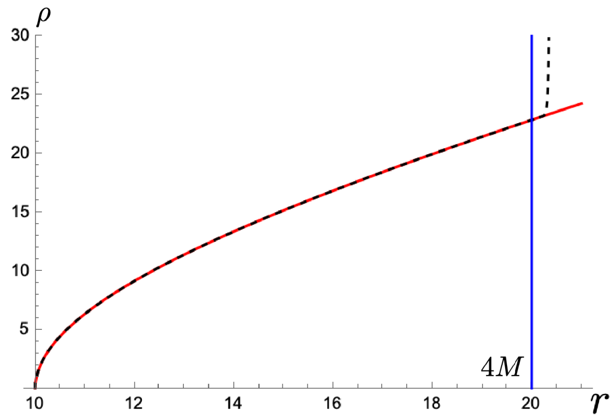

Figure 4.7: *Comparison of the series expansion (3.8) up to order $O((r-r_H)^{500-1/2})$ (dashed black line) to the analytic result (4.62) (red curve) for $M = 5$. The blue line $4M = 20$ denotes the boundary of the interval of convergence for the series expansion.*

Bonanno-Reuter black hole

For the choice (4.21) of the metric deformation (along with $f = h$), the coefficients ξ_n in the expansion (3.7) are given by

$$\begin{aligned}\xi_0 &= \frac{d_H^2}{\widetilde{\omega} + d_H^2}\,,\\ \xi_n &= \frac{(-1)^n\,(2M)^n}{(\widetilde{\omega} + d_H^2)^{n+1}} \sum_{k=1}^{\lfloor \frac{n}{2}+1 \rfloor} (-1)^k \begin{pmatrix} n+1 \\ 2k-1 \end{pmatrix} d_H^{n+2-2k}\,\widetilde{\omega}^k\,,\ \forall n \geq 1\,.\end{aligned} \tag{4.63}$$

Here the interval of convergence (for $\widetilde{\omega} < 0$) is given by $\rho \in \left[0, \frac{|d_H^2+\widetilde{\omega}|}{d_H+\sqrt{-\widetilde{\omega}}}\right)$. Moreover, since $\xi_1 = \frac{4M\,\widetilde{\omega}\,d_H}{(\widetilde{\omega}+d_H^2)^2} \neq 0$, the results of Section 3.2.1 cannot be directly applied. However, as explained in Appendix A.2, for $\widetilde{\omega} < 0$ (such that $\xi_1 < 0$), this approach can be adapted, leading to a series expansion (A.21) with coefficients $\widehat{a}_n$ in (A.24) and (A.25). This expansion provides a solution of the differential equation (3.6) (albeit with a divergent first derivative $f_H^{(1)}$ of f at the horizon). Inversion of the series (A.21) leads to an expansion of the proper distance to the horizon of the form

$$\rho_{\mathrm{BR}}(r) = \sum_{n=0}^{\infty} \widehat{b}_n\,(r - r_H)^{\frac{2+n}{3}}\,, \tag{4.64}$$

where for concreteness, we provide explicitly the first few coefficients

$$\widehat{b}_0 = \frac{1}{\widehat{a}_1^{2/3}} = \frac{3^{2/3} r_H^{1/3} (d_H + \widetilde{\omega})^{2/3}}{2^{4/3}(-d_H M \widetilde{\omega})^{1/3}}\,, \quad \widehat{b}_1 = \frac{2\widehat{a}_2}{3\widehat{a}_1^2} = \frac{(d_H + \widetilde{\omega})^2}{16 d_H M \widetilde{\omega}}\,, \quad \widehat{b}_2 = \frac{7\widehat{a}_2^2 - 6\widehat{a}_1\widehat{a}_3}{9\widehat{a}_1^{10/3}}\,. \tag{4.65}$$

A numerical plot of the three different distance functions used in Section 4.2 for the Bonanno-Reuter black hole is shown in Figure 4.8.

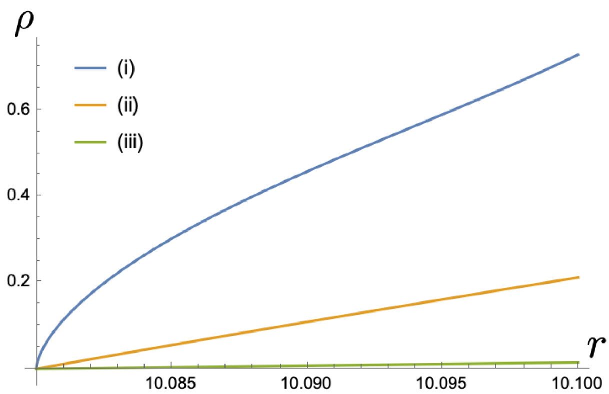

Figure 4.8: *Comparison of three different distance functions for the Bonanno-Reuter space-time:* (i) ρ_{BR} *(represented by the expansion (4.64)),* (ii) *the Schwarzschild proper distance* $\rho_S = d_S - d_H$ *and* (iii) *the approximating function* $\mathfrak{d}_S - d_H$ *in eq. (4.29). Here we have chosen* $\widetilde{\omega} = -1$, $M = 5$ *and* $r_H = 10.08$ *and* $d_H = 12.96$.

Minimal example

As a last example, we consider the metric function characterised by the minimal choice (4.2), leading to the function Φ in eq. (4.3). The first few ξ_n read explicitly

$$\xi_0 = e^{-\frac{3\phi_2}{2d_H^2}}, \qquad \xi_1 = 0, \qquad \xi_2 = \frac{(2M)^2}{d_H^4}\,\phi_2\, e^{-\frac{3\phi_2}{2d_H^2}}, \qquad \xi_3 = 0, \tag{4.66}$$

which satisfy the conditions (3.27), as expected. The leading coefficients a_n in the expansion of $r(\rho)$ in (3.8) therefore become

$$a_2 = \frac{M(1+\varpi)}{4r_H}, \quad a_3 = -\frac{2Mr_H\phi_2}{d_H^4(1+3\varpi)}, \quad a_4 = -\frac{8M^3}{1+2\varpi}\left(\frac{(1+\varpi)^3}{256r_H^3} + \frac{9r_H^3\phi_2^2}{d_H^8(1+3\varpi)^2}\right), \tag{4.67}$$

where we have again used the shorthand notation $\varpi = \sqrt{1 - 8r_H\xi_2/M}$. The series inversion yields the following coefficients for the distance function (3.8)

$$b_1 = \frac{2\sqrt{r_H}}{\sqrt{M(1+\varpi)}}, \qquad b_2 = \frac{16r_H^3\phi_2}{Md_H^4(1+\varpi)^2(1+3\varpi)},$$
$$b_3 = \sqrt{\frac{M}{r_H}}\,\frac{d_H^8(1+\varpi)^4(1+3\varpi)^3 + 256r_H^6(19+29\varpi)\phi_2}{2d_H^8(1+\varpi)^{7/2}(1+2\varpi)(1+3\varpi)^2}. \tag{4.68}$$

5 Extending the EMD

The effective metric description developed in Chapter 3 provides a well–defined and physically transparent parametrization of deformations of static and spherically symmetric black holes, ensuring regularity at the horizon and direct control over thermodynamical quantities. However, the near-horizon nature of the construction implies a limited radius of convergence for the proper-distance expansions, preventing reliable computations of observables probing regions far from the event horizon. This becomes a clear obstacle when studying quantities such as the photon sphere, the black hole shadow, or the quasi-normal modes dominated by the light ring.

The goal of this chapter, based on [49], is to overcome this limitation by extending the EMD into a framework capable of capturing both the near-horizon and the geometry near the photon sphere in a unified manner. We introduce improved approximations of the metric, including Padé rational approximations, that remain accurate well beyond the convergence domain of the original Taylor series. We then apply these methods to compute physical observables at finite radius and assess the robustness of the EMD as an effective parametrization of deformed black hole spacetimes.

5.1 Effective Metric Approach and Approximations

Our starting point is an effective metric description of a spherically symmetric and static black hole, based on the proper distance to the black hole horizon, introduced in Section 3.2. Using the metric of the form as in Eq. (3.1) with the metric functions as in Eq. (3.2) and deformation functions Ψ and Φ as in Eq. (3.7), where r_H is the position of the (simple) horizon and we assume $\rho \geq 0$ and $r \geq r_H$. Imposing the regularity conditions of all of the derivatives of the metric on the horizon, explained in Section 3.2.3, we assume that the functions Ψ and Φ can be expanded in the following form

$$\Psi(\rho) = r_H + 2M \sum_{n=1}^{\infty} \theta_{2n} \left(\frac{\rho}{2M}\right)^{2n} \quad \text{and} \quad \Phi(\rho) = r_H + 2M \sum_{n=1}^{\infty} \xi_{2n} \left(\frac{\rho}{2M}\right)^{2n} , \tag{5.1}$$

where M is the ADM mass (in units of the Planck mass) measured by an observer at space-like infinity. Furthermore, we consider the coefficients $\{\theta_{2n}\}_{n\in\mathbb{N}}$ and $\{\xi_{2n}\}_{n\in\mathbb{N}}$ (along with r_H) the effective parameters describing the black hole under consideration. For compactness of the notation, we shall also sometimes use the notation $\xi_0 = \frac{r_H}{2M} = \theta_0$ and implicitly understand $\xi_{2n+1} = \theta_{2n+1} = 0$ $\forall n \geq 0$.

The differential equation (3.6) can be solved in terms of the series expansions in eq. (3.8) and by the means explained in Section 3.2. Finally, for further convenience, we introduce two types of series expansions of the metric functions, which (assuming their convergence) are locally equivalent: first we introduce an expansion of h and f in terms of the radial coordinate as in Eq. (3.3). Here we consider the expansion coefficients $\{h_H^{(n)}\}_{n\in\mathbb{N}}$ and $\{f_H^{(n)}\}_{n\in\mathbb{N}}$ as functions of $\{\xi_{2n}\}_{n\in\mathbb{N}}$ and $\{\theta_{2n}\}_{n\in\mathbb{N}}$, for example

$$f_H^{(1)} = \frac{1+\varpi}{2r_H}\,, \tag{5.2a}$$

$$h_H^{(1)} = \frac{1}{r_H} - \frac{8r_H\theta_2/M}{r_H(1+\varpi)}\,, \tag{5.2b}$$

$$h_H^{(2)} = -\frac{1}{r_H^2} + \frac{(\varpi+1)\left[\theta_2(\varpi+1)(3\varpi+1)r_H/(4M) - \theta_4(2\varpi+1)r_H^3/M^3\right] - 32\,\theta_2\,\xi_4\,r_H^4/M^4}{r_H^2(\varpi+1)^3(2\varpi+1)}\,, \tag{5.2c}$$

where we recall from Eq. (3.13)

$$\varpi := \sqrt{1-\frac{8r_H\,\xi_2}{M}}\,. \tag{5.3}$$

The deformation to the higher-order derivatives take the form

$$\left(f_H^{(n)} - (f_H^{(n)})_{\text{class}}\right) \propto \xi_{2n} + \text{n.l.}(r_H, \xi_2, \ldots, \xi_{2n-2})\,, \tag{5.4}$$

where $(f_H^{(n)})_{\text{class}}$ is the classical expression for the derivative of the metric at the horizon (for Schwarzschild $r_H = 2M$ and $(f_H^{(n)})_{\text{class}} = (-1)^{n+1}(2M)^{-n}$) and n.l. indicates a non-linear dependence on r_H and $\{\xi_{2p}\}_{1\leq p<n}$. The same holds for $h_H^{(n)}$ with respect to θ_{2n} and $(r_H, \{\theta_{2p}\}_{1\leq p<n})$. Secondly, we consider h and f expressed as the series expansions in Eq. (3.20), in which we used Eq. (3.19). We stress that both expansions (3.3) and (3.20) in general have finite radius of convergence in a region close to the event horizon. Thus, while these expansions are crucial in (locally) solving (3.6) in a self-consistent fashion, and thus determining explicitly the geometry, they are in general not viable for computing observables at a distance from the black hole. Furthermore, even close to the horizon, convergence of (5.1) (or (3.3)) may be slow, thus making them impractical for concrete computations.[1]

The aim of this Chapter is therefore to devise a strategy for approximations of the metric that circumvent these problems: in the following Subsection 2.3 we shall briefly introduce an observable, in the form of the photon radius (which is experimentally related to the black hole shadow), which requires a description of the geometry at a distance of the black hole horizon. Furthermore, in Section 5.2 we shall introduce the Padé approximant as a means to (approximately) calculate this observable in the effective framework.

Before continuing, we would like to make a further technical remark concerning the series coefficients in (5.1) mentioned above: indeed, since Ψ and Φ encode (quantum) corrections, their effect is in a certain sense understood to be small. In fact, in many models (see Section 5.3 below for examples) there is a dedicated small parameter (denoted η in Section 5.3) that governs the size of the deformation and allows to (better) organise approximations accordingly. In order to make contact with the examples discussed in Section 5.3, we shall also define

$$r_H =: 2M\,(1+\mathfrak{c})\,, \tag{5.5}$$

[1] We note, however, that (5.1), (3.3) and (3.20) allow to compute observables that only depend on the (very near-)horizon geometry in a very efficient manner, such as the Hawking temperature of the black hole, as we demonstrated in Chapter 3.

and assume that $\{\theta_{2n}, \xi_{2n}\}$ and $\mathfrak{c}$ are small deformations. Concretely, in order to illustrate some of our conceptual points by an example, we shall consider

$$\mathfrak{c} \ll 1 \qquad \text{and} \qquad \frac{\theta_{2n}}{\mathfrak{c}} \gg \mathfrak{c}\,, \qquad \text{and} \qquad \frac{\xi_{2n}}{\mathfrak{c}} \gg \mathfrak{c}\,, \qquad \forall n \geq 2\,. \tag{5.6}$$

Assuming observables to be analytic functions in $\mathfrak{c}$, we present our results as expansions thereof, focusing mostly on the leading correction $\mathcal{O}(\mathfrak{c})$. We shall consider this, the *leading quantum correction*. As we shall see explicitly in several examples in Section 5.3, the radius of the photon sphere r_{ps} is not only larger than the radius of the event horizon r_H, but also such that the series expansions (3.6) or the expansion of the distance in (3.8) are not necessarily convergent, or at least converge very slowly. Thus, they cannot be used directly to find the solution (2.50). In the following Section we shall therefore present approximations of the metric that allow to (approximately) compute r_{ps}, the impact parameter b and ultimately the shadow b_{sh}.

5.2 Padé Approximation

In this Section we use Padé approximants (see Appendix 5.2.1 for the definition) to find approximations to the effective metric description and physical observables in a region outside of the event horizon, notably the radius of the photon ring discussed in Section 2.3. We shall introduce the concept of an order of these approximations through the number of expansion coefficients $\{\xi_{2n}, \theta_{2n}\}_{n\in\mathbb{N}}$ that we consider to be genuine and independent, which is linked to the order of the Padé approximant.

5.2.1 Padè Approximant of a Series Expansion

Let $U:\ [0, x_0] \to \mathbb{R}$ be a function with series expansion

$$U(x) = \sum_{k=0}^{\infty} \mathfrak{u}_k\, x^k\,, \tag{5.7}$$

that has radius of convergence $x_0 > 0$. We then introduce the *Padé approximant* [51] as the quotient of two polynomials

$$U_{N,M} := \frac{P_N(x)}{Q_M(x)}\,, \qquad \text{with} \qquad \begin{array}{l} P_N = \sum_{n=0}^{N} p_n\, x^n\,, \\ Q_M = 1 + \sum_{m=1}^{M} q_m\, x^m\,, \end{array} \tag{5.8}$$

such that

$$U_{N,M}(x) = \sum_{k=0}^{N+M} \mathfrak{u}_k\, x^k + \mathcal{O}(x^{N+M+1})\,. \tag{5.9}$$

If $U_{N,M}$ exists, the coefficients $\{p_n\}$ and $\{q_m\}$ are unique and given by the linear equations

$$\mathcal{M}_1 \cdot \begin{pmatrix} q_M \\ q_{M-1} \\ \vdots \\ q_1 \end{pmatrix} = -\begin{pmatrix} \mathfrak{u}_{N+1} \\ \mathfrak{u}_{N+2} \\ \vdots \\ \mathfrak{u}_{N+M} \end{pmatrix}, \quad \text{with} \quad \mathcal{M}_1 = \begin{pmatrix} \mathfrak{u}_{N-M+1} & \mathfrak{u}_{N-M+2} & \cdots & \mathfrak{u}_N \\ \mathfrak{u}_{N-M+2} & \mathfrak{u}_{N-M+3} & \cdots & \mathfrak{u}_{N+1} \\ \vdots & \vdots & & \vdots \\ \mathfrak{u}_N & \mathfrak{u}_{N+1} & \cdots & \mathfrak{u}_{N+M-1} \end{pmatrix},$$

$$\mathcal{M}_2 \cdot \begin{pmatrix} 1 \\ q_1 \\ \vdots \\ q_M \end{pmatrix} = \begin{pmatrix} p_0 \\ p_1 \\ \vdots \\ p_N \end{pmatrix}, \qquad \text{with} \quad \mathcal{M}_2 = \begin{pmatrix} 0 & 0 & \cdots & & & & 0 \\ \mathfrak{u}_1 & 0 & 0 & \cdots & & & 0 \\ \mathfrak{u}_2 & \mathfrak{u}_1 & 0 & 0 & \cdots & & 0 \\ \vdots & \vdots & \vdots & \vdots & \ddots & & \vdots \\ \mathfrak{u}_N & \mathfrak{u}_{N-1} & \mathfrak{u}_{N-2} & \cdots & & \mathfrak{u}_{N-M-1} & \mathfrak{u}_{N-M} \end{pmatrix}, \tag{5.10}$$

If it exists, an explicit form of $U_{N,M}$ can be given in the form

$$U_{N,M}(x) = \frac{\begin{vmatrix} \mathfrak{u}_{N-M+1} & \mathfrak{u}_{N-M+2} & \cdots & \mathfrak{u}_{N+1} \\ \vdots & \vdots & \ddots & \vdots \\ \mathfrak{u}_N & \mathfrak{u}_{N+1} & \cdots & \mathfrak{u}_{N+M} \\ \sum_{j=M}^{N} \mathfrak{u}_{j-M} x^j & \sum_{j=M-1}^{N} \mathfrak{u}_{j-M+1} x^j & \cdots & \sum_{j=0}^{N} \mathfrak{u}_j x^j \end{vmatrix}}{\begin{vmatrix} \mathfrak{u}_{N-M+1} & \mathfrak{u}_{N-M+2} & \cdots & \mathfrak{u}_{N+1} \\ \vdots & \vdots & \ddots & \vdots \\ \mathfrak{u}_N & \mathfrak{u}_{N+1} & \cdots & \mathfrak{u}_{N+M} \\ x^M & x^{M-1} & \cdots & 1 \end{vmatrix}}. \tag{5.11}$$

5.2.2 Padé Approximant of the Metric and Horizon Distance

While the series expansions (5.1) for the metric deformation functions, may exist close to the horizon of the black hole, they are generally expected to have finite radius of convergence. Thus (5.1) can in general not be directly used to describe the space time at an arbitrary finite distance away from the event horizon. We therefore propose to *approximate* the metric deformations Ψ and Φ by new functions, which are defined for (general) $\rho > 0$, while still representing Ψ and Φ well, close to the horizon. Concretely, we propose to approximate the deformation functions by their Padé approximants

$$\Psi(\rho) \sim r_H + \Psi_{N,M}(\rho), \qquad \text{and} \qquad \Phi(\rho) \sim r_H + \Phi_{N,M}(\rho). \tag{5.12}$$

In terms of the formalism developed in Section 3.2, this approximation implies that the coefficients $\{\theta_{2n}\}_{2n>M+N}$ and $\{\xi_{2n}\}_{2n>M+N}$ are replaced

$$\theta_{2n} \longrightarrow \widetilde{\theta}_{2n}(\theta_2,\ldots,\theta_{2L}) \quad \text{and} \quad \xi_{2n} \longrightarrow \widetilde{\xi}_{2n}(\xi_2,\ldots,\xi_{2L}), \quad \forall 2n > L := \left\lfloor \frac{M+N}{2} \right\rfloor, \tag{5.13}$$

by functions of $\theta_2,\ldots,\theta_{2L}$ and $\xi_2,\ldots,\xi_{2L}$ respectively. In the following, we shall consider these latter parameters as physically significant and interpret (5.13) (stemming from (5.12)) as an approximation.

Since, according to (3.8) and (3.14), $a_{2n}(\xi_2,\ldots,\xi_{2n})$ is independent of ξ_{2m} for $m > n$, the approximation (5.12) also leads to a modified solution $\widetilde{\rho}$ of (3.6) for the physical distance, which can be written in the form (3.8)

$$\widetilde{\rho}(r) = 2M \sum_{k=1}^{L} b_{2k-1} \left(\frac{r-r_H}{2M}\right)^{\frac{2k-1}{2}} + 2M \sum_{k=L+1}^{\infty} \widetilde{b}_{2k-1} \left(\frac{r-r_H}{2M}\right)^{\frac{2k-1}{2}}, \tag{5.14}$$

where we have also used the fact that the $b_{2n-1}(a_2,\dots,a_{2n})$ in (3.8) are independent of a_{2m} for $m>n$. The $\widetilde{b}_{2k-1}(\xi_2,\dots,\xi_{2L})$ are implicit functions of the remaining parameters $\{\xi_2,\dots,\xi_{2L}\}$, which can be obtained through series reversion of

$$r = r_H + 2M\sum_{k=1}^{L} a_{2k}\left(\frac{\rho}{2M}\right)^{2k} + 2M\sum_{k=L+1}^{\infty}\widetilde{a}_{2k}\left(\frac{\rho}{2M}\right)^{2k}\,, \tag{5.15}$$

with the coefficients

$$\widetilde{a}_p = \frac{\widetilde{\xi}_p + r_H/2M\sum_{n=3}^{p-1}(p-n+2)\,n\,\widetilde{a}_n\,\widetilde{a}_{p-n+2} + \sum_{n=2}^{p-2}\sum_{m=2}^{n}(n-m+2)\,m\,\widetilde{a}_{p-n}\,\widetilde{a}_m\,\widetilde{a}_{n-m+2}}{1-2\,p\,a_2\,r_H\,/M}\,, \tag{5.16}$$

for $p>2L$. Here we understand $\widetilde{\xi}_p=\xi_p$ and $\widetilde{a}_k=a_k$ for $k\le 2L$ with a_k given in (3.14). We remark that $\widetilde{\rho}$ is a solution of

$$\frac{\mathrm{d}\widetilde{\rho}}{\mathrm{d}r} = \frac{1}{\sqrt{\widetilde{f}(r)}} \quad \text{with} \quad \widetilde{f}(r) = 1-\frac{r_H+\Phi_{N,M}}{r}\,. \tag{5.17}$$

Notice furthermore that $a_{2k}\neq\widetilde{a}_{2k}$ for $k>L$ due to the fact that (in general) $\widetilde{\xi}_{2k'}\neq\xi_{2k'}$ for $L<k'\le k$. If the differences $|a_{2k}-\widetilde{a}_{2k}|$ are small (which certainly depends on the $\{\xi_{2n}\}_{n\in\mathbb{N}}$ and which we shall analyze in a number of examples in Section 5.3), 5.14 constitutes a good approximation for the exact physical distance (3.8). However, even if $\widetilde{\rho}$ constitutes a viable approximation, the form (5.14) may not necessarily have better convergence properties than (3.3). For this reason, we shall introduce yet another approximation

$$\widehat{\rho} := \rho_{N,M}(\sqrt{r-r_H}) = 2M\sum_{k=1}^{L} b_{2k-1}\left(\frac{r-r_H}{2M}\right)^{\frac{2k-1}{2}} + 2M\sum_{k=L+1}^{\infty}\widehat{b}_{2k-1}\left(\frac{r-r_H}{2M}\right)^{\frac{2k-1}{2}}\,, \tag{5.18}$$

namely the Padé approximant of the distance function, which is implicitly determined by the coefficients $\{b_1,\dots,b_{2L-1}\}$ that are given in terms of $\{a_2,\dots,a_{2L}\}$ and thus in terms of $\{\xi_2,\dots,\xi_{2L}\}$. Notice that $\widehat{\rho}$ only carries information about the coefficients $\xi_{2,\dots,2L}$ but not ξ_{2k} for $k>L$. In this sense, it is an approximation to the same order as (5.14), except that in general $\widetilde{b}_{2k-1}\neq\widehat{b}_{2k-1}$ for $k>L$. Furthermore, we stress that $\widehat{\rho}$ is a solution of (3.6) and of (5.17) only up to order $(r-r_H)^{\frac{2L-1}{2}}$.

To better illustrate the above discussion, we explicitly consider the example $N=M=2$, such that

$$\Psi_{2,2}(\rho) = 2M\,\frac{\begin{vmatrix} 0 & \theta_2 & 0 \\ \theta_2 & 0 & \theta_4 \\ 0 & 0 & \theta_2(\rho/2M)^2 \end{vmatrix}}{\begin{vmatrix} 0 & \theta_2 & 0 \\ \theta_2 & 0 & \theta_4 \\ (\rho/2M)^2 & \rho/2M & 1 \end{vmatrix}} = 2M\,\frac{\theta_2(\rho/2M)^2}{1-\frac{\theta_4(\rho/2M)^2}{\theta_2}}\,, \tag{5.19a}$$

$$\Phi_{2,2}(\rho) = 2M \frac{\begin{vmatrix} 0 & \xi_2 & 0 \\ \xi_2 & 0 & \xi_4 \\ 0 & 0 & \xi_2(\rho/2M)^2 \end{vmatrix}}{\begin{vmatrix} 0 & \xi_2 & 0 \\ \xi_2 & 0 & \xi_4 \\ (\rho/2M)^2 & (\rho/2M) & 1 \end{vmatrix}} = 2M \frac{\xi_2(\rho/2M)^2}{1 - \frac{\xi_4(\rho/2M)^2}{\xi_2}} \,. \tag{5.19b}$$

In this simple case, the approximation amounts to the replacement (5.13) with

$$\widetilde{\theta}_{2n} = \frac{\theta_4^{n-1}}{\theta_2^{n-2}} \,, \qquad \text{and} \qquad \widetilde{\xi}_{2n} = \frac{\xi_4^{n-1}}{\xi_2^{n-2}} \,, \qquad \forall n > 2 \,. \tag{5.20}$$

This in particular implies that the series expansions of $\Psi_{2,2}$ and $\Phi_{2,2}$ have radii of convergence $\frac{\theta_4}{\theta_2}$ and $\frac{\xi_4}{\xi_2}$, respectively.[2] Furthermore, we obtain for the coefficients (5.16)

$$a_2 = \frac{M(1+\varpi)}{4r_H} \,, \qquad a_4 = -\frac{\xi_4 + \frac{(1+\varpi)^3 M^3}{16 r_H^3}}{1+2\varpi} \,, \qquad \text{and} \qquad \widetilde{a}_{2n} = \frac{a_4^{n-1}}{a_2^{n-2}} \qquad \forall n > 2 \,. \tag{5.21}$$

We furthermore have for (5.18)

$$\widehat{\rho}\,(r) = \rho_{2,2}(r) = 2M \frac{b_1 (\frac{r-r_H}{2M})^{1/2}}{1 - \frac{b_3}{b_1}\frac{r-r_H}{2M}} \,, \qquad \text{with} \qquad \begin{aligned} b_1 &= \frac{1}{\sqrt{a_2}} \,, \\ b_3 &= -\frac{a_4}{2a_2^{5/2}} \,. \end{aligned} \tag{5.22}$$

In order to quantify the difference of $\widehat{\rho}$ and ρ we expand the coefficients $\widehat{b}_{2n-1}$ and b_{2n-1} in powers of $\mathfrak{c}$, assuming for illustrational purposes a scaling of all (initial) coefficients of the form given in (5.6)

$$\widehat{b}_5 = \frac{1}{18} + \frac{1}{108}\left(-9 + 28\,\frac{\xi_2}{\mathfrak{c}} + 192\,\frac{\xi_4}{\mathfrak{c}}\right)\mathfrak{c} + O(\mathfrak{c}^2) \,, \tag{5.23a}$$

$$b_5 = -\frac{1}{20} + \frac{1}{5}\left(\frac{3}{8} + \frac{7}{90}\,\frac{\xi_2}{\mathfrak{c}} + \frac{56}{3}\,\frac{\xi_4}{\mathfrak{c}} + 64\,\frac{\xi_6}{\mathfrak{c}}\right)\mathfrak{c} + O(\mathfrak{c}^2) \,. \tag{5.23b}$$

We stress that the differences between $\widehat{b}_5$ and b_5, have two conceptually different origins:

(i) ρ and $\widehat{\rho}$ are defined in two different ways. While this of course impacts the full form of $\widehat{b}_5$, it in particular also concerns the coefficient at order $O(\mathfrak{c}^0)$, which is independent of $\{\theta_{2n}\,, \xi_{2n}\}$: indeed, ρ and $\widehat{\rho}$ are different even in the undeformed (Schwarzschild) black hole, as is illustrated in Figure 5.1.

(ii) $\widehat{b}_5$ is obtained through a Padé approximation and therefore only depends on the coefficients $\mathfrak{c}$, ξ_2 and ξ_4, but not ξ_6, unlike b_5. Indeed, the coefficient $\widetilde{\xi}_6$ (which enters into $\widehat{b}_5$) is a function of ξ_2 and ξ_4, which thus contributes also to the numerical differences of the coefficient of order $O(\mathfrak{c})$. We notice that these modifications in fact only affect terms of order $O(\mathfrak{c})$.

[2] The functions (5.20) have a pole at $\rho = \sqrt{\frac{\theta_2}{\theta_4}}$ and $\rho = \sqrt{\frac{\xi_2}{\xi_4}}$ respectively, but are else well defined for $\rho \geq 0$.

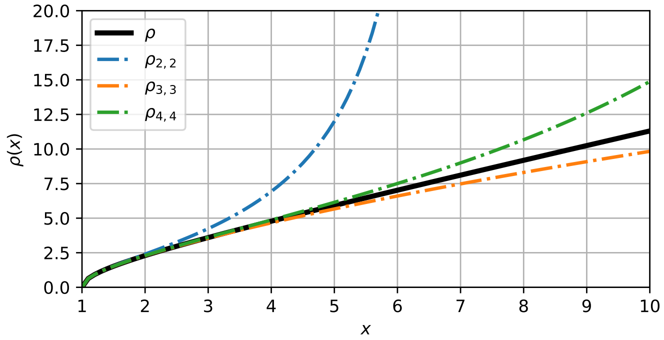

Figure 5.1: Different Padé approximants of the proper distance to the horizon ρ and its Padé approximations in the case of the Schwarzschild black hole (with $\Psi = \Phi = 2M$ and $x := r/2M$).

As we shall see in more detail below, corrections of type *(ii)* are unavoidable, but become progressively smaller (*i.e.* appear at higher and higher order in the distance expansion) for sufficiently large N, M. Corrections of the type *(i)* can be avoided for certain observables: indeed, we shall see below, that observables that are rational functions (in a certain variable) in the case of the undeformed black hole have a particular status. For such observables, the Padé approximant for the Schwarzschild black hole becomes exact beyond a certain order, such that corrections of the type *(i)* are absent at this point.

5.2.3 Padé Approximation for the Photon Radius

We next turn to the computation of the photon ring radius. Using the series expansions (5.1) and (3.8), we can write for the potential in (2.47)

$$U^2 = \sum_{p=1}^{\infty} u_{2p} \left(\frac{\rho}{2M}\right)^{2p} = \sum_{p=1}^{\infty} \left[\mathfrak{q}_{2p} - 2M \sum_{m=0}^{p} \sum_{\ell=0}^{p-m} \theta_{2(p-m-\ell)}\, \mathfrak{p}_{2\ell}\, \mathfrak{q}_{2m}\right] \left(\frac{\rho}{2M}\right)^{2p}, \tag{5.24}$$

where $\mathfrak{p}_{2n}$ is given in (3.19) and $\mathfrak{q}_{2p}$ are given from the expansion of $1/r^2$:

$$q_{2p} = \sum_{\ell=0}^{p} \mathfrak{p}_{2(p-\ell)}\, \mathfrak{p}_{2\ell}\,. \tag{5.25}$$

Concretely, the first few coefficients $u_{2,4,6}$ of U^2 read

$$u_2 = \frac{M^2(1 - 8r_H\theta_2/M + \varpi)}{2r_H^4}\,, \tag{5.26a}$$

$$u_4 = -\frac{M^4(1+\varpi)^2(7+13\varpi)}{8r_H^6(1+2\varpi)} + \frac{3M^2\theta_2(1+\varpi)}{r_H^5} - 2M\frac{\xi_4 + (1+2\varpi)\theta_4}{r_H^3(1+2\varpi)}\,, \tag{5.26b}$$

$$u_6 = -\frac{12\xi_4^2}{(3\varpi+2)(1+2\varpi)^2 r_H^2} - \frac{1}{r_H^4}\left(\frac{12M^2\theta_2\xi_4}{2\varpi+1} + 2Mr_H\left(\theta_6 + \frac{\xi_6}{3\varpi+2}\right)\right) + \tag{5.26c}$$

$$- \frac{3M^5\theta_2(\varpi+1)^2(9\varpi+5)}{4(2\varpi+1)r_H^7} + \frac{M^3(\varpi+1)\left[6\theta_4(3\varpi+2)(2\varpi+1)^2+\xi_4(13\varpi(6\varpi+7)+25)\right]}{2(2\varpi+1)^2(3\varpi+2)r_H^5} +$$
$$+ \frac{M^6(\varpi+1)^3\left[\varpi(\varpi(368\varpi+655)+386)+75\right]}{32(2\varpi+1)^2(3\varpi+2)r_H^8} \,. \tag{5.26d}$$

For finite $p > 0$, $u_{2p} = u_{2p}(r_H, \xi_{2,4,\ldots,2p}, \theta_{2,4,\ldots,2p})$ only depends on a finite number of the expansion coefficients of the metric deformations.

Following the example of the approximation of the proper distance in the previous Subsection, we can use (5.24) to compute Padé approximants of U^2, for which we can find extrema, without having to worry about convergence issues. For example, to order $(N, M) = (2, 4)$, we have

$$U^2_{2,4} = \frac{u_2^3(\rho/2M)^2}{u_2^2 + u_4^2(\rho/2M)^4 - u_2(\rho/2M)^2(u_4 + u_6(\rho/2M)^2)} \,, \tag{5.27}$$

which has a maximum at

$$\rho_{\rm ps} = 2M \frac{\sqrt{u_2}}{(u_4^2 - u_2 u_6)^{1/4}} \,. \tag{5.28}$$

In order to obtain a better intuition about this solution, we consider again a scaling of all coefficients of the form (5.6), in which case

$$\frac{\rho_{\rm ps}}{2M} = \left(\frac{15}{43}\right)^{1/4} \left[2 + 43\mathfrak{c}\left(86 - \frac{88}{3}\frac{\theta_2}{\mathfrak{c}} - 440\frac{\theta_4}{\mathfrak{c}} - 480\frac{\theta_6}{\mathfrak{c}} + \frac{864}{5}\frac{\xi_2}{\mathfrak{c}} - 8\frac{\xi_4}{\mathfrak{c}} - 96\frac{\xi_6}{\mathfrak{c}}\right) + O(\mathfrak{c}^2)\right] \,, \tag{5.29}$$

Notice, since the classical position of the photon radius is

$$r_{\rm ps}^{\rm class} = 3\,M \,, \qquad \text{or equivalently} \qquad \rho_{\rm ps}^{\rm class} = (\sqrt{3} + 2\,\text{arccoth}\sqrt{3})\,M \sim 3.04901\,M \,, \tag{5.30}$$

while $4\left(\frac{15}{43}\right)^{1/4} \sim 3.07408$, the result (5.29) is not exact, even in the undeformed case (*i.e.* for the classical Schwarzschild black hole). This is again due to corrections of the type *(i)* discussed in the previous Subsection: they are due to the fact that we are using a Padé approximation in the first place and can be made small by increasing (N, M). This, however, comes at an increased computational complexity, notably since in the terms of order $O(\mathfrak{c})$, more and more of the coefficients $\{\theta_{2n}\}$ and $\{\xi_{2n}\}$ need to be taken into account.

Fortunately, in the case of the photon radius, there is a different approximation which avoids corrections of order *(i)* and only captures corrections of type *(ii)* that are due to the deformations of the black hole geometry: indeed, as a function of r, the undeformed potential of the photon radius (*i.e.* for the case $\Psi = \Phi = 2M$)

$$U^2_{\rm class} = \frac{1 - \frac{2M}{r}}{r^2} = \frac{r - 2M}{r^3} \,, \tag{5.31}$$

is in fact a rational function in $r - r_H = r - 2M$. Therefore, any Padé approximation with $N \geq 1$ and $M \geq 3$ is in fact exact for the classical Schwarzschild black hole. For quantum deformed black holes, corrections of the type *(i)* are therefore also absent beyond this order of approximation and

N	M	σ_0	σ_1
2	1	$(1+\sqrt{3})$	$(1+\sqrt{3}) + \frac{4(8-15\sqrt{3})}{135}\,\frac{\theta_2}{\mathfrak{c}} + \left(\frac{8}{9} - \frac{16}{\sqrt{3}}\right)\,\frac{\theta_4}{\mathfrak{c}} + -\frac{32}{3}\,\frac{\theta_6}{\mathfrak{c}}$
2	2	$\frac{23+9\sqrt{3}}{13}$	$\frac{23+9\sqrt{3}}{13} - \frac{44(28+33\sqrt{3})}{4095}\,\frac{\theta_2}{\mathfrak{c}} - \frac{8(3359+1272\sqrt{3})}{2535}\,\frac{\theta_4}{\mathfrak{c}} - \frac{32(281-24\sqrt{3})}{169}\,\frac{\theta_6}{\mathfrak{c}} - \frac{768(14-3\sqrt{3})}{169}\,\frac{\theta_8}{\mathfrak{c}}$
2	3	3	$3 - \frac{13471}{14175}\,\frac{\theta_2}{\mathfrak{c}} - \frac{56128}{2835}\,\frac{\theta_4}{\mathfrak{c}} - \frac{3104}{45}\,\frac{\theta_6}{\mathfrak{c}} - \frac{1088}{9}\,\frac{\theta_8}{\mathfrak{c}} - \frac{256}{3}\,\frac{\theta_{10}}{\mathfrak{c}}$
3	3	3	$3 - \frac{443939}{467775}\,\frac{\theta_2}{\mathfrak{c}} - \frac{2625104}{127575}\,\frac{\theta_4}{\mathfrak{c}} - \frac{732448}{8505}\,\frac{\theta_6}{\mathfrak{c}} - \frac{92608}{405}\,\frac{\theta_8}{\mathfrak{c}} - \frac{9472}{27}\,\frac{\theta_{10}}{\mathfrak{c}} - \frac{2048}{9}\,\frac{\theta_{12}}{\mathfrak{c}}$

Table 5.1: Approximations of the position of the maximum of $(U^2)_{N,M}$ for different values of (N, M), using the scaling (5.6).

we are only left with corrections of the type *(ii)* that depend on (finitely many of) the physical deformation coefficients $\{\theta_{2n}\}_{n\in\mathbb{N}^*}$ and $\{\xi_{2n}\}_{n\in\mathbb{N}^*}$. We are thus lead to consider instead of (5.24) the following expansion

$$U^2 = \sum_{n=1}^{\infty} v_n\,(r-r_H)^n\,, \qquad \text{with} \qquad \begin{aligned} v_1 &= \frac{h_H^{(1)}}{r_H^2}\,,\\ v_2 &= \frac{h_H^{(2)} r_H - 4h_H^{(1)}}{2r_H^3}\,,\\ v_3 &= \frac{18h_H^{(1)} - 6r_H h_H^{(2)} + r_H^2 h_H^{(3)}}{6r_H^4}\,, \end{aligned} \tag{5.32}$$

where $h_H^{(n)}$ are the expansion coefficients of the metric deformations in (3.3) that implicitly depend on the physical coefficients $\{\theta_{2k}\}_{k\leq n}$ and $\{\xi_{2k}\}_{k\leq n}$. From this, we can compute a Padé approximation of the (square of the) potential $(U^2)_{N,M}$ in the variable $r - r_H$ along with the position of the photon radius. Using the scaling (5.6), we can write the latter in the form

$$\frac{r_{\text{ps}}}{M} = \sigma_0 + \sigma_1\,\mathfrak{c} + O(\mathfrak{c}^2)\,. \tag{5.33}$$

where $\sigma_{0,1}$ depend on the order of approximation (N, M), as can be seen in Table 5.1: for given (finite) order (N, M), σ_1 only depends on $\mathfrak{c}$ and θ_{2L} up to $2L = 2(N+M)$, thus still respecting the same order of physically relevant coefficients.

With the position r_{ps}, we can next calculate the radius of the black hole shadow in (2.49), which, assuming again the scaling (5.6), we expand as

$$\frac{b_{\text{sh}}}{M} = \tau_0 + \tau_1\,\mathfrak{c} + O(\mathfrak{c}^2)\,. \tag{5.34}$$

The expressions for $\tau_{0,1}$ depend on the order of the Padé approximation, as is shown in Table 5.2. The corrections τ_1 respect the same dependence on the number of physically relevant metric deformation coefficients as σ_1.

For approximations of the potential of the form $(U^2)_{N,3}$ we can in fact write the (approximate) result in an even more compact form. To this end, we write τ_1 as

$$\tau_1(N) = 3\sqrt{3} + \sum_{k=1}^{3+N} \beta_{2k}(N)\,\frac{\theta_{2k}}{\mathfrak{c}}\,, \tag{5.35}$$

N	M	τ_0	τ_1
2	1	$2(1+\sqrt{3})$	$2(1+\sqrt{3})+\frac{8(82+75\sqrt{3})}{135}\frac{\theta_2}{\mathfrak{c}}+\frac{16(8+3\sqrt{3})}{9}\frac{\theta_4}{\mathfrak{c}}+\frac{64}{3}\frac{\theta_6}{\mathfrak{c}}$
2	2	$2\sqrt{\frac{10}{3}+2\sqrt{3}}$	$2\sqrt{\frac{10}{3}+2\sqrt{3}}+\frac{4}{945}\sqrt{\frac{12051454}{3}+2415638\sqrt{3}}\frac{\theta_2}{\mathfrak{c}}+\frac{88}{45}\sqrt{\frac{265}{3}+59\sqrt{3}}\frac{\theta_4}{\mathfrak{c}}+\frac{32}{3}\sqrt{38\sqrt{3}-\frac{146}{3}}\frac{\theta_6}{\mathfrak{c}}+128\sqrt{\sqrt{3}-\frac{5}{3}}\frac{\theta_8}{\mathfrak{c}}$
2	3	$3\sqrt{3}$	$3\sqrt{3}+\frac{1}{\sqrt{3}}\left(\frac{98837}{4725}\frac{\theta_2}{\mathfrak{c}}+\frac{136096}{2835}\frac{\theta_4}{\mathfrak{c}}+\frac{4384}{45}\frac{\theta_6}{\mathfrak{c}}+\frac{1216}{9}\frac{\theta_8}{\mathfrak{c}}+\frac{256}{3}\frac{\theta_{10}}{\mathfrak{c}}\right)$
3	3	$3\sqrt{3}$	$3\sqrt{3}+\frac{1}{\sqrt{3}}\left(\frac{652294}{31185}\frac{\theta_2}{\mathfrak{c}}+\frac{2066276}{42525}\frac{\theta_4}{\mathfrak{c}}+\frac{62528}{567}\frac{\theta_6}{\mathfrak{c}}+\frac{29152}{135}\frac{\theta_8}{\mathfrak{c}}+\frac{2560}{9}\frac{\theta_{10}}{\mathfrak{c}}+\frac{512}{3}\frac{\theta_{12}}{\mathfrak{c}}\right)$

Table 5.2: Approximations of the value of the black hole shadow stemming from and approximation of the potential $U^2 \sim (U^2)_{N,M}$ for different values of (N, M), using the scaling (5.6).

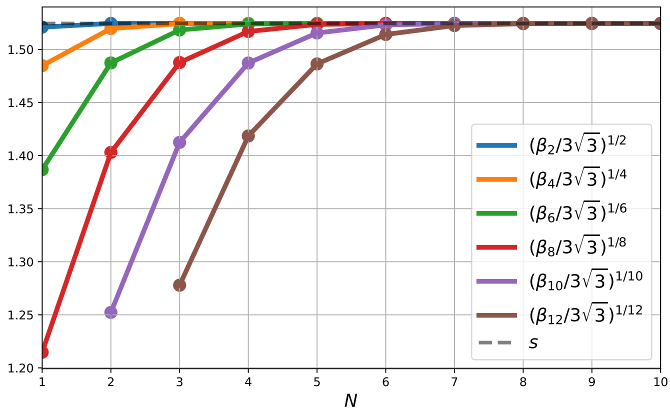

Figure 5.2: Coefficients β_{2n} in the parametrisation of the leading deformation of the black hole shadow τ_1 in (5.35) for different Padé approximations $(N, 3)$. The plot shows that rational powers of the β_{2n} converge towards a universal value for large N, as explained in eq. (5.36), which allows to resum the asymptotic value of τ_1 as in (5.37).

where β_{2k} are numerical coefficients (which for $N = 2, 3$ can be found in Table 5.2). For N sufficiently large, a fixed β_{2k} numerically changes very little when N is increased: as is shown numerically in Figure 5.2, $\beta_{2k}(N)$ approaches asymptotically a fixed numerical value, namely

$$\lim_{N\to\infty} \beta_{2k}(N) \to 3\sqrt{3}\,\mathfrak{s}^{2k} \qquad \forall k \geq 1\,, \qquad \text{with} \qquad \mathfrak{s} \sim 1.5245 \sim \frac{\rho_{\text{ps}}^{\text{class}}}{2M}\,. \tag{5.36}$$

We notice that $2M\mathfrak{s}$ is indeed numerically very close to the proper distance of the photon sphere in the case of the (classical) Schwarzschild black hole (see (5.30)). Assuming that the observation (5.36) indeed holds $\forall k \geq 1$, we can write the asymptotic behaviour of $\tau_1(N)$ in the following form

$$\lim_{N\to\infty} (\mathfrak{c}\,\tau_1(N)) = 3\sqrt{3}\,\mathfrak{c} + 3\sqrt{3}\sum_{k=1}^{\infty} \theta_{2k}\,\mathfrak{s}^{2k} = 3\sqrt{3}\,\mathfrak{c} + 3\sqrt{3}\sum_{k=1}^{\infty} \theta_{2k} \left(\frac{\rho_{\text{ps}}^{\text{class}}}{2M}\right)^{2k}\,, \tag{5.37}$$

where we have used (5.6). Using furthermore the series expansion (5.1) we can formally write

$$\lim_{N\to\infty} (\mathfrak{c}\,\tau_1(N)) = 3\sqrt{3}\,\mathfrak{c} + \frac{3\sqrt{3}}{2M}\,(\Psi(2M\,\mathfrak{s}) - r_H)\,, \tag{5.38}$$

where we have implicitly assumed that $2M\,\mathfrak{s}$ is inside the radius of convergence of (5.1).[3] Thus, using (5.5) and (5.34), to leading order, the approximate black hole shadow can be written entirely in terms of the deformation function Ψ evaluated at a particular value

$$\lim_{N\to\infty}\frac{b_{\rm sh}(N)}{M}=\frac{b_{\rm sh}}{M}\sim\frac{3\sqrt{3}}{2M}\Psi(2M\,\mathfrak{s})\,. \tag{5.39}$$

Turning this result around, we can use (5.39) to provide a bound for the size of the deformation function based on an experimental observation of the photon radius. Indeed, assuming absence of rotation (which is compatible with the experimental data), at a 1-σ confidence level, the EHT observations of M87* lead to [18]

$$\tilde{b}_{\rm sh}^{\rm EHT\ M87^*\ (\pm)}=3\sqrt{3}M_{\rm M87^*}(1\pm 0.17)\,, \tag{5.40}$$

where $M_{\rm M87^*}$ is the mass of the black hole M87*. Thus, assuming M87* to be spherically symmetric, we find based on (5.39), the following rough bound for the function governing its deviation from a Schwarzschild black hole

$$\left|\frac{\Psi(2M_{\rm M87^*}\,\mathfrak{s})}{2M_{\rm M87^*}}-1\right|\leq 0.17\,. \tag{5.41}$$

5.3 Simple Examples of Corrected Schwarzschild Geometries

In order to illustrate and showcase the formalism developed in the previous Section, we shall consider a number of models of spherically symmetric and static black holes that have previously been proposed in the literature [24, 28, 167, 191–193]. These examples have been selected on the basis that they are compatible with (5.6), such that we can use the effective expansions to leading order in the quantum deformations. Furthermore, these black holes display a wide variety on different functional dependencies on the Schwarzschild coordinate r and an explicit parameter (called ϵ) that governs the size of quantum effects. In all cases, following the philosophy of our effective approach, the theory of quantum gravity in which context these models have been proposed, plays no role.

5.3.1 Metrics and Deformation Parameters

We start with four geometries [24, 167, 191, 192] that have been proposed to describe spherically symmetric and static black holes, as deformations of the Schwarzschild geometry [2]. We label them as *simple* in the sense that they are characterised by $f(r)=h(r)\ \forall r\geq r_H$ in (3.1).

In order to describe the four models proposed in [24, 167, 191, 192] in parallel (as far as this is possible), we first introduce a unifying notation: in addition to the mass of the black hole M, all four models introduce an additional parameter, which we shall call η, to describe the deformation of the Schwarzschild space-time. While η is conceptually quite different in all models, we shall in

[3] A different way of phrasing this assumption is that $\lim_{N\to\infty}\Psi_{N,3}(2M\mathfrak{s})=\Psi(2M\mathfrak{s})-r_H$. We note that we have analysed the soundness of this assumption in a number of models of quantum black holes in Appendix 5.4 and find it to be justified at least for small values of the parameter that governs the size of quantum corrections.

the following write it in terms of a different small parameter, which can be uniformly defined. To introduce the latter, we first define

$$x := \frac{r}{2M} \quad \text{and} \quad x_H := \frac{r_H}{2M} \,. \tag{5.42}$$

in order to absorb the mass-scale in the radial coordinate. We then define the fractional deviation of the event horizon radius from the Schwarzschild radius,[4] as in [68]

$$\epsilon := \frac{2M - r_H}{r_H} = \frac{1 - x_H}{x_H} \quad \longleftrightarrow \quad x_H = \frac{1}{1+\epsilon} \,. \tag{5.43}$$

With this notation set up, Table 5.3 presents the metric deformation functions for the four models, along with the parameter η as a function of ϵ, which can take the form of a rational, exponential, or non-analytic function at $\eta = 0$. In anticipation of our further discussion, the table also indicates the leading correction of the position of the photon ring and the black hole shadow as functions of ϵ.

Model	$f = h$	$\eta(\epsilon)$	$r_{\rm ps}/M - 3$	$b_{\rm sh}/M - 3\sqrt{3}$
Hayward [24]	$1 - \frac{x^2}{x^3+\eta}$	$\frac{\epsilon}{(1+\epsilon)^3}$	$-\frac{16}{9}\epsilon + O(\epsilon^2)$	$-\frac{8}{3\sqrt{3}}\epsilon + O(\epsilon^2)$
Simpson-Visser (I) [191]	$1 - \frac{1}{\sqrt{x^2+\eta}}$	$\frac{\epsilon\,(2+\epsilon)}{(1+\epsilon)^2}$	$-\frac{20}{9}\epsilon + O(\epsilon^2)$	$-\frac{4}{\sqrt{3}}\epsilon + O(\epsilon^2)$
Simpson-Visser (II) [192]	$1 - \frac{1}{x}e^{-\eta/x}$	$\frac{\log(1+\epsilon)}{1+\epsilon}$	$-\frac{8}{3}\epsilon + O(\epsilon^2)$	$-2\sqrt{3}\,\epsilon + O(\epsilon^2)$
Dymnikova [167]	$1 - \frac{1 - e^{-x^3/\eta}}{x}$	$-\left[(1+\epsilon)^3 \log\left(\frac{\epsilon}{1+\epsilon}\right)\right]^{-1}$	$\left(\frac{81}{8}\log\epsilon - 3\right)\epsilon^{27/8} + O(\epsilon^{33/8})$	$-3\sqrt{3}\,\epsilon^{27/8} + O(\epsilon^{33/8})$

Table 5.3: Summary of the geometries of the four models studied in this Section: The first column provides the name which we shall use for each model (and the relevant reference to the literature). The second column gives the metric functions (as in (3.1), which are deformed by a small parameter η. For each model, the latter can be related to the deviation ϵ of the event horizon radius from the Schwarzschild radius (see eq. (5.43)), as shown in column three. Finally, columns four and five provide the leading corrections (in ϵ) to the photon radius and the black hole shadow, respectively.

Notice that in all models of this type, the deformation coefficients $\{\xi_{2n}\}_{n\in\mathbb{N}}$ in (5.5) (which are identical to $\{\theta_{2n}\}_{n\in\mathbb{N}}$), do not explicitly depend on the mass: in fact, from (3.6) it follows that $\rho(r) = 2\,M\,\underline{\rho}(x,\epsilon)$, where the function $\underline{\rho}(x,\epsilon)$ does not explicitly depend on M. From (3.2) and (5.1), we can then write

$$f = h = 1 - \frac{x_H + \sum_{n=1}^{\infty} \xi_{2n}\,\underline{\rho}(x,\epsilon)^{2n}}{x} \,, \tag{5.44}$$

Furthermore, from (5.43), we have $\mathfrak{c} = -\frac{\epsilon}{1+\epsilon}$ and we shall see that in all cases $\xi_{2n} = O(\epsilon)$ (such that $\frac{\xi_{2n}}{\mathfrak{c}} = O(1)$), compatible, with (5.6). In the following we shall discuss the four models in more details.

[4] For $\epsilon \ll 1$, this parametrisation ensures that we are not expanding the metric around the internal horizon that arises with the regularisation of the singularity at the origin within the models examined, but rather around the external horizon, which is expected to be close the classical Schwarzschild radius $x_H^{\rm class} = 1$.

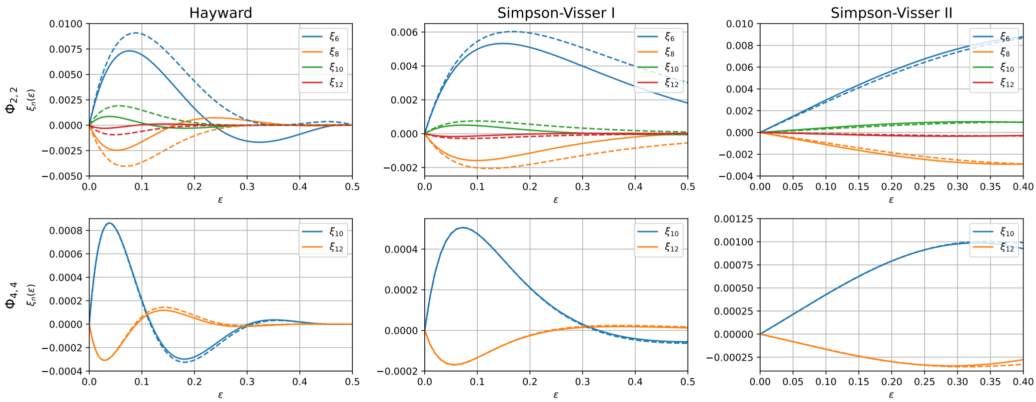

Figure 5.3: Comparison of the deformation coefficients of the metric ξ_{2n} (solid lines) with the (mass-rescaled) coefficients (5.13) stemming from a Padé approximation of Φ (dashed lines) as functions of ϵ. Top row: the coefficients $\xi_{6,8,10,12}$ and their approximations stemming from the Padé approximant $\Phi_{2,2}$ of for the Hayward metric (left column), Simpson-Visser I metric (middle column) and Simpson-Visser II metric (right column). Bottom row: the coefficients $\xi_{10,12}$ and their approximations stemming from the Padé approximant $\Phi_{4,4}$.

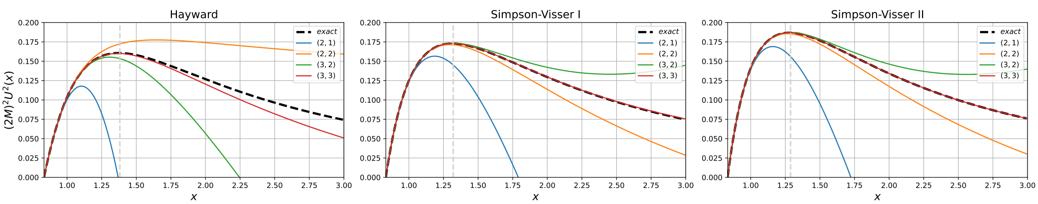

Figure 5.4: Comparison of the potential U^2 for Hayward (left panel), Simpson-Visser I (middle panel), and Simpson-Visser II (right panel) with various Padé approximants (5.32) for each model with a fixed $\epsilon = 0.2$. The vertical dashed gray line denotes the position of the maximum of the (exact) potential.

Hayward black hole: we start with the Hayward black hole, which was first introduced in [24]. Rescaling the deformation functions of the metric as in (5.5), we find explicitly for the leading ones (with $\theta_{2n} = \xi_{2n}\ \forall n \geq 1$)

$$\xi_2 = \frac{3\epsilon(1-2\epsilon)}{4(1+\epsilon)} \qquad \xi_4 = -\frac{\epsilon(1-2\epsilon)(\epsilon(7\epsilon-22)+7)}{16(1+\epsilon)}\,,$$
$$\xi_6 = \frac{\epsilon(1-2\epsilon)\left[\epsilon(\epsilon(2\epsilon(61\epsilon-899)+3225)-1600)+221\right]}{960(1+\epsilon)}\,. \tag{5.45}$$

In a first step, we can compare these coefficients $\{\xi_{2n}\}$ with their counterparts stemming from a Padé approximant $\Phi_{N,M}(=\Psi_{N,M})$ as in (5.12): Figure 5.3 (left column) shows a comparison of the exact coefficients and their approximations for $(N, M) = (2, 2)$ (upper panel) and $(N, M) = (4, 4)$ (lower panel). While in the first case, the approximations capture at least roughly the functional

dependence with respect to ϵ, in the latter case, the $\widetilde{\xi}_{2n}$ even present good approximations for finite values of ϵ.
In Figure 5.4 (left panel) we show the comparison with the analytical form of the effective potential U^2 with the Padé approximations of various orders. Similarly, Figure 5.5 (left) compares different approximations of the distance function (for a fixed value of $\epsilon = 0.2$) as functions of x: the plot highlights the finite radius of convergence of the simple series expansion (3.8) and also shows that viable approximations can already be obtained at fairly low order of the Padé approximant. The position of the maximum of the potential as well as the shadow following Tables 5.1 and 5.2 respectively, is given as follows

N	M	$\sigma_1\ \mathfrak{c}$	$\tau_1\ \mathfrak{c}$
2	1	$-\frac{11-3\sqrt{3}}{3}\,\epsilon + O(\epsilon^2)$	$\frac{1-3\sqrt{3}}{3}\,\epsilon + O(\epsilon^2)$
2	2	$\frac{3}{169}(-131+16\sqrt{3})\,\epsilon + O(\epsilon^2)$	$-\frac{1}{6}\sqrt{-\frac{965}{3}+233\sqrt{3}}\,\epsilon + O(\epsilon^2)$
2	3	$-\frac{16}{9}\,\epsilon + O(\epsilon^2)$	$-\frac{8}{3\sqrt{3}}\,\epsilon + O(\epsilon^2)$
3	3	$-\frac{16}{9}\,\epsilon + O(\epsilon^2)$	$-\frac{8}{3\sqrt{3}}\,\epsilon + O(\epsilon^2)$

Simpson-Visser I black hole: as a second example, we examine the geometry introduced in [192] and also in [131, 194]. The leading deformation coefficients are given by

$$\xi_2 = \frac{\epsilon(2+\epsilon)}{4(1+\epsilon)^3}\,,\ \xi_4 = \frac{\epsilon(2+\epsilon)(\epsilon(2+\epsilon)-11)}{96(1+\epsilon)^5}\,,\ \xi_6 = \frac{\epsilon(\epsilon+2)\left[\epsilon(\epsilon+2)(\epsilon(\epsilon+2)-121)+292\right]}{5760(\epsilon+1)^7}\,. \tag{5.46}$$

Conclusions similar to Hayward's can be drawn from Figure 5.3 (middle column), where the comparison of the $\{\xi_6, \xi_8, \xi 10, \xi_{12}\}$ with their approximations computed with a Padé approximant with $(N, M) = (2, 2)$ (upper panel) and $\{\xi_{10}, \xi_{12}\}$ with their approximation using a Padé approximation with $(N, M) = (4, 4)$ (lower panel). In Fig. 5.5 (second panel from the left) we compare the proper distance numerically computed with the exact metric and the Padé approximants of different orders. In Figure 5.4 (middle panel) we show the comparison with the analytical form of the effective potential U^2 with the Padé approximations of various orders. Finally, in Figure 5.5 (middle) we compare different approximations of the distance function numerically integrated (for a fixed value of $\epsilon = 0.2$) and the Padé approximants.[5]

The position of the maximum of the potential as well as the shadow following tables 5.1 and 5.2 respectively, is given as follows

N	M	$\sigma_1\ \mathfrak{c}$	$\tau_1\ \mathfrak{c}$
2	1	$-\frac{13}{6}\,\epsilon + O(\epsilon^2)$	$-\left(\frac{2}{3}+\sqrt{3}\right)\,\epsilon + O(\epsilon^2)$
2	2	$-\frac{15}{338}(47+2\sqrt{3})\,\epsilon + O(\epsilon^2)$	$-\frac{1}{6}\sqrt{\frac{265}{3}+59\sqrt{3}}\,\epsilon + O(\epsilon^2)$
2	3	$-\frac{20}{9}\,\epsilon + O(\epsilon^2)$	$-\frac{4}{\sqrt{3}}\,\epsilon + O(\epsilon^2)$
3	3	$-\frac{20}{9}\,\epsilon + O(\epsilon^2)$	$-\frac{4}{\sqrt{3}}\,\epsilon + O(\epsilon^2)$

[5] We noticed that Padé of order $(M, N) = (2, 2)$ introduces a vertical tangent behaviour at a position $\tilde{x} \geq x_H$ which is a feature purely due to the approximation and is effectively eliminated with a suitable choice of the Padé approximant order.

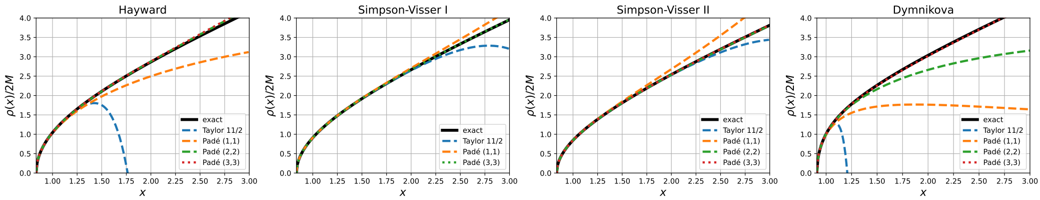

Figure 5.5: Comparison of approximations of the distance (as a function of x) in the case of the Hayward, Simpson-Visser I and Simpson-Visser II geometries (for $\epsilon = 0.2$) and Dymnikova (for $\epsilon = 0.1$): the solid black lines represent the numerical integration of (3.6), while the dashed blue lines represent the Taylor series expansion (3.8) (including terms up to order $n = 6$) and the coloured dashed and dotted lines show Padé approximants of the distance as in (5.18).

Before moving to examples with exponential dependence on the radial coordinate, we remark that the black hole geometries proposed by Bardeen [25], Frolov [195] and the one proposed in [196] have a similar functional dependence on x to the ones of Hayward and Simpson-Visser I. We therefore expect to obtain similar results in these cases as reported above.

Simpson-Visser II black hole: for the third model, we study the metric introduced in [191], where the deformation function is an exponential of the inverse the radial coordinate. This metric is constructed in such a way that at the origin a Minkowski core is recovered rather than a de Sitter one. We report the leading deformation coefficients

$$\begin{aligned}
\xi_2 &= -\frac{\overline{\epsilon}}{4}(\log(\overline{\epsilon}) - 1)\log(\overline{\epsilon}) \,, \\
\xi_4 &= \frac{(\overline{\epsilon})^3}{96}(\log(\overline{\epsilon}) - 1)\log(\overline{\epsilon})(\log(\overline{\epsilon})(4\log(\overline{\epsilon}) - 13) + 8) \,, \\
\xi_6 &= -\frac{(\overline{\epsilon})^5}{5760}(\log(\overline{\epsilon}) - 1)\log(\overline{\epsilon})\left\{\log(\overline{\epsilon})\left[\log(\overline{\epsilon})(\log(\overline{\epsilon})(34\log(\overline{\epsilon}) - 263) + 626) - 568\right] + 172\right\} \,,
\end{aligned} \tag{5.47}$$

where $\overline{\epsilon} := \epsilon + 1$. In Figure 5.3 (right column) we show the comparison of the coefficients $\{\xi_6, \xi_8, \xi_{10}, \xi_{12}\}$ with their approximations computed with a Padé approximant with $(N, M) = (2, 2)$ (upper panel) and $\{\xi_{10}, \xi_{12}\}$ with their approximation using a Padé approximation with $(N, M) = (4, 4)$ (lower panel). In Fig. 5.5 (third panel from the left) we compare the proper distance numerically computed with the exact metric and the Padé approximants of different orders. In Figure 5.4 (right panel) we show the comparison with the analytical form of the effective potential U^2 with the Padé approximations of various orders. Finally, in Figure 5.5 (middle) we compare different approximations of the distance function numerically integrated (for a fixed value of $\epsilon = 0.2$) and the Padé approximants.[6]

The position of the maximum of the potential as well as the shadow following tables 5.1 and 5.2 respectively, is given as follows

[6]We notice that the Padé approximant of order $(N, M) = (2, 2)$ introduces a vertical tangent behaviour at a point outside of the horizon, which is a feature purely due to the (low order of) approximation and is effectively eliminated with a suitable choice of the Padé approximant order.

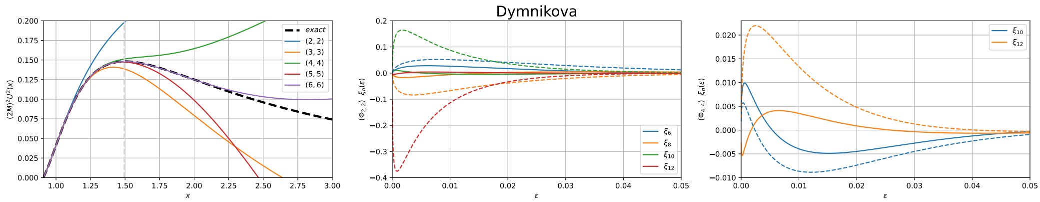

Figure 5.6: Left panel: comparison of the effective potential U^2 for the Dymnikova metric with various Padé approximants (5.32) for fixed $\epsilon = 0.1$. The vertical dashed gray line indicates the location of the maximum of the exact potential. Middle and right panels: comparison of the deformation coefficients of the Dymnikova metric ξ_{2n} (solid lines) with the (mass-rescaled) coefficients (5.13) (dashed lines) stemming from a Padé approximation $\Phi_{2,2}$ (middle panel) and $\Phi_{4,4}$ (right panel) as functions of ϵ.

N	M	$\sigma_1\,\mathfrak{c}$	$\tau_1\,\mathfrak{c}$
2	1	$-\frac{2}{3}\,(2+\sqrt{3})\,\epsilon + O(\epsilon^2)$	$-\frac{4}{3}\,(1+\sqrt{3})\,\epsilon + O(\epsilon^2)$
2	2	$-\frac{6}{13}\,(4+\sqrt{3})\,\epsilon + O(\epsilon^2)$	$-\frac{4}{3}\,\sqrt{\frac{10}{3}+2\sqrt{3}}\,\epsilon + O(\epsilon^2)$
2	3	$-\frac{8}{3}\,\epsilon + O(\epsilon^2)$	$-2\,\sqrt{3}\,\epsilon + O(\epsilon^2)$
3	3	$-\frac{8}{3}\,\epsilon + O(\epsilon^2)$	$-2\,\sqrt{3}\,\epsilon + O(\epsilon^2)$

Dymnikova black hole: special care must be paid to the Dymnikova spacetime [167], as its deformation function is non-analytic around $\eta = 0$. To address this, we use a double expansion in the power series of $u := e^{-1/\eta}$ and $\log u$. Specifically, the outer event horizon can be expanded as $x_H^{(\mathrm{Dymn})} = 1 - u + 3u^2 \log u + O(u^3)$. Since therefore the deformations of the position of the photon radius and the black hole shadow are not analytic functions of $\mathfrak{c}$, we cannot directly use the results of the tables 5.1 and 5.2. Nevertheless, we can demonstrate the efficiency of using Padé approximants to study the geometry and observables computed from it. We have plotted in the right panel of Figure 5.5 different approximations of the distance function: indeed, at order $(3,3)$, the Padé approximant represents an excellent approximation of the (numerically calculated) distance function (at $\epsilon = 0.1$). For completeness, here we report the first two deformation coefficients as in eq. (5.5) as functions of ϵ, which read

$$
\begin{aligned}
\xi_2 &= -\frac{3\epsilon}{4}(\epsilon+1)\log\left(\frac{\epsilon}{\epsilon+1}\right)\left[3\epsilon\log\left(\frac{\epsilon}{\epsilon+1}\right)+1\right] , \\
\xi_4 &= -\frac{\epsilon}{32}(\epsilon+1)^3\log\left(\frac{\epsilon}{\epsilon+1}\right)\left[3\epsilon\log\left(\frac{\epsilon}{\epsilon+1}\right)+1\right]\left[9\log\left(\frac{\epsilon}{\epsilon+1}\right)\left(2\epsilon+4\epsilon\log\left(\frac{\epsilon}{\epsilon+1}\right)+1\right)+4\right] ,
\end{aligned}
\tag{5.48}
$$

and in the middle and right panels in Fig. 5.6 we plot the higher order coefficients with their approximations with Padé of orders respectively $(N,M) = (2,2)$ and $(N,M) = (4,4)$. We can see that the expansion around $\epsilon = 0$ of such coefficients introduces a behaviour of the form $\xi_{2n} \propto \epsilon \log^n(\epsilon)$ which introduces numerical instability. Nevertheless we know that it has an analytical, but yet steep, convergence to 0, as one can see from the plots in Figure 5.6 .

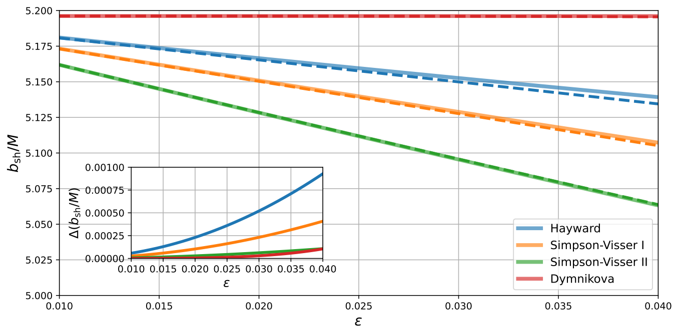

Figure 5.7: Comparison of the shadow computed from eq. (5.39) (dashed lines) to the exact numerical value (solid lines) for the models in Table 5.3. The inset plot shows the relative difference as explained in the text.

Finally, for all examples we can showcase the effective expression (5.39) for the black hole shadow, quantum-corrected to leading order: Figure 5.7 compares the result $b_{\rm sh}^{\rm app}/M$ obtained from (5.39) (dashed lines) in each case with the numerical result (solid lines) $b_{\rm sh}^{\rm exact}/M$, computed from the full metric in each case, as functions of (small) ϵ. In order to appreciate the quality of the approximation furnished by (5.39), the inset plot shows the relative difference $\Delta(b_{\rm sh}/M) = \left|\frac{b_{\rm sh}^{\rm exact}-b_{\rm sh}^{\rm app}}{b_{\rm sh}^{\rm exact}}\right|$: in all cases, for small values of ϵ, the latter is of the order of $< 0.1\%$, indicating that (5.39) indeed captures correctly the leading contribution to the black hole shadow. We note that this is in particular also the case for the Dymnikova black hole, in which case approximations of the shadow based on finite orders of the Padé approximant are in general not expected to be analytic in $\mathfrak{c}$ (or ϵ). While therefore intermediate results (notably table 5.2) cannot be directly used, the final result in (5.39) seems to correctly re-package the leading contributions in an effective manner.

5.3.2 Dilaton black hole

The black hole models of the previous Subsection have each been characterised by a single deformation function (*i.e.* these examples satisfy $f = h$ in the metric (3.1)). Here we present a different example, which is not bound by this limitation. Indeed, in [28, 193] a *dilaton-axion* system has been studied with a metric resembling a black hole. In absence of the axion field (and without spin), the line element of the latter is given

$$ds^2 = -\frac{\kappa - 2\mu}{\kappa + 2b}dt^2 + \frac{\kappa + 2b}{\kappa - 2\mu}d\kappa^2 + (\kappa^2 + 2b\kappa)d\Omega_2 \quad \text{with} \quad r^2 = \kappa^2 + 2b\kappa \quad \text{and} \quad M = \mu + b\,. \tag{5.49}$$

After changing to the same coordinates as in (3.1) we find (with $r = 2Mx$)

$$h = 1 + \frac{\eta - \sqrt{\eta^2 + 4x^2(1+\eta)^2}}{2x^2(1+\eta)}\,, \qquad f = \frac{\eta^2 + 4x^2(1+\eta)^2}{4x^2(1+\eta)^2}\left[1 + \frac{\eta - \sqrt{\eta^2 + 4x^2(1+\eta)^2}}{2x^2(1+\eta)}\right]\,,$$
$$\text{with} \qquad \eta = \frac{b}{\mu} = \epsilon(2+\epsilon)\,, \tag{5.50}$$

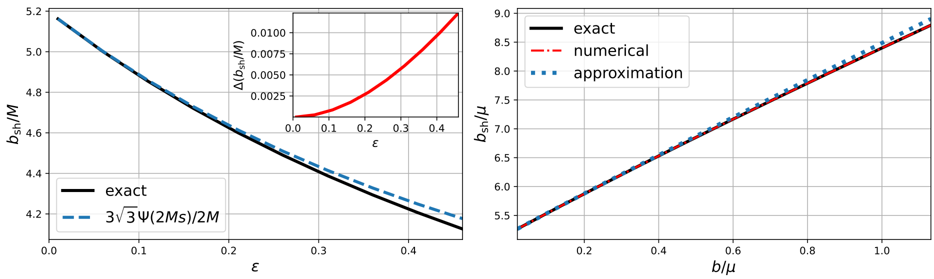

Figure 5.8: Left panel: Comparison of the shadow computed from eq. (5.39) (dashed blue line) to the exact numerical value (solid black line) for the dilaton black hole (5.50)) as a function of ϵ. The inset plot shows the relative difference between these two quantities. Right panel: Comparison to the analytic expression (5.53) of the shadow (solid black line) with a numerical computation (red line) and the approximation based on eq. (5.39) (dashed blue line), for a large range of the parameter b/μ defined in (5.50).

where ϵ is defined as in (5.43). For the coefficients (5.5) we find

$$
\begin{aligned}
\theta_2 &= \frac{\epsilon(\epsilon+2)(\epsilon(\epsilon+2)+2)\left(\sqrt{(\epsilon(\epsilon+2)+2)^2}-\epsilon(\epsilon+2)\right)}{16(\epsilon+1)\sqrt{(\epsilon(\epsilon+2)+2)^2}} = \frac{\epsilon}{4}-\frac{\epsilon^2}{8}+O(\epsilon^3)\,,\\
\theta_4 &= -\frac{\epsilon}{12}+\frac{\epsilon^2}{96}+O(\epsilon^3)\,,\\
\xi_2 &= \frac{\epsilon(\epsilon+2)(\epsilon(\epsilon+2)+2)\left(3\epsilon(\epsilon+2)\left(\epsilon(\epsilon+2)-\sqrt{(\epsilon(\epsilon+2)+2)^2}+2\right)+4\right)}{64(\epsilon+1)^3} = \frac{\epsilon}{4}-\frac{3\epsilon^2}{8}+O(\epsilon^3)\,,\\
\xi_4 &= -\frac{\epsilon}{12}+\frac{5\epsilon^2}{32}+O(\epsilon^3)\,,
\end{aligned} \tag{5.51}
$$

which indeed are all of order $O(\epsilon)$ and are thus compatible with the scaling (5.6). We can thus directly use Tables 5.1 and 5.2 to calculate the position of the photon radius and the shadow, as shown in the following table

N	M	$\sigma_1\,\mathfrak{c}$	$\tau_1\,\mathfrak{c}$
2	1	$-\frac{2}{3}\,(2+\sqrt{3})\,\epsilon+O(\epsilon^2)$	$-\frac{4}{3}\,(1+\sqrt{3})\,\epsilon+O(\epsilon^2)$
2	2	$-\frac{6}{13}\,(4+\sqrt{3})\,\epsilon+O(\epsilon^2)$	$-\frac{4}{3}\,\sqrt{\frac{10}{3}+2\sqrt{3}}\,\epsilon+O(\epsilon^2)$
2	3	$-\frac{8}{3}\,\epsilon+O(\epsilon^2)$	$-2\,\sqrt{3}\,\epsilon+O(\epsilon^2)$
3	3	$-\frac{8}{3}\,\epsilon+O(\epsilon^2)$	$-2\,\sqrt{3}\,\epsilon+O(\epsilon^2)$

We note that this table is in fact identical with the results in the case of the Simpson-Visser II black hole. Indeed, this is due to the fact that

$$
\theta_{2n}^{\text{axion-dilaton}}-\theta_{2n}^{\text{Simpson-Visser II}}=O(\epsilon^3)\,,\qquad\text{and}\qquad \xi_{2n}^{\text{axion-dilaton}}-\theta_{2n}^{\text{Simpson-Visser II}}=O(\epsilon^2)\,, \tag{5.52}
$$

thus leading to the identical results to leading order in ϵ. We also remark that an analytic expression for the black hole shadow for the geometry (5.49) was found in [197]

$$\frac{b_{\rm sh}}{M} = \frac{1}{\sqrt{2}(1+\eta)}\sqrt{27+36\eta+8\eta^2+(9+8\eta)^{3/2}} = 3\sqrt{3}-2\sqrt{3}\,\epsilon+\mathcal{O}(\epsilon)\,, \tag{5.53}$$

which indeed agrees with the result obtained from the approximations of Table 5.2 for sufficiently large (N, M). The shadow has also been computed numerically in [68] using different effective approximations. We also remark that (5.39) gives an excellent approximation for the shadow for a large range of ϵ, as is showcased in Figure 5.8.

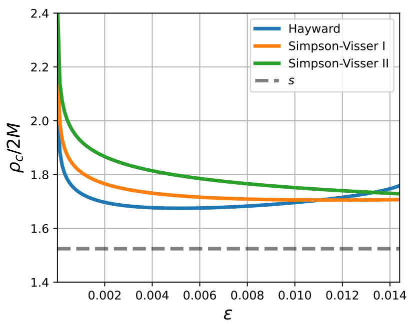

Figure 5.9: Numerical estimate of the radius of convergence in the case of the Hayward, Simpson-Visser I and Simpson-Visser II black hole. The dashed black line is the value of $\mathfrak{s}$ in (5.36).

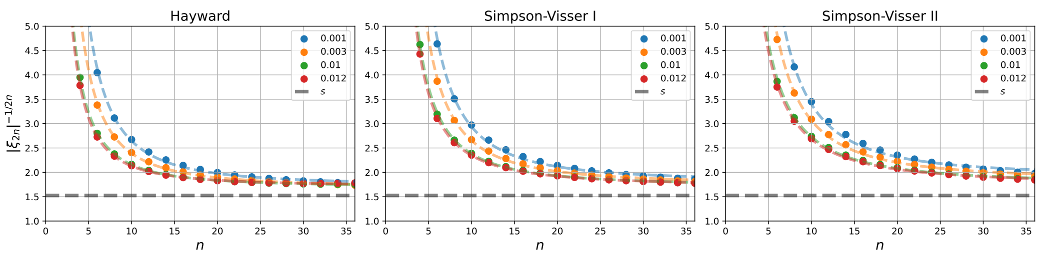

Figure 5.10: Asymptotic behaviour of $|\xi_{2n}|^{-\frac{1}{2n}}$, respectively from the left, in the case of the Hayward, Simpson-Visser I and Simpson-Visser II black holes, for different values of ϵ. The dashed coloured lines are interpolations of the form $a + \frac{b}{x^c}$, while the dashed black line is the value of $\mathfrak{s}$ in (5.36).

5.4 Convergence

In order to obtain the effective expression (5.39) of the black hole shadow in Section 5.2.3, we have implicitly assumed that the Taylor series (5.1) of the metric deformation function Ψ converges at $\rho = 2M\mathfrak{s}$. To get an intuition whether this is indeed the case, we study numerically the radii of convergence for the Hayward, Simpson-Visser I and II black hole. Indeed, the coefficients $|\xi_{2n}|^{-\frac{1}{2n}}$ up to $n = 36$ are plotted for some values of ϵ in the three panels in Figure 5.10. The dashed lines in each case represent numerical interpolations of the form $a + \frac{b}{x^c}$ (with $a, b, c \in \mathbb{R}$ and $c > 0$). The value of a in each case is a numerical approximation of the radius of convergence ρ_c of the function Ψ. Based on a more systematic study, this radius is plotted on the right in Figure 5.9 as a function of ϵ, with the dashed line representing the value of $\mathfrak{s}$. As is evident, at least for small values of ϵ, $\mathfrak{s}$ lies within the radius of convergence of the series, thus justifying the resummation leading to (5.39). Finally, due to the inherent similarity between the axion-dilaton black hole and the Simpson-Visser II geometry (see (5.52)) at leading order in ϵ, we expect a similar result also hold for the example discussed in Section 5.3.2.

6 Comparison of Parametrized Black Hole Metrics

Astrophysical BHs are natural probes of the strong-field regime of gravity, offering a unique arena to test GR under extreme curvature scales. According to GR, stationary BHs are fully characterized by their mass, charge, and angular momentum, as dictated by the *no-hair conjecture* (cf. Sec. 2.1.3). Despite their apparent simplicity, the fundamental nature of these objects remains uncertain, as current observations have not yet constrained potential deviations from the Kerr or Schwarzschild geometries with sufficient precision. This motivates the construction of agnostic frameworks capable of parametrizing possible departures from classical BH solutions while maintaining general covariance and regularity.

The objective of this chapter is twofold. First, we analyze the Johannsen–Psaltis and Rezzolla–Zhidenko parametrizations and establish their correspondence with the previously introduced proper-distance EMD parametrization near the horizon, as well as with its large-distance extension. This comparative analysis clarifies the mapping between the various sets of expansion coefficients, highlighting the complementarities and gaps among the different frameworks within a unified perspective. Second, we investigate the performance of these parametrizations in reproducing physically relevant quantities around deformed BH spacetimes, with particular emphasis on the *eikonal quasi-normal modes* (cf. Sec. 2.4.1) of representative BH models.

6.1 Agnostic parametrizations

In this section, we briefly describe the following parametrizations: Johannsen-Psaltis (JP) [65] (see Sec. 6.1.1), Rezzolla-Zhidenko (RZ) [68] (see Sec. 6.1.2). The EMD in the vicinity of the BH parametrization is also shortly reviewed using the results reported in Sections 3.2 and 5.1. Moreover, we introduce a new EMD parametrization from asymptotic series at large distance from the BH that was first used in [45] and further investigated in [46]. In Sec. 6.2 we provide the transformation maps relating the aforementioned parametrizations, where we also discuss their mathematical aspects and connections.

In all parametrizations, we consider a generic static and spherically symmetric spacetime, whose line element in Schwarzschild coordinates (t, r, θ, φ) reads

$$\mathrm{d}s^2 = g_{tt}(r)\mathrm{d}t^2 + g_{rr}(r)\mathrm{d}r^2 + r^2\left(\mathrm{d}\theta^2 + \sin^2\theta\mathrm{d}\varphi^2\right) , \tag{6.1}$$

where g_{tt} and g_{rr} are functions of the radial coordinate r only. In all the aforementioned parametrizations, we employ the experimental bounds existing on the deviations from GR in the weak-field regime, also known as parametrized post-Newtonian (PPN) constraints [198, 199].

6.1.1 Johannsen-Psaltis parametrization

The JP parametrization originates from the need to test the no-hair conjecture with observations of BHs in the electromagnetic spectrum. This approach is expressed through a parametric spacetime containing a quadrupole moment independent of both mass and spin [65]. Therefore, any deviation from GR manifests in anomalous contributions to the quadrupole moment [65, 200].

However, this framework has been generalized by the authors in [67] to overcome a series of issues. The original JP parametrization reads (cf. eq. (6.1)):

$$g_{tt}^{\text{JP}} = -[1+g(r)]\left(1-\frac{2\tilde{M}}{r}\right)\,, \quad g_{rr}^{\text{JP}} = \frac{1+g(r)}{1-\frac{2\tilde{M}}{r}}\,, \tag{6.2}$$

where the function $g(r)$ is defined as the series:

$$g(r) \coloneqq \sum_{n=1}^{\infty} \epsilon_n \left(\frac{\tilde{M}}{r}\right)^n = \sum_{n=1}^{\infty} \frac{\epsilon_n}{2^n}\left(\frac{r_H}{r}\right)^n\,, \tag{6.3}$$

with ϵ_n real constants to be determined from observations, and $\tilde{M}$ is related to the horizon position $r_H = 2\tilde{M}$ and to the gravitational mass-energy of the spacetime M through:

$$M = \tilde{M}\left(1-\frac{\epsilon_1}{2}\right)\,. \tag{6.4}$$

The revised JP parametrization becomes [67]

$$g_{tt}^{\text{JP}} = -\left[1+g^t(r)\right]\left(1-\frac{2\tilde{M}}{r}\right)\,, \quad g_{rr}^{\text{JP}} = \frac{1+g^r(r)}{1-\frac{2\tilde{M}}{r}}\,, \tag{6.5}$$

where the functions g^t and g^r are expanded as

$$g^i(r) = \sum_{n=1}^{\infty} \epsilon_n^i \left(\frac{\tilde{M}}{r}\right)^n \quad \text{with} \quad i = t, r\,, \tag{6.6}$$

and the set of s $\{\epsilon_i^t, \epsilon_i^r\}_{i\geq 1}$ has doubled with respect to the previous version of the JP parametrization. The comparison with the PPN parameters entails

$$M = \tilde{M}\left(1-\frac{\epsilon_1^t}{2}\right)\,, \tag{6.7a}$$

$$\epsilon_1^r = \gamma\,(2-\epsilon_1^t) - 2\,, \tag{6.7b}$$

$$2\epsilon_2^t = (\beta-\gamma)(\epsilon_1^t-2)^2 + 4\epsilon_1^t\,. \tag{6.7c}$$

Hence, the parameters ϵ_1^t, ϵ_2^r, and $\{\epsilon_i^t, \epsilon_i^r\}_{i\geq 3}$ are not constrained, even in the case of GR, where $\beta = \gamma = 1$.

6.1.2 Rezzolla-Zhidenko parametrization

The RZ parametrization aims to describe BH spacetimes in generic metric theories of gravity using a model-independent approach [68]. The line element of the RZ parametrization reads (cf. eq. (6.1))

$$g_{tt}^{\rm RZ} = -N^2(r) \quad \text{and} \quad g_{rr}^{\rm RZ} = \frac{B^2(r)}{N^2(r)} \,. \tag{6.8}$$

The BH event horizon is located at $r = r_H > 0$ and is defined by $N(r_H) = 0$. The radial coordinate is then compactified by introducing the dimensionless variable $x := 1 - r_H/r$, such that $x = 0$ marks the location of the event horizon, while $x = 1$ corresponds to spatial infinity.

We rewrite N as $N^2 = x\,A(x)$, where $A(x) > 0$ for $0 \leq x \leq 1$. We further express the functions A and B in terms of the parameters ϵ, a_0, and b_0, as follows:

$$A(x) = 1 - \epsilon(1-x) + (a_0 - \epsilon)(1-x)^2 + \tilde{A}(x)(1-x)^3 \,, \tag{6.9a}$$

$$B(x) = 1 + b_0(1-x) + \tilde{B}(x)(1-x)^2 \,, \tag{6.9b}$$

where ϵ encodes deviations of r_H from the Schwarzschild radius $\epsilon := \frac{2M - r_H}{r_H}$ and the functions $\tilde{A}$ and $\tilde{B}$ describe the metric near the horizon (for $x \simeq 0$) and are finite there, as well as at spatial infinity (for $x \simeq 1$).

To achieve rapid convergence, these two functions are modeled via the Padé approximants in the form of continued fractions as

$$\tilde{A}(x) = \cfrac{a_1}{1 + \cfrac{a_2 x}{1 + \cfrac{a_3 x}{1 + \dots}}} \,, \tag{6.10a}$$

$$\tilde{B}(x) = \cfrac{b_1}{1 + \cfrac{b_2 x}{1 + \cfrac{b_3 x}{1 + \dots}}} \,, \tag{6.10b}$$

where $a_1, a_2, a_3 \dots$ and $b_1, b_2, b_3 \dots$ are dimensionless constants determined from observations.

Note that by comparing the large-distance expansion in eq. (6.8) with the PPN one, we can put experimental bound on the first coefficients:

$$a_0 = \frac{(\beta - \gamma)(1+\epsilon)^2}{2} \lesssim 10^{-5} \,, \tag{6.11a}$$

$$b_0 = \frac{(\gamma - 1)(1+\epsilon)}{2} \lesssim 10^{-5} \,. \tag{6.11b}$$

6.1.3 Effective Metric Description parametrization

The EMD parametrizes the deformations of the classical Schwarzschild metric in terms of spacetime invariants, which can be measured by observers independently from the set of coordinates, and preserve the same symmetries as GR. A natural choice for such a physical quantity is the radial proper distance to the BH horizon, as extensively described in Sec. 3.2 and summarized in Sec. 5.1. The metric components can be written as

$$g_{tt}^{\rm EMD} = -h(r) \quad \text{and} \quad g_{rr}^{\rm EMD} = \frac{1}{f(r)} \,, \tag{6.12}$$

where the functions h and f are defined as in eq. (3.2):

$$h(r) = 1 - \frac{\Psi^{(\rho)}(\rho)}{r} \quad \text{and} \quad f(r) = 1 - \frac{\Phi^{(\rho)}(\rho)}{r}\,, \tag{6.13}$$

with ρ being the proper distance from the BH event horizon and defined in eq. (3.6). The functions in eq. (6.13) are positive definite for $r > r_H$ (r_H being the BH event horizon) and the deformation functions Ψ and Φ are invariant under coordinate reparametrizations and admit the Taylor expansion in eq. (3.7), where ξ_n and θ_n are real constants. As in Chap. 5, we will work under the assumptions that the series in eqs. (3.7) are assumed to have a non-vanishing radius of convergence, and all derivatives of h and f with respect to r evaluated in r_H are well defined. This implies $\xi_{2n-1} = \theta_{2n-1} = 0$ for all $n \in \mathbb{N}$, and $\xi_2 \leq M/8r_H$. The proper distance $\rho(r)$ and its inverse $r(\rho)$ can be obtained via eq. (3.7). The derivatives of the metric functions at the horizon can be written in terms of $\{\xi_{2n}, \theta_{2n}\}_{n\geq 1}$ as reported in eqs. (5.2).

EMD at large distance from the BH

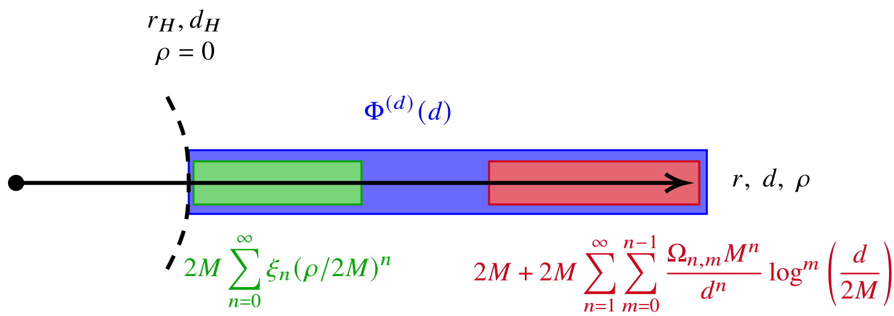

Figure 6.1: *Schematic division of the space outside of the black hole in three main regions. The curved dashed line represents the position of the event horizon. The blue region is where the full non-perturbative form of the metric functions, given in eq. (3.2) is expected to hold (namely the whole space-time outside the event horizon). For simplicity, we only give the expressions for f in the Figure, but a similar form also holds for h. The green region is where the metric is expanded as a convergent series in the proper distance from the event horizon ρ, as given in eq. (3.7). Finally, the red region refers to the asymptotically large distances from the event horizon, where the metric can be expanded in inverse powers of the proper distance, as given in eqs (6.15).*

The novel aspect introduced in this chapter is the extension of the EMD to the spacetime regions far from the BH horizon, where the spacetime is weakly curved, but still affected by the presence of the BH. Looking at the same approach introduced in Sec. 3.2, we can asymptotically expand the deformation functions and self-consistently solve for the metric functions. The full radial proper distance $d(r)$ from $r = 0$ is then given by the differential problem

$$\frac{\mathrm{d}d}{\mathrm{d}r} = \left|1 - \frac{\Phi(d)}{r}\right|^{-1/2} \quad \text{with} \quad d(0) = 0\,. \tag{6.14}$$

In order to determine the metric functions, we could start by assuming that $\Phi(d)$ and $\Psi(d)$ can be expanded in power series of $1/d$. However, solving eq. (6.14) will lead to logarithmic terms in the asymptotic expansions of $h(r)$ and $f(r)$, which are absent in the post-Newtonian expansion and in any other parametrization presented above. Therefore, to avoid any mismatch, we can reabsorb the logarithms introducing new terms in $\Phi(d)$ and $\Psi(d)$ as

$$\Phi(d) = 2M\left[1+\sum_{n=1}^{\infty}\sum_{m=0}^{n-1}\frac{\Omega_{n,m}M^n}{d^n}\log^m\left(\frac{d}{2M}\right)\right], \tag{6.15a}$$

$$\Psi(d) = 2M\left[1+\sum_{n=1}^{\infty}\sum_{m=0}^{n-1}\frac{\Gamma_{n,m}M^n}{d^n}\log^m\left(\frac{d}{2M}\right)\right], \tag{6.15b}$$

where $\Omega_{n,m}$ and $\Gamma_{n,m}$ are real constants and $\omega_n \equiv \Omega_{n,0}$ and $\gamma_n \equiv \Gamma_{n,0}$.

We consider the post-Newtonian (PN) expansion $M/r \ll 1$, (the weak-field limit $M/r \ll 1$ is related to low velocity limit $v/c \ll 1$ via the virial theorem [201], namely $M/r \sim v^2/c^2$). In this regime, we have $1/(r^i d^j) \sim 1/(r^{i+j})$ and the function $d(r)$ admits the logarithmic corrections: $(M/r)^j \log^k(r/M)$, with $\{k, j\} \in \mathbb{N}_0$ and $0 < k \leq j-1$. We PN-expand eq. (6.14) via eq. (6.15), which gives

$$\begin{aligned}
\frac{d(r)}{M} = {} & \frac{r}{M} + \log\left(\frac{r}{2M}\right) + k - \left(\frac{3}{2}+\omega_1\right)\frac{M}{r} - \left[\frac{5}{4} + \frac{\omega_1(5-2k)}{4} + \frac{\omega_2+\Omega_{2,1}}{2}\right]\frac{M^2}{r^2} \\
& + \frac{M^2(\omega_1-\Omega_{2,1})}{2r^2}\log\left(\frac{r}{2M}\right) - \left[\frac{35}{24} + \frac{(74-21k+9k^2)\omega_1}{27}\right. \\
& \left. + \frac{45\omega_1^2 + 6(7-6k)\omega_2 + 2(8+3k)\Omega_{2,1}}{54} + \frac{9\omega_3 + 3\Omega_{3,1} + 2\Omega_{3,2}}{27}\right]\frac{M^3}{r^3} \\
& + \Big[(7-6k)\omega_1 + 6\omega_2 - 2(4-3k)\Omega_{2,1} - 3\Omega_{3,1} - 2\Omega_{3,2}\Big]\frac{M^3}{9r^3}\log\left(\frac{r}{2M}\right) \\
& - [\omega_1 + 2\Omega_{2,1} - \Omega_{3,2}]\frac{M^3}{3r^3}\log^2\left(\frac{r}{2M}\right) + \mathcal{O}\left(\frac{M^4}{r^4}\right),
\end{aligned} \tag{6.16}$$

where k is a real integration constant, kept as a free parameter. It is important to note that k plays the role of the gauge for d, as its value determines the position at which $d = 0$. Any shift of the proper distance by k induces a transformation on the $\{\Omega_{n,m}\}_{n\geq 1}^{0\leq m\leq n-1}$ and hence an EMD redefinition, as shown in eqs. (3.55) and (3.59) in Sec. 3.3. Inserting eq. (6.16) into the metric functions modified with the series in eq. (6.15), we obtain the conditions to balance and cancel out (up to a given order) the logarithmic functions in eq. (6.17), which requires

$$\begin{gathered}
\Omega_{2,1} = \omega_1\,, \quad \Omega_{3,1} = -\omega_1 + 2\omega_2\,, \quad \Omega_{3,2} = \omega_1\,, \quad \Omega_{4,3} = \omega_1\,, \quad \Omega_{4,2} = -\frac{5}{2}\omega_1 + \frac{6}{2}\omega_2\,, \\
\Omega_{4,1} = \omega_1 - 2\omega_2 + 3\omega_3\,, \qquad \Omega_{5,4} = \omega_1\,, \qquad \Omega_{5,3} = -\frac{13}{3}\omega_1 + \frac{12}{3}\omega_2\,, \\
\Omega_{5,2} = \frac{9}{2}\omega_1 - \frac{14}{2}\omega_2 + \frac{12}{2}\omega_3\,, \qquad \Omega_{5,1} = -\omega_1 + 2\omega_2 - 3\omega_3 + 4\omega_4\,,
\end{gathered}$$

for the first few terms. Although it is difficult to generalize the above relations, they can be computed to arbitrary order and applied to the set $\{\Gamma_{n,m}\}_{n\geq 1}^{0\leq m\leq n-1}$. Using the above conditions, we are able to eliminate the logarithmic functions appearing in eq. (6.16) and obtain the metric functions

$$f(r) = 1 - \frac{2M}{r} - \frac{2M^2\omega_1}{r^2} + (k\omega_1 - \omega_2)\frac{2M^3}{r^3}$$

$$- \left[\left(k^2 + k + \frac{3}{2} \right) \omega_1 + \omega_1^2 - 2k\omega_2 + \omega_3 \right] \frac{2M^4}{r^4} + O\left(\frac{M^5}{r^5} \right) , \tag{6.17a}$$

$$h(r) = 1 - \frac{2M}{r} - \frac{2M^2\gamma_1}{r^2} + (k\gamma_1 - \gamma_2)\frac{2M^3}{r^3}$$
$$- \left[\left(k^2 + k + \frac{3}{2} \right) \gamma_1 + \gamma_1\omega_1 - 2k\gamma_2 + \gamma_3 \right] \frac{2M^4}{r^4} + O\left(\frac{M^5}{r^5} \right) . \tag{6.17b}$$

It is important to emphasize that the asymptotic series in eqs. (6.17) must be interpreted with care. When truncating the parametrization to a finite number of deformation parameters, for instance $(\omega_1, \ldots, \omega_n)$ and $(\gamma_1, \ldots, \gamma_n)$, only the terms up to order $1/r^{n+1}$ should be retained. Coefficients at higher orders in $1/r$ are not reliable, because they implicitly depend on additional parameters that have been set to zero by the truncation. As a consequence, the apparent $1/r^m$ term with $m > n + 1$ does not represent the true asymptotic behavior of the full parametrization, but rather a spurious artifact of the cutoff. This issue is absent in the Johannsen–Psaltis parametrization, where truncating the expansion automatically suppresses all higher-order terms, ensuring internal consistency. In contrast, in the EMD approach, truncation must be imposed manually by discarding all terms beyond the order supported by the retained number of parameters.

The combinations $k\omega_1 - \omega_2$ and $k\gamma_1 - \gamma_2$, as well as those appearing at higher orders, are independent of the choice of k. Indeed, observable quantities do not depend on the choice of this constant, as seen in Sec. 3.3. We also note that when the expansion is truncated at $O(M^4/r^4)$, the PN-expansions of f and h are equal when $\{\gamma_1, \gamma_2\}$ and $\{\omega_1, \omega_2\}$ are exchanged, whereas at the next leading order this is spoiled by the presence of mixed terms involving $\gamma_1\omega_1$.

By comparing (6.17) with the PPN expansion, we obtain:

$$|\gamma_1| = |\beta - \gamma| \lesssim 10^{-5} \quad \text{with} \quad \gamma = 1 . \tag{6.18}$$

At leading order in the PPN framework, we are able to map only γ_1 to β and γ, while ω_1 remains unconstrained. Conversely, the EMD expansion (6.17) is only able to capture a subset of PPN corrections, constrained by $\gamma = 1$.

6.2 Transformation maps relating the different parametrizations

In this section, we establish the relationships among the three distinct frameworks. Notably, while the event horizons in these parametrizations are defined through different formalisms, they all depend on free parameters. However, in all cases, they must uniquely identify the BH event horizon r_H. This observation is significant, as it facilitates the subsequent computational analyses.

JP to EMD (near horizon) parametrizations

First, we compare the temporal metric coefficients g_{tt} in the EMD (6.12) and JP (6.5) parametrizations:

$$g_{tt}^{\rm EMD} = -\sum_{n=1}^{\infty} \frac{h_H^{(n)}}{n!}(r-r_H)^n = -\frac{1+g^t(r)}{r}(r-r_H) = g_{tt}^{\rm JP} \,. \tag{6.19}$$

Dividing both sides by $(r-r_H)$ we obtain

$$\sum_{n=1}^{\infty} \frac{h_H^{(n)}}{n!}(r-r_H)^{n-1} = \frac{1+g^t(r)}{r} = \frac{1}{r}\left[1+\sum_{j=1}^{\infty}\frac{\epsilon_j^t}{2^j}\left(\frac{r_H}{r}\right)^j\right] \equiv \sum_{j=0}^{\infty}\frac{\epsilon_j^t}{2^j}\frac{r_H^j}{r^{j+1}} \,, \tag{6.20}$$

where we included additional coefficient $\epsilon_0^t = 1$ in the sum. Evaluating eq. (6.20) at $r = r_H$, we obtain for $n = 1$

$$h_H^{(1)} = \frac{1+g^t(r_H)}{r_H} = \frac{1}{r_H}\sum_{j=0}^{\infty}\frac{\epsilon_j^t}{2^j} \,. \tag{6.21}$$

The coefficients $h_H^{(n)}$ can be computed by taking n derivatives of eq. (6.20) and then evaluating it at $r = r_H$. The general expression for the coefficients $h_H^{(n)}$ is thus:

$$h_H^{(n)} = n\frac{{\rm d}^n}{{\rm d}r^n}\left(\sum_{j=1}^{\infty}\frac{\epsilon_j^t}{2^j}\frac{r_H^j}{r^{j+1}}\right)\Bigg|_{r=r_H} = \frac{(-1)^n n}{r_H^{n+1}}\sum_{j=1}^{\infty}\frac{\epsilon_j^t}{2^j}\frac{(j+n)!}{j!} \,. \tag{6.22}$$

A similar approach can be applied to the radial metric component, yielding:

$$g_{rr}^{\rm EMD} = \frac{1}{f(r)} = \frac{1+g^r(r)}{1-r_H/r} = g_{rr}^{\rm JP} \,, \tag{6.23}$$

where

$$f(r) = \sum_{n=1}^{\infty}\frac{f_H^{(n)}}{n!}(r-r_H)^n \,. \tag{6.24}$$

This can be also written as

$$f_H^{(1)} = \frac{1}{r_H[1+g^r(r_H)]} \,, \tag{6.25a}$$

$$f_H^{(n)} = n\frac{{\rm d}^n}{{\rm d}r^n}\left[\frac{1}{r(1+g^r(r))}\right]\Bigg|_{r=r_H} \,, \tag{6.25b}$$

where the general term $f_H^{(n)}$ cannot be easily found and then written in a closed form.

Comparing eqs. (6.25a) with (5.2a), eqs. (6.21) with (5.2b), and recalling that $r_H = 2M/(1-\epsilon_1^t/2)$, we finally obtain

$$\xi_2 = \frac{g^r(r_H)(2-\epsilon_1^t)}{8[1+g^r(r_H)]^2} \,, \quad \theta_2 = \frac{g^t(r_H)(\epsilon_1^t-2)}{8[1+g^r(r_H)]} \,, \tag{6.26}$$

with $g^r(r_H) \neq -1$. The case $g^r(r_H) = 1$ saturates the bound on $\xi_2 \leq (2-\epsilon_1^t)/32$. The expressions for the higher-order coefficients $\{\theta_{2n}, \xi_{2n}\}_{n\geq 2}$ are involved and we refrain from reporting them here. We note, however, that the higher-order derivatives of the metric functions depend linearly on these parameters, making their computation straightforward.

From these calculations we note that the EMD coefficients depend on an infinite number of JP terms, and vice versa. The JP coefficients can be written in terms of the EMD ones by inverting the linear system (6.22).

JP to EMD (large distance) parametrizations

The expansion of JP metric at large distance reads:

$$g_{tt}^{\rm JP} = -1 + \frac{\tilde{M}(2-\epsilon_1^t)}{r} + \frac{\tilde{M}^2(2\epsilon_1^t - \epsilon_2^t)}{r^2} + \mathcal{O}\left(\tilde{M}^3/r^3\right) , \tag{6.27a}$$

$$g_{rr}^{\rm JP} = 1 + \frac{\tilde{M}(2+\epsilon_1^r)}{r} + \frac{\tilde{M}^2(\epsilon_2^r + 2\epsilon_1^r + 4)}{r^2} + \mathcal{O}\left(\tilde{M}^3/r^3\right) . \tag{6.27b}$$

Comparing (6.27) with the EMD expansion (6.17), and taking into account the relation (6.7a), we finally obtain:

$$\epsilon_1^r = -\epsilon_1^t , \tag{6.28a}$$

$$\omega_1 = \frac{2[\epsilon_2^r + \epsilon_1^t(2-\epsilon_1^t)]}{(\epsilon_1^t - 2)^2}, \quad \gamma_1 = \frac{2(2\epsilon_1^t - \epsilon_2^t)}{(\epsilon_1^t-2)^2}, \tag{6.28b}$$

$$\omega_2 = -\frac{2}{(\epsilon_1^t-2)^3}\left\{2\epsilon_3^r + [k(\epsilon_1^t-2) - 2\epsilon_1^t](\epsilon_1^t-2)\epsilon_1^t + \epsilon_2^r[4(\epsilon_1^t-1) + k(2-\epsilon_1^t)]\right\} , \tag{6.28c}$$

$$\gamma_2 = \frac{2k(\epsilon_1^t-2)(2\epsilon_1^t-\epsilon_2^t) - 8\epsilon_2^t + 4\epsilon_3^t}{(\epsilon_1^t-2)^3} . \tag{6.28d}$$

where we write only the first few terms.

We note that this comparison can be easily carried out, because there is a one-to-one correspondence among the JP and EMD coefficients. This is due to the asymptotic expansion of the JP metric, which establishes a direct link among the two parametrizations.

JP to RZ parametrizations

We note that the map between eqs. (6.8) and (6.2) has already been presented in Ref. [68]. Here, we adapt it to the revised JP parametrization (6.5). Comparing that with eqs. (6.9a) and (6.9b), we have

$$-\epsilon\frac{r_H}{r} + (a_0 - \epsilon)\left(\frac{r_H}{r}\right)^2 + \left(\frac{r_H}{r}\right)^3 \tilde{A}\left(1 - \frac{r_H}{r}\right) = g^t(r) , \tag{6.29}$$

$$b_0\frac{r_H}{r} + \left(\frac{r_H}{r}\right)^2 \tilde{B}\left(1 - \frac{r_H}{r}\right) = g^B(r) . \tag{6.30}$$

where we introduced the auxiliary function

$$g^B(r) := \sqrt{[1+g^t(r)][1+g^r(r)]} - 1 , \tag{6.31}$$

The first few coefficients can be extracted as

$$\epsilon = -\frac{\epsilon_1^t}{2} \ , \ a_0 = \frac{1}{2}\left(\frac{\epsilon_2^t}{2} - \epsilon_1^t\right) \ , \ b_0 = \frac{\epsilon_1^t + \epsilon_1^r}{4} \ . \tag{6.32}$$

By matching the two parametrizations near the horizon, we obtain algebraic relations between the RZ coefficients $\{a_n, b_n\}_{n\geq 1}$ and the JP coefficients $\{\epsilon_n^t, \epsilon_n^r\}_{n\geq 1}$. The first few expressions are displayed below:

$$a_1 = g^t(r_H) - a_0 + 2\epsilon = \sum_{n=3}^{\infty} \frac{\epsilon_n^t}{2^n} \ , \tag{6.33a}$$

$$b_1 = g^B(r_H) - b_0 \ , \tag{6.33b}$$

$$a_2 = -\frac{(r\,g^t)' + g^t + \epsilon}{a_1}\Big|_{r=r_H} - 1 = \sum_{n=4}^{\infty} \frac{\epsilon_n^t (n-3)}{2^n} \Big/ \sum_{n=3}^{\infty} \frac{\epsilon_n^t}{2^n} \ , \tag{6.33c}$$

$$b_2 = -\frac{(r\,g^B)'}{b_1}\Bigg|_{r=r_H} - 1 \ , \tag{6.33d}$$

$$a_3 = \frac{(r^2 g^t)'' - 2a_1[1 + a_2(a_2+2)]}{2a_1 a_2}\Big|_{r=r_H} \ , \tag{6.33e}$$

$$b_3 = \frac{(r^2 g^B)''}{2b_1 b_2}\Bigg|_{r=r_H} - (b_2 + 1) \ , \tag{6.33f}$$

where the prime indicates the derivative with respect to r. Naturally, in eq. (6.33) we can easily extend to higher orders if needed.

Finally, we remark that the terms $a_1, a_2, a_3 \ldots$ do not depend on ϵ_1^t and ϵ_2^t, whereas the terms $b_1, b_2, b_3 \ldots$ follow a more complicated expression, which we chose not to display here. In the simplest case when $\epsilon_3^t \neq 0$ and $\epsilon_n^t = 0$ for $n > 3$, we have $a_2 = 0$ and the approximant for the function $N(r)$ reproduces it exactly. This illustrates how the RZ coefficients can be related to the JP ones. The inverse map can be achieved by inverting the linear system (6.33).

RZ to EMD (near horizon) parametrizations

The final map to consider is between the RZ and EMD parametrizations. Throughout the calculations we make use of the results from Sec. 6.2. By employing eqs. (6.19) and (6.25b), we obtain the following two relations:

$$g^t(r) = r\left[\sum_{n=1}^{\infty} \frac{h_H^{(n)}}{n!}(r - r_H)^{n-1}\right] - 1 \ , \tag{6.34a}$$

$$g^r(r) = \frac{1}{\sum_{n=1}^{\infty} \frac{f_H^{(n)}}{n!}(r - r_H)^{n-1}} - 1 \ . \tag{6.34b}$$

We can now exploit eq. (6.33) to express the RZ coefficients in terms of the derivatives of $g^t(r)$ and $g^r(r)$, which, in turn, are related to the EMD coefficients.

We can obtain the direct link between the first-order coefficients (θ_2, ξ_2) and (a_0, a_1, b_0, b_1) of the EMD and RZ parametrizations, respectively, by using $h_H^{(1)}$ and $f_H^{(1)}$ (cf. eqs. (6.21) and

(6.25a)) and

$$h(r) = N(r)^2 \quad \text{and} \quad f(r) = \frac{N(r)^2}{B(r)^2} \,. \tag{6.35}$$

In order to determine the relation between the coefficients, let us first define $y = r/(2M)$ and then expand the RZ metric functions up to the first order in $y - y_H$:

$$N(y)^2 = \frac{(3 + a_0 + a_1)y_H - 2}{y_H^2}(y - y_H) + O(y - y_H)^2 \,, \tag{6.36a}$$

$$\frac{N(y)^2}{B(y)^2} = \frac{(3 + a_0 + a_1)y_H - 2}{(1 + b_0 + b_1)^2\, y_H^2}(y - y_H) + O(y - y_H)^2 \,. \tag{6.36b}$$

Comparing these expansions with the first derivatives of eqs. (5.2a) and (5.2b) and solving for ξ_2 and θ_2, we obtain

$$\xi_2 = \frac{(1+\epsilon)(1+\mathcal{A}-2\epsilon)(\mathcal{B}(\mathcal{B}+2)-\mathcal{A}+2\epsilon)}{4(1+\mathcal{B})^4} \,, \tag{6.37a}$$

$$\theta_2 = \frac{(1+\epsilon)(2\epsilon-\mathcal{A})}{8}\left(1 + \frac{|1+2\mathcal{A}-\mathcal{B}(\mathcal{B}+2)-4\epsilon|}{(1+\mathcal{B})^2}\right) \,, \tag{6.37b}$$

where $\mathcal{A} \coloneqq a_0 + a_1$ and $\mathcal{B} \coloneqq b_0 + b_1$. It is worth noticing that the parameters ξ_2 and θ_2 depend on the RZ parameters only through the combinations $\mathcal{A}$ and $\mathcal{B}$. Moreover, the coefficients a_n and b_n with $n > 1$ do not contribute to the first-order parameters ξ_2 and θ_2.

Additional constraints on the parameters can be obtained by observing that, in the limit $b_0 = b_1 = 0$, we have $\mathcal{B} = 0$. At the horizon, $B(y) \equiv 1 + O\big((y - y_H)^2\big)$, so the first derivatives at the horizon in eqs. (6.36) must coincide with (5.2a) and (5.2b). This implies the additional condition $\xi_2 = \theta_2$. Furthermore, when setting $\mathcal{B} = 0$, the absolute value in eq. (6.37b) must be taken into account, which requires imposing

$$1 + 2\mathcal{A} - 4\epsilon > 0 \;\Rightarrow\; 2\epsilon - a_0 - a_1 < \frac{1}{2} \,. \tag{6.38}$$

The relations in eq. (6.37) can be inverted to obtain the coefficients $\mathcal{A}$ and $\mathcal{B}$ as functions of θ_2 and ξ_2. As previously noted, if $\theta_2 = \xi_2$, then the first derivatives of $f(y)$ and $h(y)$ at y_H must coincide. Moreover, in the limit $\epsilon \to 0$ (see under eq. (6.9)) the EMD and RZ parametrizations should recover the Schwarzschild BH. Therefore, we have:

$$\mathcal{A} = \frac{1}{2\sqrt{2}\,\xi_2}\left[8\theta_2\xi_2 + (1+\epsilon)(\xi_2-\theta_2) + \sqrt{1+\epsilon}\,(\xi_2-\theta_2)\sqrt{1+\epsilon-16\xi_2}\right]^{1/2} - 1 \,, \tag{6.39a}$$

$$\mathcal{B} = 2\epsilon - \frac{\theta_2}{2\xi_2}\left(1 - \sqrt{1 - \frac{16\xi_2}{1+\epsilon}}\right) \,. \tag{6.39b}$$

This approach can be straightforwardly generalized to higher-order coefficients by following the procedure already described for the first-order terms. The expressions beyond first order become rather cumbersome, and hence we choose not to display them here. We conclude there exists a well-defined and direct correspondence between the coefficients of the EMD and RZ parametrizations.

RZ to EMD (large distance) parametrization

The comparison between RZ and EMD parametrizations at large distance can be obtained by considering the following expansion for the RZ metric components:

$$g_{tt}^{\mathrm{RZ}} = -1 + \frac{2M}{r} - \frac{4a_0M^2}{(\epsilon+1)^2r^2} - \frac{8M^3\left[\tilde{A}(1) - a_0 + \epsilon\right]}{(\epsilon+1)^3r^3} + \mathcal{O}\left(\frac{M^4}{r^4}\right), \tag{6.40a}$$

$$g_{rr}^{\mathrm{RZ}} = 1 + \frac{2M(2b_0+\epsilon+1)}{(\epsilon+1)r} + \mathcal{O}\left(\frac{M^2}{r^2}\right). \tag{6.40b}$$

Comparing these expansions with eq. (6.17), we obtain $b_0 = 0$ and the following conditions on the first few parameters:

$$\omega_1 = \frac{4\tilde{B}(1) - 2a_0}{(\epsilon+1)^2}, \quad \gamma_1 = -\frac{2a_0}{(\epsilon+1)^2}, \quad \gamma_2 = -\frac{2\left[a_0(k(1+\epsilon)-2) + 2(\tilde{A}(1)+\epsilon)\right]}{(\epsilon+1)^3}, \tag{6.41a}$$

$$\omega_2 = -\frac{2}{(\epsilon+1)^3}\left\{a_0[k(1+\epsilon)-2] + 2\Big[\epsilon + \tilde{A}(1) + (2-k)(1+\epsilon)\tilde{B}(1) + 2\tilde{B}'(1)\Big]\right\}, \tag{6.41b}$$

where we note that the full continued fractions $\tilde{A}(1)$ and $\tilde{B}(1)$ (cf. eq. (6.10)) and their derivatives appear, with the prime denoting differentiation with respect to x defined in Sec. 6.1.2. As mentioned previously, the coefficients of RZ and EMD parametrizations at large distance are in one-to-one correspondence.

6.2.1 Eikonal limit in different parametrizations

As an application of the mapping among the three parametrizations, we now consider the eikonal limit of QNMs (cf. Sec. 2.4.1) within the framework of BH perturbation theory.

In this subsection, we investigate the eikonal limit within the three BH parametrizations introduced in Sec. 6.1. For a generic parametrization, the corresponding set of infinite coefficients is treated as independent. However, once a specific model is considered, these coefficients become functions of a finite number of free parameters.

In the next subsection, we examine small deviations from the Schwarzschild solution using models specified by the mass M and a single additional l, which quantifies the departure from the GR geometry. This introduces a displacement of the BH horizon radius r_H from its Schwarzschild value $2M$. To describe this effect, we adopt the perturbative parameter ϵ (see below eq. (6.9)), which allows for a Taylor expansion of the quantities that enter the eikonal QNM limit. Other choices, such as ϵ_1^t in the JP parametrization, are equally possible.

We then expand the physically relevant quantities in eq. (2.55) in the eikonal limit up to linear order in ϵ for each parametrization. Higher-order terms in ϵ are subsequently used to estimate the truncation error.

Rezzolla-Zhidenko parametrization

We start with the RZ parametrization, where the ϵ parameter emerges naturally. We assume the coefficients a_n and b_n admit a power-series expansion in ϵ of the form

$$a_n(\epsilon) = \sum_{p=0} A_{n,p}\,\epsilon^p \quad \text{and} \quad b_n(\epsilon) = \sum_{p=0} B_{n,p}\,\epsilon^p\,, \tag{6.42}$$

for $n \geq 0$ and $A_{0,0} = A_{1,0} = B_{0,0} = B_{1,0} = 0$. The last condition ensures that the leading contributions to the metric functions from $a_0(\epsilon)$, $a_1(\epsilon)$, $b_0(\epsilon)$, and $b_1(\epsilon)$ vanish in the Schwarzschild limit $\epsilon \longrightarrow 0$, thereby guaranteeing that the deformations associated with eqs. (6.9a) and (6.9b) are continuously switched off.

The values of the coefficients $A_{n,p}$ and $B_{n,p}$ depend on the specific model under consideration. In general, these coefficients appear in the series expansion of the quantities in eqs. (2.55) through nonlinear combinations at each order in ϵ. These expressions simplify dramatically when $A_{2,0} = B_{2,0} = 0$:

$$\frac{r^{\rm RZ}_{\rm ps}}{M} = 3 - \frac{4}{9}\left(5 + A_{0,1} + A_{1,1}\right)\,\epsilon + \mathcal{O}\!\left(\epsilon^2\right)\,, \tag{6.43a}$$

$$\Omega^{\rm RZ} M = \frac{1}{3\sqrt{3}} + \frac{2}{81\sqrt{3}}\left(6 + 3A_{0,1} + 2A_{1,1}\right)\,\epsilon + \mathcal{O}\!\left(\epsilon^2\right)\,, \tag{6.43b}$$

$$\lambda^{\rm RZ} M = \frac{1}{3\sqrt{3}} + \frac{2}{81\sqrt{3}}\left(-4 + 7A_{0,1} + 4A_{1,1} + 9B_{0,1} - 6B_{1,1}\right)\,\epsilon + \mathcal{O}\!\left(\epsilon^2\right)\,. \tag{6.43c}$$

In the following sections, we restrict our attention to BH metrics satisfying the aforementioned condition.

Johannsen-Psaltis parametrization

Following the same reasoning as for the RZ parametrization, we note that the deformation functions $g^t(r)$ and $g^r(r)$ must vanish in the Schwarzschild limit. This implies that all JP parameters $\{\epsilon^t_n, \epsilon^r_n\}_{n\geq 1}$ scale homogeneously with ϵ. Indeed, as shown in eq. (6.32), we know that $\epsilon^t_1 = -2\,\epsilon$ exactly. Therefore, for $\epsilon \longrightarrow 0$ and the scaling behavior of eq. (6.42), we generally have $\epsilon^r_1, \epsilon^t_2 \sim \mathcal{O}\!\left(\epsilon^k\right)$, with $k \geq 1$. Hence, we assume the following general power series expansion

$$\epsilon^t_n(\epsilon) = \sum_{p=1} (\epsilon^t_n)_p\,\epsilon^p \quad \text{for} \quad n \geq 2\,, \tag{6.44a}$$

$$\epsilon^r_n(\epsilon) = \sum_{p=1} (\epsilon^r_n)_p\,\epsilon^p \quad \text{for} \quad n \geq 1\,, \tag{6.44b}$$

which could be equivalently read as a power series in ϵ^t_1. The expressions for the coefficients $(\epsilon^t_n)_p$ and $(\epsilon^r_n)_p$ are determined by the model under investigation. Inserting the expansions (6.44) into eq. (2.55) written in the JP parametrization (truncated for brevity at ϵ^t_4 and ϵ^r_4), we obtain

$$\frac{r^{\rm JP}_{\rm ps}}{M} = 3 - \left(\frac{8}{3} + \frac{(\epsilon^t_2)_1}{9} + \frac{(\epsilon^t_3)_1}{18} + \frac{2(\epsilon^t_4)_1}{81}\right)\epsilon + \mathcal{O}\!\left(\epsilon^2\right)\,, \tag{6.45a}$$

$$\Omega^{\rm JP} M = \frac{1}{3\sqrt{3}} + \left(\frac{2}{9} + \frac{(\epsilon^t_2)_1}{54} + \frac{(\epsilon^t_3)_1}{162} + \frac{2(\epsilon^t_4)_1}{486}\right)\frac{\epsilon}{\sqrt{3}} + \mathcal{O}\!\left(\epsilon^2\right)\,, \tag{6.45b}$$

$$\lambda^{\rm JP} M = \frac{1}{3\sqrt{3}} + \left(\frac{5}{27} + \frac{2(\epsilon_2^t)_1}{81} + \frac{(\epsilon_3^t)_1}{162} + \frac{(\epsilon_4^t)_1}{1458} - \frac{(\epsilon_1^r)_1}{18} - \frac{(\epsilon_2^r)_1}{54} - \frac{(\epsilon_3^r)_1}{162} - \frac{(\epsilon_4^r)_1}{486}\right)\frac{\epsilon}{\sqrt{3}} + \mathcal{O}\left(\epsilon^2\right) . \tag{6.45c}$$

As expected from eqs. (6.33) and (6.43), all JP parameters enter linearly at the first order in ϵ.

EMD (near horizon) parametrization

As shown in Chapter 5, the EMD parametrization near the horizon can be extended up to the photon sphere by employing the Padé approximation [51]. In this case, the position of the event horizon is written as

$$r_H = 2M(1+\mathfrak{c}) , \tag{6.46}$$

and hence, the first of expressions reported in eq. (2.55) can be compactly written as in eq. (5.33)

$$\frac{r_{\rm ps}^{\rm EMD(nh)}}{M} = \sigma_0 + \sigma_1\, \mathfrak{c} + \mathcal{O}\left(\mathfrak{c}^2\right) , \tag{6.47}$$

where $\mathfrak{c}$ quantifies the departure of r_H from the Schwarzschild radius and is related to the RZ as

$$\mathfrak{c} = -\frac{\epsilon}{\epsilon+1} . \tag{6.48}$$

The coefficients are linear combinations of the parameters $\{\theta_{2n}, \xi_{2n}\}_{n\geq 1}$ and their explicit form depends on the order of the employed Padé approximant, and the expressions of coefficients (σ_0, σ_1) for the position of the photon sphere are reported in Table 5.1 for the first orders. A Padé approximation of order (N, M) involves a total of $N + M$ parameters. We note that the effective parameters $\{\theta_{2n}, \xi_{2n}\}_{n\geq 1}$ must still be expanded in power series of ϵ, as we will see in the subsection dedicated to specific BH models.

In the EMD framework near the horizon, the potential $U^2(r)$ can be expressed as a power series around r_H as in eq. (5.32)

$$U^2(r) = \sum_{n=1}^{\infty} v_n (r - r_H)^n, \tag{6.49}$$

where v_n depend on $\{\theta_{2k}\}$ and $\{\xi_{2k}\}$ (see eqs. (5.32) for the explicit form of these coefficients). It has been shown in Chap. 5 that, by employing Padé approximations at a sufficiently high order (N, M), the convergence radius of the series increases significantly up to the photon sphere location. This approach allows for the computation of the BH shadow radius $b_{\rm sh}$, orbital frequency Ω, and Lyapunov exponent λ. Assuming that the position of the BH horizon is defined by eq. (6.46), for small deviations $\mathfrak{c} \ll 1$ from the Schwarzschild horizon, we can write Ω and λ in eqs. (2.55b) and (2.55c) in mass units M as:

$$\Omega M = \eta_0 + \eta_1\, \mathfrak{c} + \mathcal{O}(\mathfrak{c}^2) , \tag{6.50a}$$

$$\lambda\, M = \Upsilon_0 + \Upsilon_1\, \mathfrak{c} + \mathcal{O}(\mathfrak{c}^2) . \tag{6.50b}$$

The coefficients (η_0, η_1) and (Υ_0, Υ_1) are reported in Table 6.1 and depend on the order of the Padé approximation (N, M). The Schwarzschild limit is already recovered at order $(1, 3)$. From eq. (6.50), the eikonal QNMs can be directly reconstructed at any order (N, M) of the Padé approximation using eq. (2.54). The relation between $b_{\rm sh}$ and Ω can be further exploited to

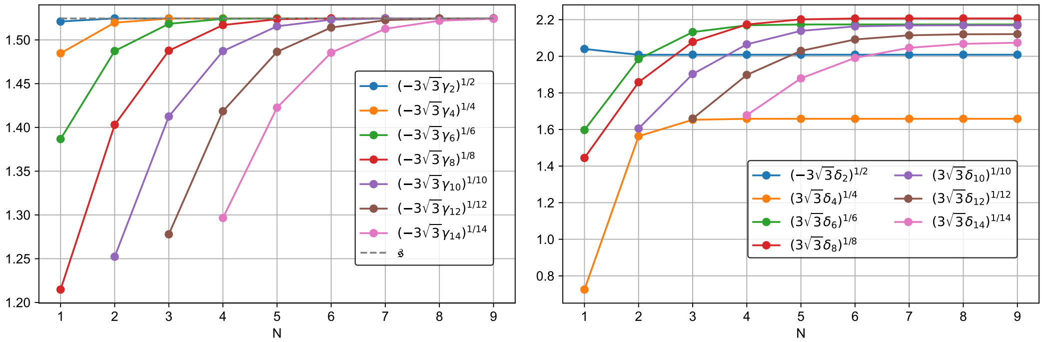

Figure 6.2: Coefficients γ_{2k} (left) and δ_{2k} (right) for different orders of the Padé approximation $(N, 3)$.

investigate the large-N limit in the Padé approximation of order $(N, 3)$. First, let us recall the expression in eq. (5.34) of the shadow radius in terms of $\mathfrak{c}$ from Sec. 5.2.3:

$$\frac{b_{\rm sh}}{M} = \tau_0 + \tau_1\,\mathfrak{c} + O(\mathfrak{c}^2)\,, \tag{6.51}$$

as well as the explicit dependence (5.35) of τ_1 on $\mathfrak{c}$ and on the order N of the Padé approximation:

$$\tau_1(N) = 3\sqrt{3} + \sum_{k=1}^{N+3} \beta_{2k}(N)\frac{\theta_{2k}}{\mathfrak{c}} \qquad \text{with} \qquad \beta_{2k}(N) = \frac{\partial}{\partial\,\theta_{2k}}\frac{1}{U_{N,3}}\bigg|_{(r_{\rm ps})_{N,3}}\,, \tag{6.52}$$

where $(r_{\rm ps})_{N,3}$ and $U_{N,3}$ correspond to the photon sphere radius and potential computed at the order $(N, 3)$ of the Padé approximation, respectively. Similarly, the coefficient η_1 of the photon sphere frequency can be expressed as

$$\eta_1(N) = -\frac{1}{3\sqrt{3}} + \sum_{k=1}^{N+3} \gamma_{2k}(N)\frac{\theta_{2k}}{\mathfrak{c}} \qquad \text{with} \qquad \gamma_{2k}(N) = \frac{\partial\, U_{N,3}}{\partial\,\theta_{2k}}\bigg|_{(r_{\rm ps})_{N,3}}\,. \tag{6.53}$$

Recalling that, at the lowest order, $U_{N,3} = 1/(3\sqrt{3})$, the coefficients $\gamma_{2k}(N)$ and $\beta_{2k}(N)$ are related by

$$\beta_{2k}(N) = \frac{\partial}{\partial\theta_{2k}}\frac{1}{U_{N,3}}\bigg|_{(r_{\rm ps})_{N,3}} = -\frac{1}{U^2_{N,3}}\gamma_{2k}(N) = -(3\sqrt{3})^2\gamma_{2k}(N)\,, \tag{6.54}$$

and the asymptotic behavior of $\gamma_{2k}(N)$ can be derived from the $N \to \infty$ limit of $\beta_{2k}(N)$ obtained in eq. (5.36)

$$\lim_{N\to\infty}\frac{\beta_{2k}(N)}{3\sqrt{3}} \longrightarrow \mathfrak{s}^{2k}\,, \qquad \mathfrak{s} \sim 1.5245. \tag{6.55}$$

This result is compatible with Fig. 6.2, where the first few coefficients γ_{2k} have been computed up to $N = 9$. Moreover, the asymptotic limit of $\eta_1(N)$ becomes

$$\lim_{N\to\infty}\mathfrak{c}\,\eta_1(N) = -\frac{\mathfrak{c}}{3\sqrt{3}} - \sum_{k=1}^{\infty}\frac{\mathfrak{s}^{2k}}{3\sqrt{3}}\theta_{2k} = -\frac{\mathfrak{c}}{3\sqrt{3}} - \frac{1}{3\sqrt{3}}\frac{1}{2M}[\Psi(2M\mathfrak{s}) - r_H], \tag{6.56}$$

and substituting it into the full expression of $\Omega = \eta_0 + \mathfrak{c}\eta_1$, we obtain

$$\lim_{N\to\infty} \Omega = \lim_{N\to\infty} (\eta_0 + \eta_1 \mathfrak{c}) = \frac{2}{3\sqrt{3}} - \frac{1}{3\sqrt{3}} \frac{1}{2M} \Psi(2M\mathfrak{s}). \tag{6.57}$$

In the case of the Lyapunov exponent, the asymptotic N limit is more intricate, since λ depends on both the photon sphere radius and the second-order derivatives of the potential. However, by analogy with Ω, we adopt a similar ansatz for $\Upsilon_1(N)$, which can be written as

$$\Upsilon_1(N) = \frac{1}{3\sqrt{3}} + \sum_{k=1}^{N+3} \delta_{2k}(N) \frac{\theta_{2k}}{\mathfrak{c}}, \tag{6.58}$$

where δ_{2k} is a suitable set of numerical coefficients. In general, δ_{2k} depend on the order of the Padé approximation and are related to the derivative of the Lyapunov exponent with respect to the parameters θ_{2k}, evaluated at the radius of the photon sphere. The coefficients δ_{2k} computed up to $k = 7$ and $N = 9$ are shown in Fig. 6.2. We remark that the individual values of δ_{2k} seem to converge to a constant value, so we expect that it is possible to write the resummation similar to the BH shadow radius and photon sphere frequency. We note that the coefficient δ_8 reaches the largest value.

Finally, we remark on the second order ϵ expansion of the EMD near-horizon parametrization. Since the ϵ dependence is encapsulated in the $\mathfrak{c}$ coefficient in eq. (6.46), it is important to study how this relation changes at second order. We have thus checked that for all BH models of interest, eq. (6.46) does not receive corrections at $O(\mathfrak{c}^2)$. Therefore, r_H acquires $O(\epsilon^2)$ contributions only from the expansion of $\mathfrak{c} = -\epsilon/(1+\epsilon)$. Moreover, the second-order expansion involves significantly more terms than the first-order one, namely linear and quadratic terms in $\{\theta_n\}$, as well as possible mixing among the linear coefficients. We find that, for a given order (N, M) of the Padé approximation, the number of coefficients at second order scales quadratically with $K = N + M$ as $(K^2 + 5K + 6)/2$. Similarly, at order ϵ^N, the number of coefficients will grow as $\sim K^N$.

EMD (at large distance) parametrization

The EMD parametrization at large distances must recover the Schwarzschild metric when the deformation parameters $\{\gamma_i, \omega_i\}_{i\geq 1}$ vanish. However, the position of the event horizon does not explicitly appear as an input, and therefore there is no direct connection to the ϵ parameter. Nevertheless, by inspecting the relations eqs. (6.41) and ansatz (6.42) (or equivalently by considering eq. (6.28) and ansatz (6.44)), we find that $\{\gamma_i, \omega_i\}_{i\geq 1}$ indeed admit a power series expansion in ϵ.

Therefore, we assume that $\{\gamma_i, \omega_i\}_{i\geq 1}$ can be expanded similarly to the previous cases, namely

$$\gamma_n(\epsilon) = \sum_{p=1} \gamma_{n,p}\, \epsilon^p \quad \text{and} \quad \omega_n(\epsilon) = \sum_{p=1} \omega_{n,p}\, \epsilon^p\ , \tag{6.59}$$

where $\{\gamma_{n,p}, \omega_{n,p}\}_{n\geq 1,\ p\geq 1}$ assume different values depending on the model under consideration. Using the metric functions in eqs. (6.17), we can express eqs. (2.55) as

$$\frac{r_{\rm ps}^{\rm EMD(ld)}}{M} = 3 + \frac{1}{9}\left[(15 - 3k + 2k^2)\gamma_{1,1} + (5 - 4k)\gamma_{2,1} + 2\gamma_{3,1}\right]\epsilon + O\left(\epsilon^2\right), \tag{6.60a}$$

$$\Omega^{\rm EMD(ld)} M = \frac{1}{3\sqrt{3}} + \frac{1}{162\sqrt{3}}\left[(-2k^2 + 4k - 21)\gamma_{1,1} + (4k - 6)\gamma_{2,2} - 2\gamma_{3,1}\right]\epsilon + O\left(\epsilon^2\right), \tag{6.60b}$$

$$\lambda^{\mathrm{EMD\,(ld)}} M = \frac{1}{3\sqrt{3}} + \frac{1}{162\sqrt{3}}\Big[(6k^2 - 4k + 21)\gamma_{1,1} + 2(5k-6)\gamma_{2,2} + 6\gamma_{3,1} - (2k^2 - 4k + 21)\omega_{1,1} + (4k-6)\omega_{2,1} - 2\omega_{3,1}\Big]\,\epsilon + \mathcal{O}\left(\epsilon^2\right), \tag{6.60c}$$

Above we kept the dependence on the gauge parameter k to keep the expressions as general as possible.

6.2.2 Application to BH models

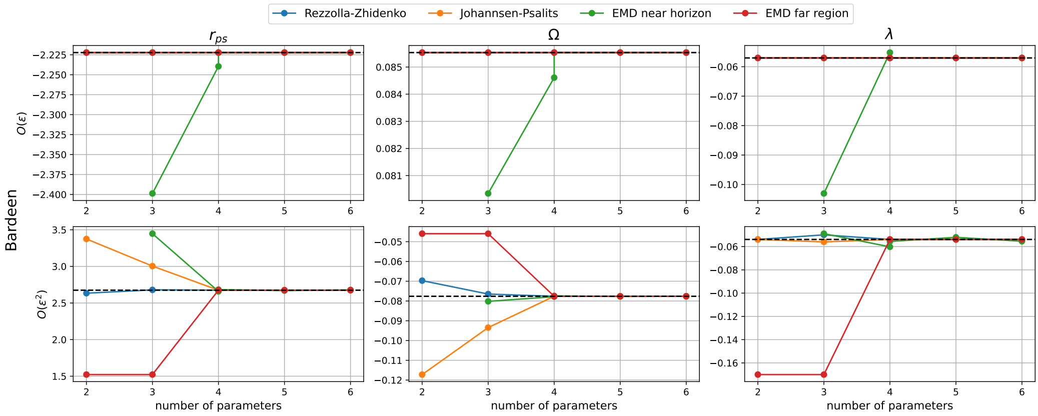

Figure 6.3: Comparison of the convergence to the linear coefficient (top row) and quadratic coefficient (bottom row) for the Bardeen BH model, varying the number of the related parameters. The horizontal dashed black line is the value computed from the model, reported in Table 6.2. For the near-horizon EMD with four parameters, two Padé approximants were used: (2,2) and (1,3), the latter being more accurate.

As an application of the formalism developed in the previous subsection, let us consider the following BH spacetimes: Hayward [24], Bardeen [162], and Simpson-Visser II [36]. These are regular BH candidates, which can be effectively described as deformations of the Schwarzschild geometry and satisfy the condition $g_{tt}\, g_{rr} = -1$. Their g_{tt} metric components read

$$-g_{tt}^{\mathrm{H}}(r) = 1 - \frac{2Mr^2}{r^3 + 2M\, l_{\mathrm{H}}^2}\,, \tag{6.61a}$$

$$-g_{tt}^{\mathrm{B}}(r) = 1 - \frac{2Mr^2}{(r^2 + l_{\mathrm{B}}^2)^{3/2}}\,, \tag{6.61b}$$

$$-g_{tt}^{\mathrm{SV2}}(r) = 1 - \frac{2M}{r}\exp\left\{-\frac{l_{\mathrm{SV2}}}{r}\right\}. \tag{6.61c}$$

The regularization length-scale parameters $(l_{\mathrm{H}}, l_{\mathrm{B}}, l_{\mathrm{SV2}})$ have different physical interpretations in each model, are allowed to vary over a finite range, and can be expressed in terms of ϵ as follows:

$$l_{\mathrm{H}} = 2M\sqrt{\frac{\epsilon}{(1+\epsilon)^3}}\,, \tag{6.62a}$$

$$l_{\rm B} = 2M\frac{\sqrt{(1+\epsilon)^{2/3}-1}}{1+\epsilon}\ , \tag{6.62b}$$

$$l_{\rm SV2} = 2M\frac{\log(1+\epsilon)}{1+\epsilon}\ . \tag{6.62c}$$

We analytically expand the quantities in Eqs. (2.55) around $\epsilon = 0$ up to quadratic order for each BH model and compare the results with those obtained in the Rezzolla–Zhidenko, Johannsen–Psaltis, near-horizon EMD, and large-distance EMD parametrizations, fixing the number of free parameters to four in Eqs. (6.43), (6.45), (6.47)-(6.50a)-(6.50b), and (6.60). The outcome of this comparison is summarized in Table 6.2. We observe that, at linear order, all parametrizations reproduce the same result for all physical quantities in all BH models. Aside from the Simpson–Visser II case, where all parametrizations trivially yield identical expansions, for the Hayward BH with four parameters no single parametrization performs significantly better than the others. On the other hand, for the Bardeen BH we see that JP and RZ already match the exact expressions.

A complementary analysis is presented in Table 6.3, where, instead of fixing the number of parameters a priori, we set the desired tolerance and let the required number of parameters vary to match the exact expressions. In the case of the EMD near-horizon parametrization, this procedure coincides with a Padé approximation of order $(N, 3)$, where the number of free parameters is controlled by the integer N. Also in this setting, no parametrization emerges as universally favored across all BH models, as their performance is model-dependent.

Finally, in Fig. 6.3 we illustrate the convergence of the linear and quadratic coefficients for the Bardeen BH as a representative example. Similar behavior is observed for all other BH models. The plots highlight that for a high enough number of coefficients all parametrizations perform on a comparable footing. Therefore, the choice of parametrization should be guided by the desired accuracy and the number of parameters one is willing to introduce. This has to be considered on a case-by-case basis for each physical observable and BH model.

N	M	η_0	η_1
2	1	$\frac{1}{4}\left(\sqrt{3}-1\right)$	$-\frac{1}{4}\left(\sqrt{3}-1\right)+\frac{1}{135}\left(61-68\sqrt{3}\right)\frac{\theta_2}{\mathfrak{c}}+\frac{2}{9}\left(2\sqrt{3}-7\right)\frac{\theta_4}{\mathfrak{c}}+\frac{8}{3}\left(\sqrt{3}-2\right)\frac{\theta_6}{\mathfrak{c}}$
2	2	$\frac{1}{4}\sqrt{9\sqrt{3}-15}$	$-\frac{1}{4}\sqrt{9\sqrt{3}-15}-\frac{1}{630}\sqrt{1274659\sqrt{3}-\frac{6386663}{3}}\frac{\theta_2}{\mathfrak{c}}-\frac{11}{15}\sqrt{\frac{1}{6}\left(627\sqrt{3}-1075\right)}\frac{\theta_4}{\mathfrak{c}}-\frac{2444\sqrt{2}}{\sqrt{\left(14\sqrt{3}-9\right)\left(85675\sqrt{3}+148401\right)}}\frac{\theta_6}{\mathfrak{c}}-\frac{16}{\sqrt{51\sqrt{3}+\frac{265}{3}}}\frac{\theta_8}{\mathfrak{c}}$
1	3	$\frac{1}{3\sqrt{3}}$	$-\frac{1}{3\sqrt{3}}-\frac{19676}{25515\sqrt{3}}\frac{\theta_2}{\mathfrak{c}}-\frac{656}{405\sqrt{3}}\frac{\theta_4}{\mathfrak{c}}-\frac{64}{27\sqrt{3}}\frac{\theta_6}{\mathfrak{c}}-\frac{128}{81\sqrt{3}}\frac{\theta_8}{\mathfrak{c}}$
2	3	$\frac{1}{3\sqrt{3}}$	$-\frac{1}{3\sqrt{3}}-\frac{98837}{127575\sqrt{3}}\frac{\theta_2}{\mathfrak{c}}-\frac{136096}{76545\sqrt{3}}\frac{\theta_4}{\mathfrak{c}}-\frac{4384}{1215\sqrt{3}}\frac{\theta_6}{\mathfrak{c}}-\frac{1216}{243\sqrt{3}}\frac{\theta_8}{\mathfrak{c}}-\frac{256}{81\sqrt{3}}\frac{\theta_{10}}{\mathfrak{c}}$
3	3	$\frac{1}{3\sqrt{3}}$	$-\frac{1}{3\sqrt{3}}-\frac{652294}{841995\sqrt{3}}\frac{\theta_2}{\mathfrak{c}}-\frac{2066276}{1148175\sqrt{3}}\frac{\theta_4}{\mathfrak{c}}-\frac{62528}{15309\sqrt{3}}\frac{\theta_6}{\mathfrak{c}}-\frac{29152}{3645\sqrt{3}}\frac{\theta_8}{\mathfrak{c}}-\frac{2560}{243\sqrt{3}}\frac{\theta_{10}}{\mathfrak{c}}-\frac{512}{81\sqrt{3}}\frac{\theta_{12}}{\mathfrak{c}}$
N	**M**	**Υ_0**	**Υ_1**
2	1	$\frac{\left(\sqrt{3}-1\right)\left(\sqrt{3}+1\right)^2}{16\sqrt[4]{3}}$	$-\frac{\left(\sqrt{3}-1\right)\left(\sqrt{3}+1\right)^2}{16\sqrt[4]{3}}+\frac{\left(13\sqrt{3}-116\right)\left(\sqrt{3}+1\right)}{180\sqrt[4]{3}}\frac{\theta_2}{\mathfrak{c}}+\frac{\left(\sqrt{3}-2\right)\left(\sqrt{3}+1\right)}{2\sqrt[4]{3}}\frac{\theta_4}{\mathfrak{c}}-\frac{2\left(\sqrt{3}-2\right)\left(\sqrt{3}+1\right)}{\sqrt[4]{3}}\frac{\theta_6}{\mathfrak{c}}$
2	2	$\frac{1}{24}\sqrt{\frac{1}{2}\left(963-529\sqrt{3}\right)}$	$-\frac{1}{24}\sqrt{\frac{1}{2}\left(963-529\sqrt{3}\right)}-\frac{\sqrt{187519473-102837005\sqrt{3}}}{3780}\frac{\theta_2}{\mathfrak{c}}+\frac{1}{60}\sqrt{162387-92399\sqrt{3}}\frac{\theta_4}{\mathfrak{c}}+\frac{78\left(9\sqrt{3}+23\right)}{\sqrt{61617\sqrt{3}+106731}}\frac{\theta_6}{\mathfrak{c}}+4796\sqrt{\frac{2}{241053\sqrt{3}+417609}}\frac{\theta_8}{\mathfrak{c}}$
1	3	$\frac{1}{3\sqrt{3}}$	$-\frac{1}{3\sqrt{3}}-\frac{35396}{25515\sqrt{3}}\frac{\theta_2}{\mathfrak{c}}+\frac{112}{1215\sqrt{3}}\frac{\theta_4}{\mathfrak{c}}+\frac{448}{81\sqrt{3}}\frac{\theta_6}{\mathfrak{c}}+\frac{512}{81\sqrt{3}}\frac{\theta_8}{\mathfrak{c}}$
2	3	$\frac{1}{3\sqrt{3}}$	$-\frac{1}{3\sqrt{3}}-\frac{171496}{127575\sqrt{3}}\frac{\theta_2}{\mathfrak{c}}+\frac{10160}{5103\sqrt{3}}\frac{\theta_4}{\mathfrak{c}}+\frac{2752}{135\sqrt{3}}\frac{\theta_6}{\mathfrak{c}}+\frac{1280}{27\sqrt{3}}\frac{\theta_8}{\mathfrak{c}}+\frac{1024}{27\sqrt{3}}\frac{\theta_{10}}{\mathfrak{c}}$
3	1	$\frac{1}{3\sqrt{3}}$	$-\frac{1}{3\sqrt{3}}-\frac{5662841}{4209975\sqrt{3}}\frac{\theta_2}{\mathfrak{c}}+\frac{2857228}{1148175\sqrt{3}}\frac{\theta_4}{\mathfrak{c}}+\frac{2398688}{76545\sqrt{3}}\frac{\theta_6}{\mathfrak{c}}+\frac{423776}{3645\sqrt{3}}\frac{\theta_8}{\mathfrak{c}}+\frac{50432}{243\sqrt{3}}\frac{\theta_{10}}{\mathfrak{c}}+\frac{11776}{81\sqrt{3}}\frac{\theta_{12}}{\mathfrak{c}}$

Table 6.1: Orbital frequency (η_0, η_1) and Lyapunov exponent (Υ_0, Υ_1) coefficients of the photon sphere obtained from eqs. (2.55b) and (2.55c) in terms of the Padé approximants of the potential $U^2_{N,M}$.

BH models	Parametrizations	$\frac{r_{\rm ps}}{M}-3$	$\Omega M-\frac{1}{3\sqrt{3}}$	$\lambda M-\frac{1}{3\sqrt{3}}$
Hayward	From the model	$-\frac{16}{9}\epsilon+\frac{80}{27}\epsilon^2$	$\frac{8}{81\sqrt{3}}\epsilon-\frac{40}{243\sqrt{3}}\epsilon^2$	$-\frac{16}{81\sqrt{3}}\epsilon+\frac{16}{243\sqrt{3}}\epsilon^2$
	Rezzolla-Zhidenko	$-\frac{16}{9}\epsilon+\frac{28892}{9801}\epsilon^2$	$\frac{8}{81\sqrt{3}}\epsilon-\frac{4012}{24057\sqrt{3}}\epsilon^2$	$-\frac{16}{81\sqrt{3}}\epsilon+\frac{173960}{2910897\sqrt{3}}\epsilon^2$
	Johannsen-Psaltis	$-\frac{16}{9}\epsilon+\frac{32}{9}\epsilon^2$	$\frac{8}{81\sqrt{3}}\epsilon-\frac{440}{2187\sqrt{3}}\epsilon^2$	$-\frac{16}{81\sqrt{3}}\epsilon+\frac{32}{243\sqrt{3}}\epsilon^2$
	EMD near horizon	$-\frac{16}{9}\epsilon+\frac{799}{243}\epsilon^2$	$\frac{8}{81\sqrt{3}}\epsilon-\frac{110}{729\sqrt{3}}\epsilon^2$	$-\frac{16}{81\sqrt{3}}\epsilon-\frac{107}{2187\sqrt{3}}\epsilon^2$
	EMD large distance	$-\frac{16}{9}\epsilon+\frac{176}{81}\epsilon^2$	$\frac{8}{81\sqrt{3}}\epsilon-\frac{296}{2187\sqrt{3}}\epsilon^2$	$-\frac{16}{81\sqrt{3}}\epsilon-\frac{368}{2187\sqrt{3}}\epsilon^2$
Bardeen	From the model	$-\frac{20}{9}\epsilon+\frac{650}{243}\epsilon^2$	$\frac{4}{27\sqrt{3}}\epsilon-\frac{98}{729\sqrt{3}}\epsilon^2$	$-\frac{8}{81\sqrt{3}}\epsilon-\frac{68}{729\sqrt{3}}\epsilon^2$
	Rezzolla-Zhidenko	$-\frac{20}{9}\epsilon+\frac{650}{243}\epsilon^2$	$\frac{4}{27\sqrt{3}}\epsilon-\frac{98}{729\sqrt{3}}\epsilon^2$	$-\frac{8}{81\sqrt{3}}\epsilon-\frac{68}{729\sqrt{3}}\epsilon^2$
	Johannsen-Psaltis	$-\frac{20}{9}\epsilon+\frac{650}{243}\epsilon^2$	$\frac{4}{27\sqrt{3}}\epsilon-\frac{98}{729\sqrt{3}}\epsilon^2$	$-\frac{8}{81\sqrt{3}}\epsilon-\frac{68}{729\sqrt{3}}\epsilon^2$
	EMD near horizon	$-\frac{20}{9}\epsilon+\frac{652}{243}\epsilon^2$	$\frac{4}{27\sqrt{3}}\epsilon-\frac{391}{2916\sqrt{3}}\epsilon^2$	$-\frac{8}{81\sqrt{3}}\epsilon-\frac{421}{4374\sqrt{3}}\epsilon^2$
	EMD large distance	$-\frac{20}{9}\epsilon+\frac{370}{243}\epsilon^2$	$\frac{4}{27\sqrt{3}}\epsilon-\frac{98}{729\sqrt{3}}\epsilon^2$	$-\frac{8}{81\sqrt{3}}\epsilon-\frac{68}{729\sqrt{3}}\epsilon^2$
Simpson-Visser II	All parametrizations	$-\frac{8}{3}\epsilon+\frac{74}{27}\epsilon^2$	$\frac{2}{9\sqrt{3}}\epsilon-\frac{7}{81\sqrt{3}}\epsilon^2$	$\frac{2}{27\sqrt{3}}\epsilon-\frac{11}{81\sqrt{3}}\epsilon^2$

Table 6.2: Expressions of the photon sphere radius $r_{\rm ps}$, orbital frequency Ω, and Lyapunov exponent λ. The values are rescaled by the BH mass M, shifted with respect to the corresponding Schwarzschild result, and computed up to quadratic order in ϵ in the case of Hayward, Bardeen, and Simpson-Visser II models using four parameters in each parametrization. For the last BH spacetime, we report only the expressions for the exact metric, as they are identical across all parametrizations.

BH models	Hayward		Bardeen		Simpson-Visser II	
order	ϵ	ϵ^2	ϵ	ϵ^2	ϵ	ϵ^2
Rezzolla-Zhidenko	2	7	2	4	1	1
Johannsen-Psaltis	3	6	2	4	1	2
EMD near horizon	4	>7	4	>7	4	4
EMD large distance	3	6	2	4	1	2

Table 6.3: Number of parameters required to reproduce the exact results for the three observables at orders ϵ and ϵ^2.

7 Concluding remarks and outlooks

In this thesis, we have developed and extensively explored the framework of *Effective Metric Descriptions* (EMDs) to study (quantum) deformed black hole (BH) geometries in a model-independent fashion. Building upon the initial proposals in [45, 46], we have systematically extended the formalism, analyzed its mathematical consistency, and applied it to a variety of BH spacetimes, ranging from Schwarzschild-like regular models to charged solutions. Our work provides a unified perspective on EMDs, consolidating several previous results and offering a robust tool to study BH physics, both in theoretical and phenomenological contexts.

At the core of our approach lies the idea that deformations of classical spherically symmetric and static BHs can be encoded in one or two functions of a *physical quantity* $\mathcal{X}$, ensuring that the deformed geometry respects the symmetries of its classical counterpart. In the majority of our analysis, $\mathcal{X}$ was chosen to be the proper distance ρ measured from the event horizon, though we have also considered curvature invariants, such as the Ricci and Kretschmann scalars, as alternative physical quantities. By defining these functions in terms of $\mathcal{X}$, we naturally enforce coordinate invariance and maintain a consistent relation between the deformed metric and classical geometry.

In the vicinity of the horizon, we solved the self-consistency conditions by employing series expansions in ρ, as introduced in [46]. This allowed us to derive regularity conditions on the metric deformations, ensuring that physical quantities such as the Ricci scalar, Kretschmann scalar, and Hawking temperature remain finite. In particular, our analysis revealed non-trivial constraints on the expansion coefficients of the deformation functions, which are essential for the physical viability of the EMD framework. We further extended these results to asymptotic expansions, thereby connecting the near-horizon behavior to the large-distance properties of the spacetime.

To overcome the limitations of Taylor expansions at larger distances from the horizon, we introduced Padé approximants [49], which allow an efficient resummation of the deformation functions and extend the range of applicability of the EMDs. This enabled accurate computations of astrophysically relevant observables, such as the radius of the photon sphere and the BH shadow, in a model-independent manner. The resulting approximations were tested across a variety of quantum-deformed BH models [24, 28, 167, 191, 192], demonstrating excellent agreement with exact or numerical results.

Our framework was further generalized to include electrically and magnetically charged BHs [48], extending the EMD formalism to Reissner–Nordström–like geometries. In this context, we derived general constraints on the metric deformation functions at the horizon and obtained expressions for the Hawking temperature, including expansions in powers of the charge. Notably, the proper time for an infalling observer emerged as a natural physical quantity for extremal BHs, enabling a consistent EMD formulation even in these limiting cases. These results provide a versatile, model-independent foundation for future studies of charged BH phenomena, including electromagnetic radiation emission, orbit stability, and superradiance [80].

In this thesis, we have developed a comprehensive framework for studying static and spherically symmetric black hole (BH) spacetimes subjected to quantum or classical deformations. The core idea behind our approach is the *Effective Metric Description* (EMD), which parametrizes deviations from classical geometries, such as Schwarzschild and Reissner–Nordström, through one or two functions of a physical quantity $\mathcal{X}$ that ensures consistency with the symmetries of the underlying classical solution. In most of our analysis, $\mathcal{X}$ was chosen to be the proper distance ρ measured from the event horizon, though we also explored alternative choices, such as curvature invariants, including the Ricci and Kretschmann scalars. By defining the deformation functions in terms of $\mathcal{X}$, the EMD framework naturally maintains coordinate invariance while providing a self-consistent description of the modified geometry.

Close to the horizon, we solved the self-consistency equations by employing series expansions in the chosen physical quantity. This procedure allowed us to systematically impose regularity conditions on the deformed metrics, ensuring that crucial physical quantities, such as curvature scalars and the Hawking temperature, remain finite at the horizon. These conditions translate into non-trivial constraints on the expansion coefficients of the deformation functions, which serve as effective parameters describing the quantum or classical deviations from the classical spacetime. We further extended these results to asymptotic expansions, providing a bridge between the near-horizon behavior and the large-distance properties of the spacetime, and allowing the connection of different EMD formulations based on distinct choices of $\mathcal{X}$.

While series expansions provide a natural description near the horizon, their radius of convergence can be limited, restricting the applicability of the framework to regions very close to the event horizon. To overcome this limitation, we introduced Padé approximants as a method to resum the series and extend the effective description to larger distances. This technique proved particularly effective for computing astrophysically relevant observables, such as the radius of the photon sphere and the apparent black hole shadow, in a manner that is independent of the underlying model. Our results demonstrate that the Padé-approximated metrics reproduce the exact or numerical predictions with high accuracy, even in cases where the original series exhibit slow convergence or non-analytic behavior. Moreover, the effective expressions obtained provide insight into the leading quantum corrections to the shadow, which can be directly compared with observational data, offering a pathway toward model-independent constraints on the deformation functions.

The EMD framework was also extended to include electrically and magnetically charged black holes. By incorporating the Reissner–Nordström geometry and its deformations, we derived general constraints on the metric functions and obtained expressions for the Hawking temperature in terms of the deformation parameters and the black hole charge. In particular, the extremal limit revealed the importance of using proper time for infalling observers as a physical quantity to formulate the EMD, ensuring a consistent description even in the most delicate regimes. This extension highlights the versatility of EMDs in accommodating additional physical properties, such as charge, and sets the stage for future studies of black hole phenomena that combine gravitational and electromagnetic radiation and superradiance [80].

A key contribution of this thesis is the establishment of explicit mappings between EMDs and other widely used BH parametrization schemes, such as Johannsen–Psaltis and Rezzolla–Zhidenko. Through this mapping, we demonstrated that different agnostic parametrizations are fundamentally equivalent: none systematically outperforms the others, and the choice of framework should be guided by the observable of interest and the physical regime under consideration. This unification also enables the translation of quantum-gravity–inspired deformations across parametrization schemes, facilitating consistent comparisons of theoretical predictions and observational results. In addition, we applied these mappings to the study of quasi-normal modes in the eikonal limit, showing how the coefficients of each parametrization can be expressed perturbatively in a small deviation parameter, and verified the approach across several regular BH models, including Hayward, Bardeen, and Simpson–Visser II.

The cumulative impact of our work is twofold. Conceptually, it establishes EMDs as a versatile and model-independent framework for encoding deformations of classical BHs, capable of handling quantum corrections, charges, and, in principle, rotation. Practically, it provides computational tools to extract physically meaningful observables, such as curvature scalars, Hawking temperature, and photon-sphere radii, in a way that is both accurate and extensible to a variety of black hole solutions. Furthermore, by relating different parametrization schemes, the framework allows a coherent translation of results across models and observables, bridging the gap between theoretical constructions and phenomenological applications.

Looking forward, several natural extensions emerge from our findings. One important direction is the incorporation of rotating black holes, enabling effective deformations of Kerr geometries [61, 202–204], which are essential for interpreting gravitational wave data and black hole imaging. Another avenue is the application of EMDs to cosmological spacetimes, including deformations of (Anti-)de Sitter and inflationary models, where quantum corrections could provide insights into early-universe physics. Additionally, extending the framework to incorporate higher-order curvature invariants or matter fields may reveal further aspects of quantum-gravity-induced modifications. On the phenomenological side, our results suggest that precise observational data from the Event Horizon Telescope, LIGO/Virgo/KAGRA, and future experiments could be used to constrain deformation functions and test predictions of quantum gravity, providing a direct link between theory and experiment.

An interesting direction for future work concerns the connection between the EMD framework and the recently proposed quantum inequalities for quantum black holes [42, 205]. These inequalities constrain the admissible deviations from classical black-hole metrics induced by quantum effects, ensuring that the resulting spacetimes remain physically consistent—free of pathological behavior such as acausal propagation or unbounded stress-energy fluctuations. Since the EMD formalism effectively parametrizes metric deformations in a covariant and model-independent manner, it provides a natural setting in which such quantum consistency bounds could be explicitly implemented. Exploring how the EMD coefficients are restricted by these inequalities would bridge phenomenological metric deformations and the general principles of semiclassical gravity, yielding a more predictive and constrained framework for quantum-corrected black holes.

In conclusion, this thesis has demonstrated that Effective Metric Descriptions constitute a powerful and flexible tool to study black hole spacetimes in a model-independent fashion. By systematically developing the mathematical formalism, extending its applicability via Padé approximants, generalizing it to charged black holes, and unifying it with other parametrization frameworks, we have created a coherent platform for theoretical analysis and phenomenological applications. This framework not only deepens our understanding of black hole physics in classical and quantum regimes but also lays the groundwork for the systematic exploitation of upcoming high-precision astrophysical observations, thereby bridging the gap between fundamental theory and measurable phenomena.

Appendix

A.1 Series relations

For the reader's convenience, we compile several series identities in this Appendix, which are too lengthy to be presented in the main body of the thesis. Firstly, we illustrate how to extract a specific term from a(n integer) power of a series. Indeed, let

$$S(x) = \sum_{k=0}^{\infty} c_k\, x^k\,, \qquad \forall |x| \leq x_c\,, \tag{A.1}$$

where x_c is the radius convergence, $c_k \in \mathbb{R}$ a set of expansion coefficients and let $n \in \mathbb{N}$. We are then interested in the expansion

$$(S(x))^n = \sum_{k=0}^{\infty} \mathfrak{c}_k\, x^k\,, \tag{A.2}$$

where the $\mathfrak{c}_k$ depend explicitly on $\{c_k\}_{k\in\mathbb{N}^*}$. To calculate $\mathfrak{c}_p$ (for given $p \in \mathbb{N}$), we consider

$$(S(x))^n = \left(\sum_{k=0}^{p} c_k\, x^k\right)^n + O(x^{p+1}) = \sum_{\ell_0=0}^{n} \binom{n}{\ell_0}\, c_0^{n-\ell_0}\, x^{\ell_0} \left(\sum_{k=1}^{p} c_k x^{k-1}\right)^{\ell_0}\,, \tag{A.3}$$

where we have used the binomial formula. This expression can be further re-written

$$(S(x))^n = \sum_{\ell_0=0}^{n} \binom{n}{\ell_0}\, c_0^{n-\ell_0}\, x^{\ell_0} \sum_{\ell_1=0}^{\ell_0} \binom{\ell_0}{\ell_1}\, c_1^{\ell_0-\ell_1}\, x^{\ell_1} \left(\sum_{k=2}^{p} c_k x^{k-2}\right)^{\ell_1}\,. \tag{A.4}$$

Iterating this procedure, we find

$$(S(x))^n = \sum_{\ell_0=0}^{n} \sum_{\ell_1=0}^{\ell_0} \cdots \sum_{\ell_{p-1}=0}^{\ell_{p-2}} \binom{n}{\ell_0}\binom{\ell_0}{\ell_1}\cdots\binom{\ell_{p-2}}{\ell_{p-1}}\, x^{\ell_0+\ell_1+\ldots+\ell_{p-1}}\, c_0^{n-\ell_0}\, c_1^{\ell_0-\ell_1}\cdots c_{p-1}^{\ell_{p-2}-\ell_{p-1}}\, c_p^{\ell_{p-1}}\,. \tag{A.5}$$

Thus, the coefficient $\mathfrak{c}_p$ in (A.2) is given by

$$\mathfrak{c}_0 = c_0^n\,,$$

$$\mathfrak{c}_p = \sum_{\substack{0\le \ell_{p-1}\le\ell_{p-2}\le\ldots\le\ell_0\le n\\ \ell_0+\ell_1+\ldots+\ell_{p-1}=p}} \frac{n!\, c_0^{n-\ell_0} c_1^{\ell_0-\ell_1}\ldots c_{p-1}^{\ell_{p-2}-\ell_{p-1}}\, c_p^{\ell_{p-1}}}{(n-\ell_0)!(\ell_0-\ell_1)!\ldots(\ell_{p-2}-\ell_{p-1})!\ell_{p-1}!}\,, \qquad \forall p\ge 1\,. \tag{A.6}$$

For $c_0 = 0$, the summation over ℓ_0 is fixed to $\ell_0 = n$, such that in this case

$$\begin{aligned} &\mathfrak{c}_0 = 0\,, \qquad \mathfrak{c}_1 = c_1\,\delta_{n,1}\,,\\ &\mathfrak{c}_p = \sum_{\substack{0\le \ell_{p-1}\le\ell_{p-2}\le\ldots\le\ell_1\le n\\ \ell_1+\ldots+\ell_{p-1}=p-n}} \frac{n!\, c_1^{n-\ell_1}\ldots c_{p-1}^{\ell_{p-2}-\ell_{p-1}}\, c_p^{\ell_{p-1}}}{(n-\ell_1)!\ldots(\ell_{p-2}-\ell_{p-1})!\ell_{p-1}!}\,, \qquad \forall p\ge 2\,. \end{aligned} \tag{A.7}$$

A.1.1 Series expansion of inverse radial coordinate

In this Section, starting from the first series in Eq. (3.8), we express the inverse radial coordinate as a series expansion in ρ. More precisely, we determine the coefficients $\mathfrak{p}_m$ in

$$P(\rho) := \frac{1}{r(\rho)} = \sum_{m=0}^{\infty} \mathfrak{p}_m \left(\frac{\rho}{2M}\right)^m\,, \qquad \text{with} \qquad \begin{aligned} &\mathfrak{p}_m \in \mathbb{R} \quad \forall m\in\mathbb{N}\,,\\ &\mathfrak{p}_0 = 1/r_H\,. \end{aligned} \tag{A.8}$$

Let us remark that, in contrast to the coefficients in Eqs. (3.7) and (3.8), the series coefficients have dimensions $[\mathfrak{p}_n] = [L]^{-1}$, $\forall n \ge 0$. Differentiating Eq. (A.8) both sides with respect to ρ and multiplying by r, we find

$$r(\rho)\,P(\rho)' = -P(\rho)\,\frac{\mathrm{d}r}{\mathrm{d}\rho}\,, \tag{A.9}$$

which with (3.8) becomes the following series identity

$$\left(r_H + 2M\sum_{n=2}^{\infty} a_n \left(\frac{\rho}{2M}\right)^n\right)\left(\sum_{m=1}^{\infty} m\,\frac{\mathfrak{p}_m}{2M}\left(\frac{\rho}{2M}\right)^{m-1}\right) = -\left(\sum_{m=0}^{\infty}\mathfrak{p}_m\left(\frac{\rho}{2M}\right)^m\right)\left(\sum_{n=2}^{\infty} n\,a_n\left(\frac{\rho}{2M}\right)^{n-1}\right)\,, \tag{A.10}$$

note that we have used the condition in $a_1 = 0$. Re-arranging both sides of this equation, we find

$$\frac{r_H\,\mathfrak{p}_1}{2M} + \left(\frac{r_H}{M}\,\mathfrak{p}_2 + 2a_2\,\mathfrak{p}_0\right)\frac{\rho}{2M} + \sum_{p=2}^{\infty}(p+1)\left[\frac{r_H}{2M}\,\mathfrak{p}_{p+1} + \mathfrak{p}_0\,a_{p+1} + \sum_{m=1}^{p-1}\mathfrak{p}_m\,a_{p+1-m}\right]\left(\frac{\rho}{2M}\right)^p = 0\,. \tag{A.11}$$

Order by order we therefore obtain the relations

$$\mathfrak{p}_1 = 0\,, \qquad \mathfrak{p}_2 = -\frac{2Ma_2}{r_H^2}\,, \qquad \mathfrak{p}_p = -\frac{2Ma_p}{r_H^2} - \frac{2M}{r_H}\sum_{m=1}^{p-2}\mathfrak{p}_m\,a_{p-m} \qquad \forall p\ge 3\,. \tag{A.12}$$

A.1.2 Power of a power series

For $\rho \in [0, d_H)$ and $n \in \mathbb{N}$, we consider the following power series

$$\left(\sum_{k=0}^{\infty}\left(-\frac{\rho}{d_H}\right)^k\right)^n = \sum_{p=0}^{\infty} \mathfrak{c}_p\, \rho^p\,. \tag{A.13}$$

For the coefficients $\mathfrak{c}_n$ we find the following explicit expression

$$\mathfrak{c}_p := \left(\sum_{k=0}^{\infty}\left(-\frac{\rho}{d_H}\right)^k\right)^n\Bigg|_{\rho^p} = \left(-\frac{1}{d_H}\right)^p \binom{n+p-1}{p} = \left(-\frac{1}{d_H}\right)^p \frac{(n+p-1)!}{p!(n-1)!}\,. \tag{A.14}$$

For $p = 0$, we indeed have $\mathfrak{c}_0 = 1$. In order to show (A.14) for $p \in \mathbb{N}$, we begin by demonstrating

$$\left(\sum_{k=0}^{p-\ell}\left(-\frac{\rho}{d_H}\right)^k\right)^\ell\Bigg|_{\rho^{p-\ell}} = \left(-\frac{1}{d_H}\right)^{p-\ell} \frac{(p-1)!}{(p-\ell)!(\ell-1)!}\,, \qquad \begin{array}{l}\forall p \in \mathbb{N}\,,\\ \forall \ell \in \{0,\ldots,p\}\,.\end{array} \tag{A.15}$$

For $p \geq 1$ it can be verified for all (finitely) many values of $\ell \in \{0, \ldots, p\}$, concretely:

- for $\ell = 0$ both sides are vanishing, since we use the convention $1/((-1)!) \to 0$.
- for $\ell = 1$ we find directly

$$\sum_{k=0}^{p}\left(-\frac{\rho}{d_H}\right)^k\Bigg|_{\rho^{p-1}} = \left(-\frac{1}{d_H}\right)^{p-1}\,, \tag{A.16}$$

  which indeed agrees with (A.15).

- for general $2 \leq \ell \leq p$ we have

$$\begin{aligned}\left(\sum_{k=0}^{p-\ell}\left(-\frac{\rho}{d_H}\right)^k\right)^\ell\Bigg|_{\rho^{p-\ell}} &= \sum_{u_2,\ldots,\ell=0}^{p-\ell}\left(\sum_{k_1=0}^{p-\ell-u_2-\ldots-u_\ell}\left(-\frac{\rho}{d_H}\right)^{k_1}\Bigg|_{\rho^{p-\ell-u_2-\ldots-u_\ell}}\right)\\ &\times\left(\sum_{k_2=0}^{u_2}\left(-\frac{\rho}{d_H}\right)^{k_2}\Bigg|_{\rho^{u_2}}\right)\times\ldots\times\left(\sum_{k_\ell=0}^{u_\ell}\left(-\frac{\rho}{d_H}\right)^{k_\ell}\Bigg|_{\rho^{u_\ell}}\right) = \left(-\frac{1}{d_H}\right)^{p-\ell}\sum_{\substack{u_2,\ldots,\ell=0\\ u_2+\ldots+u_\ell\leq p-\ell}}^{p-\ell} 1\,.\end{aligned}$$

  The last summation can be re-written in the form

$$\sum_{\substack{u_2,\ldots,\ell=0\\ u_2+\ldots+u_\ell\leq p-\ell}}^{p-\ell} 1 = \sum_{k_1=0}^{p-\ell}\sum_{\substack{u_3,\ldots,\ell=0\\ u_3+\ldots+u_\ell\leq k_1}} 1 = \sum_{k_1=0}^{p-\ell}\sum_{k_2=0}^{k_1}\ldots\sum_{k_{\ell-1}=0}^{k_{\ell-2}} 1 = \sum_{k_1=0}^{p-\ell}\sum_{k_2=0}^{k_1}\ldots\sum_{k_{\ell-2}=0}^{k_{\ell-3}}\binom{k_{\ell-2}+1}{k_{\ell-2}}\,,$$

  which, upon using the identity

$$\sum_{u=0}^{k}\binom{u+s}{u} = \binom{k+s+1}{k} \qquad \forall s \in \mathbb{N}\,, \tag{A.17}$$

leads to

$$\sum_{\substack{u_2,\ldots,\ell=0 \\ u_2+\ldots+u_\ell \leq p-\ell}}^{p-\ell} 1 = \left(\begin{array}{c} p-1 \\ p-\ell \end{array} \right) = \frac{(p-1)!}{(p-\ell)!(\ell-1)!} \,. \tag{A.18}$$

This result therefore indeed demonstrates (A.15).

With the result (A.15) we can prove (A.14) (for $p \geq 1$). To this end, we consider

$$\begin{aligned}
\left(\sum_{k=0}^{\infty}\left(-\frac{\rho}{d_H}\right)^k\right)^n \bigg|_{\rho^p} &= \left(\sum_{k=0}^{p}\left(-\frac{\rho}{d_H}\right)^k\right)^n \bigg|_{\rho^p} = \sum_{\ell=0}^{n} \left(\begin{array}{c} n \\ \ell \end{array} \right) \left(\sum_{k=1}^{p}\left(-\frac{\rho}{d_H}\right)^k\right)^\ell \bigg|_{\rho^p} \\
&= \sum_{\ell=0}^{n} \left(-\frac{\rho}{d_H}\right)^\ell \left(\begin{array}{c} n \\ \ell \end{array} \right) \left(\sum_{k=0}^{p-1}\left(-\frac{\rho}{d_H}\right)^k\right)^\ell \bigg|_{\rho^p} \\
&= \sum_{\ell=1}^{n} \left(-\frac{\rho}{d_H}\right)^\ell \left(\begin{array}{c} n \\ \ell \end{array} \right) \left[\left(\sum_{k=0}^{p-\ell}\left(-\frac{\rho}{d_H}\right)^k\right)^\ell \bigg|_{\rho^{p-\ell}}\right] .
\end{aligned} \tag{A.19}$$

With the relation (A.15) we therefore obtain

$$\begin{aligned}
\left(\sum_{k=0}^{\infty}\left(-\frac{\rho}{d_H}\right)^k\right)^n \bigg|_{\rho^p} &= \left(-\frac{1}{d_H}\right)^p \sum_{\ell=1}^{\min(n,p)} \left(\begin{array}{c} n \\ \ell \end{array} \right) \frac{(p-1)!}{(p-\ell)!(\ell-1)!} \\
&= \left(-\frac{1}{d_H}\right)^p \frac{1}{p} \sum_{\ell=1}^{\min(n,p)} \ell \left(\begin{array}{c} n \\ \ell \end{array} \right) \left(\begin{array}{c} p \\ \ell \end{array} \right) = \left(-\frac{1}{d_H}\right)^p \left(\begin{array}{c} n+p-1 \\ p \end{array} \right) ,
\end{aligned} \tag{A.20}$$

which indeed demonstrates (A.14).

A.2 Series expansions for $\xi_1 \neq 0$

For completeness, we shall generalise the approach of Section 3.2.1 also to accommodate functions Φ such that the coefficient $\xi_1 \neq 0$ in Eq. (3.7) is non-zero. Indeed, assuming that $r \sim r_H + \mathcal{O}(\rho^p)$ for some $p \in \mathbb{R}_+$, for the left-hand-side of the equation (3.9) to have a term of order $\mathcal{O}(\rho)$ requires either $p = 1$ or $p = 3/2$. Since we have seen in Section 3.2.1 that $p = 1$ still requires $\xi_1 = 0$, we shall here explore the case $p = 3/2$, *i.e.* instead of (3.22) we shall consider the expansion

$$\Phi(\rho) = r_H + \sum_{n=1}^{\infty} \xi_n \rho^n \quad \text{and} \quad r = r_H + \sum_{n=1}^{\infty} \widehat{a}_n\, \rho^{\frac{n+2}{2}} \,, \quad \text{with} \quad \widehat{a}_n \in \mathbb{R} \ \ \forall n \in \mathbb{N} \,, \tag{A.21}$$

which as before we assume to have an interval of convergence $\rho \in [0, \rho_A)$ (with some $\rho_A > 0$). We then obtain

$$r\left(1 - \left(\frac{\mathrm{d}r}{\mathrm{d}\rho}\right)^2\right) = r_H - \frac{9}{4}\,\rho\, r_H\, \widehat{a}_1^2 + \rho^{3/2}\,(\widehat{a}_1 - 6\, r_H\, \widehat{a}_1\, \widehat{a}_2) + \rho^2 \left[\widehat{a}_2 - r_H \left(4\, \widehat{a}_2^2 + \frac{15}{2}\, \widehat{a}_1\, \widehat{a}_3\right)\right]$$

$$+\sum_{p=5}^{\infty}\rho^{p/2}\Bigg[\widehat{a}_{p-2}-r_H\sum_{m=1}^{p-1}\frac{(m+2)(p-m+2)}{4}\,\widehat{a}_m\,\widehat{a}_{p-m}$$
$$-\sum_{k=1}^{p-4}\widehat{a}_k\sum_{m=1}^{p-k-3}\frac{(m+2)(p-k-m)}{4}\,\widehat{a}_m\,\widehat{a}_{p-k-m-2}\Bigg]. \quad \text{(A.22)}$$

Comparing the coefficients of ρ^0, ρ^1, $\rho^{3/2}$ and ρ^2 to the series expansion of Φ in Eq. (A.21), yields the relations

$$r_H=\xi_0\,,\quad \xi_1=-\frac{9}{4}\,r_H\,\widehat{a}_1^2\,,\quad 0=\widehat{a}_1-6\,r_H\,\widehat{a}_1\,\widehat{a}_2\,,\quad \xi_2=\widehat{a}_2-r_H\left(4\,\widehat{a}_2^2+\frac{15}{2}\,\widehat{a}_1\,\widehat{a}_3\right)\,, \quad \text{(A.23)}$$

which has solution

$$\widehat{a}_1=\pm\frac{2}{3}\sqrt{-\frac{\xi_1}{r_H}}\,,\qquad \widehat{a}_2=\frac{1}{6r_H}\,,\qquad \widehat{a}_3=\frac{1-18\,r_H\,\xi_2}{135\,\widehat{a}_1\,r_H^2}\,. \quad \text{(A.24)}$$

The coefficient $\widehat{a}_1$ is real only for $\xi_1<0$. In the case $\xi_1>0$, there exists no real solution of (3.9), which is of the form (A.21). In the following, we shall assume $\xi_1<0$ and furthermore pick the positive sign for $\widehat{a}_1$ in (A.24): indeed, for the negative sign, the function $z(\rho)$ would not be monotonically growing for $\rho>0$.

Comparing the remaining terms in (A.22) order by order, we can express $\widehat{a}_{p-1}$ in terms of $\widehat{a}_k$ with $k<p-1$

$$\widehat{a}_{p-1}=\frac{2}{3\,\widehat{a}_1\,r_H\,(p+1)}\Bigg[\widehat{a}_{p-2}-r_H\sum_{m=2}^{p-2}\frac{(m+2)(p-m+2)}{4}\,\widehat{a}_m\,\widehat{a}_{p-m}$$
$$-\sum_{k=1}^{p-4}\widehat{a}_k\sum_{m=1}^{p-k-3}\frac{(m+2)(p-k-m)}{4}\,\widehat{a}_m\,\widehat{a}_{p-k-m-2}\Bigg]-\begin{cases}0 & \text{if}\quad p\in\mathbb{N}_{\text{odd}}\\ \frac{2\xi_{p/2}}{3\widehat{a}_1\,r_H\,(p+1)} & \text{if}\quad p\in\mathbb{N}_{\text{even}}\end{cases}$$
$$\text{(A.25)}$$

A.3 Transition from Ricci to Distance EMD

Identifying the coefficients $\{\tau_n\}_{n=0,1,2,3}$ in (3.80) with those in (3.84) leads to the following solutions of $(R_0,R_1,\widetilde{q}_0,\widetilde{q}_1)$ in terms of $(\xi_0,\xi_2,\xi_4,\xi_6)$

$$R_0=\frac{3+5\varpi-3\varpi^2-5\varpi^3+384r_H^3\xi_4}{2r_H^2(1+\varpi)(1+2\varpi)}\,,$$
$$R_1=\frac{7680r_H^2}{(1+\varpi)^2(2+3\varpi)}\,\xi_6-\frac{9+61\varpi+73\varpi^2-53\varpi^3-90\varpi^4}{4r_H^3(1+2\varpi)^2(2+3\varpi)}$$
$$+\frac{96(19+41\varpi+30\varpi^2)}{(1+\varpi)(1+2\varpi)^2(2+3\varpi)}\,\xi_4+\frac{24576r_H^3(7+8\varpi)}{(1+\varpi)^3(1+2\varpi)^2(2+3\varpi)}\,\xi_4^2\,,$$
$$\widetilde{q}_0=\frac{\xi_0}{2M}\,,$$

$$\widetilde{q}_1 = \left[\frac{30720 r_H^2 M \xi_6}{(1-\varpi)(1+\varpi)^2(2+3\varpi)\xi_2} - \frac{(9+70\varpi+143\varpi^2+90\varpi^3)M}{r_H^3(1+2\varpi)^2(2+3\varpi)} + \frac{384(19+41\varpi+30\varpi^2)M\xi_4}{(1-\varpi)(1+\varpi)(1+2\varpi)^2(2+3\varpi)} + \frac{98304 r_H^3(7+8\varpi)M\xi_4^2}{(1-\varpi)(1+\varpi)^3(1+2\varpi)^2(2+3\varpi)}\right]^{-1} \tag{A.26}$$

These relations can also be inverted to express $(\xi_0, \xi_2, \xi_4, \xi_6)$ in terms of $(R_0, R_1, \widetilde{q}_0, \widetilde{q}_1)$ as follows

$$\begin{aligned}
\xi_0 &= 2M\,\widetilde{q}_0\,,\\
\xi_2 &= \frac{\widetilde{q}_1 R_1 M}{2M}\,(1-2\widetilde{q}_1\,R_1\,M)\,,\\
\xi_4 &= \frac{(1+\sigma)^3\left(R_0 r_H^2(1+2\sigma)-8\widetilde{q}_1 R_1 M(1+\sigma-\widetilde{q}_1 R_1 M)\right)}{384 r_H^3\left(1+\sigma-4\widetilde{q}_1 R_1 M+8\widetilde{q}_1 R_1^2 M^2\right)}\,,\\
\xi_6 &= \frac{(1+\sigma)^4(2+3\sigma)M}{46080 r_H^3 u}\left[\frac{36\widetilde{q}_1 R_1}{r_H^2} - \frac{3R_0}{M} + \frac{3R_1 r_H}{M} - \frac{(1+\sigma)^2}{r_H^2 M(1+2\sigma)u^2}\right.\\
&\qquad\times\left(R_0 r_H^2(1+2\sigma)-8\widetilde{q}_1 R_1 M(1+\sigma+\widetilde{q}_1 R_1 M)\right)\\
&\qquad\times\left(R_0 r_H^2(1+2\sigma)+(1+\sigma-4\widetilde{q}_1 R_1 M)(3-8\widetilde{q}_1 R_1 M)\right)\\
&\quad-\frac{2\widetilde{q}_1 R_1(1+\sigma)(1-2\widetilde{q}_1 R_1 M)}{u^2 r_H^2(1+2\sigma)^2(2+3\sigma)}\left(2R_0^2 r_H^4\left(32\widetilde{q}_1 R_1(4\sigma+7)M-32\sigma-31-64\widetilde{q}_1^2 R_1^2(4\sigma+7)M^2\right)\right.\\
&\qquad+R_0 r_H^2(\sigma(16\widetilde{q}_1 R_1 M(2\widetilde{q}_1 R_1 M(128\widetilde{q}_1 R_1 M-107)+75)-117)\\
&\qquad+4\widetilde{q}_1 R_1 M(417-2\widetilde{q}_1 R_1 M(64\widetilde{q}_1 R_1 M(17\widetilde{q}_1 R_1 M-31)+1013))-117)\\
&\qquad\left.\left.-2(3-8\widetilde{q}_1 R_1 M)^2(4\widetilde{q}_1 R_1 M(17\widetilde{q}_1 R_1 M-7)-1)(-4\widetilde{q}_1 R_1 M+\sigma+1)\right)\right]
\end{aligned} \tag{A.27}$$

with $\sigma = |1-4\widetilde{q}_1 R_1 M|$ and $u = 1+\sigma-4\widetilde{q}_1 R_1 M(1-\widetilde{q}_1 R_1 M)$.

A.4 Signs in the Kretschmann Scalar EMD

The sign choice appearing in the definition of the Kretschmann scalar EMD in Section 3.5 a priori have an impact on the type of solutions that can be described within this EMD. Indeed, in Section 3.2, following [46], we have fixed a similar choice in Eq. (3.14) by demanding that the corresponding geometry allows a smooth limit recovering the Schwarzschild space-time. A similar condition also fixes certain signs in the Kretschmann scalar EMD (and its connection to the distance EMD). To illustrate this idea, we start with the distance EMDfor the particular choice $\xi_{2n} = 0\;\forall n > 1$, such that the only non-trivial remaining parameter is ξ_2, or equivalently ϖ. The classical limit, which indeed reproduces the Schwarzschild space-time, is $\varpi \to 1$. For this particular choice of parameters we find

$$\tau_0 = \frac{r_H}{2M}\,,\quad \tau_1 = \frac{1-\varpi^2}{4M(1+\varpi)}\,,\quad \tau_2 = \frac{1-\varpi^2}{8Mr_H(1+2\varpi)}\,,\quad \tau_3 = \frac{(1-\varpi)(1+\varpi)^2(1-2\varpi)}{16Mr_H^2(2+3\varpi)(1+2\varpi)^2}\,.$$

Thus, identification with the Kretschmann scalar EMD leads to

$$\begin{aligned} K_0 &= \frac{29 + 124\varpi + 170\varpi^2 + 84\varpi^3 + 25\varpi^4}{4r_H^4(1+2\varpi)^2} = \frac{12}{r_H^4} + O(\varpi - 1)\,, \\ K_1 &= -\frac{323 + 2593\varpi + 8128\varpi^2 + 12658\varpi^3 + 10235\varpi^4 + 4157\varpi^5 + 786\varpi^6}{4r_H^5(1+2\varpi)^3(2+3\varpi)} \\ &= -\frac{72}{r_H^5} + O(\varpi - 1)\,, \end{aligned} \tag{A.28}$$

and for $\zeta_{1,2}$ in (3.96) we obtain

$$\begin{aligned} \zeta_1 &= -\frac{r_H^5(1+2\varpi)^3(2+\varpi-3\varpi^2)}{M(323 + 2593\varpi + 8128\varpi^2 + 12658\varpi^3 + 10235\varpi^4 + 4157\varpi^5 + 786\varpi^6)} \\ &= \frac{r_H^5}{288M}(\varpi - 1) + O((\varpi-1)^2)\,, \\ \zeta_2 &= \frac{(2\varpi+1)^5 r_H^9}{M(3+4\varpi)\left(786\varpi^6 + 4157\varpi^5 + 10235\varpi^4 + 12658\varpi^3 + 8128\varpi^2 + 2593\varpi + 323\right)^3} \\ &\quad \times \big(68694 + 901511\varpi + 5091799\varpi^2 + 15949627\varpi^3 + 29316755\varpi^4 + 28823217\varpi^5 \\ &\quad + 4572149\varpi^6 - 24913951\varpi^7 - 32758909\varpi^8 - 19894452\varpi^9 - 6289848\varpi^{10} - 866592\varpi^{11}\big) \\ &= -\frac{25r_H^9}{124416M}(\varpi - 1) + O((\varpi-1)^2)\,. \end{aligned} \tag{A.29}$$

Inserting (A.28) and (A.29) into (3.95) we find

$$K_2 = \begin{cases} \frac{252}{r_H^6} + \frac{5116}{35r_H^6}(\varpi - 1) + O(\varpi - 1) & \text{if} \quad u = +1 \text{ and } \varpi \geq 1\,, \\ \frac{252}{r_H^6} + \frac{5116}{35r_H^6}(\varpi - 1) + O(\varpi - 1) & \text{if} \quad u = -1 \text{ and } \varpi \leq 1\,. \end{cases} \tag{A.30}$$

Thus, depending on how the limit $\varpi \to 1$ is taken, *i.e.* depending on the sign of ξ_2, only one choice of the sign u in (3.95) yields a viable solution, which moreover leads to a finite limit for the Kretschmann scalar as a function of ϖ. Notice also, that in this case (A.28) and (A.30) are compatible with the expansion of the Kretschmann scalar for the (classical) Schwarzschild space-time

$$K_{\text{class}} = \frac{48M^2}{r^6} = \frac{12}{r_H^4} - \frac{72}{r_H^5}(r - r_H) + \frac{252}{r_H^6}(r - r_H)^2 + O((z - r_H)^3)\,, \tag{A.31}$$

where we have used $r_H = 2M$ for the classical Schwarzschild black hole.

A.5 Conditions in the extremal case with $Q^2 \neq M\,r_H$

Here, we collect all conditions on the deformation functions coefficients for an extremal black hole with $\widetilde{\Gamma} \neq \widetilde{\Omega}$ and $Q^2 \neq M r_H$ discussed in Subsection 3.6.5. In particular, requiring $\widetilde{a}_1 \in \mathbb{R}$ and (3.161), we have:

$$\widetilde{\xi}_0 = \widetilde{\theta}_0 = \frac{r_H^2}{2Mr_H - Q^2}\,, \quad \widetilde{\xi}_1 = \widetilde{\theta}_1 = \widetilde{a}_1 \frac{2\widetilde{\xi}_0^2\left(Mr_H - Q^2\right)}{r_H^3}\,, \quad \widetilde{\xi}_2 > \widetilde{\theta}_2\,,$$

- $\dfrac{Q^2}{2} < M\,r_H < Q^2\,,\ \widetilde{a}_2 < \dfrac{r_H\left(4\widetilde{\theta}_2 r_H^2\left(Q^2 - M\,r_H\right)^2 + \widetilde{\xi}_1^2 Q^4\left(Q^2 - 2M\,r_H\right)\right)}{4\widetilde{\xi}_0^2\left(M\,r_H - Q^2\right)^3}\,,$

- $M\,r_H < \dfrac{Q^2}{2}\,,\ \widetilde{a}_2 > \dfrac{r_H\left(4\widetilde{\xi}_2 r_H^2\left(Q^2 - Mr_H\right)^2 + \widetilde{\xi}_1^2 Q^4\left(Q^2 - 2Mr_H\right)\right)}{4\widetilde{\xi}_0^2\left(Mr_H - Q^2\right)^3}\,,$

- $M\,r_H > Q^2\,,\ \widetilde{a}_2 > \dfrac{r_H\left(4\widetilde{\theta}_2 r_H^2\left(Q^2 - Mr_H\right)^2 + \widetilde{\xi}_1^2 Q^4\left(Q^2 - 2Mr_H\right)\right)}{4\widetilde{\xi}_0^2\left(Mr_H - Q^2\right)^3}\,.$

If $\left.\frac{\mathrm{d}^2 f}{\mathrm{d}r^2}\right|_{r=r_H} = \left.\frac{\mathrm{d}^2 h}{\mathrm{d}r^2}\right|_{r=r_H}$, then $\widetilde{a}_1 = 1$, and the relation $\widetilde{\xi}_2 > \widetilde{\theta}_2$ becomes $\widetilde{\xi}_2 = \widetilde{\theta}_2$, such that:

$$\widetilde{\xi}_0 = \widetilde{\theta}_0 = \frac{z_H^2}{2Mr_H - Q^2}\,, \quad \widetilde{\xi}_1 = \widetilde{\theta}_1 = \frac{2\widetilde{\xi}_0^2\left(Mr_H - Q^2\right)}{r_H^3}\,, \quad \widetilde{\xi}_2 = \widetilde{\theta}_2\,,$$

- $\dfrac{Q^2}{2} < M\,r_H\,, \quad \widetilde{\xi}_2 < -\dfrac{Q^4}{\left(Q^2 - 2Mr_H\right)^3},$

- $M\,r_H < \dfrac{Q^2}{2}\,, \quad \widetilde{\xi}_2 > -\dfrac{Q^4}{\left(Q^2 - 2Mr_H\right)^3}\,.$

Bibliography

[1] K. Schwarzschild, *On the gravitational field of a mass point according to Einstein's theory*, Sitzungsber. Preuss. Akad. Wiss. Berlin (Math. Phys.) **1916**, 189–196 (1916), arXiv:physics/9905030 .

[2] R. M. Wald, *General Relativity* (Chicago Univ. Pr., Chicago, USA, 1984).

[3] S. Chandrasekhar, *The mathematical theory of black holes* (1985).

[4] J. A. Wheeler, *No Hair Conjecture and the Physics of Black Holes*, Proc. Ecole d'Eté de Physique Théorique, Les Houches **1**, 121–208 (1971), reprinted in: Black Holes (Les Houches Lectures), C. DeWitt and B. DeWitt (eds.), Gordon and Breach, New York (1973).

[5] W. Israel, *Event horizons in static vacuum space-times*, Phys. Rev. **164**, 1776–1779 (1967).

[6] B. Carter, *Axisymmetric Black Hole Has Only Two Degrees of Freedom*, Phys. Rev. Lett. **26**, 331–333 (1971).

[7] D. C. Robinson, *Uniqueness of the Kerr black hole*, Phys. Rev. Lett. **34**, 905–906 (1975).

[8] J. D. Bekenstein, *Transcendence of the law of baryon-number conservation in black hole physics*, Phys. Rev. Lett. **28**, 452–455 (1972).

[9] J. D. Bekenstein, *Nonexistence of baryon number for static black holes*, Phys. Rev. D **5**, 1239–1246 (1972).

[10] M. Heusler, *No hair theorems and black holes with hair*, Helv. Phys. Acta **69**, 501–528 (1996), arXiv:gr-qc/9610019 .

[11] P. T. Chruściel, J. L. Costa, and M. Heusler, *Stationary Black Holes: Uniqueness and Beyond*, Living Rev. Rel. **15**, 7 (2012), arXiv:1205.6112 [gr-qc] .

[12] C. A. R. Herdeiro and E. Radu, *Asymptotically flat black holes with scalar hair: A review*, International Journal of Modern Physics D **24**, 1542014 (2015), https://doi.org/10.1142/S0218271815420146 .

[13] H. Reissner, *Über die eigengravitation des elektrischen feldes nach der einsteinschen theorie*, Annalen der Physik **355**, 106–120 (1916), https://onlinelibrary.wiley.com/doi/pdf/10.1002/andp.19163550905 .

[14] H. Weyl, *Zur gravitationstheorie*, Annalen der Physik **359**, 117–145 (1917), https://onlinelibrary.wiley.com/doi/pdf/10.1002/andp.19173591804 .

[15] G. Nordstrom, *On the energy of the gravitational field in einstein's theory*, Verhandl. Koninkl. Ned. Akad. Wetenschap., Afdel. Natuurk. (Amsterdam) **26**, 1201–1208 (1918).

[16] S. M. Carroll, M. C. Johnson, and L. Randall, *Extremal limits and black hole entropy*, JHEP **11**, 109, arXiv:0901.0931 [hep-th] .

[17] K. Akiyama *et al.* (Event Horizon Telescope), *First M87 Event Horizon Telescope Results. I. The Shadow of the Supermassive Black Hole*, Astrophys. J. Lett. **875**, L1 (2019), arXiv:1906.11238 [astro-ph.GA] .

[18] P. Kocherlakota *et al.* (Event Horizon Telescope), *Constraints on black-hole charges with the 2017 EHT observations of M87**, Phys. Rev. D **103**, 104047 (2021), arXiv:2105.09343 [gr-qc] .

[19] K. Akiyama *et al.* (Event Horizon Telescope), *First Sagittarius A* Event Horizon Telescope Results. I. The Shadow of the Supermassive Black Hole in the Center of the Milky Way*, Astrophys. J. Lett. **930**, L12 (2022), arXiv:2311.08680 [astro-ph.HE] .

[20] K. Akiyama *et al.* (Event Horizon Telescope), *First Sagittarius A* Event Horizon Telescope Results. VI. Testing the Black Hole Metric*, Astrophys. J. Lett. **930**, L17 (2022), arXiv:2311.09484 [astro-ph.HE] .

[21] B. P. Abbott *et al.* (LIGO Scientific, Virgo), *Observation of Gravitational Waves from a Binary Black Hole Merger*, Phys. Rev. Lett. **116**, 061102 (2016), arXiv:1602.03837 [gr-qc] .

[22] R. Abbott *et al.* (LIGO Scientific, Virgo), *Tests of general relativity with binary black holes from the second LIGO-Virgo gravitational-wave transient catalog*, Phys. Rev. D **103**, 122002 (2021), arXiv:2010.14529 [gr-qc] .

[23] R. Abbott *et al.* (LIGO Scientific, Virgo), *GW190412: Observation of a Binary-Black-Hole Coalescence with Asymmetric Masses*, Phys. Rev. D **102**, 043015 (2020), arXiv:2004.08342 [astro-ph.HE] .

[24] S. A. Hayward, *Formation and evaporation of nonsingular black holes*, Physical Review Letters **96**, 10.1103/physrevlett.96.031103 (2006).

[25] J. Bardeen, in *Proceedings of the 5th International Conference on Gravitation and the Theory of Relativity* (1968) p. 87.

[26] I. Dymnikova, *Vacuum nonsingular black hole*, General relativity and gravitation **24**, 235–242 (1992).

[27] I. Dymnikova and E. Galaktionov, *Stability of a vacuum nonsingular black hole*, Class. Quant. Grav. **22**, 2331–2358 (2005), arXiv:gr-qc/0409049 .

[28] A. García, D. Galtsov, and O. Kechkin, *Class of stationary axisymmetric solutions of the einstein-maxwell-dilaton-axion field equations*, Phys. Rev. Lett. **74**, 1276–1279 (1995).

[29] N. E. J. Bjerrum-Bohr, J. F. Donoghue, and B. R. Holstein, *Quantum corrections to the Schwarzschild and Kerr metrics*, Phys. Rev. D **68**, 084005 (2003), [Erratum: Phys.Rev.D 71, 069904 (2005)], arXiv:hep-th/0211071 .

[30] J. F. Donoghue, B. R. Holstein, B. Garbrecht, and T. Konstandin, *Quantum corrections to the Reissner-Nordström and Kerr-Newman metrics*, Phys. Lett. B **529**, 132–142 (2002), [Erratum: Phys.Lett.B 612, 311–312 (2005)], arXiv:hep-th/0112237 .

[31] G. G. Kirilin, *Quantum corrections to the Schwarzschild metric and reparametrization transformations*, Phys. Rev. D **75**, 108501 (2007), arXiv:gr-qc/0601020 .

[32] V. P. Frolov, *Notes on nonsingular models of black holes*, Phys. Rev. D **94**, 104056 (2016), arXiv:1609.01758 [gr-qc] .

[33] X. Calmet and B. K. El-Menoufi, *Quantum Corrections to Schwarzschild Black Hole*, Eur. Phys. J. C **77**, 243 (2017), arXiv:1704.00261 [hep-th] .

[34] X. Calmet, R. Casadio, and F. Kuipers, *Quantum Gravitational Corrections to a Star Metric and the Black Hole Limit*, Phys. Rev. D **100**, 086010 (2019), arXiv:1909.13277 [hep-th] .

[35] A. Simpson and M. Visser, *Black-bounce to traversable wormhole*, JCAP **02**, 042, arXiv:1812.07114 [gr-qc] .

[36] A. Simpson and M. Visser, *Regular black holes with asymptotically Minkowski cores*, Universe **6**, 8 (2019), arXiv:1911.01020 [gr-qc] .

[37] P. Nicolini, E. Spallucci, and M. F. Wondrak, *Quantum Corrected Black Holes from String T-Duality*, Phys. Lett. B **797**, 134888 (2019), arXiv:1902.11242 [gr-qc] .

[38] X. Calmet and F. Kuipers, *Quantum gravitational corrections to the entropy of a Schwarzschild black hole*, Phys. Rev. D **104**, 066012 (2021), arXiv:2108.06824 [hep-th] .

[39] E. Battista, *Quantum Schwarzschild geometry in effective field theory models of gravity*, Phys. Rev. D **109**, 026004 (2024), arXiv:2312.00450 [gr-qc] .

[40] R. Carballo-Rubio, *Master field equations for spherically symmetric gravitational fields beyond general relativity* (2025), arXiv:2507.15920 [gr-qc] .

[41] R. Carballo-Rubio *et al.*, *Towards a non-singular paradigm of black hole physics*, JCAP **05**, 003, arXiv:2501.05505 [gr-qc] .

[42] R. Emparan, A. M. Frassino, and B. Way, *Quantum BTZ black hole*, JHEP **11**, 137, arXiv:2007.15999 [hep-th] .

[43] R. Emparan, A. M. Frassino, M. Sasieta, and M. Tomašević, *Holographic complexity of quantum black holes*, JHEP **02**, 204, arXiv:2112.04860 [hep-th] .

[44] S. Vagnozzi *et al.*, *Horizon-scale tests of gravity theories and fundamental physics from the Event Horizon Telescope image of Sagittarius A*, Class. Quant. Grav. **40**, 165007 (2023), arXiv:2205.07787 [gr-qc] .

[45] E. Binetti, M. Del Piano, S. Hohenegger, F. Pezzella, and F. Sannino, *Effective theory of quantum black holes*, Phys. Rev. D **106**, 046006 (2022), arXiv:2203.13515 [gr-qc] .

[46] M. Del Piano, S. Hohenegger, and F. Sannino, *Quantum black hole physics from the event horizon*, Phys. Rev. D **109**, 024045 (2024), arXiv:2307.13489 [gr-qc] .

[47] M. Del Piano, S. Hohenegger, and F. Sannino, *Effective metric descriptions of quantum black*

holes, Eur. Phys. J. C **84**, 1273 (2024), arXiv:2403.12679 [gr-qc] .

[48] M. Damia Paciarini, M. Del Piano, S. Hohenegger, and F. Sannino, *Effective metric description of charged black holes*, Eur. Phys. J. C **85**, 848 (2025), arXiv:2504.20810 [gr-qc] .

[49] M. Del Piano, S. Hohenegger, and F. Sannino, *Black hole shadow and other observables away from the horizon: Extending the effective metric descriptions*, Phys. Rev. D **111**, 064070 (2025), arXiv:2412.13673 [gr-qc] .

[50] A. D'Alise, G. Fabiano, D. Frattulillo, S. Hohenegger, D. Iacobacci, F. Pezzella, and F. Sannino, *Positivity conditions for generalized Schwarzschild space-times*, Phys. Rev. D **108**, 084042 (2023), arXiv:2305.12965 [gr-qc] .

[51] C. M. Bender and S. A. Orszag, *Advanced Mathematical Methods for Scientists and Engineers* (McGraw-Hill, 1978).

[52] N. A. Dondi, G. V. Dunne, M. Reichert, and F. Sannino, *Analytic Coupling Structure of Large N_f (Super) QED and QCD*, Phys. Rev. D **100**, 015013 (2019), arXiv:1903.02568 [hep-th] .

[53] N. A. Dondi, G. V. Dunne, M. Reichert, and F. Sannino, *Towards the qed beta function and renormalons at $1/N_f^2$ and $1/N_f^3$*, Phys. Rev. D **102**, 035005 (2020).

[54] C. Gruber and O. Luongo, *Cosmographic analysis of the equation of state of the universe through Padé approximations*, Phys. Rev. D **89**, 103506 (2014), arXiv:1309.3215 [gr-qc] .

[55] A. M. Sultan, A. Batool, G. Abbas, A. Jawad, and S. Shaymatov, *Padé approximated traversable wormholes in f(R,T) gravity*, Nucl. Phys. B **1013**, 116838 (2025).

[56] A. H. Mroue, L. E. Kidder, and S. A. Teukolsky, *Ineffectiveness of Pade resummation techniques in post-Newtonian approximations*, Phys. Rev. D **78**, 044004 (2008), arXiv:0805.2390 [gr-qc] .

[57] E. Berti, *Black hole quasinormal modes: Hints of quantum gravity?*, Conf. Proc. C **0405132**, 145–186 (2004), arXiv:gr-qc/0411025 .

[58] E. Berti, V. Cardoso, M. H.-Y. Cheung, F. Di Filippo, F. Duque, P. Martens, and S. Mukohyama, *Stability of the fundamental quasinormal mode in time-domain observations against small perturbations*, Phys. Rev. D **106**, 084011 (2022), arXiv:2205.08547 [gr-qc] .

[59] E. Berti, V. Cardoso, and A. O. Starinets, *Quasinormal modes of black holes and black branes*, Class. Quant. Grav. **26**, 163001 (2009), arXiv:0905.2975 [gr-qc] .

[60] R. A. Konoplya and Z. Stuchlík, *Are eikonal quasinormal modes linked to the unstable circular null geodesics?*, Phys. Lett. B **771**, 597–602 (2017), arXiv:1705.05928 [gr-qc] .

[61] R. Konoplya, L. Rezzolla, and A. Zhidenko, *General parametrization of axisymmetric black holes in metric theories of gravity*, Phys. Rev. D **93**, 064015 (2016), arXiv:1602.02378 [gr-qc] .

[62] I. Z. Stefanov, S. S. Yazadjiev, and G. G. Gyulchev, *Connection between Black-Hole Quasinormal Modes and Lensing in the Strong Deflection Limit*, Phys. Rev. Lett. **104**, 251103 (2010), arXiv:1003.1609 [gr-qc] .

[63] V. Cardoso, A. S. Miranda, E. Berti, H. Witek, and V. T. Zanchin, *Geodesic stability, Lyapunov exponents and quasinormal modes*, Phys. Rev. D **79**, 064016 (2009), arXiv:0812.1806 [hep-th] .

[64] S. R. Dolan, *The Quasinormal Mode Spectrum of a Kerr Black Hole in the Eikonal Limit*, Phys. Rev. D **82**, 104003 (2010), arXiv:1007.5097 [gr-qc] .

[65] T. Johannsen and D. Psaltis, *Testing the No-Hair Theorem with Observations in the Electromagnetic Spectrum: I. Properties of a Quasi-Kerr Spacetime*, Astrophys. J. **716**, 187–197 (2010), arXiv:1003.3415 [astro-ph.HE] .

[66] T. Johannsen and D. Psaltis, *A Metric for Rapidly Spinning Black Holes Suitable for Strong-Field Tests of the No-Hair Theorem*, Phys. Rev. D **83**, 124015 (2011), arXiv:1105.3191 [gr-qc] .

[67] V. Cardoso, P. Pani, and J. Rico, *On generic parametrizations of spinning black-hole geometries*, Phys. Rev. D **89**, 064007 (2014), arXiv:1401.0528 [gr-qc] .

[68] L. Rezzolla and A. Zhidenko, *New parametrization for spherically symmetric black holes in metric theories of gravity*, Phys. Rev. D **90**, 084009 (2014), arXiv:1407.3086 [gr-qc] .

[69] M. Del Piano, C. De Simone, M. Damia Paciarini, V. De Falco, M. Myszkowski, F. Sannino, and V. Vellucci, *Toward a unified view of agnostic parametrizations for deformed black holes*, Submitted to Phys. Rev. D (2025), arXiv:2510.14707 [gr-qc] .

[70] Y.-Z. Li and X.-M. Kuang, *Precession of bounded orbits and shadow in quantum black hole spacetime*, Phys. Rev. D **107**, 064052 (2023).

[71] A. Belfiglio, O. Luongo, S. Mancini, and S. Tomasi, *Entanglement entropy in quantum black holes*, Class. Quant. Grav. **42**, 035006 (2025), arXiv:2404.00715 [gr-qc] .

[72] M. Damia Paciarini, S. Hohenegger, M. Myszkowski, and F. Sannino, *Effective metric description of 2+1 dimensional quantum black holes*, Eur. Phys. J. C **85**, 611 (2025), arXiv:2412.15960 [gr-qc] .

[73] M. Damia Paciarini, M. Myszkowski, F. Sannino, and V. Vellucci, *Regular Spacetimes in the Effective Metric Description* (2025), arXiv:2506.12620 [gr-qc] .

[74] S. Hohenegger, *Probing Effective Black Hole Deformations* (2025), arXiv:2508.17781 [gr-qc] .

[75] R. P. Kerr, *Gravitational field of a spinning mass as an example of algebraically special metrics*, Phys. Rev. Lett. **11**, 237–238 (1963).

[76] R. Penrose, *Gravitational collapse: The role of general relativity*, Riv. Nuovo Cim. **1**, 252–276 (1969).

[77] J. M. Bardeen, W. H. Press, and S. A. Teukolsky, *Rotating black holes: Locally nonrotating frames, energy extraction, and scalar synchrotron radiation*, Astrophys. J. **178**, 347 (1972).

[78] W. H. Press and S. A. Teukolsky, *Floating Orbits, Superradiant Scattering and the Black-hole Bomb*, Nature **238**, 211–212 (1972).

[79] T. Damour and R. Ruffini, *Black Hole Evaporation in the Klein-Sauter-Heisenberg-Euler*

Formalism, Phys. Rev. D **14**, 332–334 (1976).

[80] R. Brito, V. Cardoso, and P. Pani, *Superradiance: New Frontiers in Black Hole Physics*, Lect. Notes Phys. **906**, pp.1–237 (2015), arXiv:1501.06570 [gr-qc] .

[81] R. Penrose, *Naked singularities*, Annals N. Y. Acad. Sci. **224**, 125–134 (1973).

[82] R. Penrose, *Gravitational collapse and space-time singularities*, Phys. Rev. Lett. **14**, 57–59 (1965).

[83] G. B. Jeffery and L. N. G. Filon, *The field of an electron on einstein's theory of gravitation*, Proceedings of the Royal Society of London. Series A, Containing Papers of a Mathematical and Physical Character **99**, 123–134 (1921).

[84] S. Carroll, *Spacetime and Geometry: An Introduction to General Relativity* (Benjamin Cummings, 2003).

[85] R. A. Matzner, N. Zamorano, and V. D. Sandberg, *Instability of the Cauchy horizon of Reissner-Nordstrom black holes*, Phys. Rev. D **19**, 2821–2826 (1979).

[86] E. Poisson and W. Israel, *Inner-horizon instability and mass inflation in black holes*, Phys. Rev. Lett. **63**, 1663–1666 (1989).

[87] S. Chandrasekhar and J. B. Hartle, *On crossing the cauchy horizon of a reissner-nordström black-hole*, Proceedings of the Royal Society of London. Series A, Mathematical and Physical Sciences **384**, 301–315 (1982).

[88] S. Hollands, R. M. Wald, and J. Zahn, *Quantum instability of the Cauchy horizon in Reissner–Nordström–deSitter spacetime*, Class. Quant. Grav. **37**, 115009 (2020), arXiv:1912.06047 [gr-qc] .

[89] N. N. Bogoljubov, *On a new method in the theory of superconductivity*, Il Nuovo Cimento **7**, 794–805 (1958).

[90] S. Sarkar, S. Shankaranarayanan, and L. Sriramkumar, *Sub-leading contributions to the black hole entropy in the brick wall approach*, Phys. Rev. D **78**, 024003 (2008), arXiv:0710.2013 [gr-qc] .

[91] S. W. Hawking, *Particle creation by black holes*, Communications in Mathematical Physics **43**, 199–220 (1975).

[92] N. D. Birrell and P. C. W. Davies, *Quantum Fields in Curved Space*, Cambridge Monographs on Mathematical Physics (Cambridge University Press, 1982).

[93] J. D. Bekenstein, *Black holes and entropy*, Phys. Rev. D **7**, 2333–2346 (1973).

[94] R. M. Wald, *Black hole entropy is the Noether charge*, Phys. Rev. D **48**, R3427–R3431 (1993), arXiv:gr-qc/9307038 .

[95] J. M. Maldacena, *The Large N limit of superconformal field theories and supergravity*, Adv. Theor. Math. Phys. **2**, 231–252 (1998), arXiv:hep-th/9711200 .

[96] S. S. Gubser, I. R. Klebanov, and A. M. Polyakov, *Gauge theory correlators from noncritical string theory*, Phys. Lett. B **428**, 105–114 (1998), arXiv:hep-th/9802109 [hep-th] .

[97] E. Witten, *Anti-de Sitter space and holography*, Adv. Theor. Math. Phys. **2**, 253–291 (1998), arXiv:hep-th/9802150 [hep-th] .

[98] V. E. Hubeny, M. Rangamani, and T. Takayanagi, *A Covariant Holographic Entanglement Entropy Proposal*, JHEP **07**, 062, arXiv:0705.0016 [hep-th] .

[99] T. Nishioka, S. Ryu, and T. Takayanagi, *Holographic Entanglement Entropy: An Overview*, J. Phys. A **42**, 504008 (2009), arXiv:0905.0932 [hep-th] .

[100] M. Rangamani and T. Takayanagi, *Holographic Entanglement Entropy*, Lecture Notes in Physics, Vol. 931 (Springer, 2017) arXiv:1609.01287 [hep-th] .

[101] S. Ryu and T. Takayanagi, *Holographic derivation of entanglement entropy from AdS/CFT*, Phys. Rev. Lett. **96**, 181602 (2006), arXiv:hep-th/0603001 .

[102] S. Ryu and T. Takayanagi, *Aspects of Holographic Entanglement Entropy*, JHEP **08**, 045, arXiv:hep-th/0605073 [hep-th] .

[103] D. V. Fursaev, *Temperature and entropy of a quantum black hole and conformal anomaly*, Phys. Rev. D **51**, 5352–5355 (1995), arXiv:hep-th/9412161 .

[104] Y. Xiao and Y. Tian, *Logarithmic correction to black hole entropy from the nonlocality of quantum gravity*, Phys. Rev. D **105**, 044013 (2022), arXiv:2104.14902 [gr-qc] .

[105] S. N. Solodukhin, *Entanglement entropy of black holes*, Living Rev. Rel. **14**, 8 (2011), arXiv:1104.3712 [hep-th] .

[106] S. N. Solodukhin, *The Conical singularity and quantum corrections to entropy of black hole*, Phys. Rev. D **51**, 609–617 (1995), arXiv:hep-th/9407001 .

[107] A. Sen, *Logarithmic Corrections to Schwarzschild and Other Non-extremal Black Hole Entropy in Different Dimensions*, JHEP **04**, 156, arXiv:1205.0971 [hep-th] .

[108] B. K. El-Menoufi, *Quantum gravity of Kerr-Schild spacetimes and the logarithmic correction to Schwarzschild black hole entropy*, JHEP **05**, 035, arXiv:1511.08816 [hep-th] .

[109] R.-G. Cai, L.-M. Cao, and N. Ohta, *Black Holes in Gravity with Conformal Anomaly and Logarithmic Term in Black Hole Entropy*, JHEP **04**, 082, arXiv:0911.4379 [hep-th] .

[110] S. Carlip, *Logarithmic corrections to black hole entropy from the Cardy formula*, Class. Quant. Grav. **17**, 4175–4186 (2000), arXiv:gr-qc/0005017 .

[111] R. Banerjee and B. R. Majhi, *Quantum Tunneling Beyond Semiclassical Approximation*, JHEP **06**, 095, arXiv:0805.2220 [hep-th] .

[112] R. Banerjee and B. R. Majhi, *Quantum Tunneling, Trace Anomaly and Effective Metric*, Phys. Lett. B **674**, 218–222 (2009), arXiv:0808.3688 [hep-th] .

[113] R. K. Kaul and P. Majumdar, *Logarithmic correction to the Bekenstein-Hawking entropy*, Phys. Rev. Lett. **84**, 5255–5257 (2000), arXiv:gr-qc/0002040 .

[114] T. Jacobson, *Thermodynamics of space-time: The Einstein equation of state*, Phys. Rev. Lett. **75**, 1260–1263 (1995), arXiv:gr-qc/9504004 .

[115] T. Jacobson, G. Kang, and R. C. Myers, *On black hole entropy*, Phys. Rev. D **49**, 6587–6598

(1994), arXiv:gr-qc/9312023 .

[116] C. Eling, R. Guedens, and T. Jacobson, *Non-equilibrium thermodynamics of spacetime*, Phys. Rev. Lett. **96**, 121301 (2006), arXiv:gr-qc/0602001 .

[117] T. Jacobson, *Entanglement Equilibrium and the Einstein Equation*, Phys. Rev. Lett. **116**, 201101 (2016), arXiv:1505.04753 [gr-qc] .

[118] A. Alonso-Serrano and M. Liška, *Quantum phenomenological gravitational dynamics: A general view from thermodynamics of spacetime*, JHEP **12**, 196, arXiv:2009.03826 [gr-qc] .

[119] A. Alonso-Serrano, M. de Cesare, and M. Del Piano, *Black hole solutions in quantum phenomenological gravitational dynamics*, Phys. Rev. D **112**, 084031 (2025), arXiv:2504.01539 [gr-qc] .

[120] D. N. Page, in *5th Canadian Conference on General Relativity and Relativistic Astrophysics (5CCGRRA)* (1993) arXiv:hep-th/9305040 .

[121] E. Bianchi, M. Christodoulou, F. D'Ambrosio, H. M. Haggard, and C. Rovelli, *White Holes as Remnants: A Surprising Scenario for the End of a Black Hole*, Class. Quant. Grav. **35**, 225003 (2018), arXiv:1802.04264 [gr-qc] .

[122] P. Chen, Y. C. Ong, and D.-h. Yeom, *Black Hole Remnants and the Information Loss Paradox*, Phys. Rept. **603**, 1–45 (2015), arXiv:1412.8366 [gr-qc] .

[123] V. Perlick and O. Y. Tsupko, *Calculating black hole shadows: Review of analytical studies*, Phys. Rept. **947**, 1–39 (2022), arXiv:2105.07101 [gr-qc] .

[124] S. M. Carroll, *Spacetime and Geometry* (Cambridge University Press, 2019).

[125] C. W. Misner, K. S. Thorne, and J. A. Wheeler, *Gravitation* (Macmillan, 1973).

[126] V. Bozza, *Gravitational lensing in the strong field limit*, Phys. Rev. D **66**, 103001 (2002), arXiv:gr-qc/0208075 .

[127] J. L. Synge, *The Escape of Photons from Gravitationally Intense Stars*, Monthly Notices of the Royal Astronomical Society **131**, 463–466 (1966), https://academic.oup.com/mnras/article-pdf/131/3/463/8076763/mnras131-0463.pdf .

[128] V. Perlick, O. Y. Tsupko, and G. S. Bisnovatyi-Kogan, *Influence of a plasma on the shadow of a spherically symmetric black hole*, Phys. Rev. D **92**, 104031 (2015), arXiv:1507.04217 [gr-qc] .

[129] K. S. Virbhadra and G. F. R. Ellis, *Gravitational lensing by naked singularities*, Phys. Rev. D **65**, 103004 (2002).

[130] Q. Gan, P. Wang, H. Wu, and H. Yang, *Photon spheres and spherical accretion image of a hairy black hole*, Phys. Rev. D **104**, 024003 (2021), arXiv:2104.08703 [gr-qc] .

[131] P. V. P. Cunha and C. A. R. Herdeiro, *Stationary black holes and light rings*, Phys. Rev. Lett. **124**, 181101 (2020), arXiv:2003.06445 [gr-qc] .

[132] C.-M. Claudel, K. S. Virbhadra, and G. F. R. Ellis, *The Geometry of photon surfaces*, J. Math. Phys. **42**, 818–838 (2001), arXiv:gr-qc/0005050 .

[133] C. V. Vishveshwara, *Scattering of gravitational radiation by a Schwarzschild black-hole*, Nature **227**, 936–938 (1970).

[134] W. H. Press, *Long Wave Trains of Gravitational Waves from a Vibrating Black Hole*, Astrophys. J. Lett. **170**, L105–L108 (1971).

[135] S. Chandrasekhar and S. Detweiler, *The quasi-normal modes of the Schwarzschild black hole*, Proc. Roy. Soc. Lond. A **344**, 441–452 (1975).

[136] K. D. Kokkotas and B. G. Schmidt, *Quasi-normal modes of stars and black holes*, Living Rev. Rel. **2**, 2 (1999), arXiv:gr-qc/9909058 .

[137] H. P. Nollert, *Quasinormal modes: The characteristic 'sound' of black holes and neutron stars*, Class. Quant. Grav. **16**, R159–R216 (1999).

[138] E. Berti, V. Cardoso, and A. O. Starinets, *Quasinormal modes of black holes and black branes*, Class. Quant. Grav. **26**, 163001 (2009), arXiv:0905.2975 [gr-qc] .

[139] T. Regge and J. A. Wheeler, *Stability of a Schwarzschild singularity*, Phys. Rev. **108**, 1063–1069 (1957).

[140] F. J. Zerilli, *Effective potential for even parity Regge-Wheeler gravitational perturbation equations*, Phys. Rev. Lett. **24**, 737–738 (1970).

[141] R. A. Konoplya and A. Zhidenko, *Quasinormal modes of black holes: From astrophysics to string theory*, Rev. Mod. Phys. **83**, 793–836 (2011), arXiv:1102.4014 [gr-qc] .

[142] B. P. Abbott *et al.* (LIGO Scientific and Virgo), *Observation of Gravitational Waves from a Binary Black Hole Merger*, Phys. Rev. Lett. **116**, 061102 (2016), arXiv:1602.03837 [gr-qc] .

[143] B. P. Abbott *et al.* (LIGO Scientific and Virgo), *Tests of general relativity with GW150914*, Phys. Rev. Lett. **116**, 221101 (2016), arXiv:1602.03841 [gr-qc] .

[144] A. Maselli, S. Yi, L. Pierini, V. Vellucci, L. Reali, L. Gualtieri, and E. Berti, *Black hole spectroscopy beyond Kerr: Agnostic and theory-based tests with next-generation interferometers*, Phys. Rev. D **109**, 064060 (2024), arXiv:2311.14803 [gr-qc] .

[145] V. Cardoso and P. Pani, *Tests for the existence of horizons through gravitational wave echoes*, Nat. Astron. **1**, 586–591 (2017), arXiv:1709.01525 [gr-qc] .

[146] E. Berti *et al.*, *Testing General Relativity with Present and Future Astrophysical Observations*, Class. Quant. Grav. **35**, 053001 (2018), arXiv:1806.05195 [gr-qc] .

[147] L. Barack *et al.*, *Black holes, gravitational waves and fundamental physics: a roadmap*, Class. Quant. Grav. **36**, 143001 (2019), arXiv:1806.05195 [gr-qc] .

[148] H.-J. Blome and B. Mashhoon, *Quasi-normal oscillations of a schwarzschild black hole*, Phys. Lett. A **100**, 231–234 (1981).

[149] B. F. Schutz and C. M. Will, *Black Hole Normal Modes: A Semianalytic Approach*, Astrophys. J. Lett. **291**, L33–L36 (1985).

[150] S. Iyer and C. M. Will, *Black-hole normal modes: A WKB approach. I. Foundations and application of a higher-order WKB analysis of potential-barrier scattering*, Phys. Rev. D **35**, 3621–3631 (1987).

[151] R. A. Konoplya, *Quasinormal behavior of the D-dimensional Schwarzschild black hole and higher order WKB approach*, Phys. Rev. D **68**, 024018 (2003), arXiv:gr-qc/0303052 .

[152] J. Matyjasek and M. Opala, *Quasinormal modes of black holes: The improved semianalytic approach*, Phys. Rev. D **96**, 024011 (2017), arXiv:1704.00361 [gr-qc] .

[153] E. W. Leaver, *An analytic representation for the quasi-normal modes of Kerr black holes*, Proc. Roy. Soc. Lond. A **402**, 285–298 (1985).

[154] C. Gundlach, R. H. Price, and J. Pullin, *Late time behavior of stellar collapse and explosions: 1. Linearized perturbations*, Phys. Rev. D **49**, 883–889 (1994), arXiv:gr-qc/9307009 .

[155] V. Cardoso, A. S. Miranda, E. Berti, H. Witek, and V. T. Zanchin, *Geodesic stability, Lyapunov exponents and quasinormal modes*, Phys. Rev. D **79**, 064016 (2009), arXiv:0812.1806 [hep-th] .

[156] E. Berti *et al.*, *Black hole spectroscopy: from theory to experiment* (2025), arXiv:2505.23895 [gr-qc] .

[157] A. Bonanno and M. Reuter, *Renormalization group improved black hole space-times*, Phys. Rev. D **62**, 043008 (2000), arXiv:hep-th/0002196 .

[158] H. S. Ruse, *Taylor's theorem in the tensor calculus*, Proceedings of the London Mathematical Society **s2-32**, 87–92 (1931), https://londmathsoc.onlinelibrary.wiley.com/doi/pdf/10.1112/plms/s2-32.1.87 .

[159] J. L. Synge, *A characteristic function in riemannian space and its application to the solution of geodesic triangles*, Proceedings of the London Mathematical Society **s2-32**, 241–258 (1931), https://londmathsoc.onlinelibrary.wiley.com/doi/pdf/10.1112/plms/s2-32.1.241 .

[160] B. S. DeWitt and R. W. Brehme, *Radiation damping in a gravitational field*, Annals of Physics **9**, 220–259 (1960).

[161] A. Held, *Invariant Renormalization-Group improvement* (2021), arXiv:2105.11458 [gr-qc] .

[162] J. M. Bardeen, *Non-singular general relativistic gravitational collapse*, Proceedings of the International Conference GR5 (1968).

[163] E. Kretschmann, *über die prinzipielle bestimmbarkeit der berechtigten bezugssysteme beliebiger relativitätstheorien (i), (ii)*, Annalen der Physik **48**, 907–942, 943–982 (1915).

[164] R. Balbinot, A. Fabbri, S. Farese, and R. Parentani, *Hawking radiation from extremal and non-extremal black holes*, Phys. Rev. D **76**, 124010 (2007), arXiv:0710.0388 [hep-th] .

[165] R. C. Delgado, *Quantum gravitational corrections to the entropy of a reissner–nordström black hole*, The European Physical Journal C **82**, 10.1140/epjc/s10052-022-10232-0 (2022).

[166] E. T. Whittaker, *On the reversion of series*, Gaz. Mat. Lisboa. **12(50)**, 1 (1950).

[167] I. Dymnikova, *Vacuum nonsingular black hole*, Gen. Rel. Grav. **24**, 235–242 (1992).

[168] E. Palti, *The Swampland: Introduction and Review*, Fortsch. Phys. **67**, 1900037 (2019), arXiv:1903.06239 [hep-th] .

[169] C. Vafa, *The String landscape and the swampland* (2005), arXiv:hep-th/0509212 .

[170] N. Arkani-Hamed, L. Motl, A. Nicolis, and C. Vafa, *The String landscape, black holes and gravity as the weakest force*, JHEP **06**, 060, arXiv:hep-th/0601001 .

[171] S. Weinberg, *Ultraviolet divergences in quantum theories of gravitation*, In *General Relativity: An Einstein Centenary Survey*, eds. S. W. Hawking and W. Israel (1979).

[172] M. Reuter, *Nonperturbative evolution equation for quantum gravity*, Phys. Rev. D **57**, 971–985 (1998), arXiv:hep-th/9605030 .

[173] M. Niedermaier and M. Reuter, *The Asymptotic Safety Scenario in Quantum Gravity*, Living Rev. Rel. **9**, 5–173 (2006).

[174] R. Percacci, *Asymptotic safety*, In *Oriti, D. (ed.): Approaches to Quantum Gravity* 111–128 (2009), arXiv:0709.3851 [hep-th] .

[175] A. Eichhorn, *An asymptotically safe guide to quantum gravity and matter*, Front. Astron. Space Sci. **5**, 47 (2018), arXiv:1810.07615 [hep-th] .

[176] A. Eichhorn and A. Held, *Black holes in asymptotically safe gravity and beyond* (2022), arXiv:2212.09495 [gr-qc] .

[177] M. Reichert, *Lecture notes: Functional Renormalisation Group and Asymptotically Safe Quantum Gravity*, PoS **Modave2019**, 005 (2020).

[178] J. F. Donoghue, *Leading quantum correction to the Newtonian potential*, Phys. Rev. Lett. **72**, 2996–2999 (1994), arXiv:gr-qc/9310024 .

[179] J. F. Donoghue, *General relativity as an effective field theory: The leading quantum corrections*, Phys. Rev. D **50**, 3874–3888 (1994), arXiv:gr-qc/9405057 .

[180] H. W. Hamber and S. Liu, *On the quantum corrections to the Newtonian potential*, Phys. Lett. B **357**, 51–56 (1995), arXiv:hep-th/9505182 .

[181] N. E. J. Bjerrum-Bohr, J. F. Donoghue, and B. R. Holstein, *Quantum gravitational corrections to the nonrelativistic scattering potential of two masses*, Phys. Rev. D **67**, 084033 (2003), [Erratum: Phys.Rev.D 71, 069903 (2005)], arXiv:hep-th/0211072 .

[182] J. F. Donoghue, *Nonlocal partner to the cosmological constant*, Phys. Rev. D **105**, 105025 (2022), arXiv:2201.12217 [hep-th] .

[183] H. Ooguri and C. Vafa, *On the Geometry of the String Landscape and the Swampland*, Nucl. Phys. B **766**, 21–33 (2007), arXiv:hep-th/0605264 .

[184] N. B. Agmon, A. Bedroya, M. J. Kang, and C. Vafa, *Lectures on the string landscape and the Swampland* (2022), arXiv:2212.06187 [hep-th] .

[185] D. Harlow, B. Heidenreich, M. Reece, and T. Rudelius, *Weak gravity conjecture*, Rev. Mod. Phys. **95**, 035003 (2023), arXiv:2201.08380 [hep-th] .

[186] O. Antipin, J. Bersini, F. Sannino, Z.-W. Wang, and C. Zhang, *More on the weak gravity conjecture via convexity of charged operators*, JHEP **12**, 204, arXiv:2109.04946 [hep-th] .

[187] T. Antonelli and X. Calmet, *The weak gravity conjecture in the Vilkovisky-DeWitt effective action of quantum gravity*, Phys. Lett. B **864**, 139403 (2025), arXiv:2503.09227 [hep-th] .

[188] E. Meissel, *Über Reihen, denen man bei der numerischen Lösung des Dreikörperproblems begegnet, wenn die Anfangsgeschwindigkeiten Null sind*, Jahresbericht über die Realschule in Kiel während des Schuljahres 1881/82 , 1–11 (1882).

[189] S. K. Foong, *From moon-fall to motions under inverse square laws*, European Journal of Physics **29**, 987 (2008).

[190] J. Peetre, Ernst meissel and the pythagorean problem - the dreikörper-problem in the nachlass meissel (1997).

[191] A. Simpson and M. Visser, *Black-bounce to traversable wormhole*, JCAP **02**, 042, arXiv:1812.07114 [gr-qc] .

[192] A. Simpson and M. Visser, *Regular black holes with asymptotically Minkowski cores*, Universe **6**, 8 (2019), arXiv:1911.01020 [gr-qc] .

[193] A. García, D. Galtsov, and O. Kechkin, *Class of stationary axisymmetric solutions of the einstein-maxwell-dilaton-axion field equations*, Phys. Rev. Lett. **74**, 1276–1279 (1995).

[194] H. Culetu, *On a regular charged black hole with a nonlinear electric source*, Int. J. Theor. Phys. **54**, 2855–2863 (2015), arXiv:1408.3334 [gr-qc] .

[195] V. P. Frolov, *Notes on nonsingular models of black holes*, Phys. Rev. D **94**, 104056 (2016).

[196] M. Cadoni, M. De Laurentis, I. De Martino, R. Della Monica, M. Oi, and A. P. Sanna, *Are nonsingular black holes with super-Planckian hair ruled out by S2 star data?*, Phys. Rev. D **107**, 044038 (2023), arXiv:2211.11585 [gr-qc] .

[197] S.-W. Wei and Y.-X. Liu, *Observing the shadow of Einstein-Maxwell-Dilaton-Axion black hole*, JCAP **11**, 063, arXiv:1311.4251 [gr-qc] .

[198] C. M. Will, *The Confrontation between General Relativity and Experiment*, Living Rev. Rel. **17**, 4 (2014), arXiv:1403.7377 [gr-qc] .

[199] J. G. Williams, S. G. Turyshev, and D. H. Boggs, *Progress in lunar laser ranging tests of relativistic gravity*, Phys. Rev. Lett. **93**, 261101 (2004), arXiv:gr-qc/0411113 .

[200] K. Glampedakis and S. Babak, *Mapping spacetimes with LISA: Inspiral of a test-body in a 'quasi-Kerr' field*, Class. Quant. Grav. **23**, 4167–4188 (2006), arXiv:gr-qc/0510057 .

[201] M. Maggiore, *Gravitational Waves. Vol. 1: Theory and Experiments* (Oxford University Press, 2007).

[202] A. Chowdhuri, A. Bhattacharyya, and S. Kumar, *Prospects of detecting deviations to Kerr geometry with radiation reaction effects in EMRIs*, JCAP **04**, 001, arXiv:2311.05983 [gr-qc] .

[203] J. Ben Achour, E. Gourgoulhon, and H. Roussille, *Black hole photon ring beyond General Relativity: an integrable parametrization*, JCAP **10**, 012, arXiv:2506.09882 [gr-qc] .

[204] S. Kumar, R. K. Singh, A. Chowdhuri, and A. Bhattacharyya, *Exploring waveforms with non-GR deviations for extreme mass-ratio inspirals*, JCAP **10**, 047, arXiv:2405.18508 [gr-qc] .

[205] A. M. Frassino, R. A. Hennigar, J. F. Pedraza, and A. Svesko, *Quantum Inequalities for*

Quantum Black Holes, Phys. Rev. Lett. **133**, 181501 (2024), arXiv:2406.17860 [hep-th]